



Master's Thesis

The Development of a Next Generation Total Disc Replacement Prosthesis

Author: Benjamin Scott McCarl

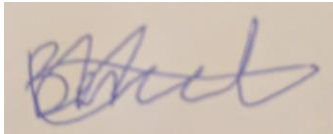
Supervisors: Assoc Prof John Costi and Prof Mark Taylor

Submitted to the School of Computer Science, Engineering, and Mathematics in the Faculty
of Science and Engineering in partial fulfilment of the requirements for the degree of
Batchelor of Engineering (Biomedical)(Honours) / Master of Engineering (Biomedical) at
Flinders University - Adelaide Australia

Declaration

I certify that this work does not incorporate without acknowledgment any material previously submitted for a degree or diploma in any university; and that to the best of my knowledge and belief it does not contain any material previously published or written by another person except where due reference is made in the text.

Benjamin McCarl



Date: 6/2/2017

Acknowledgments

I would like to first acknowledge my supervisors Associate Professor John Costi and Professor Mark Taylor for their continued aid and guidance throughout the completion of my thesis. I would particularly like to thank John, for reading and editing a number of lengthy drafts as I compiled my thesis, and Mark for his aid in the data analysis of the FEA component of the project.

I would also like to thank Dermmot O'Rourke, Rami Al-Dirini, Maged Awadalla and Hamed Ziaei Poor for their generous help with countless FEA minor issues. I would also like to recognise Dr Ashish Dhar Diwan for his generous donation of a Prodisc-L TDR device which will be used in the future of the project. I would also like to recognise Robbie Trott and Daniel Thomas for their support through the year.

Lastly, I would like to thank my family for supporting me throughout the past six years of tertiary study, without which I may not have been able to accomplish my goals of becoming a biomedical engineer. I cannot thank you enough for the opportunities you have provided which have allowed me to follow my dreams and aspirations.

Contents

Declaration.....	ii
Acknowledgments.....	iii
List of Figures.....	xvi
List of Tables.....	xxiii
List of Abbreviations.....	xxviii
Abstract.....	1
Chapter 1. Introduction.....	3
1.1 Project Goals.....	4
Chapter 2. Background.....	5
2.1 Low Back Pain.....	5
2.2 Financial Burden of Back Pain.....	7
2.3 Degenerative Disc Disease.....	10
Chapter 3. Design Process and Problem Definition.....	14
3.1 Design Process.....	14
3.2 Problem Definition.....	14
3.3 Design Requirements.....	15
3.3.1 Geometric Requirements.....	15
3.3.2 Material Requirements.....	15
3.3.3 Mechanical Requirements.....	15
3.3.4 Brainstorm Necessary Information for the Design.....	16
Chapter 4. Literature Review.....	17
4.1 Anatomy.....	17
4.1.1 Lumbar Spine.....	17
4.1.2 Facet Joints.....	19
4.1.3 Intervertebral Disc.....	19
4.1.3.1 Nucleus Pulposus.....	20

4.1.3.2	Annulus Fibrosis.....	20
4.1.3.3	Vertebral Endplate.....	20
4.1.4	Functional Spinal Unit.....	21
4.2	Lumbar Morphology.....	22
4.2.1	Vertebral Body Height and Bone Density.....	22
4.2.2	Endplate Area and Shape.....	22
4.2.3	Facet Joints.....	27
4.2.3.1	Angle of Facet Joints.....	28
4.2.3.2	Facet Joint Linear Dimensions.....	30
4.2.4	Facet Joint Area.....	31
4.3	Lordosis Angle.....	32
4.4	Lordosis Angle in Healthy Individuals.....	34
4.5	Intervertebral Disc Angle.....	35
4.6	Segmental Lordosis.....	36
4.7	Disc Height.....	37
4.8	Lateral Annulus Fibrosis Thickness.....	39
4.9	Biomechanical Behaviour of the Lumbar Spine.....	40
4.9.1	Biomechanics of Lumbar Functional Spinal Units.....	41
4.9.2	Compression.....	42
4.9.3	Torsion.....	44
4.9.4	Shear.....	44
4.9.5	Flexion/Extension.....	45
4.9.6	Lateral Bending.....	45
4.9.7	Fatigue Strength of Spinal Functional Units.....	46
4.9.7.1	Compression.....	46
4.9.7.2	Shear.....	47
4.10	Biomechanics of the Facet Joints.....	47

4.10.1	Shear	47
4.10.2	Torsion	48
4.10.3	Flexion/Extension	49
4.11	Summary of Failure Loads for the Lumbar Spine.....	51
4.12	Range of Motion of the Spine	51
4.13	Centre of Rotation	53
4.14	Assessment of LBP	57
4.14.1	Visual Analogue Scale (VAS)	57
4.14.2	Oswestry Disability Index (ODI).....	58
4.15	Different Solutions of LBP	58
4.15.1	Non-Surgical	58
4.15.2	Surgical	58
4.15.2.1	Tissue Engineering	59
4.15.2.2	Facet Replacement.....	59
4.15.2.3	Fusion	60
4.15.2.3.1	Adjacent Disc Degeneration.....	60
4.16	Total Disc Replacements.....	61
4.17	TDR Devices	61
4.17.1	Ball and Socket	63
4.17.2	Mobile Core	63
4.17.3	Elastomer Core.....	63
4.18	Surgical Insertion	64
Chapter 5.	Review of TDRs	67
5.1	Unknown Market Status.....	67
5.1.1	eDisc™	67
5.1.1.1	Design Features	67
5.1.1.1.1	Unique Design Features.....	68

5.1.1.2	Mechanical Testing.....	68
5.1.1.3	Clinical Trials	70
5.2	TDRs Removed from the Market.....	70
5.2.1	CHARITÉ™	71
5.2.1.1	Design Features	71
5.2.1.1.1	Unique Design Features.....	72
5.2.1.2	Mechanical Testing.....	72
5.2.1.3	Clinical Trials	76
5.2.2	AcroFlex	77
5.2.2.1	Design Features	77
5.2.2.1.1	Unique Design Features.....	78
5.2.2.2	Mechanical Testing.....	78
5.2.2.3	Clinical Trials	79
5.2.3	FlexiCore®	80
5.2.3.1	Design Features	80
5.2.3.1.1	Unique Design Features.....	81
5.2.3.2	Mechanical Testing.....	82
5.2.3.3	Clinical Trials	83
5.2.4	Kineflex.....	83
5.2.4.1	Design Features	83
5.2.4.1.1	Unique Design features	84
5.2.4.2	Clinical Trials	84
5.3	Currently on the Market	85
5.3.1	M6-L®	85
5.3.1.1	Design Features	85
5.3.1.1.1	Unique Design Features.....	85
5.3.1.2	Mechanical Testing.....	85

5.3.1.3	Clinical Data	86
5.3.2	MobiDisc L	87
5.3.2.1	Design Features	87
5.3.2.1.1	Unique Design Features.....	87
5.3.2.2	Mechanical Testing.....	88
5.3.2.3	Clinical Trials	89
5.3.3	XL TDR®	89
5.3.3.1	Design Features	89
5.3.3.1.1	Unique Design features	90
5.3.3.2	Mechanical Testing.....	90
5.3.3.3	Radiological Testing.....	91
5.3.3.4	Clinical Testing.....	91
5.3.4	LP-ESP®.....	92
5.3.4.1	Design Features	92
5.3.4.1.1	Unique Design Features.....	92
5.3.4.2	Mechanical Testing.....	95
5.3.4.2.1	Creep.....	96
5.3.4.2.2	Combined compression and rotation	96
5.3.4.2.3	Adhesion of endplates to annuls.....	97
5.3.4.2.4	Compression Tests.....	97
5.3.4.2.5	Endplate coating test.....	97
5.3.4.3	Clinical Trials	98
5.3.5	ActivL®	98
5.3.5.1	Design Features	98
5.3.5.2	Unique Design Features.....	98
5.3.5.3	Mechanical Testing.....	99
5.3.5.4	Clinical Trials	104

5.3.6	Prodisc®-L.....	104
5.3.6.1	Design Features	104
5.3.6.2	Mechanical Testing.....	105
5.3.6.3	Static Compression Shear Test.....	105
5.3.6.4	Dynamic Compression Shear Test	106
5.3.6.5	Creep.....	107
5.3.6.6	Static Inlay Push Out Test	107
5.3.6.7	Dynamic Inlay Push Out Test.....	108
5.3.6.8	Wear Testing.....	109
5.3.6.9	Hysteresis Test.....	109
5.3.6.10	Expulsion Test	109
5.3.6.11	Clinical Trials	110
5.3.7	Maverick™	110
5.3.7.1	Design Features	110
5.3.7.2	Clinical Trials	111
5.3.8	Freedom® Lumbar Disc	111
5.3.8.1	Design Features	111
5.3.8.2	Unique Design Features.....	111
5.3.8.3	Mechanical Testing.....	112
5.3.8.4	Range of Motion.....	113
5.3.8.4.1	Compression and Axial Rotation CoR	113
5.3.8.4.2	Flexion Extension RoM.....	113
5.3.8.5	Static Compression	114
5.3.8.6	Fatigue	114
5.3.8.6.1	Compression	114
5.3.8.6.2	Compressive Shear	115
5.3.8.6.3	Wear Fatigue.....	117

5.3.8.7	Clinical Trials	118
5.3.9	Baguera L.....	118
5.3.9.1	Design Features	118
5.3.9.2	Unique Design Features.....	119
5.3.9.3	Clinical Trials	119
5.3.10	Physio-L.....	119
5.3.10.1	Design Features	119
5.3.10.2	Radiographic RoM and Height Testing.....	119
5.3.10.3	Clinical Trials	120
5.4	Summary of Clinical Trials	121
5.4.1	ODI	121
5.4.2	VAS.....	123
5.5	Summary of Commercially Available TDR Parameters.....	125
5.6	Problems with TDR.....	131
5.6.1	Adjacent Disc Degeneration	131
5.6.2	Facet Joint Degeneration.....	131
5.6.3	Subsidence	131
Chapter 6.	Specifications.....	133
6.1	TDR Type.....	133
6.2	Material Specifications.....	133
6.2.1	Elastomer Core.....	133
6.2.2	Metal Endplates	133
6.3	Mechanical Specifications.....	134
6.4	Geometric Specifications	134
6.4.1	Endplate Design Specifications	134
6.4.1.1	Lordosis of Endplates	134
6.4.1.2	Keel/spike Height	137

6.4.1.3	Endplate Shape	137
6.4.1.4	Anterior Posterior Endplate Width	138
6.4.1.5	Lateral Endplate Width.....	138
6.4.1.6	Endplate Area	139
6.5	Range of Motion.....	139
6.6	Centre of Rotation	140
6.7	Total Height.....	140
6.8	Summary of Key Design Specifications	141
Chapter 7.	Design Concepts	142
7.1	Printed Magnetic Endplates	142
7.1.1	Advantages.....	142
7.1.2	Disadvantages	142
7.2	Internally Assembled Endplates.....	143
7.2.1	Advantages.....	143
7.2.2	Disadvantages	143
7.3	Modular Core	143
7.3.1	Advantages.....	144
7.3.2	Disadvantages	144
7.4	Velodrome TDR.....	145
7.4.1	Advantages.....	145
7.4.2	Disadvantages	146
Chapter 8.	Ranking of Design Concepts	147
8.1	Justification of Weighting	147
8.1.1	Safety	147
8.1.2	Biocompatibility	147
8.1.3	Range of Motion	147
8.1.4	Centre of Rotation.....	147

8.1.5	Surgical Invasiveness.....	148
8.1.6	Cost.....	148
8.1.7	Fatigue Life.....	148
8.1.8	Biomechanical Behaviour.....	148
8.2	Concept Scores.....	148
8.2.1	Printed Magnetic Endplates.....	149
8.2.2	Internally Assembled Endplates.....	149
8.2.3	Modular Core.....	150
8.2.4	Velodrome TDR.....	150
Chapter 9.	Design Iterations of the Velodrome TDR.....	152
9.1	The Final Design.....	154
Chapter 10.	CAD Automation.....	160
10.1	Automation Justification.....	161
10.1.1	CAD software.....	162
10.2	Initial CAD Automation System.....	162
10.3	Final CAD Part Automation System.....	163
10.3.1	Minor Functions.....	164
10.4	Assembly Creation.....	164
10.5	Dimension limitations.....	167
10.6	Disadvantages of Automation System.....	168
Chapter 11.	FEA Study.....	169
11.1	Aim of FEA.....	169
11.2	Development of FEA model.....	169
11.2.1	Additional Parts.....	170
11.3	Segmentation of Parts.....	171
11.4	Material Properties.....	172
11.5	Assembly.....	173

11.6	Constraints.....	174
11.7	Boundary Conditions.....	174
11.8	Loading Regime	174
11.9	Parametric Study	174
11.9.1	Control Parameters.....	174
11.10	Investigated Design Iterations	175
11.11	Measurement of CoR	176
11.12	Measurement of RoM.....	177
11.13	Convergence Study	177
11.13.1	Convergence Study Method	177
11.14	Mesh Size and Type	178
11.15	FEA Automation	178
11.16	Batch Analysis.....	179
11.17	Post Processing.....	179
11.18	Results	180
11.18.1	Parametric Analysis.....	182
11.19	Discussion	187
11.19.1	Automation Clarification.....	187
11.19.2	Proof of Concept	189
11.19.3	CoR location.....	190
11.19.4	Sample Size	190
11.19.5	Additional Data	190
11.19.6	Assumptions	191
11.19.7	RoM.....	191
11.19.8	Specification and Design Requirement Priority.....	191
11.19.9	Further Analysis	191
11.20	FEA Conclusion	192

11.21 CAD and FEA Automation System	193
Chapter 12. Future Work	197
12.1 Expansion on levels of Intended Use	197
12.2 Automatic Screen Scaling and Directory Creation	197
12.3 Automation of More Complex Post Processing	197
12.4 Design of Experiment.....	198
12.5 Automation System Troubleshooting	199
12.6 Automated Iteration Generation.....	199
12.7 Validation of the FEA	199
12.8 Expand Parametric Analysis	200
12.9 Material properties	200
12.10 Expansion of Mechanical Testing Simulation	200
12.11 Mechanical Performance Prioritisation.....	201
12.12 In-vitro testing	201
12.13 Facet Joint Specifications.....	201
12.14 Endplate Optimisation.....	202
12.14.1 Endplate Lordosis.....	202
12.14.2 Elastomer Core to Endplate Fixation	202
12.15 Hyper-elastic Mooney Rivlin Material Properties	203
12.16 Design Optimisation.....	203
12.17 Patent Search and Application	203
12.18 Single Core.....	204
12.19 Additional Applications	204
Chapter 13. Conclusion.....	205
Chapter 14. Bibliography.....	207
Chapter 15. Appendix	224

List of Figures

Figure 1: The percentage of bodily locations that were referenced for serious claims. (injuries that were awarded compensation and required one or more weeks of time off work) made in the 2012-13 financial year according to Australian Workers Compensation Statistics 2012-2013 (Safe Work Australia 2015).....	6
Figure 2: The prevalence of back problems by age based on the 2011-12 National Health survey by the Australian Bureau of Statistics (Australian Institute of Health and Welfare 2015).....	7
Figure 3: A summary of the direct and indirect cost of LBP from around the world. Japan (Shinohara et al. 1998), UK (Maniadakis & Gray 2000), Belgium (Van, ZJ, Van 2005), Sweden (Ekman et al. 2016), Australia (Walker, B.F, Muller, R., Grant 2003), Netherlands (Boonen et al. 2005), Switzerland (Wieser, Horisberger, Schmidhauser & Eisenring 2011) and the US (Katz 2006). All figures were converted using the corresponding currency conversion from the Westpac Financial year average exchange rate (Sterling & Sterling 2014).	10
Figure 4: A healthy disc (left) and a degenerative disc (right). Highlighting the loss of disc height and the differences made to the facet joint contact that can result in facet joint osteoarthritis and the narrowing of the vertebral foreman that can cause compression of the spinal nerves (Baliga et al. 2015).	12
Figure 5: The process of lumbar disc degeneration shown in human lumbar intervertebral discs (Da Silva Baptista et al. 2015). A=a healthy disc with a well hydrated nucleus and well aligned annulus fibrosis. As the degeneration of the disc continues (A to F) tears begin to occur, the annulus begins to lose its highly aligned orientation and lose of disc height becomes more extensive (Da Silva Baptista et al. 2015).	12
Figure 6: Image of an adult spine, showing the curvature and different regions of the spine (OpenStax College 2013).	17
Figure 7: A typical vertebrae, showing the different processes that comprise the posterior elements, the vertebral body, the spinal cord and the facet joints (OpenStax College 2013).....	18
Figure 8: The lumbar vertebrae. Distinctive characteristics include the large thick vertebral body and the short rounded spinous process.	19
Figure 9: Schematic of the intervertebral disc (Cortes & Elliott 2014).....	20

Figure 10: General sagittal cross sectional shape of the lumbar vertebral bodies and the intervertebral discs. Note the concave shape of the inferior endplate of the superior vertebral body, the convex shape of the superior endplate of the inferior vertebral body, the wedge shape of the intervertebral disc and the greater anterior disc height compared to the posterior height causing the disc to contribute to the lordotic shape of the lower lumbar spine.21

Figure 11: The relationship between 2 years postoperative Oswestry Disability Index (ODI) score and the percentage of total area of the endplate that the prosthesis covers. The error bars indicate the stand error (Gornet et al. 2014).23

Figure 12: Image depicting the location of the lateral (A) and anterior posterior(B) diameters of the endplates (Hall et al. 1997).....24

Figure 13: The average shape of male and female endplates of the inferior L4 (top left), superior L5 (top right), inferior L5 (bottom left) and superior S1 (bottom right)(Hall et al. 1997).26

Figure 14: Angles of the facet joints (Jaumard & Welch, William C, Winkelstein 2011).28

Figure 15: Diagram depicting the different measurements taken by Panjabi (left) and the legend of measurement acronyms (right) (Panjabi et al. 1993).30

Figure 16: Cobb method of measuring spinal curvature (Vrtovec et al. 2009).33

Figure 17: X- ray lumbar lordosis (LL) and segmental lordosis (SL) angle measurements for an intact spine (left) and implanted with TDR spine (right)(Cakir et al. 2005).36

Figure 18: The creep test input (constant stress (σ) over a time period (t)) (left (a)) and stress relaxation input (constant strain (ϵ) over a time period (t)) (right (a)) The different creep (left) and stress relaxation (right) responses of different types of materials (elastic=b, viscoelastic solid=c and viscoelastic fluid =d)40

Figure 19: The six degree of freedom mechanical behaviour of human intervertebral lumbar disc motion segments (without FJs) when loaded at different strain rates. This illustrates the non-linear, strain rate dependent, viscoelastic and anisotropic behaviour of the disc (Costi et al. 2011).41

Figure 20: Annulus fibrosis fibres under tensile loads when the disc is exposed to shear (left) axial torsion (centre) and axial tensile (right) loading (Bogduk 1997).43

Figure 21: The different regions of the tensile stress strain response of the Annulus Fibrosis fibres.43

Figure 22: The approximate centre or rotation (CoR) of the lumbar spine (O). Note that the CoR is not positioned more dorsally at the centre of curvature of the facet joints (O').

Also not that one of the facets is in compression and the others is in tension when loaded in torsion.(Adams et al. 2013).	49
Figure 23: The calculation of the instantaneous centre of rotation (ICR)(Pearcy & Bogduk 1988).....	54
Figure 24: The mean instantaneous centre of rotation (ICR) of the three movements on a standardised diagram of the lumbar spine in the sagittal plane. A=upright to flexion movement, B=upright to extension and C= extension to flexion. The inner ellipse describes two standard deviations from the mean ICR for the 10 subjects measured. The outer and middle ellipses indicate the 96% confidence limits of the inter and intra-observer reliability (Pearcy & Bogduk 1988).....	55
Figure 25: An example of different types of Visual Analogue Scale (VAS). A simple non-scaled VAS (top), a VAS with a descriptive sale (middle) and a VAS with a numeric scale (bottom)(Mannion et al. 2007).	57
Figure 26: The difference in back and leg pain from a Visual Analogue Scale over a 24-month period, comparing the non-surgical and surgical (fusion) group. The mean and 95% confidence values are presented (Fritzell et al. 2001).....	59
Figure 27: A facet replacement system (Goel et al. 2007).	60
Figure 28: A demonstration of how a mobile core translates during flexion (left) to extension (right) within the disc space (Geisler 2006).	63
Figure 29: The 'French Position' (Vital & Boissière 2014).	64
Figure 30: A drawing in the transverse plane of the approach often used to implant a lumbar TDR (Vital & Boissière 2014).....	65
Figure 31: The distraction of the left common iliac vein and artery to expose the L5-S1 disc before TDR implantation (McAfee et al. 2006).	65
Figure 32: Assembled eDisc TDR (left) and eDisc with exposed electronics (right)(Hunt et al. 2007)(McMillin 2006).....	68
Figure 33: The SN curve illustrating cycles to failure of a number of different biomaterials compared to TH200 (eDisc polymer)(Hunt et al. 2007).	69
Figure 34: The effect of hydrolytic aging on tensile strength for a number of different biomaterials (left) and the effect of oxidative aging on tensile strength for a number of different biomaterials (right)(Hunt et al. 2007).	70
Figure 35: CHARRITE artificial lumbar disc (top) and the InMotion disc (bottom) (Geisler 2006)(Serhan et al. 2011).	72

Figure 36: The original AcroFlex endplate design, with flat endplates and a crescent moon ridge (left) and the refined designed endplate with central anterior posterior ridge and finned teeth (right) (Fraser et al. 2004).....	78
Figure 37: AcroFlex axial compression load-displacement response at 8, 80 and 800 N/sec loading rates (Manuscript & Proximity 2011).....	79
Figure 38: Deconstructed FlexiCore TDR (Valdevit & Errico 2004).	81
Figure 39: Assembled FlexiCore artificial disc. Note the unique domed vertebral endplates (Cheung et al. 2016).	82
Figure 40: Kineflex TDR. (a) The baseplate and metal mobile core, (b) an assembled Kineflex TDR and (c) the base plate and superior endplate (Cheung et al. 2016).....	84
Figure 41: M6-L cross section exposing the different components of the design; artificial nucleus, artificial annulus, sheath and titanium endplates (left) and an assembled M6-L TDR (Spinal Kinetics 2009).	85
Figure 42: Comparison of the intact L4-L5FSU load displacement curves for a 400N follower load (left) and 800N follower load (right)(Spinal Kinetics 2009).....	86
Figure 43: An assembled MobiDisc-L TDR (left) and the mobile core of the MobiDisc-L that allows semi constrained translation in the transverse plane and axial rotation(right) (Zimmer Biomet 2016).	87
Figure 44: The self-guided insertion tool used to insert the MobiDisc-L anchors (Zimmer Biomet 2016).	88
Figure 45: Mean CoR position pre-op and 2 years after MobiDisc-L implantation calculated from SpineView software (Delécrin et al. 2007).....	89
Figure 46: Assembled XL TDR coronal view (left) and lateral view (right)(AIMIS Spine 2014).....	89
Figure 47: The XL TDR neutral zone motion in flexion/extension, lateral bending and axial rotation compared to the intact for both non and resected AF and ligaments conditions (Pimenta et al. 2015).....	91
Figure 48: CAD exploded view showing the LP-ESP inner silicone gel core and polycarbonate urethane ring (A-C). The actual LP-ESP TDR with titanium endplates and five spikes for fixation (D-G)(Lazennec et al. 2012).	92
Figure 49: LP-ESP component schematic (Lazennec et al. 2012).....	94
Figure 50: Test setup used to investigate the cohesion of the annulus to the endplates (Lazennec et al. 2012).	97

Figure 51: The ActivL different components. Inferior endplate (left), inlay (centre) and superior endplate (right) (Miller et al. 2016).....	98
Figure 52: The standard shape of the ActivL TDR (left) and the specialised S1 endplate shape (right) (Miller et al. 2016).....	99
Figure 53: ActivL keel (left) and spike (right) endplate design(FDA 2015b).....	99
Figure 54: Prodisc-L exploded view showing the superior endplate, inlay core and inferior endplate (top left), the Prodisc-L in lateral bending (top right), the Prodisc-L in flexion and extension bottom left and an assembled Prodisc-L (bottom right) (Synthes Spine 2006).....	105
Figure 55: The Prodisc-L snap in core feature used to lock the inlay into place (Marnay & Beyersdorff 2005).....	106
Figure 56: The two different endplates of the Maverick TDR (left). Note the polished articulating core and an assembled Maverick TDR (right) (Serhan et al. 2011; Errico 2005).....	110
Figure 57: The Freedom TDR from Axiomed (Axiomed 2008a).....	111
Figure 58: Cross section of the Freedom TDR. Illustrating the unique keels on the top and bottom top caps, void between the endplates, and the metal beads on both the outer endplate surface (for bone ingrowth) and inner endplate surface (for elastomer bond strength)(Axiomed 2008a).....	112
Figure 59: Freedom TDR compression stiffness test response. The dashed vertical line illustrates the boundary (displacement =0.04 mm) between the neutral zone (left) and the elastic zone (right) (Benzel et al. 2011).....	114
Figure 60: Axial compressive fatigue curve of the Freedom TDR (Benzel et al. 2011; Axiomed 2008a).....	115
Figure 61:45° compressive shear fatigue curve of the Freedom TDR. The applied compressive shear loads on 1200 to 2000 N correspond to 1697 to 2828 N of anterior shear load (Benzel et al. 2011; Axiomed 2008a).....	116
Figure 62: The Freedom TDR tested in a 45° compressive shear test. Note that the core and the endplates remain attached during testing (AxioMed 2008).....	117
Figure 63: Assembled Bagueira L TDR (Spine Art n.d.).....	118
Figure 64: Physio-L TDR (Pimenta et al. 2010).....	119
Figure 65: Comparison of mean ODI outcome of different TDR devices (For a tabulated comparison of the data and references to the clinical trials see Appendix C) (Pre-op=before operation).....	122

Figure 66: Comparison of VAS outcome of different TDR devices. (scores were scaled to 0-10 values) (For a tabulated comparison of the data and references to the clinical trials) (Pre-op=before operation) For a tabulated comparison of the data and references to the clinical trials see Appendix D) (Pre-op=before operation).. 124

Figure 67: The sites at which the anterior posterior (AP) and two mediolateral (ML1 and ML2) measurement were taken to investigate endplate and total disc replacement endplate size mismatch (Michaela et al. 2008)..... 132

Figure 68: The location of the centre of rotation (CoR) for the 6° (top) and 11° (bottom) Prodisc-L prosthesis with non-distributed (old implant) and distributed (new implant) lordosis angle endplates compared to the intact CoR (Tsitsopoulos et al. 2012)..... 136

Figure 69: Different endplate shapes of various commercial TDRs. Activ-L standard endplate (top left), Activ-L S1 Endplate (top middle), Baguera-L (top right), CHARITE (bottom left), MobiDisc (bottom left-middle), Prodisc-L (bottom right-middle) and Maverick (bottom right)..... 138

Figure 70: Example of two different 3D printed magnetic fields that are used to create a locking mechanism (Polymagnet 2016). 142

Figure 71: CAD drawing of the internally assembled endplate concept. 143

Figure 72: Drawing of the modular core concept assembled (top) and with the core unassembled (bottom). 144

Figure 73: A mini velodrome (Track Cycling News 2011)..... 145

Figure 74: The first design of the bottom core. 152

Figure 75: The sketches used by the loft tool to create the initial bottom core design..... 153

Figure 76: The initial bottom core design with a sharp top edge..... 153

Figure 77: First design iteration with flat top edge and filet between raised edges and bottom of the bottom core..... 154

Figure 78: An iteration of the final bottom core design..... 154

Figure 79: Cross section of the bottom core indicating the different geometric parameters that can be altered. A sagittal plane cross section (top) of the bottom core illustrating the anterior (left) and posterior (right) cross sections. A coronal plane cross section of the bottom core revealing the lateral cross sections (bottom). 155

Figure 80: Inner core of the TDR design concept..... 156

Figure 81: The assembled bottom core and inner core (left,) and the inner core (right) indicating the smaller size to the anterior posterior and lateral dimensions of the bottom core, but greater diameters than the base measurements..... 157

Figure 82: Early endplate design. 158

Figure 83: A CAD iteration of the final design chosen to proceed with the parametric analysis. (A) The assembled TDR and (B & C) exploded views illustrating the five different components of the design. (D-E) A picture of the Prodisc-L TDR components compared to (F-I) a 3D printed prototype of the Velodrome TDR concept components. 159

Figure 84: The different additional parameters of the endplates and total height of the TDR. 160

Figure 85: The automation process utilised to create different iterations of the CAD parts. 163

Figure 86: Section of the assembly creation window. The place button (red, dot dashed box), the model window (black, solid box), part and part origin box (blue, line dot line dashed box) and the assembly window (yellow, dashed line). 166

Figure 87: The internal trapezium geometries that are lofted around the outer ellipse rail... 167

Figure 88: The maximum outer height of the bottom core = Total TDR height - 1 mm - Superior Endplate Thickness - Inferior Endplate Thickness. 168

Figure 89: Initial point load simulation causing large local deformations. 170

Figure 90: The developed model with the 'box like structure' used to apply the bending moment to the designed TDR. The model before deformation (left) and after (right)... 171

Figure 91: Superior endplate with the front and back tracking nodes selected in red. 171

Figure 92: The pressure loads applied to the front and back halves of the 'box' part. 172

Figure 93: The results from two different iterations of the Velodrome TDR design. Dashed ellipse = two standard deviations from the L4-L5 CoR mean, solid ellipse = two standard deviations from the mean CoR for the L5-S1 index level, x= mean CoR of the TDR, o=the instantaneous change in position (posterior to anterior (left to right)) of the CoR as the TDR undergoes flexion. 181

Figure 94: The bottom core sloped surface which would fail to be defined for particular design iterations. Note that the point used by the findAt() function does lie on surface as indicated by the reference point. 188

Figure 95: Summary of the CAD and FEA automation system. 194

Figure 96: Hollow pyramid-like concept to increase surface area. 203

List of Tables

Table 1: Breakdown of the 2008-09 Australian Institute of Health and Welfare disease expenditure data on the associated costs to back problems (Australian Institute of Health and Welfare 2015).	8
Table 2: Summary of the direct and indirect Human Capital and Functional Cost estimates of the costs of LBP in Switzerland for 2005 (Wieser et al. 2011). The estimates were converted from Swiss Francs (CHF) to euro at the average 2005 exchange rate of the Swiss National Bank (0646 €/CHF); GDP= Gross Domestic Product and then converted to Australian dollars using Westpac financial year average exchange rates for 2005 (1AUD=0.6144Euro)(Sterling & Sterling 2014).....	9
Table 3: Estimates of the direct costs of LBP in the United States from the 1989 National Ambulatory Medical Survey reported in the 2001 Institute of Medicine Report and the Healthcare Cost and Utilization Project (Katz 2006).	9
Table 4: Table of FDA approved TDRs.	15
Table 5: Mean and Standard Deviation Vertebral Body Anterior and Posterior Heights (mm)(Zhou et al. 2000).	22
Table 6: Comparing mean and standard deviation of the anterior posterior and lateral dimensions of the vertebral endplates for male and female specimens (Hall et al. 1997) (Zhou et al. 2000).	25
Table 7: Summary of human lumbar endplate areas.	27
Table 8: Angles of the lumbar facet joints taken in the transverse plane relative to the sagittal plane (α angle of Figure 14A).	29
Table 9: Summary of the transverse plane angles measured by Panjabi (Panjabi et al. 1993).	29
Table 10: The mean and (standard error of the mean) of the superior articular facet linear dimensions (mm). FCW_{sr} = superior right facet width, FCW_{sl} = superior left facet width, FCH_{sr} = superior right Facet Height, FCH_{sl} = Superior left Facet Height. See Figure 15 for measurement locations(Panjabi et al. 1993).	30
Table 11: The mean and (standard error of the mean) of the inferior articular facet linear dimensions (mm). FCW_{ir} = inferior right facet width, FCW_{il} = inferior left facet width, FCH_{ir} = inferior right facet height, FCH_{il} = inferior left facet height. See Figure 15 for measurement locations (Panjabi et al. 1993).	31

Table 12: The mean and (standard error of the mean) of the interfacet Distances (mm). IFWs=superior interfacet Width, IFWi=inferior interfacet width, IFHr=right interfacet height, IFHl=left interfacet Height. See Figure 15 for measurement locations (Panjabi et al. 1993).	31
Table 13: The mean and (standard error of the mean) of the superior articular facet surface areas (mm ²). FCA _{sr} =superior right facet surface area, FCA _{sl} =superior left facet surface area, FCA _{ir} =inferior right facet surface area, FCA _{il} =inferior left facet surface area. See Figure 15 for measurement locations (Panjabi et al. 1993).	31
Table 14: The mean and standard deviation (SD) of the facet joint articulation overlap measured from sagittal CT images (Liu et al. 2006).	32
Table 15: Overall lumbar lordosis measurements from multiple sources.	34
Table 16: Table comparing female and male lumbar lordosis.	34
Table 17: Summary of different Intervertebral disc angles.	35
Table 18: Summary of segmental lumbar lordosis angles.	37
Table 19: Different lumbar disc heights from the literature.	38
Table 20: The different RoMs, segmental lordosis and neural foramen size of the lumbar spine for different TDR heights (Gaffey et al. 2010).	38
Table 21: The probability of functional spinal unit fatigue failure (%) after a specific number of cycles while being loading at a particular range of compressive force relative to the FSU's ultimate strength (Brinckmann et al. 1988).	46
Table 22: Summary of the loads need to fail lumbar functional spinal units. * = functional spinal unit with facet joints removed.	51
Table 23: Recorded ranges of motion of the human lumbar spine.	52
Table 24: Comparison of the preoperative (top section) and postoperative (bottom section) pain scores between patients with RoM \leq 5° and RoM $>$ 5°. (* = statistically significant using a Spearman correlation) (Huang et al. 2005).	53
Table 25: The mean (and standard deviation) instantaneous centre of rotation (ICR) of the lumbar spine. Measurements are relative to an origin at the posterior superior corner of the lower vertebra of the applicable functional spinal unit (FSU). The location of the ICR is in terms of the proportion of the depth (x) and height (y) from the defined origin of the lower vertebrae of the applicable FSU in the sagittal plane (Pearcy & Bogduk 1988).	56
Table 26: Summary of the different types of TDR devices available on the market as of 2014. The table shows the type of bearing surfaces (MoM=metal on metal, MoP=metal on	

polymer, PoP=polymer on polymer and 1P=one piece), the biomaterial the devices are made of, the bearing design or type and the manufacture (Veruva et al. 2014).....	62
Table 27: The mechanical properties of the eDisc polymer (Hunt et al. 2007).....	68
Table 28: Summary of the chemical properties of TH200 the polymer used in the eDisc (Hunt et al. 2007).....	69
Table 29: Summary of CHARITE static tests (FDA 2004).....	73
Table 30: Summary of CHARITE dynamic testing (FDA 2004).....	75
Table 31: The range of motion of the AcroFlex implanted FSU with simulated fibrosis tissue compared to the intact FSU for flexion/Extension, lateral bending and axial rotation (Manuscript & Proximity 2011).	79
Table 32: Comparison of the LP-ESP to the natural disc when loaded in flexion/extension, lateral flexion (also known as lateral bending), torsion, axial compression and elastic recovery (Lazennec et al. 2013; Lazennec et al. 2012).	96
Table 33: Series of mechanical tests submitted as part of the ActivL FDA approval process (FDA 2015b).	100
Table 34: Mean and standard deviation of the ultimate force and displacement at ultimate force from the Prodisc-L static compression shear test (FDA 2006).	106
Table 35: The mean and standard deviation ultimate force (N) and displacement (mm) at the ultimate force for the static inlay push out test (FDA 2006).....	108
Table 36: Prodisc-L dynamic inlay push out test results.	108
Table 37: Mean and standard deviation of the shear force needed to expel the Prodisc-L TDR from the polyurethane block and the corresponding displacement recorded (FDA 2006).	109
Table 38: Freedom RoM test results compared to human lumbar RoM (Benzel et al. 2011).	113
Table 39: Comparison of the Freedom TDR (FLD) wear test data to the CHARITE and Prodisc-L data (Axiomed 2008a).	118
Table 40: A summary of the different anteriorposterior (top row) and lateral (bottom row) widths (mm) of a number of different total disc replacements endplates. Note the CHARITE sizes in the table correspond to the size 2,3,4 and 5 prosthesis and that the Mobidisc-L comes in two different lateral widths (34 and 39mm) for 3 different anteriorposterior widths.....	125
Table 41: Summary of the different total heights of different TDRs (mm).....	125
Table 42: Summary of the different inlay sizes of different TDRs (mm).	126

Table 43: A summary of the different lordosis angles available from different TDR devices.	126
Table 44: Summary of the RoM of different TDR devices. Merged flexion and extension data signifies the combined flexion/extension RoM.	128
Table 45: The maximum ranges of motion of the ActivL TDR. *= The inlay translation is limited on endplate size which effect flexion RoM (FDA 2015b).	129
Table 46: Material properties of common orthopaedic biomaterials (Hallab et al. 2003).	130
Table 47: Mechanical failure specifications.	134
Table 48: The comparison of the range of motion of the lumbar spine in flexion/extension, lateral bending and axial rotation to the intact state for different TDR endplate lordosis angles (Tsitsopoulos et al. 2012).	135
Table 49: The global mean RoM of the L4-L5 and L5-S1 spinal segments from literature and the final specified RoM.	139
Table 50: Centre of rotation specifications. (values given as proportion of x=width and y=height of the inferior spinal segment).	140
Table 51: Summary of key design specifications.	141
Table 52: Weighting matrix used to decide which design concept to pursue.	147
Table 53: Printed magnetic endplate decision matrix.	149
Table 54: Internally assembled endplate decision matrix.	149
Table 55: Modular core decision matrix.	150
Table 56: Velodrome TDR decision matrix.	150
Table 57: Summary of different Velodrome TDR parameters.	161
Table 58: Different subroutine functions that are used during the creation of the CAD parts.	164
Table 59: Material properties of the elastomer core.	173
Table 60: Constant variables for FEA.	175
Table 61: The parameters used in the parametric analysis of the prototype design. (PB=Posterior base, AB= Anterior base, LB=Lateral base, POH=Posterior outer height, AOH=Anterior outer height, LOH=Lateral outer height, PTE=Posterior outer height, LTE=Lateral outer height).	176
Table 62: Convergence study results.	177
Table 63: The model coordinates of the physiological CoR x and y coordinates and the two standard deviation ranges.	180

Table 64: FEA simulation results for the 19 different design iterations. (Final instantaneous X CoR= The final frame CoR x coordinate, Final instantaneous Y CoR= The final frame CoR y coordinate, Mean CoR X = mean centre of rotation x coordinate, Mean CoR Y = mean centre of rotation y coordinate, RoM = range of motion)..... 182

Table 65: Additional design iterations that were tested..... 184

Table 66: Additional iteration simulations results. (Final instantaneous X CoR= The final frame CoR x coordinate, Final instantaneous Y CoR= The final frame CoR y coordinate, Mean CoR X = mean centre of rotation x coordinate, Mean CoR Y = mean centre of rotation y coordinate, RoM = range of motion). 185

Table 67: The refined iterations dimension parameters (PB=Posterior base, AB= Anterior base, LB=Lateral base, POH=Posterior outer height, AOH=Anterior outer height, LOH=Lateral outer height, PTE=Posterior outer height, LTE=Lateral outer height).... 186

Table 68: Refined iteration simulations results. (Final instantaneous X CoR= The final frame CoR x coordinate, Final instantaneous Y CoR= The final frame CoR y coordinate, Mean CoR X = mean centre of rotation x coordinate, Mean CoR Y = mean centre of rotation y coordinate, RoM = range of motion). 186

Table 69: Updated material properties used to investigate the effect of the bottom core to top core elastic modulus ratio, on the variance between different design iterations. 186

Table 70: The original results (left column) compared to the updated results (right column). 187

List of Abbreviations

6DOF = Six degree of freedom
ADD = Adjacent disc degeneration
AF = Annulus fibrosis
BMD = Bone mineral density
CAD = Computer aided design
CoR = Centre of rotation
CT = Computer tomography
DALYs = Daily adjusted life years
DDD = Degenerative disc disease
Disc = Intervertebral disc
DW = Disability weighting
EP = Endplate
FEA = Finite element analysis
FJ = Facet joints
FSU = Functional spinal unit
GBD = Global burden of disease study
ICR = Instantaneous centre of rotation
IDEs = Investigational device exemption studies
LBP = Low back pain
MRI = Magnetic Resonance Imaging
NP = Nucleus pulpous
ODI = Oswestry disability index
PGs= Proteoglycans
RoM = Range of motion
TDR = Total disc replacement
VAS = Visual analogue scale
YLD = Years lived with a disease
YLL = Years of life lost to premature mortality

Abstract

Low back pain (LBP) has been ranked as the number one disability in terms of years lived with, according to the 2010 Global Burden of Disease study. Furthermore 80% of people will experience low back pain during their lives, with 10% of these eventually developing chronic pain. Once all non-surgical measures have been exhausted there are mainly only two options of surgical prostheses: spinal fusion or a total disc replacement (TDR).

All FDA approved TDRs are based on the concept of ball and socket hip replacements, which do not restore the complex biomechanics of the lumbar spine. Nevertheless, they are superior to fusion in terms of allowing a more physiological range of motion. Elastomer core TDRs appear to be the future. A small number of these have been released on to the market with some level of success, however none have yet gained FDA approval.

The aim of the project was to commence the early stages of design for a new next generation elastomer core TDR with the aid of finite element analysis (FEA). A parametric study investigating different prototype design geometries was performed to investigate their mechanical response.

An extensive literature review summarised relevant studies to the design process including an overview of: the problem of LBP and its financial implications, lumbar spinal morphology, lumbar biomechanics, and a detailed review of both previous and current TDR designs.

A novel ‘velodrome’ composite elastomer core prototype has been designed. The name of the prototype signifies the general shape of the bottom core, which has different levels of raised anterior, posterior and lateral edges that are used to alter the mechanical properties of the TDR and to mould the upper core. The core is comprised of three parts: a bottom, inner and top core. These parts have been designed to have different material properties to further aid the customisation of the early design.

An automated system created in MATLAB has been developed. This software successfully creates XML files that are uploaded into Autodesk Inventor, which changes the desired dimensions of the different template prototype parts. The CAD files are then automatically exported in the correct format so they can undergo FEA in an external software package (Abaqus v6.13 Dassault Systèmes, Providence, RI, USA). The Abaqus FEA simulation process is also automated by a python script that is created concurrently with the generation of the different iterations of the design in MATLAB. The FEA study will investigate the

centre of rotation of the prototype when undergoing flexion as an early stage proof of concept of the TDRs customisable design.

The project when completed may potentially lead to the development of a commercially viable device.

Keywords: Lumbar Disc Replacement, Total Disc Replacement, Low Back Pain, Costs of Low Back Pain, Total Disc Prosthesis, Lumbar Prosthesis, Design.

Chapter 1. Introduction

Low Back pain (LBP) is a serious problem in society, with a large proportion of the population experiencing it at some point in their lives (Dreischarf et al. 2015; Fritzell et al. 2001; Longo et al. 2010; Ruiz et al. 2014). Approximately one in ten LBP sufferers go on to develop chronic LBP (Baliga et al. 2015). LBP has been ranked number one in terms of years lived with a disability (Hoy et al. 2014). Once all non-surgical LBP pain treatments (Section 4.15.1) have been exhausted there are two main lumbar prostheses that are used in an attempt to fix the pain: spinal fusion or TDR.

The aim of this thesis was to complete the early stages of the design process of a novel total disc replacement (TDR). The goal of the design was to develop a TDR that best mimics the natural biomechanical properties of the intervertebral disc (disc). Computer aided design (CAD) models of potential prototypes have been developed and then simulated using finite element analysis (FEA), which was used to investigate the different mechanical response of the designs, and to illustrate the design concept. This FEA data was then used to identify how to refine the design of the TDR.

Chapter 2 covers the background of LBP, its influence on society and the likely causes. Chapter 3 describes the design process that has been followed to create the TDR, and 3.3 defines the design requirements derived from literature.

The extensive literature review in Chapter 4 provides the vast array of information necessary for the design of a TDR. Levels L3 to S1 of the lumbar spine were studied as they are applicable to TDRs (FDA 2006). The design itself focused on the L4-L5 and L5-S1 lumbar spinal segments, as these are the most commonly replaced levels (Rothwell et al. 2014; Michaela et al. 2008). The literature review includes lumbar anatomy and morphology, which were used to derive the TDR's geometric specifications. Lumbar spine biomechanics was also reviewed to understand the complex mechanical response of the disc segment. A comprehensive review, investigating the dimensions, design features, mechanical testing and clinical outcomes of both past and present TDRs that have been released onto the market was also conducted.

The information obtained from the literature review was then used to create design specifications for the development of the next generation TDR in Chapter 6, and summarised in 6.8. A number of different design concepts that followed the defined requirements and

specifications were then created in Chapter 7. These design concepts were then graded and ranked in Chapter 8. The superior design concept was then selected and the accompanying design iteration process was undertaken in Chapter 9.

An automated CAD system was defined and developed in Chapter 10, which allowed the creation of different geometric iterations of the design. The design process and an explanation of the system and how it works was also presented. Chapter 11 shows the accompanying FEA Section of the project which was undertaken to demonstrate proof of design concept and analyses the designs centre of rotation during flexion bending. A summary of the developed CAD and FEA automation system has been completed in 0. The future work and direction of the project has been discussed in Chapter 12, before the conclusion of the project in Chapter 13.

1.1 Project Goals

The main project goal was to commence the design process of a next generation TDR. The design process of TDRs is long, with the LP-ESP (Section 5.3.4) TDR requiring 20 years of research and development to produce the current design (Lazennec et al. 2012). It was not practical to completely develop a TDR during this half-year full-time equivalent project. Therefore, the following practical project goals were implemented:

1. Undertake an extensive literature review that provides the background information needed to design a TDR.
2. Develop a TDR design concept with the aid of CAD software.
3. Automate the CAD development to allow different parametric iterations of the design to be created.
4. Create a system which allows the CAD geometries to be uploaded into Abaqus FEA software via a python script.
5. Automatically simulate the designs and use the results to illustrate design concepts of the proposed design.

Chapter 2. Background

2.1 Low Back Pain

Low back pain (LBP) has been estimated to affect 80% of all adults at some point of their lives (Dreischarf et al. 2015; Fritzell et al. 2001; Longo et al. 2010; Ruiz et al. 2014) and is a major problem in today's society. The majority of these 80% do not seek medical attention, however approximately 10% of these individuals eventually develop chronic LBP (Baliga et al. 2015).

LBP has been defined as:

‘Pain in the area on the posterior aspect of the body from the lower margin of the twelfth ribs to the lower gluteal folds with or without pain referred into one or both of the lower limbs that lasts for at least one day’ (Hoy et al. 2014).

Disability-adjusted life years (DALYs) is a useful metric in determining the severity of LBP (Murray et al. 2012). DALYs are calculated as the sum of years of life lost to premature mortality (YLL), and the years lived with a disability (YLD). The definition of a disability for the context of the Global Burden of Disease study (GBD) was ‘any short-term or long-term health loss, other than death’ (Murray et al. 2012). The 2010 GBD highlighted the significance of LBP on a global and national level (Bourne et al. 2014; Hoy et al. 2014).

Since there is no link to mortality and LBP, an alternative method was used to calculate DALYS as $YLL=YLD$. In order to account for this a series of disability weightings (DW) were developed (Salomon et al. 2012). The DWs were developed through either face to face, telephone or online surveys where participants were given a comparative hypothetical scenario in which they would decide which, out of the two health states described to them, was more severe (Salomon et al. 2012).

The classification of DWs for LBP were broken down into two major categories; pain with or without leg pain, and then into another four subcategories of mild or severe, chronic or acute LBP. The mean overall DW was then multiplied by the age/sex/region-specific prevalence for the years 1990, 2005 and 2010 to YLDs to calculate the resulting DALYs.

Of the 291 conditions that were studied, LBP ranked number one in terms of years lived with a disability and sixth in DALYs having increased from the 1990 GBD rank of 11 (Hoy et al.

2014). The prevalence of LBP in individuals within the ages of 0-100 was estimated to be 9.4% with a 95% confidence interval of 9.0% to 9.8% (Hoy et al. 2014).

According to the Australian Workers Compensation Statistics, 2012-13, back pain including upper and LBP was the most common location injured that resulted in a serious claim (22%); resulting in compensation being awarded and the individual missing one or more weeks from work (excluding fatalities) (Safe Work Australia 2013). Although the back injury claims have decreased by 27% between 2000-01 and 2012-13, back injuries were still the number one form of injury with 25,750 claims made in the 2012-2013 financial year (Figure 1) (Safe Work Australia 2013).

Percentage of serious claims by bodily location of injury or disease, 2012–13p

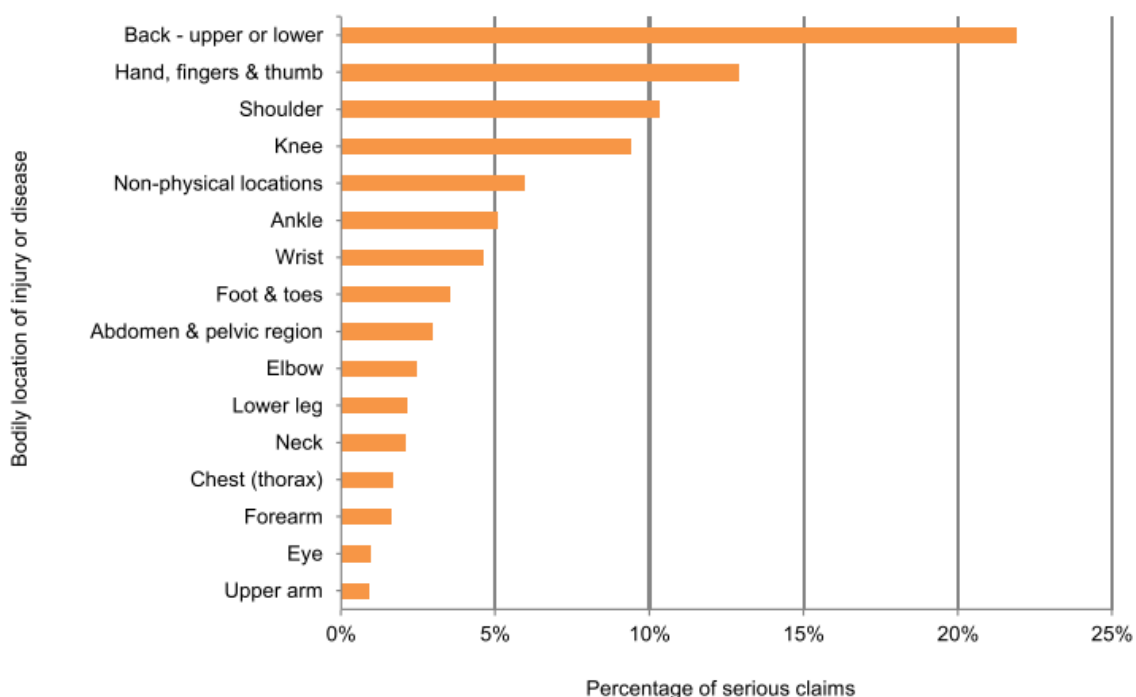


Figure 1: The percentage of bodily locations that were referenced for serious claims. (injuries that were awarded compensation and required one or more weeks of time off work) made in the 2012-13 financial year according to Australian Workers Compensation Statistics 2012-2013 (Safe Work Australia 2015).

Age is also a factor for back problems. It most commonly occurs in those aged between 65-79 according to the 2011-12 Bureau of Statistic National Health Survey (Australian Institute of Health and Welfare 2015). However, the prevalence of back pain does increase significantly after the age of 35 (Figure 2).

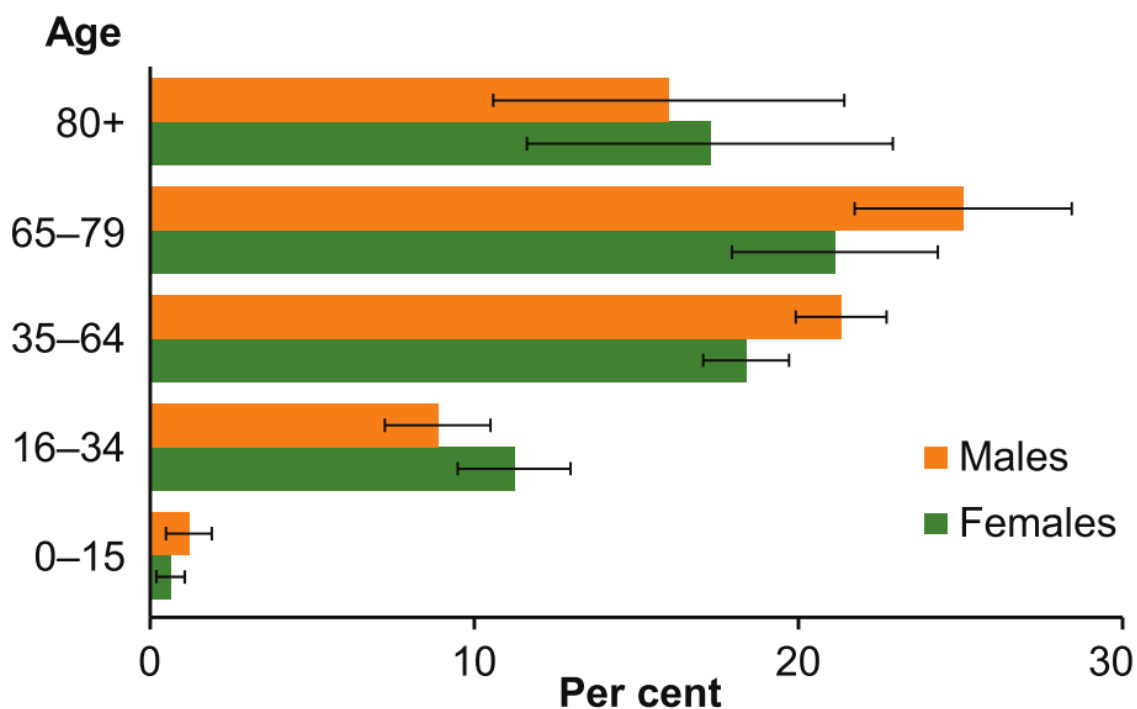


Figure 2: The prevalence of back problems by age based on the 2011-12 National Health survey by the Australian Bureau of Statistics (Australian Institute of Health and Welfare 2015).

Estimates from the Healthcare Cost and Utilization Project Nationwide Inpatient Sample suggest there has been a significant 137% increase from 174,223 to 413,171 ($P < 0.001$) spinal fusions that were performed in the US between 1998 and 2008 (Rajae et al. 2012). These findings clearly demonstrate that LBP is a significant problem in today's society, which has led to the development of a number of different treatments; including lumbar total disc replacements.

2.2 Financial Burden of Back Pain

With the prevalence of LBP being so high in today's society there is a significant accompanying economic burden.

The direct costs of LBP that are associated with the diagnosis, treatment and rehabilitation within Australia were estimated to be \$1.02 billion AUD in 2001 (Walker, B.F, Muller, R., Grant 2003). However, this amount is dwarfed by the indirect costs of \$8.15 billion that mainly contribute to loss of productivity due to work absences.

The economic burden of back pain in general is increasing, which is due to the aging population (Productivity Commission 2013). Expenditure data from the Australian Institute of Health and Welfare disease revealed this; as the direct costs due to back problems

increased to \$1.2 billion AUD for the 2008-09 period that can be broken down into three main categories (Table 1)(Australian Institute of Health and Welfare 2015).

Table 1: Breakdown of the 2008-09 Australian Institute of Health and Welfare disease expenditure data on the associated costs to back problems (Australian Institute of Health and Welfare 2015).

Type of Expenditure	Cost (AUD)	Percent of Total Expenditure
Admitted Patient Costs	\$560 million	47.6%
Out of Hospital Costs	\$464 million	39.4%
Prescription Pharmaceuticals	\$153 million	13.0%

These high direct and indirect costs are not unique to Australia. In 2005, Swiss data (Table 2) regarding the direct and indirect costs of LBP also supported this by utilising two separate methods for calculating the costs of LBP (Wieser, Horisberger, Schmidhauser, Eisenring, et al. 2011):

The Human Capital Approach (HC), which was defined as the product of work time lost due to LBP and gross earnings lost to the individual. This method has been criticized by Drummond (Drummond 1992) and Bjorn (Lindergren 1981) as they believed that it over estimated the productivity loss (Wieser, Horisberger, Schmidhauser, Eisenring, et al. 2011). Therefore, a new measure, defined as the Friction Cost (FC) was also used. The Functional Cost takes into consideration the time taken to restore the initial production level that was reduced due to the injury. This was defined as friction time (Young et al. 2000). This results in the Functional Cost method being a lower estimate than Human Capital Approach.

Table 2: Summary of the direct and indirect Human Capital and Functional Cost estimates of the costs of LBP in Switzerland for 2005 (Wieser et al. 2011). The estimates were converted from Swiss Francs (CHF) to euro at the average 2005 exchange rate of the Swiss National Bank (0646 €/CHF); GDP= Gross Domestic Product and then converted to Australian dollars using Westpac financial year average exchange rates for 2005 (1AUD=0.6144Euro)(Sterling & Sterling 2014).

	Total Direct Costs per LBP sufferer (AUD)	Total Direct Costs of LBP in Switzerland (AUD)
Total Direct Costs	\$3 billion	\$4.2 billion
Indirect Costs (HC)	\$4.8 billion	\$6.6 billion
Indirect Costs (FC)	\$2.5 billion	\$3.5 billion
Total Cost (HC)	\$7.8 billion	\$10.8 billion (2.3% GPD)
Total Cost (FC)	\$5.5 billion	\$7.8 billion (1.6% GPD)

The direct costs of LBP in the United States have also been studied (Katz 2006)(Table 3) .

Table 3: Estimates of the direct costs of LBP in the United States from the 1989 National Ambulatory Medical Survey reported in the 2001 Institute of Medicine Report and the Healthcare Cost and Utilization Project (Katz 2006).

Type of Expense	Number of Expenses per Year	Median Cost (US Dollars)	Total Cost (US Dollars)
Office Visits for LBP	19 million	\$150	\$3 billion
Medical Admissions for LBP	225,000	\$9000	\$2 billion
Laminectomy and Discectomy	286,000	\$14,000	\$4 billion
Lumbar Fusion Procedures	298,000	\$37,000	\$11 billion
		Total Cost	\$20 billion

A substantial number of studies from around the world all highlight the extreme cost of LBP, with a vast majority of these studies finding that the indirect costs outweigh the direct costs (Figure 3) (Dagenais et al. 2008).

Although the direct costs of LBP in the US are high (Table 3), the indirect costs outweigh the direct costs (Dagenais et al. 2008). The total costs of LBP in the US however dwarf the costs of any other nation (Duthey 2013; Katz 2006) (Figure 3).

A systematic review on the international costs of low back pain investigated a number of different cost of illness studies (Dagenais et al. 2008). The most recent studies; that provided

both the total indirect and direct costs of LBP, and the other studies have been summarised in (Figure 3).

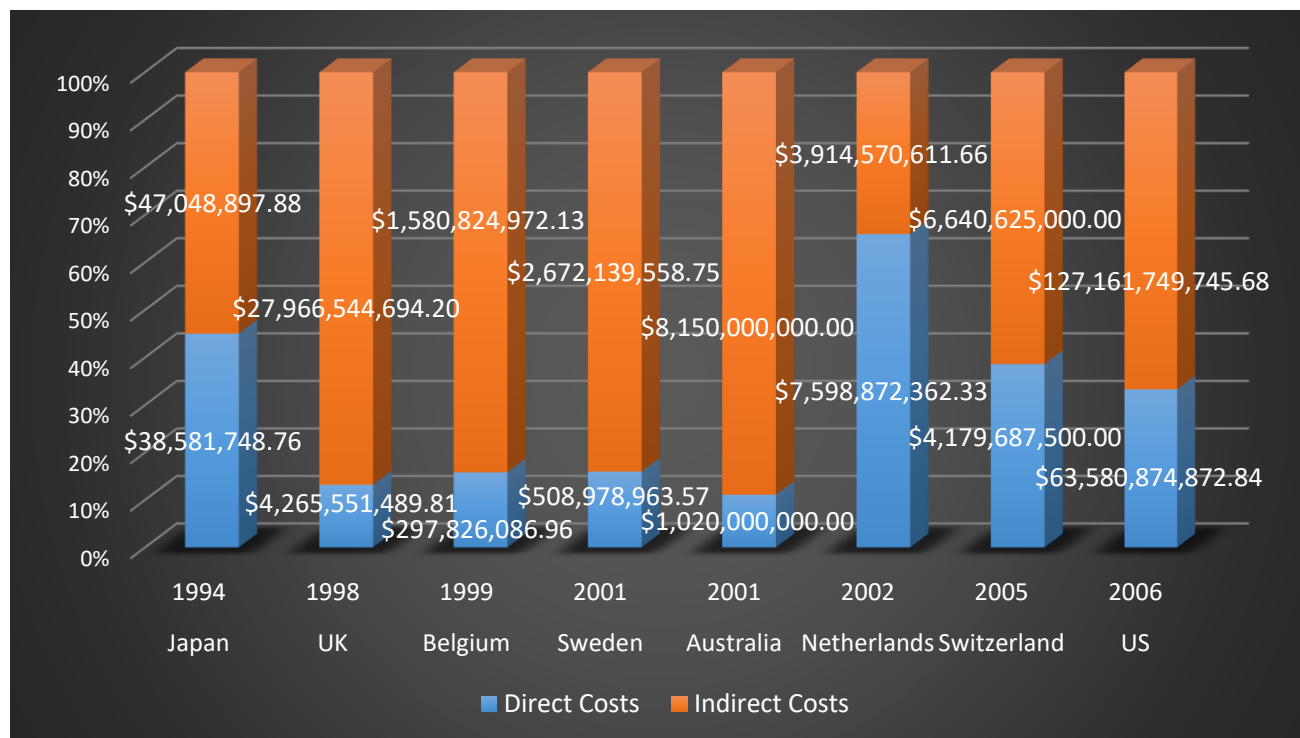


Figure 3: A summary of the direct and indirect cost of LBP from around the world. Japan (Shinohara et al. 1998), UK (Maniadakis & Gray 2000), Belgium (Van, ZJ, Van 2005), Sweden (Ekman et al. 2016), Australia (Walker, B.F, Muller, R., Grant 2003), Netherlands (Boonen et al. 2005), Switzerland (Wieser, Horisberger, Schmidhauser & Eisenring 2011) and the US (Katz 2006). All figures were converted using the corresponding currency conversion from the Westpac Financial year average exchange rate (Sterling & Sterling 2014).

As a result of the high cost of LBP in the world, it is clear that the market for a device that could help alleviate pain while maintaining physiological function of the lumbar spine will be in great demand.

2.3 Degenerative Disc Disease

Degenerative disc disease (DDD) is strongly linked to LBP and is understood to be a part of the normal aging process (Battie et al. 2014; Whatley & Wen 2012; Nerurkar et al. 2010). However, the exact mechanism of degeneration is not yet fully understood (Whatley & Wen 2012). The intervertebral discs begin to degenerate at a much earlier age than other musculoskeletal tissues with signs of degeneration already visible in the lumbar spine for those aged between 11 and 16 years (Baliga et al. 2015; Boos et al. 2002).

Many factors are believed to play a role in accelerating the natural degeneration of the disc such as age, hereditary traits, level of manual labour, trauma injuries and smoking status (Whatley & Wen 2012; Cortes & Elliott 2014). Heritability has been investigated in how it affects Magnetic Resonance Imaging (MRI) signal loss; which is associated with disc, degeneration, height loss and bulging (Battié et al. 2008). The study estimated that the genetic influence on LBP varied from 29%-54% depending on the disc degeneration phenotype and the lumbar segments location (Battié et al. 2008).

The process of DDD is considered to be both biological and mechanical and believed to begin in the nucleus pulposus (NP) (Section 4.1.3.1) where a reduction in cells, proteins and proteoglycans (PGs) occurs (Cortes & Elliott 2014). This affects the NP's ability to maintain the collagen matrix and withhold water causing a permanent loss in osmotic pressure (Costi et al. 2011; Luk & Ruan 2008). The relation of lumbar disc height measured with lateral radiographs and signs of degeneration from magnetic resonance imaging have been investigated. A total of 43 randomly selected patients from a cohort that were being examined for potential disc degeneration due to long term lifting were included in the study. The study concluded that early signs of degeneration did not correlate with loss of disc height. However as degeneration progresses disc height loss is more evident (Frobin et al. 2001).

The loss of water in the NP is believed to be a key factor in loss of disc height. This in turn affects the disc's mechanical response and causes increased facet joint contact forces. These increased forces can then lead to the development of facet joint osteoarthritis and/or place pressure on the spinal nerves, due to stenosis causing pain (Whatley & Wen 2012; Liu et al. 2006; Baliga et al. 2015; Frobin et al. 2001; Dunlop et al. 1984)(Figure 4). Decreases of 1 to 3 mm in disc height have been shown to cause these increases in facet joint contact forces (Dunlop et al. 1984; Adams et al. 2013).

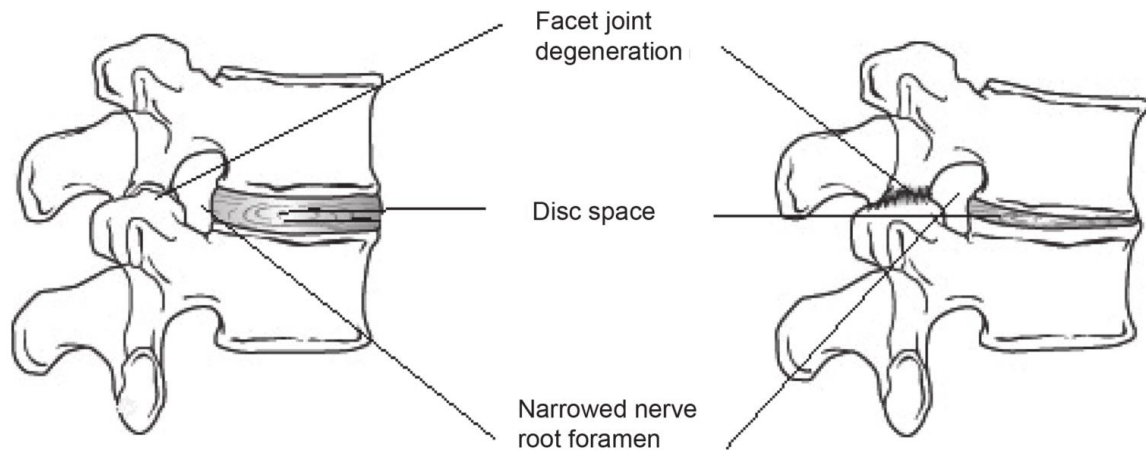


Figure 4: A healthy disc (left) and a degenerative disc (right). Highlighting the loss of disc height and the differences made to the facet joint contact that can result in facet joint osteoarthritis and the narrowing of the vertebral foreman that can cause compression of the spinal nerves (Baliga et al. 2015).

As the disc continues to degenerate and lose height the nucleus further dehydrates and tears in the NP and the peripheral annulus fibrosus (AF) (Section 4.1.3.2) begin to occur. The NP may begin to eject into the endplate (EP) (Section 4.1.3.3), the alignment of the AF begins to worsen and the disc begins to stiffen (Da Silva Baptista et al. 2015). The disc eventually loses significant height and the differentiation between the NP and the AF becomes almost impossible (Figure 5).

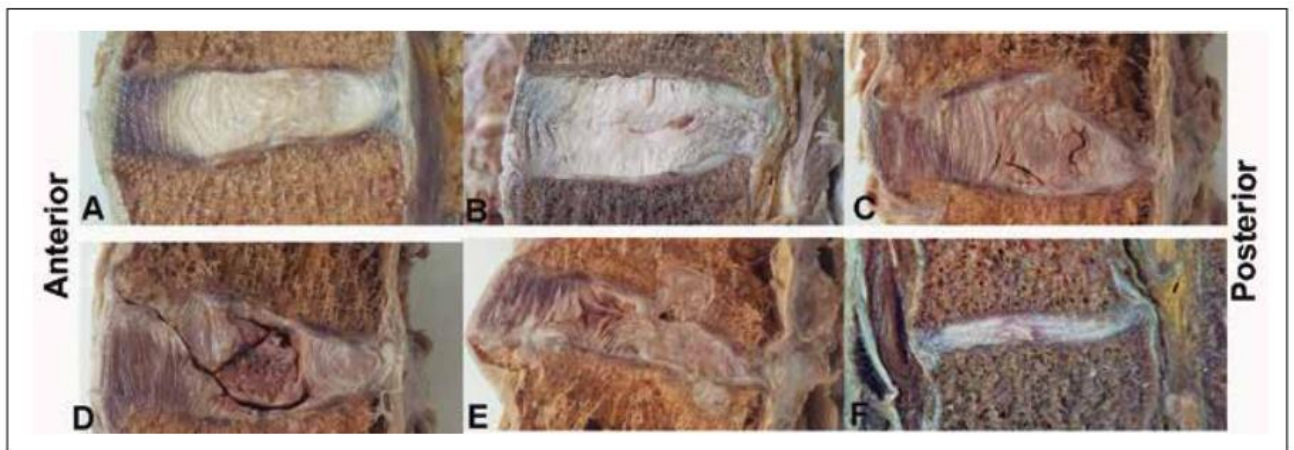


Figure 5: The process of lumbar disc degeneration shown in human lumbar intervertebral discs (Da Silva Baptista et al. 2015). A=a healthy disc with a well hydrated nucleus and well aligned annulus fibrosus. As the degeneration of the disc continues (A to F) tears begin to occur, the annulus begins to lose its highly aligned orientation and lose of disc height becomes more extensive (Da Silva Baptista et al. 2015).

Even though disc delegation appears to be a key indicator of LBP, it does not always correlate with back pain. Herniated discs, which often follow DDD due to fatigue or trauma,

do not always cause symptoms in all individuals (Battie et al. 2014). However, DDD is now the most common diagnosis used to prescribe surgical intervention after alternative non-invasive methods have been exhausted (Battie et al. 2014; Baliga et al. 2015). DDD is most commonly diagnosed from MRI; the recorded signal loss of the NP has also allowed detection of degeneration before evident disc height loss (Frobin et al. 2001).

Chapter 3. Design Process and Problem Definition

3.1 Design Process

It is clear that LBP is a significant problem in today's society and that current treatments (Section 4.15) are not yet perfect. A multi stage design process was employed during the development of a next generation TDR device. The design process followed a structured procedure that was adapted from the Engineering Design Process textbook (Haik & Shahin 2011).

The key steps of the design process are listed below:

1. Problem definition.
2. The development of a set of design requirements.
3. The identification of information that must be obtained via literature review.
4. Updating design requirements based on relevant literature.
5. The development of a series of design specifications derived from literature.
6. The generation of a number of design concepts.
7. Ranking of design concepts.
8. Selection of the final design.
9. Design iteration process.
10. Development of automated CAD design.
11. Development of automated FEA process.
12. Analysis of FEA results.
13. Proof of design concept.
14. Design modification.

3.2 Problem Definition

A solution neutral definition of the underlying problem for the project was defined as: 'the treatment of lower back pain.' This is the key goal of the project to develop a prosthesis that can aid in the treatment of LBP.

The major problem gap that the project is attempting to address, is that no elastomer core TDRs has gained the U.S Food and Drug Association (FDA) approval; which is needed to enter the largest LBP market in the world (Section 2.2). Only three devices (Table 4) have gained the necessary approval however, these were either ball and socket or mobile core TDRs (Section 4.16).

Table 4: Table of FDA approved TDRs.

TDR Prosthesis	Year of Approval	Type of TDR
CHARITE	2004	Mobile Core
Prodisc-L	2006	Ball and Socket
ActivL	2015	Mobile Core

3.3 Design Requirements

A set of design requirements of the final completed design were initially developed via a brainstorming process. These requirements were expanded due to inspiration from the literature review. In particular, the review of different TDRs that are/or have been available on the market to treat LBP and restore spine mechanics, was used to highlight features or characteristics of successful TDR devices (Section 1.1). In addition, the identification of current problems that TDRs face was also investigated for design inspiration (Chapter 1). The final set of design requirements were broken down into three different categories:

3.3.1 Geometric Requirements

- The TDR must be constrained within the lumbar intervertebral disc space (Benzel et al. 2011).
- The TDR must restore sagittal balance (Benzel et al. 2011).
- The TDR must be able to be implanted through a typical TDR surgical approach.

3.3.2 Material Requirements

- The TDR must be made from biocompatible materials that are already used in market approved devices.

3.3.3 Mechanical Requirements

- The TDR strength must significantly exceed maximum physiological loads while also restoring physiological biomechanical properties at active daily living loads (Benzel et al. 2011).
- The TDR must restore a physiological range of motion (RoM).
- The TDR must restore a natural centre of rotation (CoR) to the affects lumbar segment(s)(Benzel et al. 2011).
- The TDR must have a high fatigue life (Benzel et al. 2011).

These design requirements that have been generated are consistent with recommendations from literature with a number of different papers highlighting similar requirements for TDRs (Cunningham 2004; Costi et al. 2011).

3.3.4 Brainstorm Necessary Information for the Design

Upon completion of the design requirement stage, the identification of the necessary additional information needed in order to complete the design of the next generation TDR was accomplished. The main categories of information needed that were covered in the literature review included: information regarding the lumbar anatomy and morphology, the biomechanics of the lumbar spine, and the review and analysis of past and present TDRs.

Chapter 4. Literature Review

4.1 Anatomy

4.1.1 Lumbar Spine

An understanding of the natural lumbar anatomy is key as it plays an important role in the natural biomechanics of the disc and also will provide insight into the geometry of the disc space.

The lumbar region of the spine is situated between the Sacrum and the Thoracic spine (OpenStax College 2013)(Figure 6).

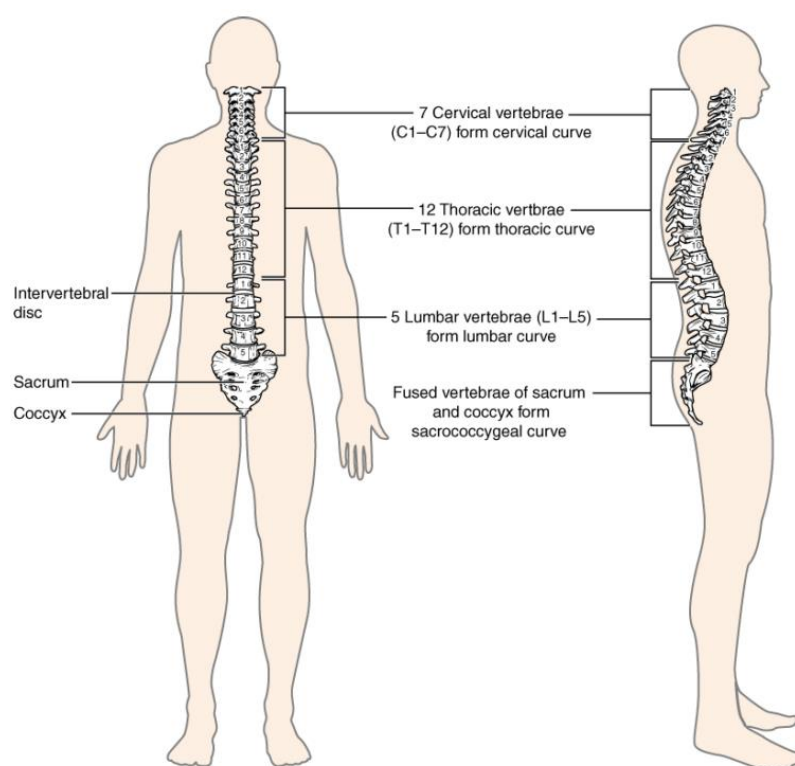


Figure 6: Image of an adult spine, showing the curvature and different regions of the spine (OpenStax College 2013).

The lumbar spine comprises of five vertebrae that share a common basic structure. The most anterior part of the vertebrae is the vertebral body. The vertebral body is responsible for the majority (80%) of the compressive load bearing (Frelinghuysen et al. 2005). A number of different bony processes radiate from the dorsal side of the vertebral body forming the posterior elements.

These processes include the lamina and pedicles that form the vertebral arch that encases the spinal nerves forming the vertebral foramen, the transverse processes, the spinous process that radiates dorsally from the midline of the vertebrae, and the inferior and superior articular processes (Figure 7) that form the facet joints (FJ) and help join adjacent vertebrae (OpenStax College 2013).

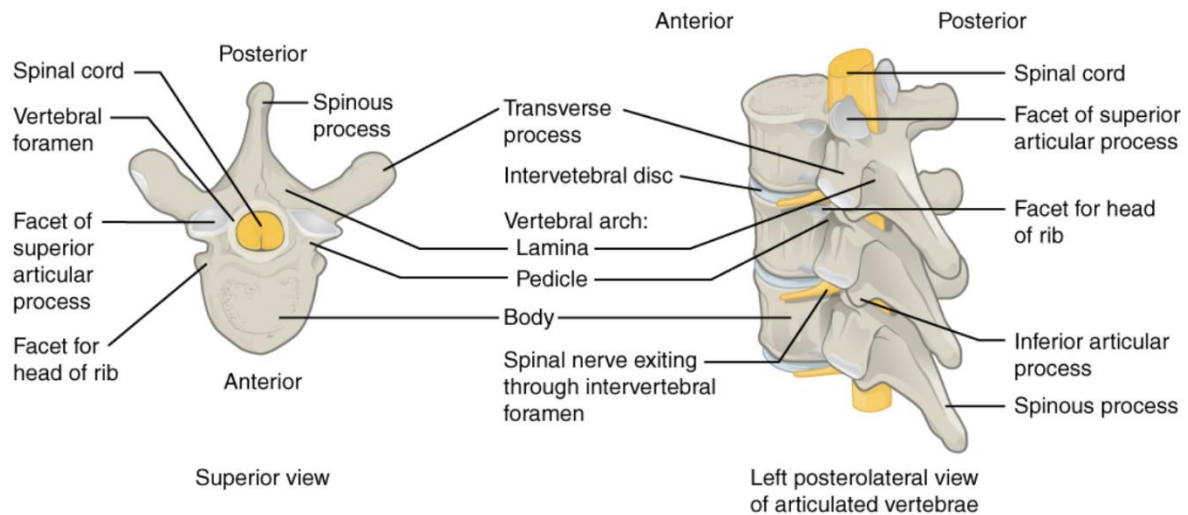


Figure 7: A typical vertebrae, showing the different processes that comprise the posterior elements, the vertebral body, the spinal cord and the facet joints (OpenStax College 2013).

The lumbar vertebrae structure differentiates itself from other regions of the spine due to the larger thick vertebral bodies, short transverse processors and short rounded spinous process(OpenStax College 2013)(Figure 8).

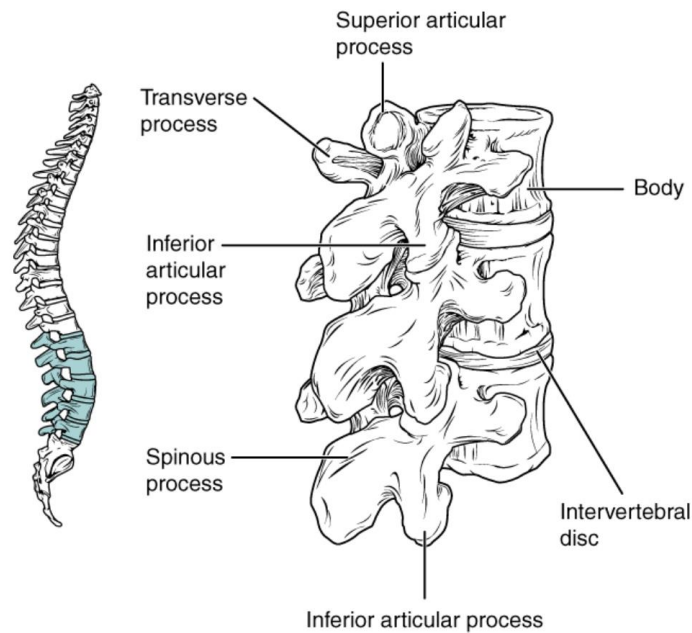


Figure 8: The lumbar vertebrae. Distinctive characteristics include the large thick vertebral body and the short rounded spinous process.

4.1.2 Facet Joints

The two FJs are located on the postero-lateral sides of each adjacent lumbar vertebrae pair (Figure 7)(Jaumard et al. 2011). The joints are also known as the zygapophyseal and are diarthrodial (synovial) in nature (Jaumard et al. 2011). The two articular processes are covered in hyaline cartilage, which is thickest in the centre (approximately 1 mm) and are encased in a synovial capsule allowing for near-frictionless motion (Jaumard & Welch, William C, Winkelstein 2011). Ligaments, muscles and soft tissues also form part of the joint and aid in providing joint stability (Gellhorn et al. 2013).

4.1.3 Intervertebral Disc

The vertebral bodies of adjacent vertebrae are separated by intervertebral discs (disc). There are two distinct regions of a disc; the inner NP and the surrounding AF. The disc is constrained superiorly and inferiorly by the EPs (Whatley & Wen 2012)(Figure 9).

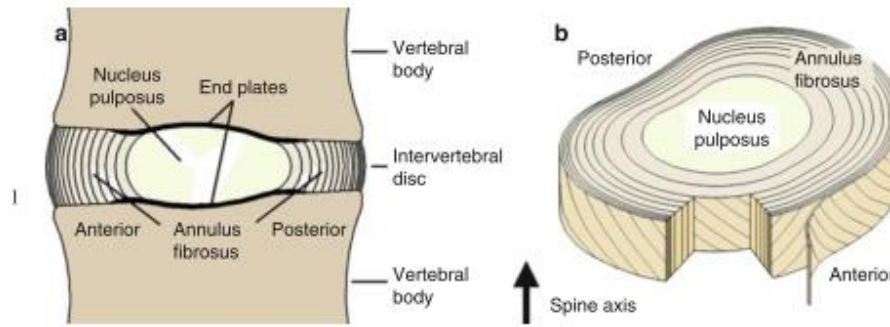


Figure 9: Schematic of the intervertebral disc (Cortes & Elliott 2014).

4.1.3.1 Nucleus Pulposus

The NP is a gel like material that is isotropic in structure and mechanical properties. It comprises of a matrix-like structure of type II collagen fibres, proteoglycans, water molecules and cells (Nerurkar et al. 2010). The PGs are hydrophilic and cause the NP to withhold water which accounts for 70-90% of its contents (Jongeneelen 2006).

4.1.3.2 Annulus Fibrosus

The Annulus Fibrosus is made of fibrocartilage with mainly highly aligned collagen I fibres (50-70% dry weight), PGs (10-20% dry weight), elastin and water (Bron et al. 2009; Whatley & Wen 2012). The fibres are arranged in a minimum of 15 concentric layers posteriorly and a maximum of 25 layers laterally (Bron et al. 2009; Arun et al. 2009; Marchand & Ahmed 1990). Each alternating layer is positioned in the opposite direction with the angle of the fibres reducing from 62° in the periphery of the AF to 45° relative to the transverse plane (Whatley & Wen 2012)(Figure 9). The space between each layer is known as the interlamellar septae and contains a complex structure of linking elements and PG aggregates causing cohesion between the layers (Bron et al. 2009).

4.1.3.3 Vertebral Endplate

The vertebral endplates are the boundaries between the vertebral body and the intervertebral disc. The superior EP has a convex shape and the inferior EP has a concave shape (Figure 10). The hyaline cartilage of the EP integrates with the bone of the vertebral body and helps to provide nutrients to the avascular disc (Wang & Griffith 2011; Fibrosus 2010; Whatley & Wen 2012; Arun et al. 2009). Some fibres from the outer edges of the disc known as Sharpey's fibres penetrate through the EP and infiltrate into the bone of the vertebral body (Bron et al. 2009). Other AF fibres especially those in the centre of the disc integrate into the vertebral endplate or bend around the NP (Bron et al. 2009).

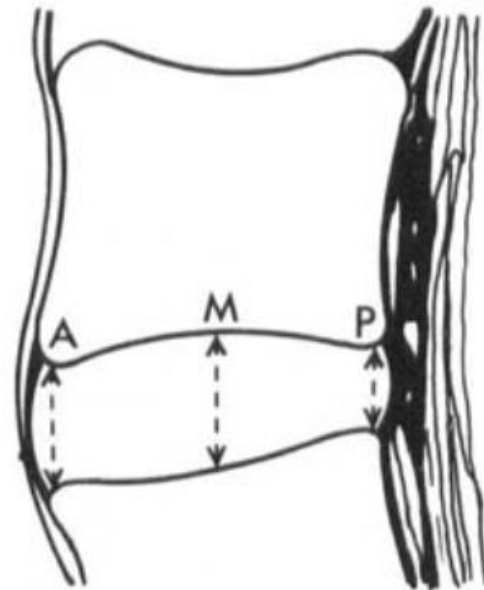


**Figure 1. Intervertebral disc. Convexity index = $M/A + P$.
M = mid-disc height,
A = anterior height,
P = posterior height.**

Figure 10: General sagittal cross sectional shape of the lumbar vertebral bodies and the intervertebral discs. Note the concave shape of the inferior endplate of the superior vertebral body, the convex shape of the superior endplate of the inferior vertebral body, the wedge shape of the intervertebral disc and the greater anterior disc height compared to the posterior height causing the disc to contribute to the lordotic shape of the lower lumbar spine.

4.1.4 Functional Spinal Unit

A functional spinal unit (FSU) or motion segment is the smallest physiological motion unit of the spine. It contains what is known as a ‘three joint complex’ that is comprised of the two adjacent vertebrae and the adjoining articulating FJs and the disc, together with the ligaments surrounding and spanning across each FSU.

4.2 Lumbar Morphology

The lumbar morphology is a critical aspect of the geometric design of the TDR. The height of the vertebral bodies will dictate the limits for potential spike or keel heights for initial TDR stability, the endplate area and shape will limit the size of the TDR endplates and the disc height will dictate the total height of the TDR.

4.2.1 Vertebral Body Height and Bone Density

Vertebral body height measurements investigated from Computer Tomography (CT) images of 126 LBP patients measured the anterior and posterior vertebral body heights (Table 5)(Zhou et al. 2000).

Table 5: Mean and Standard Deviation Vertebral Body Anterior and Posterior Heights (mm)(Zhou et al. 2000).

Mean and Standard Deviation Vertebral Body Heights (mm)					
Anterior Height			Posterior Height		
L3	L4	L5	L3	L4	L5
30.2±2.1	30.1±2.4	30.8±2.5	29.6 ±2.4	28.7±2.3	25.9±2.0

The vertebral body height constrains the height of the spikes and/or keels that are used to gain initial fixation for a TDR into the vertebral bone. The keels and spikes help to prevent shifting in position of the TDRs once they are inserted, and the keels in particular can be used as a guide to insert the TDR once a guide slit has been cut into the vertebrae during surgery. CT analysis of human lumbar vertebral bodies have illustrated that the superior third and the inferior third of the vertebral body have very similar bone mineral density's (BMDs), of approximately 180 mg/cm³. Compared to the central region, which has a lower BMD of approximately 140 mg/cm³ (Briggs et al. 2012).

4.2.2 Endplate Area and Shape

The EP area coverage is an important parameter in the success of TDR devices, and it has been recommended that at least 85% of the EP should be covered by the prosthesis (Gornet et al. 2014). A statistically significant superior outcome at 24 months postoperatively was found in terms of Oswestry Disability Index (ODI) score (Section 4.14.2) when a greater total area of the vertebral EP was covered by the prosthesis (p=0.024) (Figure 11). It was also found that the risk of subsidence (Section 5.6.3) of a TDR was less likely if coverage was greater than 60% and 62% of the vertebral EP at the L4 and L5 level respectively (Punt et al. 2013).

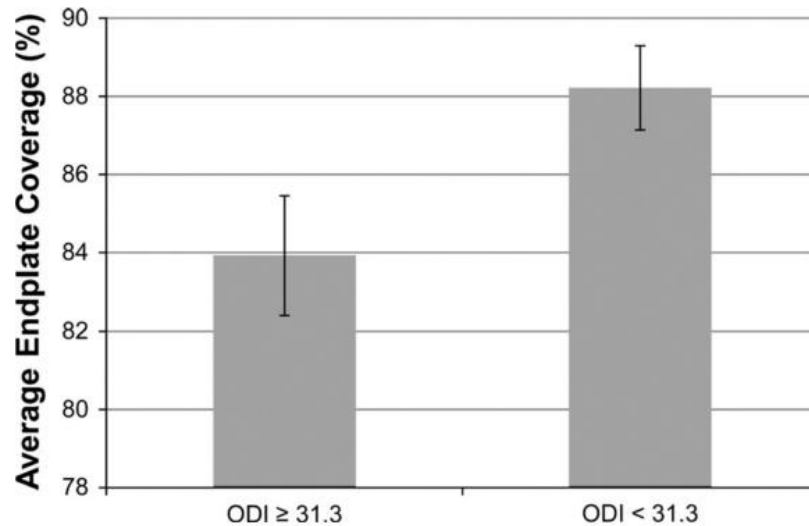


Figure 11: The relationship between 2 years postoperative Oswestry Disability Index (ODI) score and the percentage of total area of the endplate that the prosthesis covers. The error bars indicate the stand error (Gornet et al. 2014).

The vertebral EPs have a cardioid shape (Figure 12 & Figure 13) which becomes more elliptical from the inferior L4 to the superior S1 EP (Hall et al. 1997). The lateral (A) and anterior posterior (B) diameter as well as the shape of lower lumbar EPs from CT images of LBP suffers (Figure 12)(Hall et al. 1997). The investigation illustrated that females have smaller EP areas but have similar shape to males (Hall et al. 1997; Tang et al. 2016; Zhou et al. 2000)(Table 6)(Figure 13).

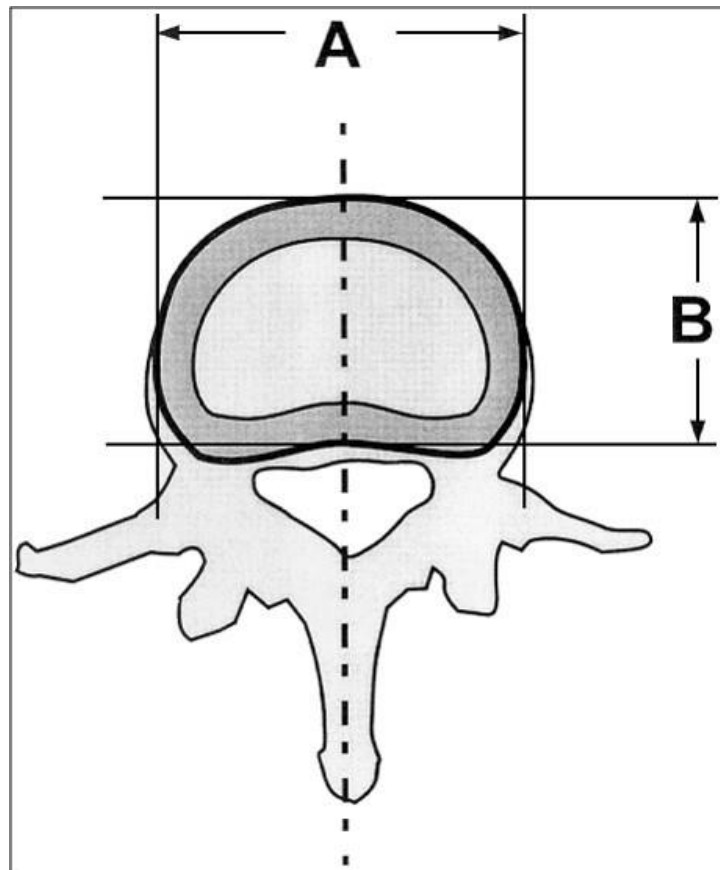


Figure 12: Image depicting the location of the lateral (A) and anterior posterior(B) diameters of the endplates (Hall et al. 1997).

Table 6: Comparing mean and standard deviation of the anterior posterior and lateral dimensions of the vertebral endplates for male and female specimens (Hall et al. 1997) (Zhou et al. 2000).

	Inferior L4	Superior L5	Inferior L5	Superior S1	Reference
<u>Anterior Posterior Diameter (mm)</u>					
Male	37.0 ± 3.4	36.5 ± 3.3	36.0 ± 3.2	34.7 ± 3.2	(Hall et al. 1997)
	38.6 ± 3.4	37.6 ± 3.1	38.3 ± 3.8		(Zhou et al. 2000)
Male Grand Mean	37.8	37.05	37.15	34.7	
Female	32.6 ± 2.0	32.8 ± 2.2	32.6 ± 1.9	30.7 ± 2.1	(Hall et al. 1997)
	34.4 ± 2.8	34.3 ± 3.5	34.3 ± 3.3		(Zhou et al. 2000)
Female Grand Mean	33.5	33.55	33.45	30.7	
Grand Mean Both Sexes	35.65	35.3	35.3	32.7	
<u>Lateral Diameter (mm)</u>					
Male	54.2 ± 3.8	54.1 ± 3.8	53.5 ± 3.7	54.0 ± 3.8	(Hall et al. 1997)
	55.1 ± 4.1	54.4 ± 4.9	56.7 ± 5.3		(Zhou et al. 2000)
Male Grand Mean	54.65	54.25	55.1	54.0	
Female	46.8 ± 2.9	48.7 ± 2.2	48.0 ± 2.9	48.3 ± 2.1	(Hall et al. 1997)
	50.4 ± 4.2	50.4 ± 4.4	50.4 ± 4.9		(Zhou et al. 2000)
Female Grand Mean	48.6	49.55	49.2	48.3	
Grand Mean Both Sexes	51.63	51.9	52.15	51.17	

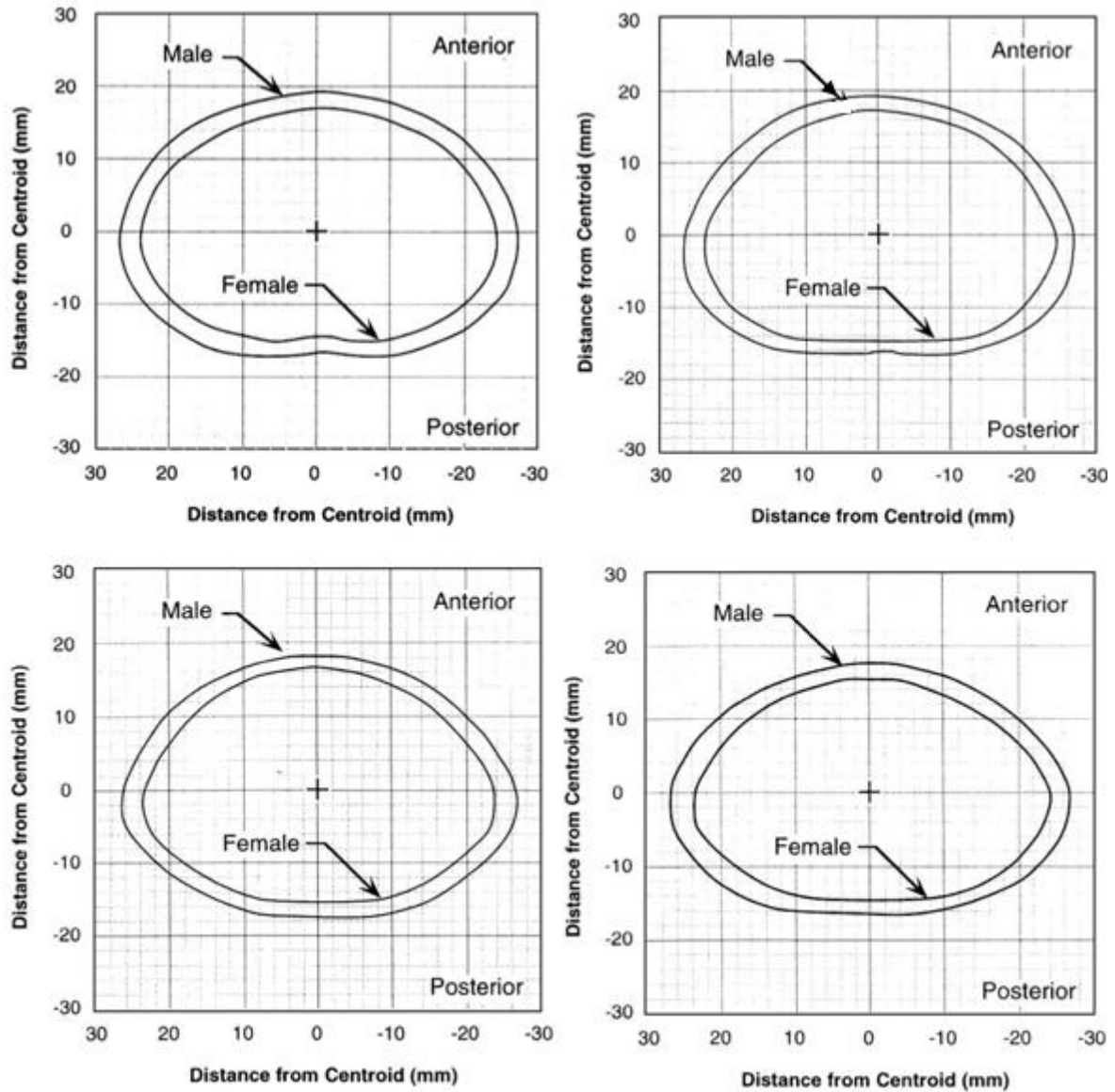


Figure 13: The average shape of male and female endplates of the inferior L4 (top left), superior L5 (top right), inferior L5 (bottom left) and superior S1 (bottom right)(Hall et al. 1997).

The area of the EPs varies depending on lumbar index level (Table 7).

Table 7: Summary of human lumbar endplate areas.

Lumbar Vertebrae	Mean Area (mm ²) and Standard Deviation	Reference
L3-L4 (average of inferior L5 EP and S1 EP)	1385 ± 214	(Tang et al. 2016)
L3 (inferior EP)	1290 ± 64.35	(Panjabi et al. 1992)
	1560 ± 210	(Y. Wang et al. 2012)
L4-L5 (average of L5 lower and S1 upper)	1492 ± 173.8	(Zhou et al. 2000)
	1375 ± 210	(Tang et al. 2016)
L4 (upper)	1239 ± 58.41	(Panjabi et al. 1992)
	1580 ± 240	(Y. Wang et al. 2012)
L4 (lower)	1273 ± 51.72	(Panjabi et al. 1992)
	1670 ± 240	(Y. Wang et al. 2012)
L5-S1 (average of L5 lower and S1 upper)	1308 ± 223	(Tang et al. 2016)
L5 (upper)	1237 ± 58.48	(Panjabi et al. 1992)
	1610 ± 250	(Y. Wang et al. 2012)
L5 (lower)	1218 ± 59.43	(Panjabi et al. 1992)
	1580 ± 300	(Y. Wang et al. 2012)
S1 (upper)	1510 ± 280	(Y. Wang et al. 2012)

An investigation into the possibility of 3D printing the EPs of TDRs to identify the effect of having a conforming shape compared to a flat EP, revealed that the more area of the EP that the implant covers the higher the maximum failure load in compression ($p < 0.0001$) (Beer & Merwe 2013). This concept was also utilised by the design team of the FlexiCore TDR (Valdevit & Errico 2004). The study unfortunately only tested the L2/L3 lumbar levels, however the resulting increase in stiffness and failure load due to the increase in contact area was encouraging and supports that a design should attempt to cover as most of the EP as possible. This increasing in stiffness and strength of the EP-implant interface has also been indicated to reduce the chance of subsidence of the implant (Section 5.6.3) (Beer & Merwe 2013).

4.2.3 Facet Joints

The restoration of the FJ orientation is also a key parameter in the success of TDR due to the facets role in both the natural kinematics and biomechanics of the FSU (Jaumard et al. 2011). The clinical success of TDR have also been linked to FJ orientation due to the development of LBP if correct facet alignment is not achieved (Shin et al. 2013).

4.2.3.1 Angle of Facet Joints

The orientation of the articulating surfaces of the lumbar FJ vary greatly for different levels of the spine. Two different angles are used to define the FJ articulation angles. The first is taken in the transverse plane and gives the angle relative to the sagittal plane (angle α in Figure 14A). The other is taken in the sagittal plane relative to the transverse plane (angle β in Figure 14B).

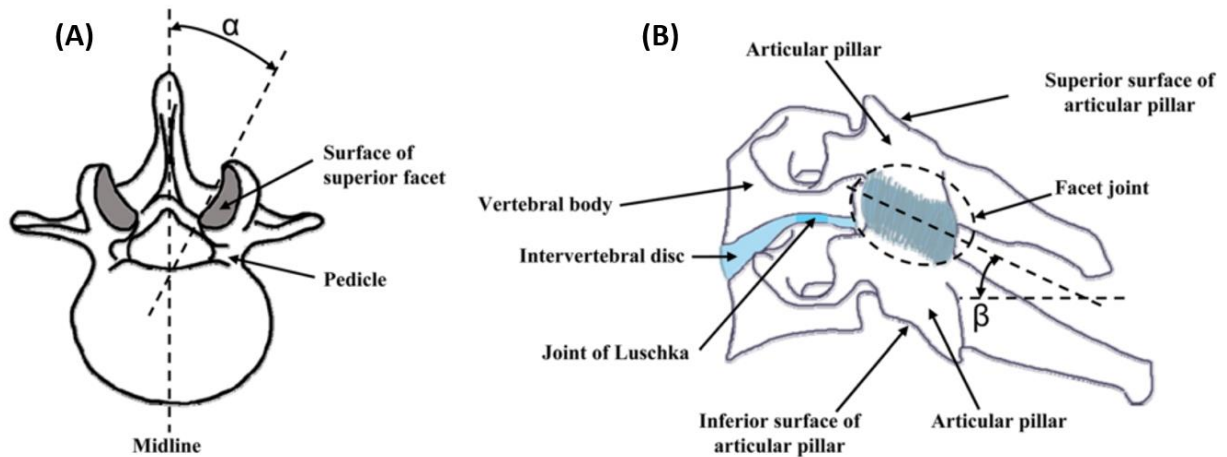


Figure 14: Angles of the facet joints (Jaumard & Welch, William C, Winkelstein 2011).

The angles corresponding to the angle ‘ α ’ in Figure 14A have been summarised in Table 8.

Table 8: Angles of the lumbar facet joints taken in the transverse plane relative to the sagittal plane (α angle of Figure 14A).

Lumbar Level	Mean Angle (°)	Lower Range (°)	Upper Range (°)	Reference
L1-L2	25	15	47	(Pilitsis et al. 2007)
L2-L3	28	17	51	(Pilitsis et al. 2007)
L3-L4	37	15	57	(Pilitsis et al. 2007)
	39.6	17.6	57	(Noren et al. 1991)
	37.1	17	57	(Van Schaik, Jan, Verbiest, Henk, Van Schaik 1984)
L4-L5	48	13	70	(Pilitsis et al. 2007)
	48.4	30	64.5	(Noren et al. 1991)
	48.2	29.5	75	(Van Schaik, Jan, Verbiest, Henk, Van Schaik 1984)
	43	10	70	(Farfan 1973)
L5-S1	53	36	70	(Pilitsis et al. 2007)
	53.9	29	77.5	(Noren et al. 1991)
	53.1	36	70	(Van Schaik, Jan, Verbiest, Henk, Van Schaik 1984)
	52	20	90	(Farfan 1973)

These angles are in general agreement to range of 15 to 70° proposed by other studies (Jaumard et al. 2011).

Three dimensional qualitative measurements from CT images of 12 complete spines (C2 to L5), revealed a number of different morphological parameters of the FJs including the angle of the FJs in relation to the transverse plane which correspond to the β angle in Figure 14B (Panjabi et al. 1993)(Table 9).

Table 9: Summary of the transverse plane angles measured by Panjabi (Panjabi et al. 1993).

Transverse Plane Angles								
Superior Articular Facet Orientation (°)					Inferior Articular Facet Orientation (°)			
	Right		Left		Right		Left	
	Mean	SD	Mean	SD	Mean	SD	Mean	SD
L1	82.9	1.4	81.3	2.7	81.4	1.6	81.8	1.9
L2	85.7	0.9	83.8	1.3	82.8	2.5	78.7	4.0
L3	81.9	1.6	84.1	1.5	75.6	4.1	77.8	3.3
L4	81.2	1.6	81.3	2.5	70.5	6.7	80.3	1.2
L5	86	1	85.1	1.2	71	3.7	81.6	1.2

Again, these measurements are in agreement to the range of β angles (82° to 86°) given for the FJs orientation by other studies (Jaumard et al. 2011).

4.2.3.2 Facet Joint Linear Dimensions

A number of other dimensions of the FJs can be measured (Figure 15)(Table 10-Table 14)(Panjabi et al. 1993).

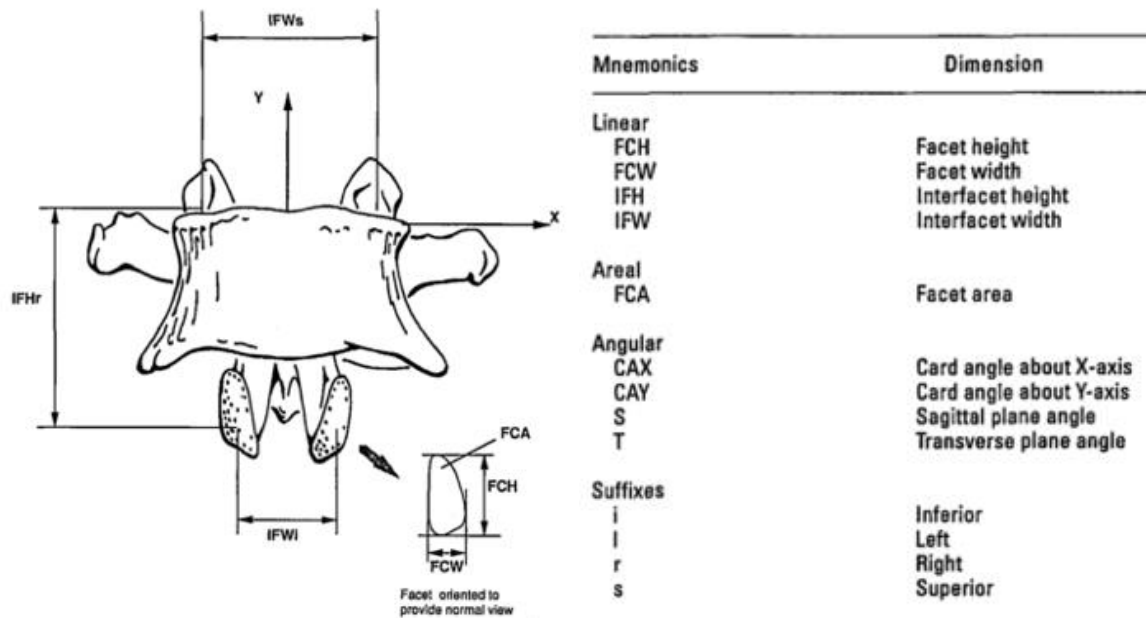


Figure 15: Diagram depicting the different measurements taken by Panjabi (left) and the legend of measurement acronyms (right) (Panjabi et al. 1993).

Table 10: The mean and (standard error of the mean) of the superior articular facet linear dimensions (mm). FCW_{sr} = superior right facet width, FCW_{sl} = superior left facet width, FCH_{sr} = superior right Facet Height, FCH_{sl} = Superior left Facet Height. See Figure 15 for measurement locations(Panjabi et al. 1993).

Vertebra	FCW _{sr}	FCW _{sl}	FCH _{sr}	FCH _{sl}
L1	10.2 (0.6)	10.5 (0.6)	12.7 (0.3)	12.2 (0.7)
L2	11.1 (0.7)	11.4 (1.0)	14.6 (0.6)	14.6 (0.7)
L3	13.8 (0.9)	13.9 (0.7)	16.0 (0.8)	15.9 (0.8)
L4	14.1 (1.0)	15.3 (0.6)	16.1 (0.5)	17.3 (0.7)
L5	16.3 (0.7)	14.9 (0.6)	17.4 (0.7)	17.5 (0.7)

Table 11: The mean and (standard error of the mean) of the inferior articular facet linear dimensions (mm). FCWir = inferior right facet width, FCWil = inferior left facet width, FCHir = inferior right facet height, FCHil = inferior left facet height. See Figure 15 for measurement locations (Panjabi et al. 1993).

Vertebra	FCWir	FCWil	FCHir	FCHil
L1	12.4 (0.7)	10.7 (0.5)	15.3 (0.7)	15.7 (0.6)
L2	12.7 (0.7)	12.7 (0.8)	16.0 (0.6)	16.3 (0.6)
L3	13.8 (0.4)	13.4 (0.4)	15.7 (0.3)	16.4 (0.5)
L4	14.7 (0.5)	14.1 (0.6)	16.2 (0.7)	15.6 (0.7)
L5	15.6 (0.9)	16.1 (0.9)	18.4 (1.0)	17.3 (1.0)

Table 12: The mean and (standard error of the mean) of the interfacet Distances (mm). IFWs=superior interfacet Width, IFWi=inferior interfacet width, IFHr=right interfacet height, IFHl=left interfacet Height. See Figure 15 for measurement locations (Panjabi et al. 1993).

Vertebra	IFW _s	IFW _i	IFH _r	IFH _l
L1	26.2 (0.6)	24.8 (0.8)	32.5 (0.5)	31.8 (1.0)
L2	26.4 (0.9)	26.6 (0.9)	33.0 (0.7)	32.4 (0.6)
L3	28.6 (1.0)	29.1 (1.5)	32.4 (0.9)	31.6 (0.7)
L4	31.4 (1.6)	34.8 (1.7)	28.5 (1.0)	28.3 (1.3)
L5	35.0 (2.1)	40.6 (2.0)	26.1 (1.8)	26.4 (1.5)

Table 13: The mean and (standard error of the mean) of the superior articular facet surface areas (mm²). FCA_{sr}=superior right facet surface area, FCA_{sl}=superior left facet surface area, FCA_{ir}=inferior right facet surface area, FCA_{il}=inferior left facet surface area. See Figure 15 for measurement locations (Panjabi et al. 1993).

Vertebra	FCA _{sr}	FCA _{sl}	FCA _{ir}	FCA _{il}
L1	96.7 (6.2)	99.2 (11.4)	127.9 (7.5)	125.9 (6.9)
L2	138.0 (11.4)	148.2 (12.8)	150.9 (9.8)	153.6 (10.1)
L3	170.3 (13.1)	164.4 (12.0)	159.8 (4.8)	167.9 (9.7)
L4	175.0 (7.0)	194.3 (11.0)	182.1 (15.6)	167.9 (11.8)
L5	211.9 (14.0)	199.1 (12.0)	197.3 (21.8)	182.7 (17.2)

4.2.4 Facet Joint Area

The mean and standard deviation of articulation overlap of the FJs in the sagittal plane from CT images of the 10 lumbar spine segments revealed that the level of overlap increases and the lumbar spinal index decreases (Table 14) (Liu et al. 2006).

Table 14: The mean and standard deviation (SD) of the facet joint articulation overlap measured from sagittal CT images (Liu et al. 2006).

Spine Level	Left		Right	
	Mean (mm)	SD (mm)	Mean (mm)	SD (mm)
L3-L4	16.29	1.2	16.22	1.16
L4-L5	17.81	1.18	17.74	1.18
L5-S1	18.18	1.18	18.23	1.15

4.3 Lordosis Angle

Lordosis is the inward curvature of the spine (i.e. concave anteriorly) found in the cervical and lumbar regions during normal standing. The lordosis angle varies greatly between individuals and many factors have been investigated to identify their influence (Been & Kalichman 2014; Damasceno et al. 2006; Dreischarf et al. 2014). Lordosis is contributed by the intervertebral disc and the lumbar vertebrae (Been & Kalichman 2014); with majority of the lumbar lordosis being produced by the final two segments (L4-L5, L5-S1)(Been et al. 2010; Been & Kalichman 2014; Damasceno et al. 2006). Lumbar lordosis along with sacral and pelvic tilt play a critical role in sagittal balance, which when restored has been associated with the success of TDR clinical trials (Adams et al. 2013; Gornet et al. 2014; Tsitsopoulos et al. 2012; Le Huec et al. 2005).

The local segmented lordosis at the implanted level following TDR is often increased (Cakir et al. 2005; Le Huec et al. 2005). Increases and preservation in overall global lordosis (Tournier et al. 2007; Gornet et al. 2014; Cakir et al. 2005; Le Huec et al. 2005) have also been discovered. The increase in segmental lordosis but the retention of global lordosis while using a Prodisc-L device showed no influence on short-term (12 to 35 months post op) clinical outcome even though the lordosis of adjacent segments was decreased (Cakir et al. 2005).

Lumbar lordosis after TDR and its correlation to clinical outcome are not yet confirmed (Lu et al. 2015; Been & Kalichman 2014). However as previously mentioned normal physiological lordosis has been shown to be restored or preserved following TDR implantation (Lu et al. 2015; Le Huec et al. 2005). This potential clinical improvement maybe due to the fact that both hyper and hypo lumbar lordosis have been linked to LBP (Cakir et al. 2005; Garges et al. 2008a; Lu et al. 2015). It is hypothesised that this rebuilding of lordosis maybe due to the restoration of disc height after a TDR as well as the reinstatement of normal spinal biomechanics (Lu et al. 2015). This makes some intuitive

sense since the lordotic curvature helps to balance compressive forces (Evcik & Yücel 2003) and makes it easier to maintain balance by distributing the body's mass away from the central axis of rotation of the spine, by increasing the moment of inertia about this axis (Adams et al. 2013).

Sacral tilt and lumbar lordosis have been shown to be significantly correlated (Le Huec et al. 2005). A comparison of fusion patients with and without pain postoperatively revealed that pelvic tilt was significantly higher and sacral tilt was significantly lower in patients with pain (Le Huec et al. 2005; Lazennec et al. 2000). These clinical findings maybe be translatable to TDR to highlight the importance of restoring sagittal balance of which lumbar lordosis is a contributor.

The Cobb method or a modified Cobb method is the gold standard for measuring lumbar lordosis from radiographs (Figure 16)(Been & Kalichman 2014; Vrtovec et al. 2009). A summary of different lordosis angles that have been measured using the Cobb method in healthy individuals can be seen in Table 15.

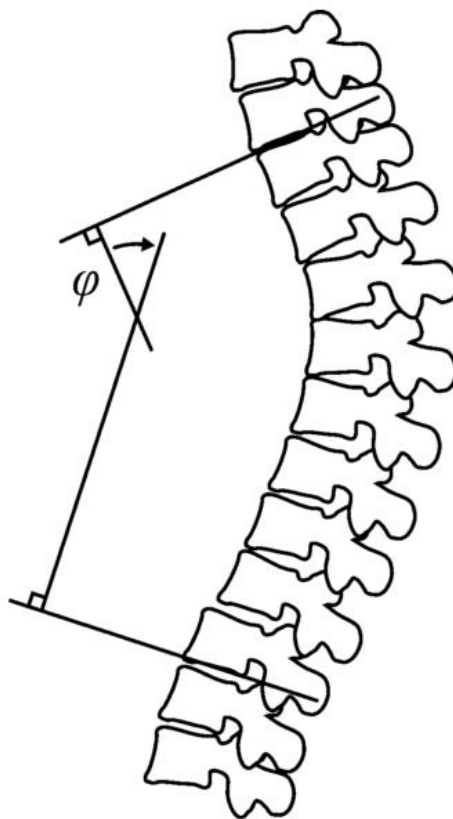


Figure 16: Cobb method of measuring spinal curvature (Vrtovec et al. 2009).

4.4 Lordosis Angle in Healthy Individuals

Table 15: Overall lumbar lordosis measurements from multiple sources.

Lumbar Segment Range	Mean Angle (°)	Standard Deviation	Range (°) (min to max)	Reference
L1-S1 (superior L1 endplate to S1 superior endplate)	60.9	10.65	33 to 89	(Damasceno et al. 2006)
	60.2	10.3	30 to 89	(Vialle et al. 2005)
	60.9	12	31 to 88	(Jackson & McManus 1994)
	53.7	11.7	-	(Cakir et al. 2005)
	74	7	-	(Pearcy et al. 1984)
L1-L5 (superior L1 endplate to S1 superior endplate)	45.1	10.8	15 to 78	(Damasceno et al. 2006)

L1-L5 ($p=0.003$) and L1-S1 ($p=0.019$) lumbar lordosis has also been shown to be similar for males and females, with females having slightly greater lordosis angles (Table 16)(Damasceno et al. 2006; Been & Kalichman 2014).

Table 16: Table comparing female and male lumbar lordosis.

Lumbar Segment Range	Gender	Mean Angle (°)	Standard Deviation	Range (°) (min to max)	Reference
L1-S1 (superior L1 endplate to S1 superior endplate)	Female	62.01	10.46	33.0 to 88	(Damasceno et al. 2006)
	Female	62	10	-	(Vialle et al. 2005)
	Male	59.3	10.46	33 to 89	(Damasceno et al. 2006)
	Male	59.2	10.12	-	(Vialle et al. 2005)
L1-L5 (superior L1 endplate to L5 superior endplate)	Female	46.53	10.61	20 to 77	(Damasceno et al. 2006)
	Female	46.2	11	-	(Vialle et al. 2005)
	Male	43.02	10.77	15 to 78	(Damasceno et al. 2006)
	Male	41.4	11		(Vialle et al. 2005)

4.5 Intervertebral Disc Angle

The lumbar disc has a wedge-like shape that contributes to lumbar lordosis. This angle is due to the anterior height of the disc being larger than the posterior height (Figure 10). The discs in the lumbar spine do not all have the same wedge angle and therefore different discs have a different influence on the overall lumbar curvature (Table 17). The L4-L5 and L5-S1 have the strongest influence on the overall curvature of the lumbar spine and therefore restoration of this angle is an important design (Damasceno et al. 2006; Gornet et al. 2014).

Table 17: Summary of different Intervertebral disc angles.

Lumbar Disc	Mean Angle (°)	Standard Deviation	Range (°) (min to max)	Reference
L3-L4	9.25	2.54	2 to 20	(Damasceno et al. 2006)
	9	3.2	-	(Been et al. 2010)
Grand Mean	9.125			
L4-L5	12.29	3.39	2 to 26	(Damasceno et al. 2006)
	11.2	3.5		(Been et al. 2010)
Grand Mean	11.745			
L5-S1	15.58	5.43	4 to 35	(Damasceno et al. 2006)
	11.7	3.5		(Been et al. 2010)
Grand Mean	13.64			

4.6 Segmental Lordosis

The segmental lordosis; the angle from the superior EP of one vertebrae to the inferior EP of the adjacent vertebrae is an important parameter in order to evaluate if a potential prosthesis is able to restore segmental balance and for fitting purposes (Figure 17)(Table 18).

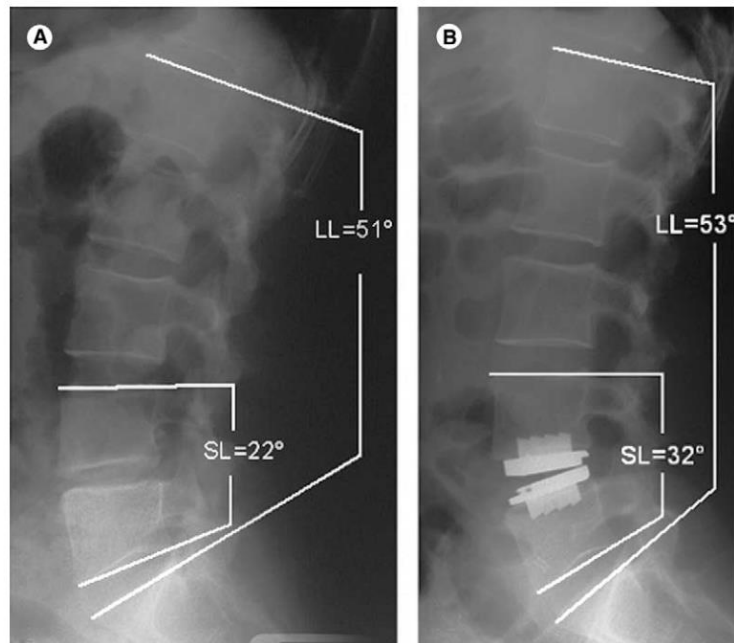


Figure 17: X- ray lumbar lordosis (LL) and segmental lordosis (SL) angle measurements for an intact spine (left) and implanted with TDR spine (right)(Cakir et al. 2005).

Table 18: Summary of segmental lumbar lordosis angles.

Lumbar Segment	Mean Angle (°)	Standard Deviation	Reference
L1-L2	2.5	3.5	(Been et al. 2010)
	2.8		(Damasceno et al. 2006)
	2	5	(Pearcy et al. 1984)
Grand Mean	2.43		
L2-L3	6.1	3.0	(Been et al. 2010)
	7.2		(Damasceno et al. 2006)
	7	4	(Pearcy et al. 1984)
Grand Mean	6.76		
L3-L4	8.8	3.5	(Been et al. 2010)
	10.8		(Damasceno et al. 2006)
	11	3	(Pearcy et al. 1984)
	10.2		
L4-L5	13.6	4.1	(Been et al. 2010)
	15.2		(Damasceno et al. 2006)
	17	5	(Pearcy et al. 1984)
Grand Mean	15.26		
L5-S1	19.8	4.9	(Been et al. 2010)
	24.8		(Damasceno et al. 2006)
	38	6	(Pearcy et al. 1984)
Grand Mean	27.53		

4.7 Disc Height

Restoration of disc height; to physiological levels (Table 19), following TDR is also an important parameter in the success of the treatment. A study investigating a single cohort of 99 patients implanted with the Maverick TDR found that the outcome is superior if the disc height after TDR implantation is less than 8 mm (Gornet et al. 2014).

Table 19: Different lumbar disc heights from the literature.

Lumbar Section	Mean and standard deviation lumbar disc height (mm)	Reference
L3-L4	9.71 ± 0.65	(Neubert et al. 2014)
	9.64	(Hong et al. 2010)
	11.6 ± 1.8	(Zhou et al. 2000)
L4-L5	10.89 ± 1.12	(Brinckmann & Grootenboer 1991)
	10.32 ± 1.16	(Neubert et al. 2014)
	10.05	(Hong et al. 2010)
	11.3 ± 2.1	(Zhou et al. 2000)
L5-S1	9.58	(Hong et al. 2010)
	10.7 ± 2.1	(Zhou et al. 2000)
Grand Mean of L4-L5 and L5-S1	10.47	
Lumbar discs in general	9 to 17	(Cortes & Elliott 2014)
	5 to 10	(Adams et al. 2013)
	11	(Zhou et al. 2000)

A different study investigating varying heights of Prodisc-L using either the 10 mm or 14 mm height prosthesis also suggested that disc height should be kept to a minimum to optimise range of motion and improve sagittal balance (Gaffey et al. 2010). The study measured the influence on the range of motion, segmental lordosis and neural foramen size in a cadaveric model with seven L1-S1 spines (Figure 7)(Table 20). The TDRs were implanted at the L4-L5 and tested at 8Nm in flexion and -6 Nm in extension with a 400 N follower preload. They were also tested without a follower preload at ±6 Nm and ±5 Nm in lateral bending and axial rotation respectively (Gaffey et al. 2010). All three available Prodisc-L heights were used (10, 12 and 14 mm see Section 5.5)).

Table 20: The different RoMs, segmental lordosis and neural foramen size of the lumbar spine for different TDR heights (Gaffey et al. 2010).

	Flexion/Extension	Lateral Bending	Axial Rotation	Segmental Lordosis	Neural foraminal size (mm)
Intact	8.1 ± 2.3°	8.0 ± 2.3°	4.0 ± 2.6°	-	8.9 ± 0.87
10 mm	9.2 ± 1.9°	5.7 ± 2.8°	3.9 ± 1.9°	9.7 ± 2.9°	9.4 ± 1.3
12 mm	7.7 ± 2.0°	4.6 ± 2.6°	3.2 ± 2.0°	14.0 ± 4.6°	9.7 ± 1.3
14 mm	5.8 ± 2.4°	3.6 ± 1.7°	3.0 ± 2.2°	16.1 ± 5.1°	9.9 ± 1.4

Flexion/extension and lateral bending decreased significantly with increasing height ($p < 0.05$) when comparing the 10 mm to 12 mm and 12 mm to 14 mm heights (Gaffey et al. 2010).

Axial rotation also decreased with increasing TDR height however this was only significant when increasing from 10 mm to 12 mm TDR heights. Increasing implant height also caused significant ($p < 0.05$) increases in both segmental lordosis and neural foraminal size for all of the three comparisons (Gaffey et al. 2010).

4.8 Lateral Annulus Fibrosis Thickness

The lateral AF is left intact when TDRs are implanted. Therefore, the thickness of the lateral AF should be taken into consideration in designing the lateral width of a TDR. The lateral width of the disc and the NP have been found to be 55.38 and 36.54 mm respectively (Showalter et al. 2012). The corresponding lateral AF thickness can be calculated to be approximately 18.84 mm.

4.9 Biomechanical Behaviour of the Lumbar Spine

Both the vertebrae and the intervertebral disc of the spine are viscoelastic. A material is defined as viscoelastic if it displays mechanical behaviour that is typical to both viscous and solid materials and thus demonstrates strain-rate and time dependent behaviour. This results in changes to the mechanical behaviour depending on the rate of loading (Cortes & Elliott 2014).

This viscoelastic behaviour can be displayed in both creep and stress relaxation (Figure 18). Creep is defined as change in displacement (strain) over time under the application of a constant force (stress). Stress relaxation is defined as the change in force (stress) over time under the application of a constant displacement (strain).

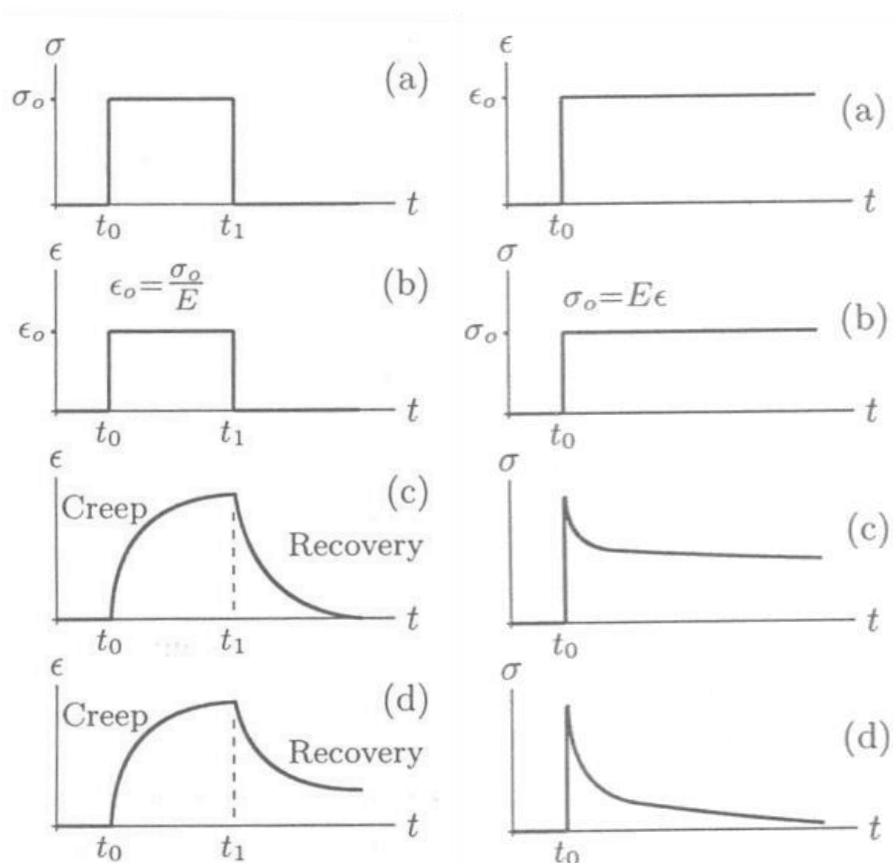


Figure 18: The creep test input (constant stress (σ) over a time period (t)) (left (a)) and stress relaxation input (constant strain (ϵ) over a time period (t)) (right (a)). The different creep (left) and stress relaxation (right) responses of different types of materials (elastic=b, viscoelastic solid=c and viscoelastic fluid =d).

4.9.1 Biomechanics of Lumbar Functional Spinal Units

Both the biomechanics of the lumbar FSU and the lumbar discs are important in the design of a TDR. The restored FSU should hopefully re-establish some or all of the natural biomechanics to the treated level and the whole lumbar spine (to prevent future damage). This biomechanical behaviour will help to form specifications for the mechanical behaviour of the disc.

The intervertebral disc is heterogeneous and exhibits non-linear strain rate dependent anisotropic viscoelastic mechanical behaviour that differs based on the direction of displacement in all six degrees of freedom (6 DOF)(Costi et al. 2011). The disc can be tested in six primary modes of loading: compression, axial rotation, lateral bending, flexion/extension, anteroposterior shear and lateral shear or a combination of these (Figure 19).

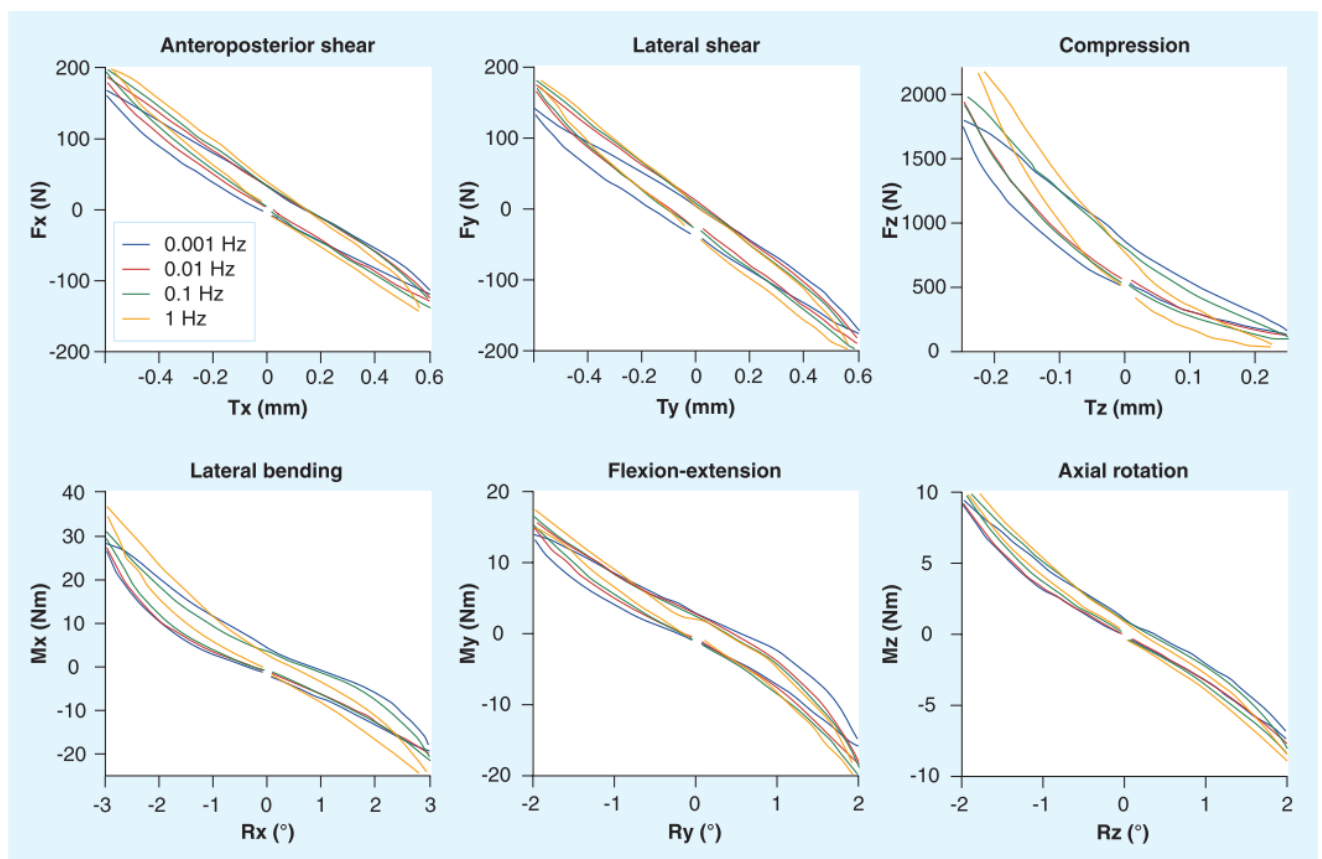


Figure 19: The six degree of freedom mechanical behaviour of human intervertebral lumbar disc motion segments (without FJs) when loaded at different strain rates. This illustrates the

non-linear, strain rate dependent, viscoelastic and anisotropic behaviour of the disc (Costi et al. 2011).

Figure 19 also illustrates the disc hysteresis characteristics when it is non-destructively deformed. The area between loading (top curve) and the unloading (bottom curve) represents the amount of strain energy that the disc absorbs and dissipates in the form of heat (Adams et al. 2013).

4.9.2 Compression

The NP has predominately biphasic (solid and fluid phase) strain rate dependent biomechanical properties, but also comprises of chemical and electrical phases. These properties are strongly influenced by the interactions between water and the hydrophilic glycosaminoglycan chains of the PGs (fluid phase) and the collagen matrix of the NP and AF (solid phase).

Swelling and shrinking of the NP and AF occurs on a diurnal cycle due to the transportation of water molecules in and out of disc (van den Broek et al. 2012). When subjected to stresses that cause volume deformation, such as compression, the PGs generate drag forces that resist the flow of water out of the NP (Costi et al. 2011). Under high strain rate compressive loading, there is inadequate time for the fluid phase of the NP to exit, resulting in the fluid phase bearing the majority of the load. Lower strain rates allow more of the fluid phase to exit the matrix causing the solid matrix phase to carry a greater majority of the load.

Compression loading also causes an increase in hydrostatic and osmotic pressures that causes the AF to budge radially outwards (Cortes & Elliott 2014). This results in tensile hoop stresses being applied to the AF (Schroeder et al. 2006). The orientation of the collagen fibres is important in the AF's ability to withstand the tensile loads. The AF is subjected to tensile forces when the disc is loaded under compressive, shear, tensile, bending, and axial torsion loads (Figure 20).

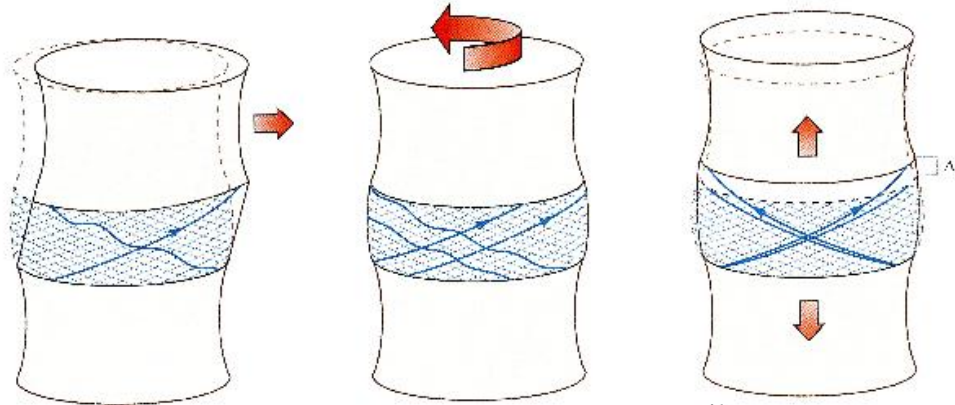


Figure 20: Annulus fibrosis fibres under tensile loads when the disc is exposed to shear (left) axial torsion (centre) and axial tensile (right) loading (Bogduk 1997).

Collagen type I fibres are dominant in the outer AF, as the fibres are straightened they initially apply extremely low, negligible resistance to the loading (Cortes & Elliott 2014). They begin to unravel and recruitment of nearby fibres occurs. As the amount of strain increases, more and more fibres are recruited and a greater majority of the collagen fibres are uncrimped and straightened (Costi et al. 2011). This increases stiffness of the AF in a non-linear response to increasing strain (Figure 21)(Cortes & Elliott 2014).

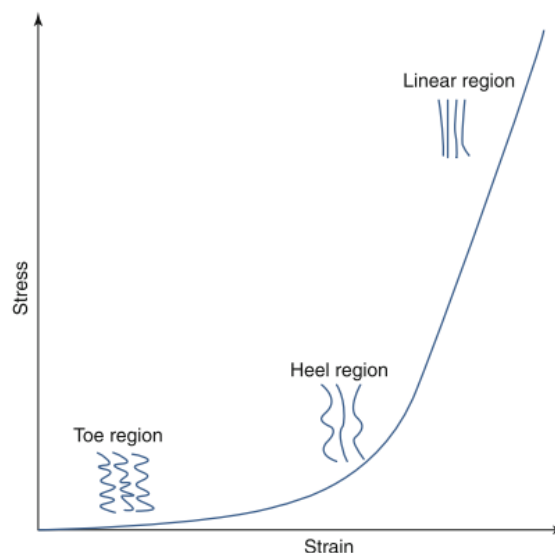


Figure 21: The different regions of the tensile stress strain response of the Annulus Fibrosis fibres.

During compressive loading, the disc does not fail, with failure occurring in the vertebral body or EP (M Adams, McNally, et al. 1994). The amount of load needed to fail lumbar FSUs in compression varies in average individuals from 2 to 14kN (Brinckmann et al. 1989;

Adams et al. 2013; Granhed et al. 1987). This variance is based on a number of factors including sex, age, body weight and bone mineral density (BMD)(Adams et al. 2013). It has been suggested that the compressive strength of the lumbar spine can be predicted through a relationship between EP area and vertebral body bone density acquired through a quantitative CT scan (Brinckmann et al. 1989; Granhed et al. 1987). This relationship suggests that an athlete's lumbar spine may be able to withstand upwards of 20kN of compressive loading (Adams et al. 2013; Granhed et al. 1987). The amount of compressive strength also increases from the superior to inferior lumbar spine by approximately 0.3kN per lumbar segment (Adams et al. 2013).

4.9.3 Torsion

Torsion has been identified as the main cause of injury in the spine, in particular when it is combined with compression (Garges et al. 2008b). During low levels of torque there is little resistance from the FSU as the FJs are either not compressed or the pedicles undergo passive bending (Adams & Hutton 1981). This results in the disc resisting the majority of the loading while the AF collagen fibres are often only in the toe to heel region (Figure 21)(Adams et al. 2013). As the amount of torque and the resulting rotation increases to approximately 1-2° (the approximate range of motion for axial rotation of the lumbar spine (Section 4.12)), compressive yielding of the FJ can begin to occur (Adams & Hutton 1981). The range of motion of the disc in torsion before failure is much higher when the FJs are removed (Adams et al. 2013). The failure load of FSUs with the FJs removed is between 10 to 31Nm (Adams et al. 2013).

4.9.4 Shear

Shear forces are greatest in the lower lumbar region due to the greater inclination of the disc (Adams et al. 2013)(Table 17). The anteroposterior shear typically occurs in-vivo while coupled with flexion/extension bending (Lu et al. 2005). In vivo shear forces in the lumbar spine often fall within the range of 400 to 800 N (Lu et al. 2005), however spinal muscles are responsible for carrying the majority of this load. In terms of the FSU, the disc is not well suited to resist shear loads which results in the FJs bearing the majority of the loading (Section 4.10.1) (Adams et al. 2013). The ultimate shear strength of the FSU in pure shear has been reported to be between 0.6 to 3.2 kN (Gallagher & Marras 2012; Adams et al. 2013) and between 1100 to 2760 N when coupled with flexion (Lu et al. 2005).

The isolated disc has also been tested in shear. These findings illustrate the importance of the FJs in this mode of loading due to the significantly lower reported failure loads of 0.5 kN for the disc compared to the much higher intact FSU failure loads (Adams et al. 2013).

4.9.5 Flexion/Extension

The FSU initially offers little resistance to flexion (known as the neutral zone) which occurs in-vivo coupled with compression and shear (Adams & Dolan 1991; Adams et al. 2013). As the FSU continues to flex, the disc begins to resist the majority of the bending for approximately the final half of the FSU's range of motion (Adams et al. 2013). During this period of bending the outer posterior AF is under tension and the anterior disc is compressed causing bulging (approximately 0.1 mm per degree of flexion) (Adams et al. 2013). This tension also prevents the migration of the nucleus that is pushed away from the compressed anterior vertebral space during flexion or the vice versa during extension (Valdevit & Errico 2004). The final stages of flexion cause a shift from the disc to the FJs in terms of resisting the loading (Section 4.10.3). The lumbar spine is often injured in flexion at bending moments ranging from 50 to 80 Nm (Adams et al. 2013; Green et al. 1994; Michael Adams, Green, et al. 1994). The disc fails at an average of 33 ± 12.8 Nm which is much lower than the average lumbar FSU at 72.8 ± 18.1 Nm.

When the spine is extended within the elastic limit, 60 to 70% of the resistance to the bending moment is resisted by the vertebral arch (Adams et al. 2013). Bony contact from either the spinous process and/or the FJs begins to occur after approximately 2° of extension (Adams et al. 1988). On average it takes 655 N acting 41 mm posterior to the discs CoR in order to reach the maximum physiological extension angle (Adams et al. 1988). Damage of the lumbar FSU begins to occur on average for an extension angle of 5° (3 to 8°) and can occur from bending moments ranging from 28 to 45 Nm (Green et al. 1994; Adams et al. 1988; Adams et al. 2013) During extension, stress concentrations begin to accumulate in the posterior AF after approximately 2° of extension (Adams et al. 2013). The majority of the resistance to extension comes from the posterior elements (Section 4.10.3) with the disc resisting roughly $22 \pm 11\%$ and $33 \pm 12\%$ of the backwards bending for the L4-L5 and L5-S1 lumbar levels respectively (Adams et al. 1988).

4.9.6 Lateral Bending

The axis of bending during lateral bending lies approximately in the sagittal plane. This mode of loading is resisted by the compressed FJ on the side of bending, and from tension in the

AF and FJ capsule ligaments on the collateral side to bending (Adams et al. 2013). During low loads, the majority of the resistance to lateral bending comes from the disc with 10 Nm causing 4 to 6° of bending (Adams et al. 2013). During lateral bending 60 Nm can fail lumbar FSUs, producing 12-15° of angular rotation (Miller et al. 1986). Pure lateral bending is unlikely during physiological loading with lateral bending often accompanied with flexion and/or axial rotation (Adams et al. 2013).

4.9.7 Fatigue Strength of Spinal Functional Units

The fatigue strength of a TDR is of great importance as it has been projected that the spine undergoes 125,000 cycles of flexion/extension bending per year (Hedman et al. 1990; Axiomed 2008a). TDRs have been implanted in patients as young as 19 (Delamarter et al. 2005) but are typically implanted in individuals aged between 35 to 50 years (Hedman et al. 1990; Enker et al. 1993; Delamarter et al. 2005). Therefore the implant must last for approximately 40 years which equates to approximately 5 million flexion/extension cycles (Axiomed 2008a).

4.9.7.1 Compression

The fatigue strength of 58 lumbar FSUs from 30 different lumbar spines were tested under cyclic compressive loading (Brinckmann et al. 1988). One random FSU from each spine was tested to failure to determine the ultimate strength. The FSUs were tested for 5000 cycles at varying levels of load relative to the particular spines respective ultimate strength.

The probability of failure after 10, 100, 500, 1000 and 5000 cycles while loading at a load relative to the ultimate strength was then calculated (Table 21).

Table 21: The probability of functional spinal unit fatigue failure (%) after a specific number of cycles while being loading at a particular range of compressive force relative to the FSU's ultimate strength (Brinckmann et al. 1988).

Relative Load (% of ultimate strength)	Number of Cycles				
	10	100	500	1000	5000
30-40	0	0	21	21	36
40-50	0	38	56	56	67
50-60	0	45	64	82	91
60-70	8	62	76	84	9

Stiffness and ultimate strength measurements are not the only important parameters to consider in TDR design. Failure of implant fixation to bone are strongly related to cyclic

loading. These loads are often applied during locomotion and external sources of vibration from machines (Huber et al. 2016).

4.9.7.2 Shear

Similar to the compressive strength the shear fatigue strength of lumbar FSUs has also been positively correlated with BMD (Skrzypiec et al. 2012). The lumbar vertebrae are most likely to fail at the pars interarticularis of the vertebral arch when exposed to shear forces (Cryon & Hutton 1978; Adams et al. 2013). Loading the lumbar spine in ranges of 30-40% of the ultimate shear strength for over 1000 cycles has been estimated to be below the failure threshold. Increasing the loading to 40-60% of the ultimate shear strength for 100 cycles has been reported to cause failure in 10% of specimens and increasing the loading above 60% causes rapid damage (Gallagher & Marras 2012; Cryon & Hutton 1978). It was therefore recommended that shear loading of the lumbar spine should be below 1kN for 100 cycles or less a day and below 700N for 100 to 1000 cycles per day (Gallagher & Marras 2012).

4.10 Biomechanics of the Facet Joints

The FJs limit the amount of axial rotation, resist anterior translation of the superior vertebral body, and limit flexion and especially extension of the spine (Cortes & Elliott 2014; Anon 1983) They also aid in the transmission of loads and have been shown to be responsible for carrying approximately 20% of the compressive loads to the spine (Jaumard & Welch, William C, Winkelstein 2011).

4.10.1 Shear

Due to the disc's viscoelastic properties, most of the shear forces that the spine is exposed to are transmitted through the FJ, except for high strain rate transient shear forces which are taken up by both the disc and the FJs (Serhan et al. 2007; Lu et al. 2005). This was illustrated by a study that tested a total of 16 lumbar spine segments (L2-3 and L4-L5) at a neutral position that were tested in a non-destructive pure shear test (Lu et al. 2005). The discs were first tested in an intact state under load control to a maximum of 250 N of anteroposterior shear at a loading rate of 25 N/s. The specimens were then tested under displacement control to 0.4 mm at a rate of 0.02 mm/s. Each disc was tested 3 times for each of the load and displacement controlled tests; and was allowed to 'rest' at zero displacement between changing of direction for the displacement tests to reduce hysteresis.

The discs were separated into 2 groups; Group A (N=8) had the disc cut including the anterior and posterior ligaments with a single sharp incision. The posterior elements were

removed from the remaining discs (Group B (N=8)). The testing methods for the intact discs were then repeated with the displacement controlled tests being executed first. The study found that the intact spinal segment was stiffer in anterior shear compared to posterior shear (Lu et al. 2005). This difference is caused by the angle of the FJs articulation and that anterior shear compressed the FJs together. Whereas posterior shear acts to separate the FJs resulting in the FJ capsule ligaments resisting excessive separation. They also reported that the anterior column (vertebral body and the disc) contributed to only 22.8% and 23.9% of the anterior and posterior shear stiffness respectively when comparing the intact state to the cut disc state. However, there was a difference in anterior and posterior stiffness of 77.7% and 79% respectively from the intact state to the removed posterior elements state. The results from the load controlled tests resulted in an increase in anterior deformation (mm) of 12.4% and 101.7% respectively for the disc and FJ dissected specimens compared to the intact states. Similar results of an 18.8% and 117% increase for posterior deformation were reported. The paper concluded that the posterior elements are more efficient in withstanding anterior and posterior shear load compared to the disc (Lu et al. 2005). However, the paper also concluded that the FJ and the disc do not act independently to each other when resisting shear loads which is important in defining the biomechanics of the spinal functional unit.

4.10.2 Torsion

The FJs in the FSU are responsible for withstanding the majority of torsional forces. During torsion one of the FJs is in compression and the other is in tension (Figure 22). As the FSU degenerates the range of motion of the FSU in torsion also increases and the amount of rotation needed for the facets to begin to compress increases from 1-2° to 8° (Adams & Hutton 1981). The FSUs begin to fail when these compressive forces reach 250 to 500 N. The range of the maximum recorded failure FJ compressive loads were 217 to 1280 N (Adams & Hutton 1981). These failures often occur when 10 to 30 Nm of torque is applied to the FSU with the maximum recorded failure torque being 88 Nm (Adams & Hutton 1981; Adams et al. 2013).

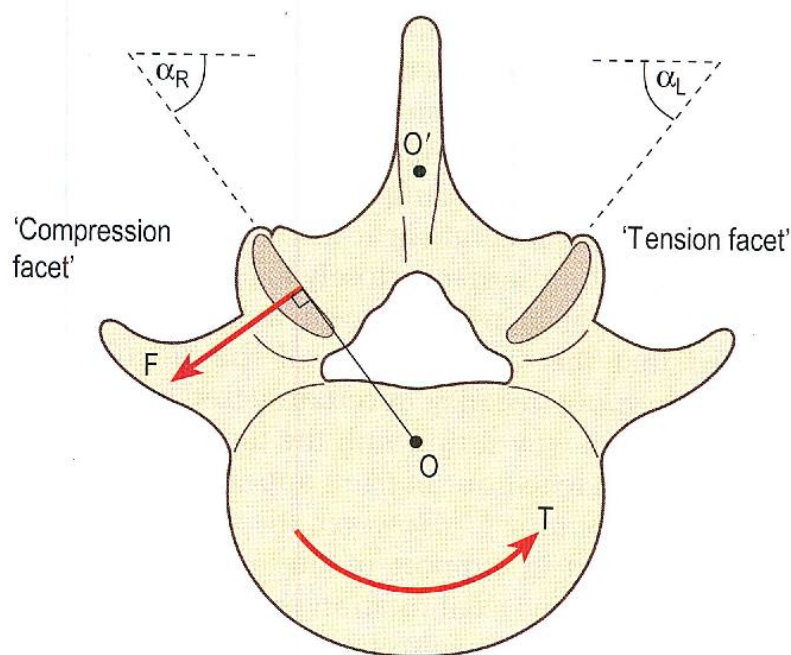


Figure 22: The approximate centre of rotation (CoR) of the lumbar spine (O). Note that the CoR is not positioned more dorsally at the centre of curvature of the facet joints (O'). Also note that one of the facets is in compression and the other is in tension when loaded in torsion. (Adams et al. 2013).

4.10.3 Flexion/Extension

In flexion the FJs aid in the resistance of the posterior tensile forces. The level of involvement increases dramatically for the final 2-3° of flexion with 39% of resistance coming from the FJ joint capsule ligaments (Adams et al. 2013). The FJs also limit the amount of flexion of the lumbar spine and in doing so prevents the disc from reaching the elastic limit by approximately 4°.

During hyperextension the FJs as well as the interspinous ligaments (which become compressed) are believed to be the first structures of the FSU to become damaged (Adams et al. 2013). The damage to the FJs is particularly common in individuals with widely spaced spinous processes (Adams et al. 1988). The spinous process resists the majority of the bending during extension; $59 \pm 25\%$ and $38 \pm 18\%$ for the L4-L5 and L5-S1 levels respectively. The remaining $19 \pm 15\%$ and $29 \pm 19\%$ is resisted from the FJs (Adams et al. 1988). When flexion is combined with compression; as is in vivo, compressive forces as low as 500 N can cause damage (M Adams, McNally, et al. 1994). A compressive force of 190 N combined with 10 Nm of extension bending causes 200 N of compressive force on the

FJs. Furthermore, 3 kN of compression at 4° of flexion can cause 570 N of compressive force on the FJs (Adams et al. 2013).

4.11 Summary of Failure Loads for the Lumbar Spine

It is important to summarise the different failure loads of the lumbar FSU to obtain benchmark values that a potential TDR must withstand (Table 22).

Table 22: Summary of the loads need to fail lumbar functional spinal units. * = functional spinal unit with facet joints removed.

Functional Spinal Unit		
Mode of loading	Failure Load	Reference
Compression	2 to 20kN	(Adams et al. 2013)
Shear	0.6 to 3.2kN	(Gallagher & Marras 2012)
	0.5kN*	(Adams et al. 2013)
Torsion	10 to 88Nm	(Adams & Hutton 1981; Adams et al. 2013)
	10 to 30Nm*	(Adams et al. 2013)
Flexion	50 to 81.5Nm	(Michael Adams, Green, et al. 1994)
	64.6Nm*	(Michael Adams, Green, et al. 1994)
Extension	28 to 45Nm	(Green et al. 1994)
Lateral Bending	60Nm	(Miller et al. 1986)

4.12 Range of Motion of the Spine

The range of motion of the lumbar spine is of great importance for clinicians. As a result, a number of different studies have investigated the natural RoM of the lumbar spine (Table 23).

Table 23: Recorded ranges of motion of the human lumbar spine.

Lumbar Level	Flexion (°)		Extension (°)		Lateral Bending (°)		Axial Rotation (°)		Reference
	Mean	SD	Mean	SD	Mean	Range	Mean	Range	
L4-L5	13	4	2	1	6	1 to 9	3	1 to 5	(Pearcy et al. 1984; Pearcy & Tibrewal 1984)
	8.9	-	5.8	-	5.9	-	2.7		(Yamamoto et al. 1989)
	-	-	4.1	1.1	-	-	-	-	(Adams et al. 1988)
	17.125		3.4						(Green et al. 1994)
					8		4		(Gaffey et al. 2010)
Global Mean	13		3.83		6.63		3.23		
L5-S1	9	6	5	4	3	1 to 6	2	0-3	(Pearcy et al. 1984; Pearcy & Tibrewal 1984)
	10		7.8		5.7		1.5		(Yamamoto et al. 1989)
			5.0	0.8					(Adams et al. 1988)
Global Mean	9.5		5.93		4.35		1.75		

The average combined flexion/extension RoM of the lumbar spine in asymptomatic individuals was discovered to be 13° and 14° with a range of 2-20° and 2-27° for the L4-L5 and L5-S1 lumbar regions respectively (Hayes et al. 1989).

A statistically significant and moderately clinically relevant correlation relating RoM at TDR treated levels and pain scores was identified in a mean 8.6 year follow up study (Huang et al. 2006). They discovered that when average flexion/extension RoM (measured from lateral x-rays using the Cobb method) postoperatively at the implanted level was greater or equal to 5°, patients had statistically significant and clinically modest improvement in both ODI (p=0.26)(Section 4.14.2) and modified Stauffer-Coventry Score pain scores (Appendix A)(p=0.015)(Huang et al. 2005). This threshold of 5° RoM for flexion/extension has also been suggested as a baseline to prevent adjacent disc degeneration (Gaffey et al. 2010). The

study investigated a total of 38 patients with average RoM for multi-level TDR replacements used to give each patient a single value. The patients were split into two groups: patients with $\text{RoM} \leq 5^\circ$ ($n=28$) and those with $\text{RoM} > 5^\circ$ ($n=10$) (Huang et al. 2005). The pre and post-operative pain scores were then compared (Table 24).

Table 24: Comparison of the preoperative (top section) and postoperative (bottom section) pain scores between patients with $\text{RoM} \leq 5^\circ$ and $\text{RoM} > 5^\circ$. (* = statistically significant using a Spearman correlation) (Huang et al. 2005).

	$\leq 5^\circ$ ROM	$> 5^\circ$ ROM	P Value
Age	45.1 \pm 5.5	44.1 \pm 12.2	0.72
Weight	73.7 \pm 15.3	67.9 \pm 11.0	0.29
Males	60.7%	50.0%	0.71
Previous lumbar surgery	46.4%	60.0%	0.71
Back pain	2.8 \pm 0.50	2.6 \pm 0.70	0.56
Leg pain	2.6 \pm 0.88	2.3 \pm 1.3	0.64
Disability	3.1 \pm 0.72	2.5 \pm 0.97	0.12
Modified Stauffer-Coventry score	7.1 \pm 2.9	6.6 \pm 3.9	0.87
Back pain	1.46 \pm 0.79	0.90 \pm 0.74	0.080
Leg pain	0.71 \pm 0.90	0.50 \pm 0.85	0.51
Disability	1.89 \pm 0.74	1.20 \pm 0.42	0.016*
Oswestry Disability Questionnaire	21.6 \pm 16.6	9.0 \pm 10.2	0.026*
Modified Stauffer-Coventry score	15.6 \pm 2.6	17.8 \pm 1.9	0.015*

From these findings it is clear that a total flexion/extension RoM that is greater than 5° should be achieved when using a TDR for a superior clinical outcome due to the correlated increase RoM and decrease pain score (Huang et al. 2005).

4.13 Centre of Rotation

The FSU is comprised of a unique three joint complex (Section 4.1.4). This special type of articulation causes the spine to have a non-fixed centre of rotation unlike relatively constrained joints such as ball and socket joints or hinge joints. A major design flaw in some TDR designs is that they introduce a non-physiological centre of rotations due to translational or rotational constraints. It has also been theorised, but not statistically proven from a clinical study, that abnormal CoRs may be caused by malpositioning, or due to bone growth after implantation that cause the CoR to shift into non physiological position (Tournier et al. 2007).

These non-physiological CoRs can lead to abnormal loading on the FSU and in particular cause an increase or decrease in facet joint forces depending on the change in CoR caused by the TDR (Sears et al. 2006). These fixed CoRs also can cause movement at the bone-TDR interface or deformation of the TDR itself if the TDR is forced to displace out of its constrained range of motion trajectory (Sears et al. 2006).

During physiological flexion/extension the vertebrae undergo rotation and translation in the sagittal plane (Pearcy & Bogduk 1988). This motion can geometrically be simply defined as a single rotation about a fixed centre of rotation known as an instantaneous centre of rotation (ICR) (Figure 23).

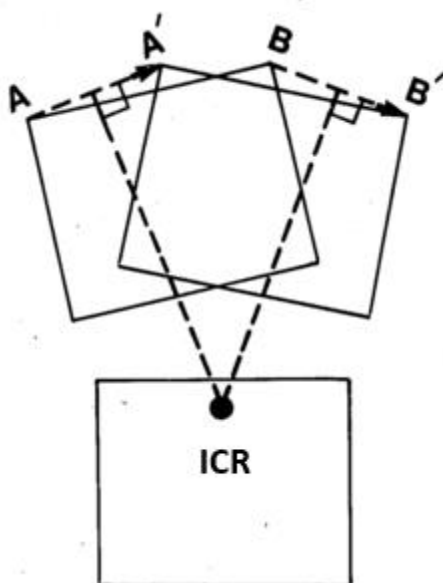


Figure 23: The calculation of the instantaneous centre of rotation (ICR)(Pearcy & Bogduk 1988).

The ICR however often shifts during a particular movement and the locations of the series of ICRs can be defined within a certain area (for 2D analysis) or locus known as the centre of motion (CoM)(Pearcy & Bogduk 1988).

An abnormal CoR of the lumbar spine has been suggested to occur in patients with sagittal imbalance which if not corrected it can limit TDR success (Pearcy & Bogduk 1988; Adams et al. 2013; Gornet et al. 2014; Tsitsopoulos et al. 2012; Le Huec et al. 2005).

A method to measure the CoR in-vivo from bilateral radiographs has been developed from 10 healthy male subjects. The CoR was measured from x-ray images at an upright standing position to flexion, upright to extension and extension to flexion (Pearcy & Bogduk 1988).

The distribution of the mean ICRs from the 10 subjects in the three different movements varies (Figure 24).

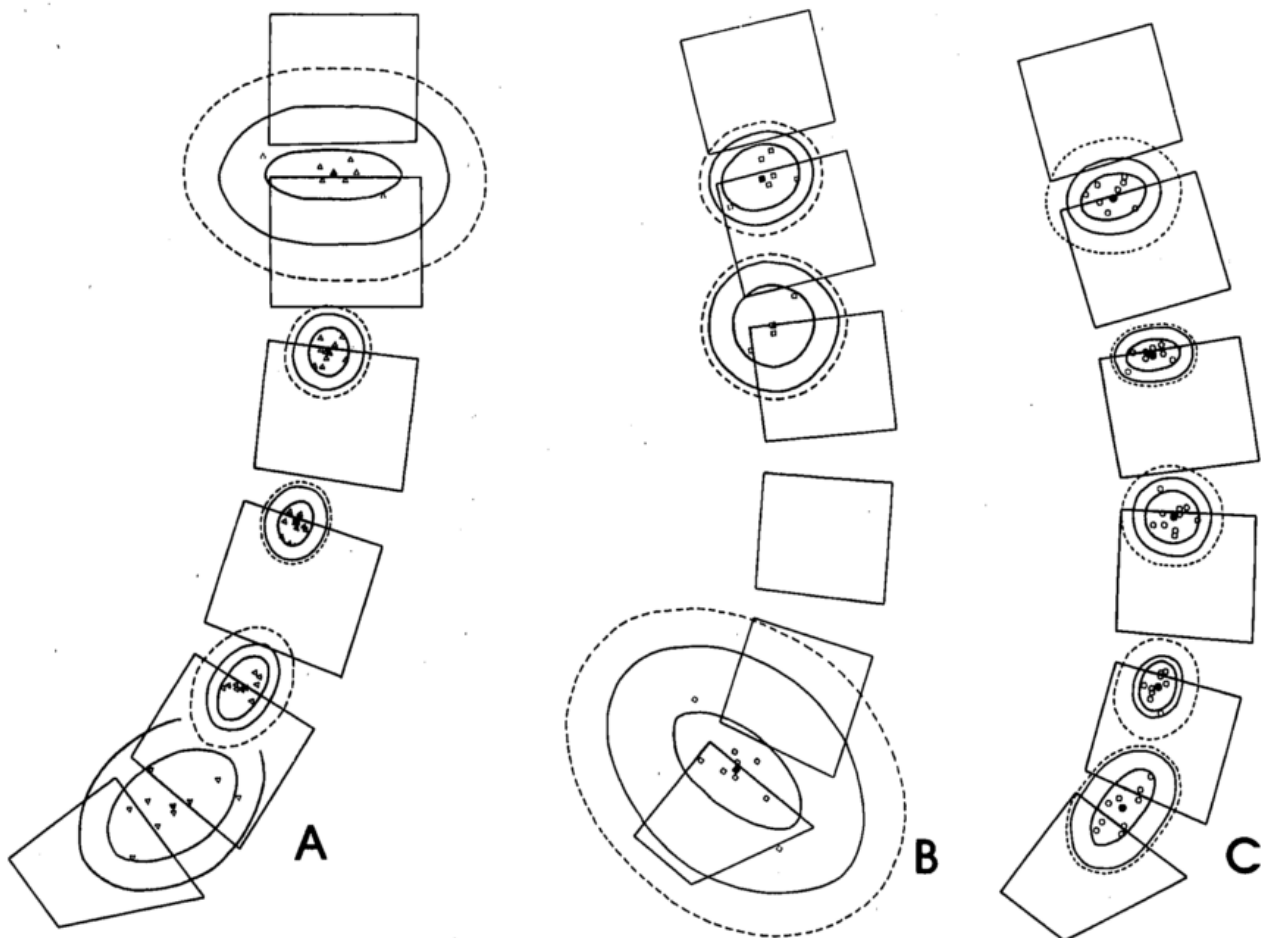


Figure 24: The mean instantaneous centre of rotation (ICR) of the three movements on a standardised diagram of the lumbar spine in the sagittal plane. A=upright to flexion movement, B=upright to extension and C= extension to flexion. The inner ellipse describes two standard deviations from the mean ICR for the 10 subjects measured. The outer and middle ellipses indicate the 96% confidence limits of the inter and intra-observer reliability (Percy & Bogduk 1988).

It is clear (Figure 24) that the ICR is not fixed in the lumbar spine and that the superior vertebrae does not simply rotate about the NP (Adams et al. 2013). This variation in the ICR causing the variable CoR is due to the complex biomechanics of the FSU and how the proportions of compression and bending vary continuously. This continuous variation also occurs to the proportion of translation and rotation of the FSU during physiological loading (Adams et al. 2013). It has been discovered that the ICR remains below the centre of the disc for small movements and then migrates anteriorly and posteriorly for flexion and extension respectively (Adams et al. 2013). DDD (Section 2.3) has also been shown to affect the

position of the CoR, causing it to migrate posteriorly to the FJs and inferiorly into the vertebral body (Zhao et al. 2005).

The location of the mean ICR have also been summarised (Pearcy & Bogduk 1988)(Table 25).

Table 25: The mean (and standard deviation) instantaneous centre of rotation (ICR) of the lumbar spine. Measurements are relative to an origin at the posterior superior corner of the lower vertebra of the applicable functional spinal unit (FSU). The location of the ICR is in terms of the proportion of the depth (x) and height (y) from the defined origin of the lower vertebrae of the applicable FSU in the sagittal plane (Pearcy & Bogduk 1988).

Joint	Upright to flexion		Upright to extension		Extension to flexion	
	x	y	x	y	x	y
L1-2	0.43(0.23)	0.03(0.09)	0.36(0.15)	-0.05(0.14)	0.39(0.12)	-0.01(0.10)
L2-3	0.40(0.07)	-0.04(0.09)	0.17(0.15)	-0.02(0.17)	0.36(0.10)	-0.04(0.06)
L3-4	0.38(0.06)	-0.05(0.09)	—	—	0.38(0.10)	-0.04(0.11)
L4-5	0.41(0.07)	-0.04(0.14)	—	—	0.36(0.07)	-0.10(0.11)
L5-S1	0.38(0.15)	0.19(0.26)	0.28(0.30)	-0.04(0.14)	0.33(0.07)	0.12(0.17)

These mean ICRs are helpful in designing a TDR which mimics the natural biomechanics as closely as possible. The recent development of elastomer core TDRs (Section 4.17.3) attempt to mimic this characteristic by not constraining the CoR like ball and socket designs.

The CoR in axial torsion is also not fixed (Adams et al. 2013). The CoR of the FSU lies approximately in or slightly outside the posterior AF (Figure 22)(Adams et al. 2013). The CoR for the L4-L5 or L5-S1 level in a neutral position when subjected to torsion lied 4 mm (-15 to 0 mm) dorsally of the posterior AF and 1.33 mm (-11 to 18 mm) inwards of the disc from the posterior AF for the particular levels respectively (Adams & Hutton 1981).

4.14 Assessment of LBP

Pain is a very difficult metric to measure due to the personal nature of its perception. Pain has been defined as ‘unpleasant sensory and emotional experience associated with the actual or potential tissue damage, or described in terms of such damage’ (Mannion et al. 2007).

There are two main pain questionnaires that are used to determine LBP especially in the lumbar region: the Visual Analogue Scale (VAS) and the Oswestry Disability Index (ODI) (Ruiz et al. 2014; Longo et al. 2010). These two metrics are useful in quantitatively accessing the clinical outcome of different LBP treatments, and have been used in clinical trials to obtain entry to the market. This is often achieved by comparing pre-treatment scores with post-treatment scores or by comparing the amount of improvement of two or more treatments.

4.14.1 Visual Analogue Scale (VAS)

The VAS consists of a line that is often 100mm long (Ostelo & de Vet 2005; Mannion et al. 2007). The beginning of the line is labelled as no pain and the other end is labelled as the most severe pain that the participant can imagine. The participant of the test is then asked to place a mark on the line indicating their individual perception of the level of pain they are in. The distance between the beginning of the line and the mark from the participant is used to give a score often described simply as the measured value i.e. a VAS score of 15 is 15 mm from the start of the line to the mark on a line of 100 mm in length. Modifications to this system may be adapted with such adaptations including separating the line into different sections for ‘mild’, ‘moderate’ and ‘severe’ pain or giving a numeric scale below the line (Figure 25).

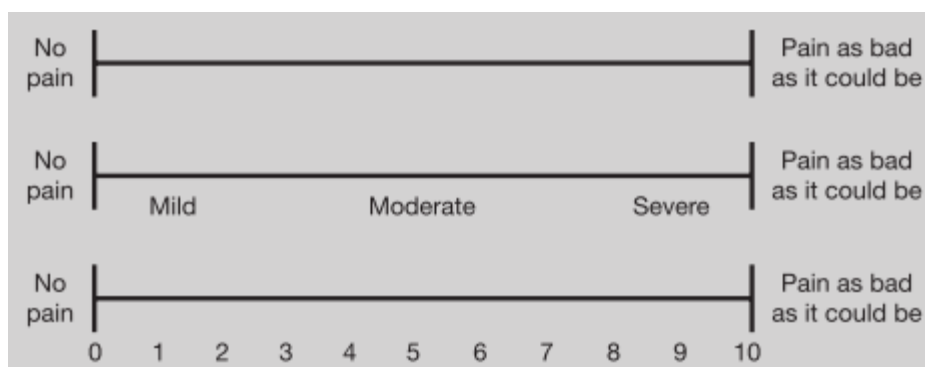


Figure 25: An example of different types of Visual Analogue Scale (VAS). A simple non-scaled VAS (top), a VAS with a descriptive scale (middle) and a VAS with a numeric scale (bottom)(Mannion et al. 2007).

4.14.2 Oswestry Disability Index (ODI)

The ODI or a modified version of the ODI is a very common method of grading both spinal fusion techniques and TDR devices in terms effectiveness and patient satisfaction from clinical studies. The method has been stated as the gold standard test for lower back functional outcomes (Fairbank & Pynsent 2000). There are two main versions of ODI that are used; ODI version 1.0 and ODI version 2.0. Both comprise of 10 sections (Appendix B).

The scoring system works by giving each statement in each section a score. The first statement is worth 0, the second is worth 2 and so on. The overall score is then often presented as a percentage. If a section is inapplicable the total score is adjusted. Therefore, the higher the ODI score the greater the level of pain. The ODI has been shown to have sufficient reliability and has been validated (in multiple languages) to be suited for clinical LBP grading (Davidson & Keating 2002; Fairbank & Pynsent 2000; Longo et al. 2010). The ODI is also believed to be superior to VAS as a predictor when considering functional movement parameters in a clinical setting. This is due to the ODI's greater predictive abilities for overall lumbar range of motion and functional range of motion when performing average daily living activities (Ruiz et al. 2014).

4.15 Different Solutions of LBP

There are a number of different methods for treating LBP which can be sorted into two main categories; surgical and non-surgical. For obvious reasons non-surgical methods should be exhausted first before invasive treatments are recommended.

4.15.1 Non-Surgical

Non-surgical approaches to treating LBP include pain injections, manipulative therapy, medications and transcutaneous electrical therapy (Baliga et al. 2015). Lifestyle changes are also often recommended for LBP dependant on the type and severity of the pain. These changes may include simply resting or exercise programs (Whatley & Wen 2012).

4.15.2 Surgical

When non-invasive treatment methods have failed surgical methods have been shown to be scientifically valid in terms of treating LBP (Fritzell et al. 2001). This was concluded after a multicentre, randomised controlled trial that compared the outcomes of L4/L5 and/or L5-S1 fusion surgery to non-invasive methods (Figure 26)(Fritzell et al. 2001). This clearly illustrates how surgical methods are a superior approach once non-surgical treatments have been exhausted.

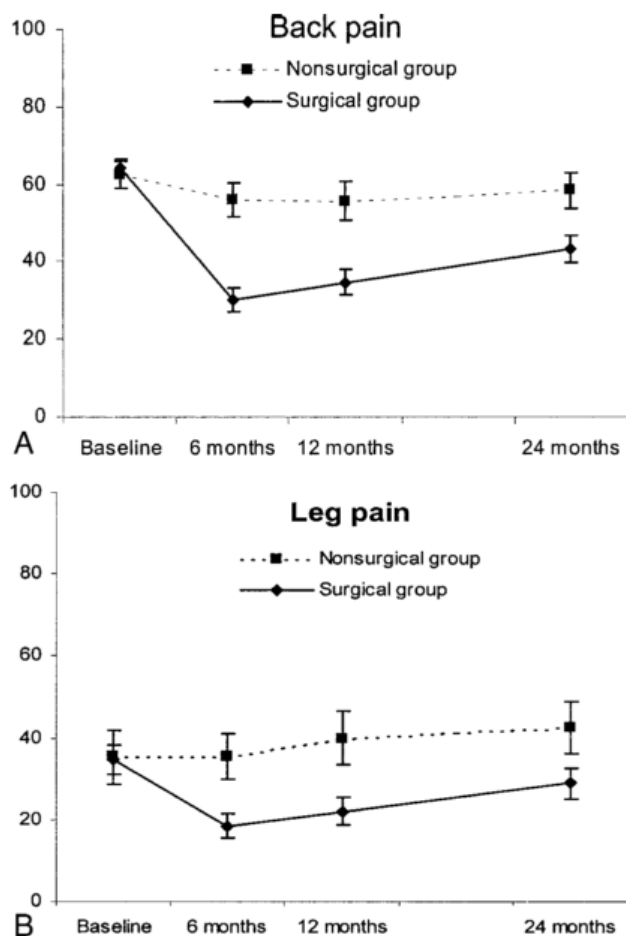


Figure 26: The difference in back and leg pain from a Visual Analogue Scale over a 24-month period, comparing the non-surgical and surgical (fusion) group. The mean and 95% confidence values are presented (Fritzell et al. 2001).

4.15.2.1 Tissue Engineering

Stem cell research and tissue engineering has also been applied to the lumbar disc however the application of these ‘biological’ disc replacements are still years away from becoming clinically and commercially viable (Baliga et al. 2015).

4.15.2.2 Facet Replacement

Facet degeneration (Section 2.3) is also a cause of LBP. As a result, a number of different facet replacement prophesises have also been developed (Figure 27). The main rationale behind these devices is to remove painful FJs which may be due to osteoarthritis or facet tropism with an artificial articulating device to restore natural facet function in a painless manner (Anekstein et al. 2015; Goel et al. 2007).

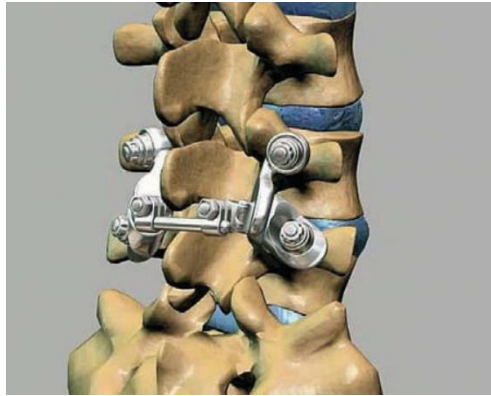


Figure 27: A facet replacement system (Goel et al. 2007).

4.15.2.3 Fusion

Fusion is the ‘gold standard’ for surgical treatment of severe DDD (Errico 2005; Siepe et al. 2007). The rationale behind the treatment is to provide axial relief and provide stability of the affected lumbar segments by fusing them together to disallow movement between affected vertebrae (Baliga et al. 2015). This essentially progresses the process of lumbar disc degeneration to the final stage (Errico 2005).

4.15.2.3.1 Adjacent Disc Degeneration

A major problem with lumbar fusion is the development or advancement of disc degeneration of the adjacent disc(s) to the fused level(s). This adjacent disc degeneration (ADD) is believed to be caused by the increase in stiffness to the operated construct after surgery and/or the loss of motion. This in turn alters the mechanical behaviour of the adjacent discs causing accelerated DDD (J. C. Wang et al. 2012). In order to maintain a normal range of RoM adjacent discs to the fused level would also have to increase their RoM to compensate for its loss at the fused level. This would cause higher disc stresses resulting in at advancement of disc degeneration.

4.16 Total Disc Replacements

Apart from fusion, TDRs are the next most common surgical prosthesis used to treat LBP.

The advantages for total disc replacements include:

- Restoration of normal spinal kinematics and the range and quality of motion (Liu et al. 2006).
- Restoration of disc height (Fattor et al. 2016; Liu et al. 2006).
- Preventing adjacent disc degeneration by limiting abnormal loading of adjacent discs (J. C. Wang et al. 2012; Liu et al. 2006; Huang et al. 2006).
- Preventing abnormal facet loading at the operated level to avoid FJ osteoarthritis.
- Restoration of more natural lumbar biomechanics (Liu et al. 2006).
- Restoration of lumbar lordosis (Fattor et al. 2016).
- Decrease in operating time (Whatley & Wen 2012).
- Decreased blood loss during surgery (Whatley & Wen 2012).
- Decreased length of hospital stay (Whatley & Wen 2012).

TDR devices first gained entrance to the US medical market in 2004 after they were proven to be a comparable to fusion for treatment for LPB (Thavaneswaran & Vandeppeer 2014).

In addition, TDR offers a number of advantages compared to fusion:

- They restore some level of motion to the affected spinal level, believed to reduce the risk of ADD (Benzel et al. 2011).
- They do not pose the risk of bone graft location pain or infection as no grafts are needed (Benzel et al. 2011; Park 2015).

4.17 TDR Devices

TDR devices can be separated into three main categories based on the type of mechanical articulation the design incorporates. These categories are ball and socket designs; with a fixed centre of rotation, mobile core; articulating ball and socket designs, and elastomer core designs (Table 26).

Chapter 4. Literature Review

Table 26: Summary of the different types of TDR devices available on the market as of 2014. The table shows the type of bearing surfaces (MoM=metal on metal, MoP=metal on polymer, PoP=polymer on polymer and 1P=one piece), the biomaterial the devices are made of, the bearing design or type and the manufacture (Veruva et al. 2014).

Device	Manufacturer	Classification	Biomaterials	Bearing design	IDE trial status (www.clinicaltrials.gov)	Current regulatory status (as of January 2014)
CHARITÉ	DePuy Synthes Spine, Raynham, MA, USA	MoP	CoCr-UHMWPE	Mobile	Completed	FDA-approved but withdrawn from US/OUS market after DePuy Synthes merger, 2012
ProDisc-L	DePuy Synthes Spine, West Chester, PA, USA	MoP	CoCr-UHMWPE	Fixed	Completed	FDA-approved, available US/OUS
Activ-L	Aesculap AG, Tuttlingen, Germany	MoP	CoCr-UHMWPE	Mobile	Active; not recruiting	Available OUS
Mobidisc	LDR Spine, Troyes, France	MoP	CoCr-UHMWPE	Mobile	Terminated	Withdrawn
Maverick	Medtronic, Memphis, TN, USA	MoM	CoCr-CoCr	Fixed	Completed	Available OUS
Kineflex	Spinal Motion Inc, Mountainview, CA, USA	MoP	CoCr-CoCr	Mobile	Terminated	Withdrawn
Flexicore	Stryker Spine, Allendale, NJ, USA	MoP	CoCr-CoCr	Constrained	Not registered	Withdrawn
Baguera L	Spineart, Geneva, Switzerland	MoP	Diamolith-coated Ti-UHMWPE	Fixed	Not registered	Available OUS
CAdisc-L	Ranier Technology, Cambridge, UK	1P	1-piece polyurethane	One-piece	Completed	Available OUS
Freedom	Axiomed, Garfield, OH, USA	1P	Ti plates and elastomer core	One-piece	Recruiting	Available OUS
eDisc	Integra Spine, Vista, CA, USA	1P	Ti plates and elastomer core	One-piece	Not registered	Available OUS
Physio-L	Nexgen Spine, Whippany, NJ, USA	1P	Ti plates and elastomer core	One-piece	Not registered	Available OUS
M6-L	Spinal Kinetics Sunnyvale, CA, USA	1P	Ti plates and polyurethane- UHMWPE fiber core	One-piece	Withdrawn	NA

IDE = Investigational Device Exemption; MoP = metal-on-polyethylene; MoM = metal-on-metal; 1P = one-piece; CoCr = cobalt-chromium; UHMWPE = ultrahigh-molecular-weight polyethylene; Ti = titanium; OUS = outside United States; NA = not available.

4.17.1 Ball and Socket

The inspiration of these ball and socket devices came from hip joint replacements (Reeks & Liang 2015; Benzel et al. 2011). The main problem with these types of devices is that the FSU is not a ball and socket joint (Section 4.1.4 and 4.13) but comprises of a three joint complex. Therefore these type of devices do not restore natural lumbar biomechanics (Benzel et al. 2011). In addition, due to the articulating surfaces of ball and socket joint TDRs wear is also an issue (Hyde et al. 2015; Grupp et al. 2014). Although these TDRs have their limitations and do not completely restore physiological biomechanics, they have shown to be clinically viable, with some of the longest follow up periods of any type of TDR (Park et al. 2016).

4.17.2 Mobile Core

Mobile core TDRs have been around since the beginning of modern TDR devices with the first FDA approved TDR; the CHARITE, having a sliding core (Depuy Spine a Johnson & Johnson Company 2004; Geisler 2006). These types of devices still use a ball and socket articulation and therefore still have the associated risks of wear. However, the mobile nature of the sliding cores allows the CoR to translate in a constrained manner to in an attempt allow for a more physiological CoR (Section 4.13) (Figure 28) compared to the completely constrained ball and socket like devices (Sears et al. 2006).



Figure 28: A demonstration of how a mobile core translates during flexion (left) to extension (right) within the disc space (Geisler 2006).

4.17.3 Elastomer Core

Viscoelastic elastomer core TDRs seem to be the future. The major advantage of these types of TDRs compared to the previously mentioned ball and socket and mobile core devices is the completely unconstrained CoR and the viscoelastic mechanical properties that most closely mimic the natural biomechanics of the disc (Section 1.1).

4.18 Surgical Insertion

TDRs are typically inserted with an anterior approach (Park 2015). It is important to have some understanding on the operation procedure used to implant TDR as depending on the size of the operating window the TDR may not be able to be implanted.

A typical TDR implantation surgery involves having the patient lie on their back with their legs spread in a 'French Position'(Figure 29)(Vital & Boissière 2014).



Figure 29: The 'French Position' (Vital & Boissière 2014).

An incision is made on the central side of the rectus abdominus muscle and the hand is often used to open a wide enough field of view (Figure 30)(Vital & Boissière 2014).

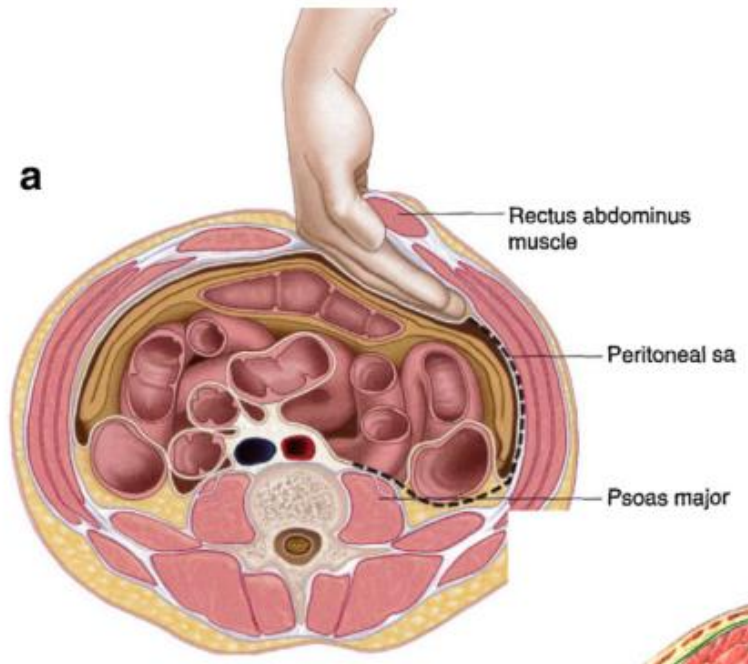


Figure 30: A drawing in the transverse plane of the approach often used to implant a lumbar TDR (Vital & Boissière 2014).

Once the disc has been partially exposed the left common iliac vein and artery are distracted to expose the disc prior to removal so TDR implantation can begin (McAfee et al. 2006). The lateral annulus fibrosis is often left intact.

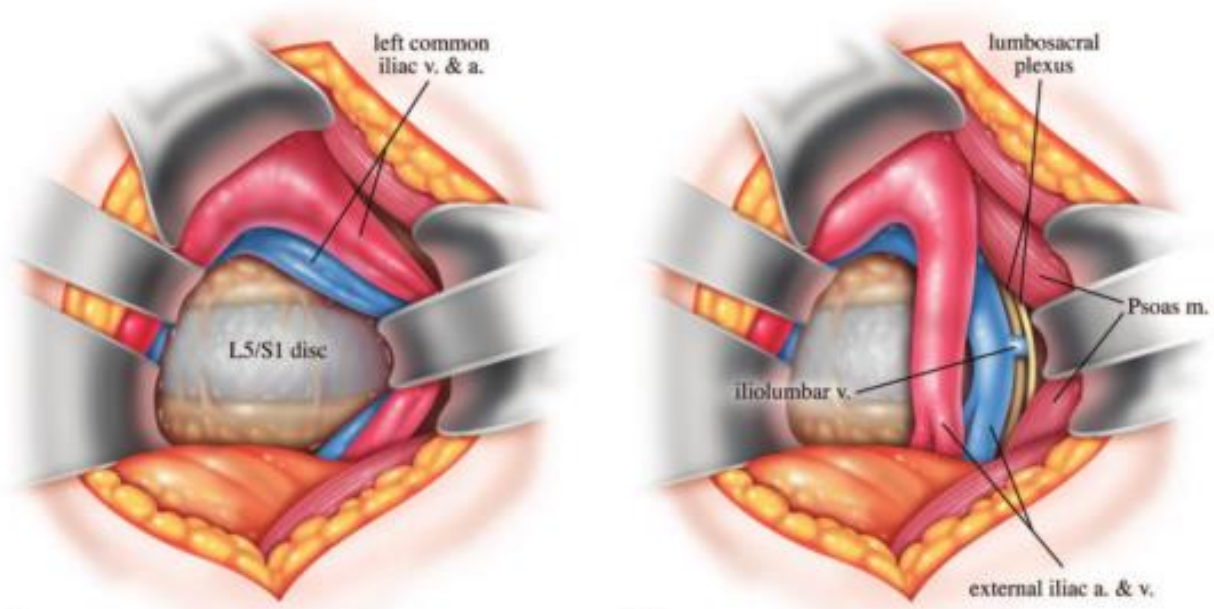


Figure 31: The distraction of the left common iliac vein and artery to expose the L5-S1 disc before TDR implantation (McAfee et al. 2006).

Special implantation guide tools have been developed to help position and guide the TDR into place (Section 5.3.2.1.1).

Chapter 5. Review of TDRs

Commercially available or previously available TDRs have been reviewed in sections 5.1, 5.2 and 5.3. These sections have highlighted the design feature of each TDR, describe any published mechanical testing and review any clinical studies of each device. These design features were used for inspiration when developing novel features of the designed TDR. The mechanical testing provided information on different loading regimes which TDRs have been subjected to before market release. In particular, the testing from the CHARITE, Prodisc-L and ActivL was derived from the FDA safety summary sheets which described the testing that was performed prior to market approval. These test protocols can be incorporated into future FEA simulations and then replicated; in vitro, once a substantial prototype has been developed to demonstrate that the design is at least adequate to existing devices. The clinical outcomes provided information that was helpful in deciding which type of TDR device should be utilised in the design.

5.1 Unknown Market Status

The market status of a number of TDRs is unknown. This problem is believed to be caused by two major factors. One, the TDR was quietly removed from the market in order to preserve company reputation or the company has been acquired by another and the TDR is no longer in production.

5.1.1 eDisc™

5.1.1.1 Design Features

The eDisc was developed by Theken and is a one piece TDR which is made of a thermoplastic polyurethane elastomer core with titanium endplates (Figure 32)(St. John 2014; Serhan et al. 2011).



Figure 32: Assembled eDisc TDR (left) and eDisc with exposed electronics (right)(Hunt et al. 2007)(McMillin 2006).

5.1.1.1.1 Unique Design Features

The eDisc is revolutionary as it is one of the first TDRs to have self-recharging microelectronics with force transducers which allow patient monitoring (Krijnen et al. 2004; Veruva et al. 2014; Serhan et al. 2011). The eDisc communicates with a hand held PDA device which allows surgeons to monitor their patients in real time and also record data. The eDisc also has the capabilities to alert patients via a buzzer when they are incorrectly loading their spines via excessive movements (Hunt et al. 2007). The polymer that the eDisc is made of (TH200) was developed over two years by Theken and has been shown to be twice to ten times more fatigue resistant than competing elastomer cores (Krijnen et al. 2004; Hunt et al. 2007).

5.1.1.2 Mechanical Testing

TH200 has undergone a number of different ASTM standard tests (Table 27).

Table 27: The mechanical properties of the eDisc polymer (Hunt et al. 2007).

Property	Test Method	Value
Hardness (Shore A)	ASTM D2240	82 typical
Compression Set	ASTM D395A	3% max
Ultimate Tensile Strength	ASTM D412	27.5 to 34.5 MPa typical
Ultimate Tensile Strain	ASTM D412	350 to 450% typical
25% Modulus	ASTM D412	2.4 to 3.4 MPa typical
100% Modulus	ASTM D412	5.5 to 7.2 MPa typical
Tear die C	ASTM D624	70 to 87.6 kN typical
Tear die T	ASTM D624	52.5 to 70 kN typical

The fatigue strength of the eDisc when tested for one million cycles and compared to other biocompatible elastomers that had been tested (Figure 33).

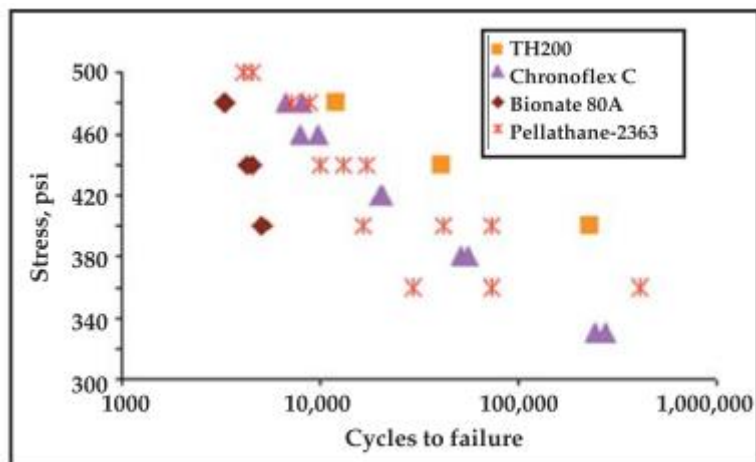


Figure 33: The SN curve illustrating cycles to failure of a number of different biomaterials compared to TH200 (eDisc polymer)(Hunt et al. 2007).

This shows TH200 is superior to a number of different commercially available elastomers in terms of fatigue life.

The eDisc polymer also underwent extensive biocompatibility tests (Table 28).

Table 28: Summary of the chemical properties of TH200 the polymer used in the eDisc (Hunt et al. 2007).

Properties	Test Method	Value
Dilute solution viscosity	ASTM D2857	0.95 to 1.05 dL/g
Molecular weight	ASTM D5259	130,000 to 170,000 g/mol
Glass transition temperature	ASTM D4092	-20 to -30°C typical

Hydrolysis and oxidation have been shown to be a lead cause of degradation of thermoplastic polyurethanes (Hunt et al. 2007). In vitro tests designed to simulate accelerated in vivo conditions of hydrolysis or oxidation aging comparing TH200 to other biomaterials (Figure 34). Note that the tensile strength of the TH200 is superior when unaged or aged compared to other materials.

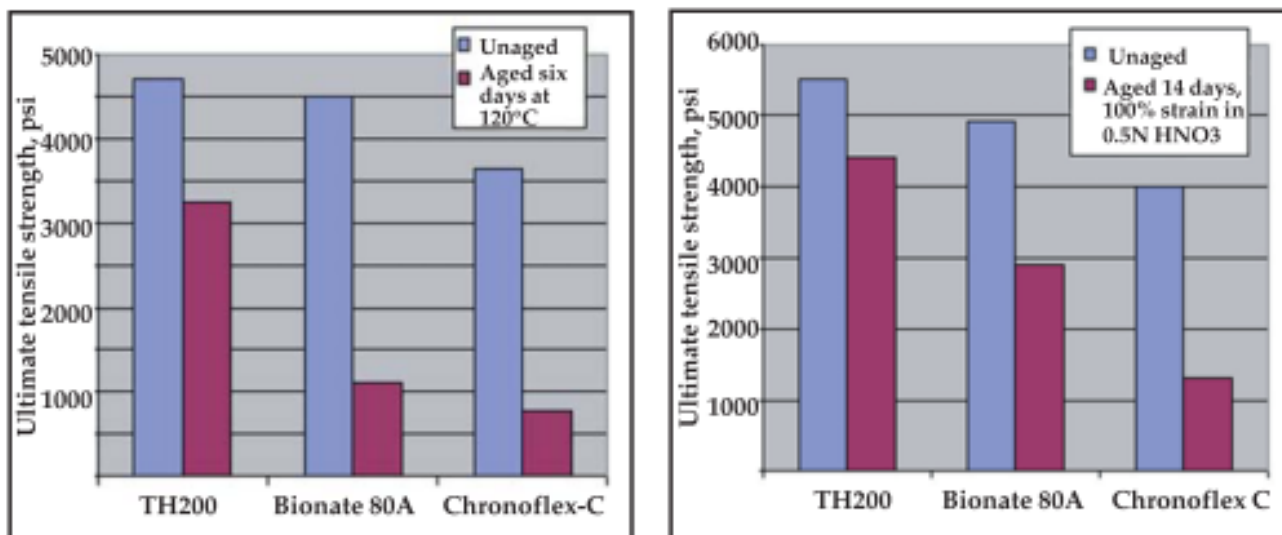


Figure 34: The effect of hydrolytic aging on tensile strength for a number of different biomaterials (left) and the effect of oxidative aging on tensile strength for a number of different biomaterials (right)(Hunt et al. 2007).

TH200 has also been tested for material leaching, cytotoxicity, reactivity, sensitivity, systemic toxicity, genotoxicity and hemocompatibility, all of which were deemed safe under ISO10993 guidelines (Hunt et al. 2007).

The eDisc design focused on compression and flexion as these are the main modes of loading of the natural disc (Nevarro et al. 2008). Rationale for this decision was justified as it would be impractical when using of a homogeneous polymer core to attempt to mimic the whole 6DOF spinal mechanical properties (Nevarro et al. 2008). A finite element model of the L3-L4 FSU revealed that under 2600 N of compressive force the disc bears 99% of the load and under 10 Nm of extension bending the disc bears 54.2%, the FJs 26.3%, and the ligaments 19.5% (Nevarro et al. 2008). The eDisc was shown to be able to replicate this 54.2% based on cadaveric test data.

5.1.1.3 Clinical Trials

The eDisc has been implanted in a baboon animal trial. This trial was used to show that the eDisc can survive the implantation procedure, activate the communication electronics when required, transmit data outside of the body and recharge the battery (Nevarro et al. 2008). No known human trials have been completed.

5.2 TDRs Removed from the Market

A number of the TDR devices that have been released on the market were eventually removed or withdrawn from FDA investigational device exemption studies (IDEs). These

IDE studies provide exceptions for newly developed devices to undergo controlled and strictly regulated clinical trials which if successful will allow the device to eventually gain US medical market approval (FDA 2015a). The reasons for market withdrawal are not always known due to attempts to preserve company reputation.

5.2.1 CHARITÈ™

5.2.1.1 Design Features

The CHARITE TDR was developed in Germany during the early 1980s, with the first device being implanted in 1984 (Guyer et al. 2009; Bono & Garfin 2004; Mayer & Siepe 2007; Guyer et al. 2016). The CHARITE was later acquired by Depuy Spine and then went on to become the first TDR to gain FDA approval in 2004 (FDA 2004). The device itself is comprised of two cobalt chromium molybdenum (CoCrMo) endplates that have six spiked teeth; for initial fixation, and is coated in plasma sprayed titanium and bio-active calcium phosphate to promote bone ingrowth. The endplates are separated by a semi constrained sliding mobile ultra-high molecular weight polyethylene (UHMWPE) biconvex core; that has a metal wire along its centre circumference for radiographic marking (Figure 35) (Mayer & Siepe 2007; Geisler 2006; Depuy Spine a Johnson & Johnson Company 2004; Serhan et al. 2011). The CHARITE was eventually removed from the market in 2012 due to the Depuy Synthes merger and was slightly modified and rebranded as the InMotion® disc (Figure 35)(Serhan et al. 2011). However, the InMotion is no longer marketed in the US and Depuy Synthes now purely sell the Prodisc-L (Premera Blue Cross 2016).



Figure 35: CHARRITE artificial lumbar disc (top) and the InMotion disc (bottom) (Geisler 2006)(Serhan et al. 2011).

5.2.1.1.1 Unique Design Features

The major unique design feature of the CHARITE compared to other TDR devices are the metal wire used for radiographic tracking of the mobile core. This doesn't offer advantages for the mechanical performance of the TDR but does aids in patient monitoring, TDR placement analysis and RoM assessment.

5.2.1.2 Mechanical Testing

The CHARITE TDR was exhibited to a number of static and dynamic mechanical tests prior to FDA approval (Table 29 and Table 30).

Table 29: Summary of CHARITE static tests (FDA 2004).

Test	Test Description	Test Samples	Method	Results
1	Preliminary Test of Compressive Strength	Twenty 7.5 mm cores; ten with parallel and ten with oblique endplates.	Axial compression to failure, with eccentric / off centre axis loading onto the outer rim of the core.	Deformation did not exceed 50%. Ultimate Strength (kN); <ul style="list-style-type: none"> Parallel= 7.55 ± 2.75 Off axis loading on outer rim = 1.37 ± 0.06
2	Preliminary Test of Bending Compressive Strength	Twenty 7.5 mm cores; ten with parallel and ten with oblique endplates.	Bending compression to failure, with eccentric loading onto the outer rim of the core.	Ultimate Strength (kN); <ul style="list-style-type: none"> Parallel= 2.32 ± 0.05 Off axis loading on outer rim = 2.36 ± 0.16
3	Creep	Nine 7.5 mm cores with parallel	50 hours of max load followed by 48 hours with no load; samples in 37°C water bath; at least two samples tested at each load: 1, 2, 3 or 4 kN.	Max initial height deformation (immediately after 50 hours of load) = 7.6% (0.57 mm) Max Height deformation after relaxation = 2.3% (0.17 mm)
4	Range of Motion	Eight Cadaveric spines (L2-S1) with L4-L5 reconstructions using CHARITE disc, interbody fusion cage, and interbody fusion cage with pedicle screw system.	± 8 Nm moment applied to produce flexion/extension, lateral bending and axial rotation movements; intact spine compared to the reconstructed spines for RoM distribution from L3-S1 and for location of centre of rotation	A 3% increase in flexion/extension, 16% increase in lateral bending and 44% increase in axial rotation compared to intact specimens. Mean segmental translation: CHARITE = 2.06 ± 0.77 mm Intact = 1.9 ± 0.98 mm Centre of rotation was in the posterior 1/3 of the operated and adjacent discs for the CHARITE and intact specimens.
5	Supplemental test of Axial Compression with Flexion	Thirty 7.5 mm cores and thirty 9.5 mm cores. 15 of each core used	Implant tested at neutral (0°), max flexion (13.5°) and max extension (7.5°).	Min yield @ 0° = 16.38 ± 0.29 kN Min yield @ 13.5° = 4.899 ± 0.345 kN

	and Extension	with parallel and 15 with oblique endplates.		<p>Min yield @ 7.5° = 16.58 ± 1.67 kN</p> <p>Max Deformation = 9-20% after 50-60% recovery.</p>
--	---------------	--	--	---

When loaded eccentrically in tests 1 and 2 the CHARITE TDR exhibited a flexion/extension displacement greater than 32° which resulted in the outer edges of the core bearing the majority of the load instead of the centre. Since the physiological range of motion is approximately 0-20° (Section 4.12) these failure loads are likely the worst case scenario that will not likely occur in vivo (FDA 2004).

The TDRs were exposed to both axial compressive and eccentric (load applied at an off axis at the outer rim of the core) compressive strength tests. A total of 20 TDRs with 7.5 mm core heights were tested. 10 flat endplate TDRs and 10 oblique endplates TDRs were tested. The ultimate strengths were 7.55±2.75 kN and 1.37±0.06 kN respectively for the axial and eccentric loading conditions (FDA 2004). The same number and types of TDRs were also tested in bending compressive strengths tests with the loading again applied eccentrically onto the outer rim of the core. The ultimate strength was 2.36±0.16 kN (FDA 2004).

Creep tests revealed that the worst case of permanent deformation was a height loss of 0.57 mm for the 4 kN compressive load.

Table 30: Summary of CHARITE dynamic testing (FDA 2004).

Test	Test Description	Test Samples	Method	Results
1	Preliminary Axial load fatigue testing	Six 7.5 mm cores with parallel endplates. Test	Test was performed for 10 million cycles at 10 Hz; with 200 N preload in a 37°C water bath and R~10; Two specimens @ 3.77kN peak, two specimens @ 7.5 kN peak, and two specimens @ 10 kN peak.	Endurance limit approximately 3.77 kN to 10 million cycles.
2	Supplemental Axial Fatigue Testing	Five CHARITE disc devices with 7.5 mm cores.	10 million cycles at 1 Hz with R=10 in 37°C saline bath; 375 N- 3.75 kN axial load/each device.	Deformation~ 5.9- 8.8% Mean Deformation= 6.8% No gross or catastrophic damage to the core or endplates was observed in tested specimens
3	Supplemental Compressive Shear Fatigue Testing	Five CHARITE disc devices with 7.5 mm cores.	10 million cycles at 1 Hz with R=10 in 37°C saline bath; @ 2 kN compressive shear loading	Deformation = 3.3 -7.5% Mean Deformation= 5.2% No gross or catastrophic damage to the core or endplates was observed in tested specimens. All other cores were observed to have a thin layer of white amorphous material on the outer portions of the top and bottom domes.
4	Dynamic Compression Simulation	Ten 7.5 mm cores and ten 9.5 mm cores.	24-hours cyclic loading in 3 phases: 4 hrs@ 0.5Hz, 12 hrs@ 0.017 Hz, 8 hrs@ 0.00028 Hz; 37°C water bath; peak load of 2.5 kN for 5 of each core height; test repeated with peak	Calculated 10-year deformation based on strain data to be less than 8%. During 4.5 kN loading, the twisted x- ray wire on the 7.5 mm cores broke.

			load of 4.5 for 5 of each core height.	
5a	Hysteresis	Five CHARITE disc devices with 7.5 mm cores and parallel endplates.	Five sequential axial compressions at 4.2 kN.	No hysteresis loss was observed in any of the samples.
5b		Five CHARITE disc devices with 7.5 mm cores and parallel endplates.	Five sequential axial compressions at 10.5 kN.	Hysteresis loss was observed.
5c		One CHARITE disc devices with 7.5 mm cores and parallel endplates.	Implant placed in L4-L5 position of cadaver spine and cycled at 5 Hz and 10 Hz for 20 million cycles with increasing load	Endplate teeth over penetrated vertebral body at 3 kN; bone started to fail at 7.7 kN and endplate subsided into bone at 10.8 kN.

The dynamic testing revealed the estimated fatigue life of the CHARITE to be greater than 10 million cycles (Table 30 test 3). They also investigated the load needed to correctly implant the TDR into the bone and the load needed to cause subsidence (test 5c Table 30).

5.2.1.3 Clinical Trials

The CHARITE TDR due to its extensive time on the market has had numerous clinical studies investigating the devices effectiveness. The CHARITE was originally compared to spinal fusion during the product approval stage to illustrate that it was at least comparable clinically (Geisler 2006). Due to the success of the CHARITE pioneering the way for TDRs to enter the US medical market. The CHARITE has also extensively been used as a control to compare to new TDR designs wishing to gain market entry (Yue & Mo 2010; Guyer et al. 2016). A number of the clinical trials have investigated the ODI and VAS scores at different time points following CHARITE implantation (Figure 65, Figure 66).

5.2.2 AcroFlex

5.2.2.1 Design Features

The AcroFlex prosthesis (DePuy Spine) was one of the first one piece elastomeric core with titanium (ASTM F-136 Ti-6Al-4V ELI alloy) endplates TDR designs (Fraser et al. 2004). The rationale behind the use of an elastomeric core was that it would replicate the elasticity of the natural disc. Initially the elastomer core comprised of a polyolefin-based rubber core; which was successfully implanted in five out of six human trials during 1988 to 1989, however this was then substituted with a silicone core. The refined core design was then implanted in a total of eight patients between 1993 and 1994, with one mechanical failure occurring after just 6 months from implantation (Fraser et al. 2004). The design was then remodified again to use the original rubber core. The endplate design was also altered to incorporate domed endplates in the coronal and sagittal plane, compared to the original flat with a crescent ridge on the superior endplate. It was also altered with a central anterior posterior ridge, four to six fin like teeth and a porous beaded coating for ease of alignment, initial stability and bone ingrowth respectively (Figure 36)(Fraser et al. 2004). The bonding between the rubber core and the titanium endplates incorporated a chemical bond with the use of Chemlok 205 primer and Chemlok 250 adhesive. A mechanical bonding component from sintered titanium balls that allow the rubber to flow between the balls during the moulding processes and increases the surface area between the endplates and the elastomer core was also used (Fraser et al. 2004).

The lordosis of the implant was generated from the endplates, as opposed to the elastomer core. This decision was due to findings from a finite element analysis that predicted better stress distribution between the rubber to endplate surface (Fraser et al. 2004).

The rubber core also has a smaller inner diameter compared to the superior and inferior diameter at the endplate interface. This shape was incorporated to prevent or reduce the change of nicking or tearing due to bulging during in vivo loading.



Figure 36: The original AcroFlex endplate design, with flat endplates and a crescent moon ridge (left) and the refined designed endplate with central anterior posterior ridge and finned teeth (right) (Fraser et al. 2004).

5.2.2.1.1 Unique Design Features

The AcroFlex is the only known TDR device to use a hexane based polyolefin rubber core.

5.2.2.2 Mechanical Testing

The AcroFlex was tested in vitro with a total of twelve lumbar FSUs (6 L3-L4 and 6 L4-L5) (Manuscript & Proximity 2011). The intact FSU, the FSU implanted with the AcroFlex TDR and the FSU with simulated fibrosis tissue made of household silicone with an elastic modulus of approximately 0.9 MPa were tested (Manuscript & Proximity 2011). The different FSUs underwent axial compressive, flexion/extension, lateral bending and axial rotation testing. For the axial compressive tests, a sinusoidal waveform was used to apply a maximum load of 1500 N at three different loading rates 8, 80, and 800 (N/sec) for three cycles each. A 10 second dwell time was applied between each cycle.

For loads less than 400 N the axial compressive stiffness for a loading rate of 80 N/s was 1.46 ± 1.07 kN/mm and 0.38 ± 0.22 kN/mm for the intact and TDR implanted specimens respectively. For loads greater than 400 N the axial compressive stiffnesses were 3.01 ± 0.86 kN/mm and 1.02 ± 0.32 kN/mm for the intact and implanted specimens (Manuscript & Proximity 2011). The AcroFlex TDR did manage to have a non-linear sigmoidal response to axial compressive loading (Figure 37) which is very similar shape to the natural disc. However, the magnitude of the stiffness is dissimilar to that found in (Figure 19).

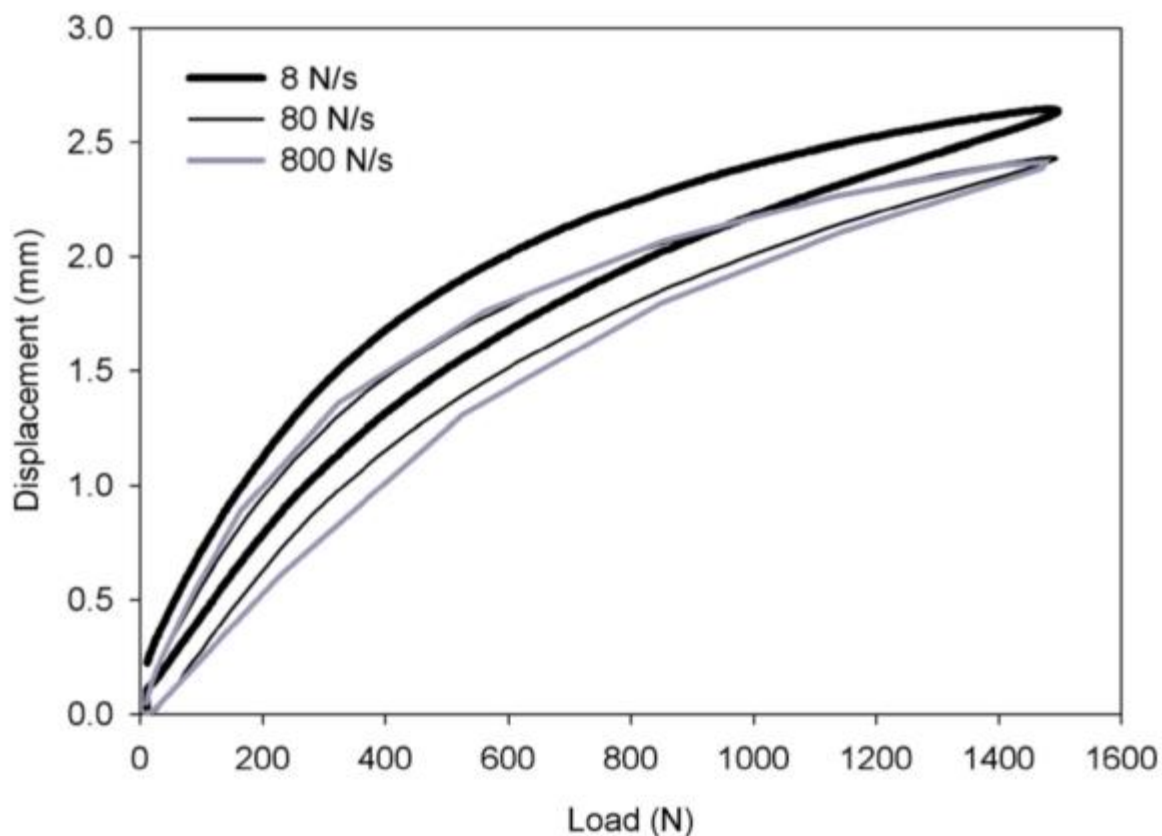


Figure 37: AcroFlex axial compression load-displacement response at 8, 80 and 800 N/sec loading rates (Manuscript & Proximity 2011).

For the remaining tests a sinusoidal ± 7.5 Nm bending moment combined with 100 N of compression was applied at a 0.04 Hz. Again the shape of the AcroFlex response to bending was similar to that of a natural disc (Figure 19). The range of motion of the AcroFlex and intact FSU for the different bending and axial rotation regimes was also measured (Table 31).

Table 31: The range of motion of the AcroFlex implanted FSU with simulated fibrosis tissue compared to the intact FSU for flexion/Extension, lateral bending and axial rotation (Manuscript & Proximity 2011).

Type of Loading	Intact	AcroFlex
Flexion/Extension	$8.7^\circ \pm 4.5^\circ$	$9.0^\circ \pm 3.7^\circ$
Lateral Bending	$8.9^\circ \pm 2.5^\circ$	$10.6^\circ \pm 3.4^\circ$
Axial Rotation	$1.8^\circ \pm 1.1^\circ$	$2.8^\circ \pm 1.4^\circ$

5.2.2.3 Clinical Trials

The AcroFlex underwent a baboon animal model biomechanical, histological and biological ingrowth investigation (Cunningham, Dmitriev, et al. 2003). The testing revealed no loosening and good ingrowth at the endplate bone interface. Histology tests revealed no local

or systemic accumulation of wear particles. However, the AcroFlex group did show decreases in axial rotation, flexion/extension and lateral bending after 6 months of implantation.

Unfortunately, during the two human pilot tests the AcroFlex mechanically failed due to the development of tears in the rubber core and wear related osteolysis. These failures were not obvious from regular clinical CT and were discovered from thin section CT images with an accuracy of 0.25 mm (Fraser et al. 2004). The total number of patients enrolled in the two pilot tests was 28; with 11 receiving the original flat endplates (pilot 1) and 17 receiving the modified central ridge endplate design (pilot 2). A total of 7 devices failed due to minor anterior tears in the elastomer core (3 from pilot 1 and 4 from pilot 2). Another 3 had large anterior tears (2 from pilot 1 and 1 from pilot 2) (Fraser et al. 2004). These mechanical failures were unexpected as the in vitro biomechanical testing indicated that the AcroFlex would be capable of withstanding in vivo loads and was estimated to have an in vivo fatigue life of at least 10 years (Section 5.2.2.2) (Fraser et al. 2004; Manuscript & Proximity 2011; Meir et al. 2013).

A 10-year clinical outcome study was also performed on those that still had the AcroFlex implanted from the pilot studies. The cumulative survival of the AcroFlex was 60.7% from the 28 subjects included in the study. The most common mode of failure was due to device failure occurring in 7 patients followed by severe pain that occurred in 4 patients (Meir et al. 2013). Mean ODI at ten years was 25 ± 17.6 and 41.8 ± 26 for non-revision and revision patients respectively. Improvement of ODI for successful patients was 17.9 ± 16.9 at 10 years compared to 12 ± 16.1 for revision patients (Meir et al. 2013).

The failure of the AcroFlex in vivo was believed to be due to the coupled moments that occur on the annulus of the disc being greater than first thought (Fraser et al. 2004). The poor clinical outcomes in terms of premature failure resulted in the AcroFlex not reaching further developmental stages (Meir et al. 2013).

5.2.3 FlexiCore®

5.2.3.1 Design Features

The FlexiCore was developed by Stryker and is a metal on metal cobalt-chrome ball and socket TDR (Cheung et al. 2016; Premera Blue Cross 2016). The device is packaged in two pieces which are press fit into a single unit which are linked by a captured ball and socket before implantation (Errico 2005; Frelinghuysen et al. 2005). The cobalt-chrome endplates have three 1.5 mm tall teeth on lateral edges of each endplate (Figure 39)(six in total) for

initial stability and they are covered by a titanium plasma to assist with bone ingrowth (Cheung et al. 2016; Frelinghuysen et al. 2005).

The rationale behind containing the CoR for the FlexiCore was that they believed in healthy individuals minimal motion of the NP occurs during bending; in particular during flexion and extension, due the resistance by the side of the AF that is in tension (posterior for flexion and posterior for flexion)(Valdevit & Errico 2004). The chosen location of the CoR for the FlexiCore was in the middle of the disc which doesn't agree with the literature from Section 4.13.

5.2.3.1.1 Unique Design Features

Unique design features of the FlexiCore is that it has channels and a shield in the ball and socket articulation that limits rotation to less than 7.5° in flexion or extension and 3° in lateral bending (Valdevit & Errico 2004). The shield and ball and socket articulation also fully constrain the CoR (Figure 38)(Frelinghuysen et al. 2005; Errico 2005).



Figure 38: Deconstructed FlexiCore TDR (Valdevit & Errico 2004).

Another key design feature is the dome shaped endplates that are 1.5 mm at the domes apex and approximate the concavities of the vertebral endplate to allow a closer fit (Figure 39)(Cheung et al. 2016; Frelinghuysen et al. 2005)

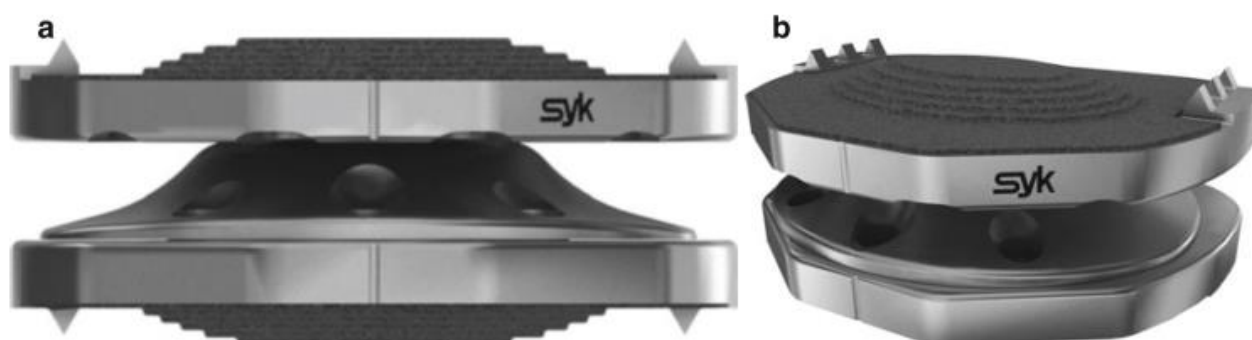


Figure 39: Assembled FlexiCore artificial disc. Note the unique domed vertebral endplates (Cheung et al. 2016).

5.2.3.2 Mechanical Testing

The FlexiCore was mechanically tested in a number of ways. The plasma spray coating was tested in a tensile test statically to determine the detachment strength. A peak stress of approximately 70 MPa was recorded and there was good reproducibility between the different TDRs that were tested (Valdevit & Errico 2004).

The fatigue strength of the FlexiCore was also tested in axial compression and in axial shear (placed 45° to the horizontal and then axially loaded). The test was conducted for 10 million cycles; which is reasonable number of cycles at a peak physiological load during activities of daily living, or until failure in order to determine the stress vs number of cycles (S/N) curve (Valdevit & Errico 2004). Axial compression tests were loaded at 60 Hz and shear at 40 Hz. The valley and peak compressive force applied in each of the test were -300 N and -3250 N respectively (Valdevit & Errico 2004). Data was acquired at 15,000 cycles and then at intervals of 250,000 cycles and net deflection was calculated. The loading and unloading phases of the tests were then analysed using linear regression to calculate the stiffness from the slope of the load deformation curves in the linear region. The stiffness was calculated initially and then at 1,2,5 and 10 million cycles. ANOVA analysis was then performed to compare the stiffness at the different stages of testing (Valdevit & Errico 2004). No significant changes in deflexion were detected beyond 250,000 cycles (Valdevit & Errico 2004). A significant difference ($p < 0.05$) in the stiffness between the initial stiffness of the TDR and the following stiffness's at the different number of cycles was observed during axial fatigue testing. However, no significant changes in stiffness were found between 1, 2, 5, and

10 million cycles of loading. The shear fatigue tests revealed that the stiffness was significantly different between the initial and all other cycles. The stiffness after one million and ten million cycles were also significantly different.

5.2.3.3 Clinical Trials

The FlexiCore was enrolled in a FDA IDE trial which has since been completed. However the FlexiCore is no longer commercially available (Cheung et al. 2016). The ODI and VAS scores of the FlexiCore from a 2-year comparative study to fusion has been completed (Figure 65, Figure 66). The clinical trial compared the FlexiCore TDR group (N=44) to a fusion control group (N=23). The mean preoperative ODI scores for the FlexiCore and fusion groups were 62 and 58 respectively. The scores then fell to 6 and 12 respectively after 24 months (Sasso et al. 2008). The VAS scores also fell from 86 to 16 for the FlexiCore group compared to 82 to 20 for the control after two years.

5.2.4 Kineflex

5.2.4.1 Design Features

The Kineflex (originally Centurion) is a metal on metal mobile core lumbar TDR developed in South Africa. It was first implanted during clinical trials in 2002 (Hahnle et al. 2007). The Kineflex has CoCrMo endplates with a sliding core (Figure 40). Each endplate is fitted with a keel to allow initial stability. The Kineflex allow 12° of flexion/extension and lateral bending. The inferior baseplate has a retaining ring that limits all translations of the TDR to 2 mm from the neutral central position, resulting in a total of 4 mm of translation being possible (Hahnle et al. 2007)(Figure 40). A re-centring force generated by the core will act to oppose translations greater than the described limits (Hahnle et al. 2007).



Figure 40: Kineflex TDR. (a) The baseplate and metal mobile core, (b) an assembled Kineflex TDR and (c) the base plate and superior endplate (Cheung et al. 2016).

5.2.4.1.1 Unique Design features

The sliding core of the Kineflex TDR is available in CoCrMo and polyethylene; which is quite different to other mobile core TDRs such as the CHARITE; which are only available with a polymer core (Section 5.2.1.1)(Cheung et al. 2016; Hahnle et al. 2007).

5.2.4.2 Clinical Trials

A five-year clinical trial comparing the outcome of the Kineflex (N=204) and a CHARITE control group (N=190) has been completed (Guyer et al. 2016) (Figure 65, Figure 66). ODI scores for both groups were approximately 60 preoperatively and decreased to approximately 20 after both a two and five year follow up. A large proportion of both groups meet the 15-point decrease in ODI score at 24 months, with 86.5% and 84.9% of the Kineflex and control group showing this improvement respectively (Guyer et al. 2016). VAS scores like ODI score significantly decreased after 6 weeks and remained significantly reduced compared to preoperative score at five years postoperatively (Guyer et al. 2016).

5.3 Currently on the Market

5.3.1 M6-L®

5.3.1.1 Design Features

The M6-L is an elastomer core TDR (Veruva et al. 2014). It is comprised of two titanium endplates with a double low profile keels sprayed with titanium plasma, an artificial polycarbonate – polyurethane viscoelastic nucleus, ultra-high molecular weight polyethylene (UHMWPE) artificial annulus and a viscoelastic sheath (Figure 41) (Spinal Kinetics 2009; Reeks & Liang 2015).



Figure 41: M6-L cross section exposing the different components of the design; artificial nucleus, artificial annulus, sheath and titanium endplates (left) and an assembled M6-L TDR (Spinal Kinetics 2009).

5.3.1.1.1 Unique Design Features

The multi component design of M6-L is unlike any other TDR. It incorporates separate parts to attempt to mimic the different physiological components of the natural disc and has a separate NP and AF respectively.

5.3.1.2 Mechanical Testing

The kinematics of the M6-L have been compared to the L4-L5 index levels of the natural disc for two different magnitudes of follower loads. The resulting load displacements curves of the intact spines and the implanted spines have been calculated (Figure 42).

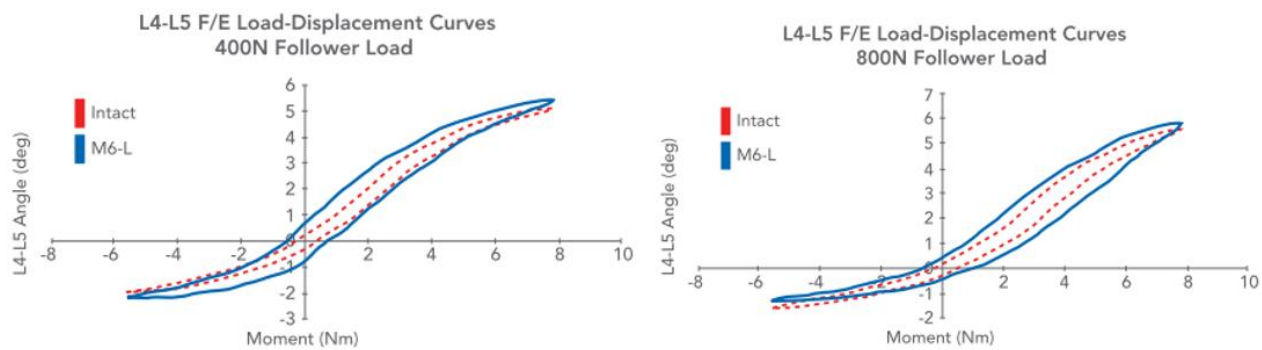


Figure 42: Comparison of the intact L4-L5FSU load displacement curves for a 400N follower load (left) and 800N follower load (right)(Spinal Kinetics 2009).

5.3.1.3 Clinical Data

The M6-L underwent a 2 year clinical trial, investigating not only single but multi-level TDR implantations (Schätz et al. 2015). Forty-nine patients were implanted at the single level and the remaining 34 had multiple M6-Ls implanted. Resulting in a total of 121 M6-L disc being implanted (Schätz et al. 2015). Both the ODI and VAS scores were measured pre operatively and at different time points post operatively (Figure 65, Figure 66).

5.3.2 MobiDisc L

5.3.2.1 Design Features

The MobiDisc L was developed by LDR; before being acquired by Zimmer Biomet. It has since been removed from its US FDA IDE trial but is still available elsewhere outside of the US (Kurtz et al. 2009). The TDR comprises of cobalt chromium molybdenum endplates and a UHMWPE unconstrained sliding core (Figure 43)(Zimmer Biomet 2016).



Figure 43: An assembled MobiDisc-L TDR (left) and the mobile core of the MobiDisc-L that allows semi constrained translation in the transverse plane and axial rotation(right) (Zimmer Biomet 2016).

5.3.2.1.1 Unique Design Features

The four peripheral stops that help to control the mobility of the inner core are unique to the MobiDisc-L. These stops allow the core to self-position, theoretically helping to restore the physiological mobility and CoR. It also aids to reduce stresses on the FJs and those generated around and/or within the TDR (LDR 2014). Another unique design feature of the MobiDisc is its anchoring system that fixates the device into the vertebral body (Figure 43,Figure 44). These anchors are self-guiding and are inserted through a special implantation device. Once the anchors have successfully been implanted they clip into the endplates which differs greatly from the keels and spikes used by other TDRs.

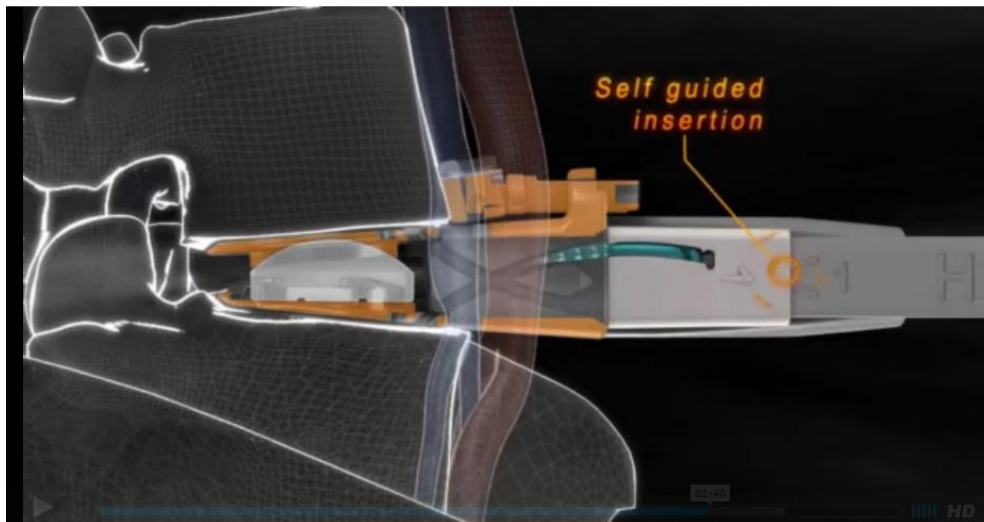


Figure 44: The self-guided insertion tool used to insert the MobiDisc-L anchors (Zimmer Biomet 2016).

5.3.2.2 Mechanical Testing

The RoM and CoR of the MobiDisc-L has been investigated in a minimum 2 year follow up clinical trial. The cohort consisted of 80 patients (Delécrin et al. 2007). After 2 years of implantation 83.1% of the patients had a flexion/extension RoM greater or equal to 2° at the L5-S1 prosthesis level. A further 59.6% of the patients had a RoM greater or equal to 5° at the same level. A similar trend followed at the L4-L5 level with 87% and 66.7% of the patients having a RoM greater or equal to 2° or 5° respectively, two years from implantation (Delécrin et al. 2007).

87% of the patient were also believed to have a physiological CoR restored after TDR implantation (Figure 45).

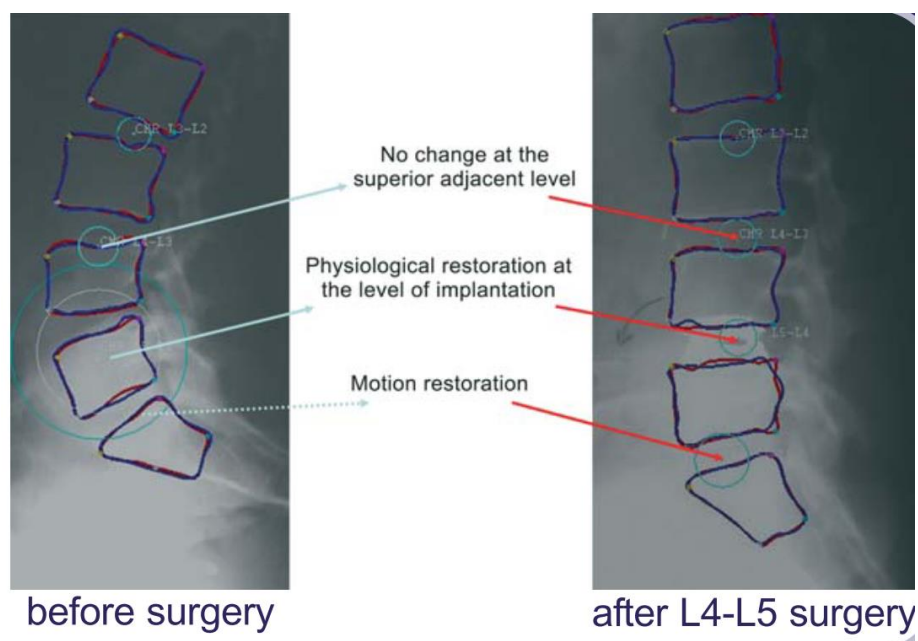


Figure 45: Mean CoR position pre-op and 2 years after MobiDisc-L implantation calculated from SpineView software (Delécrin et al. 2007).

5.3.2.3 Clinical Trials

A two year follow up clinical trial of the MobiDisc-L device has been completed (Figure 65, Figure 66). Eighty patients with a mean age of 41 years were implanted with a MobiDisc-L TDR. Both ODI and VAS scores significantly decreased compared to preoperative scores (Delécrin et al. 2007). After the 24 month follow up, 75% of the patients were satisfied in terms of back pain with 74.4% of the patients record having a ODI score decrease of at least 15 points (Delécrin et al. 2007). No mechanical failures of the TDRs were reported.

5.3.3 XL TDR®

5.3.3.1 Design Features

The XL TDR is a metal on metal TDR that has been developed by Nuvasive (Figure 46).



Figure 46: Assembled XL TDR coronal view (left) and lateral view (right)(AIMIS Spine 2014).

5.3.3.1.1 Unique Design features

XL TDR implantation uses a unique lateral surgical approach as opposed to the regular anterior approach (Section 4.18). The rationale for using a lateral approach is that the resection of the anterior longitudinal ligament and the anterior AF during normal TDR implantation can lead to instability (Pimenta et al. 2015).

5.3.3.2 Mechanical Testing

Six human cadaveric L2-S1 lumbar specimens were subjected to non-destructive multi directional testing. The total intact specimen RoM after ± 8 Nm loading was first recorded and then was reapplied to the specimens after they were implanted with a XL TDR and then reapplied after resection of the AF and ligaments (Pimenta et al. 2015). Flexion, extension and the full flexion/extension bending RoM including both the neutral and elastic zones was calculated. These tests were also performed in lateral bending and axial rotation.

Following XL TDR implantation RoM decreased for all directions of loading and was statistically significant ($p < 0.06$) for all loading cases except for flexion and lateral bending. The neutral zone of loading was also not changed from the intact state ($p < 0.05$) (Figure 47). The removal of the AF and ligaments resulted in a significant increase ($p < 0.003$) in RoM for all loading directions (Figure 47)(Pimenta et al. 2015).

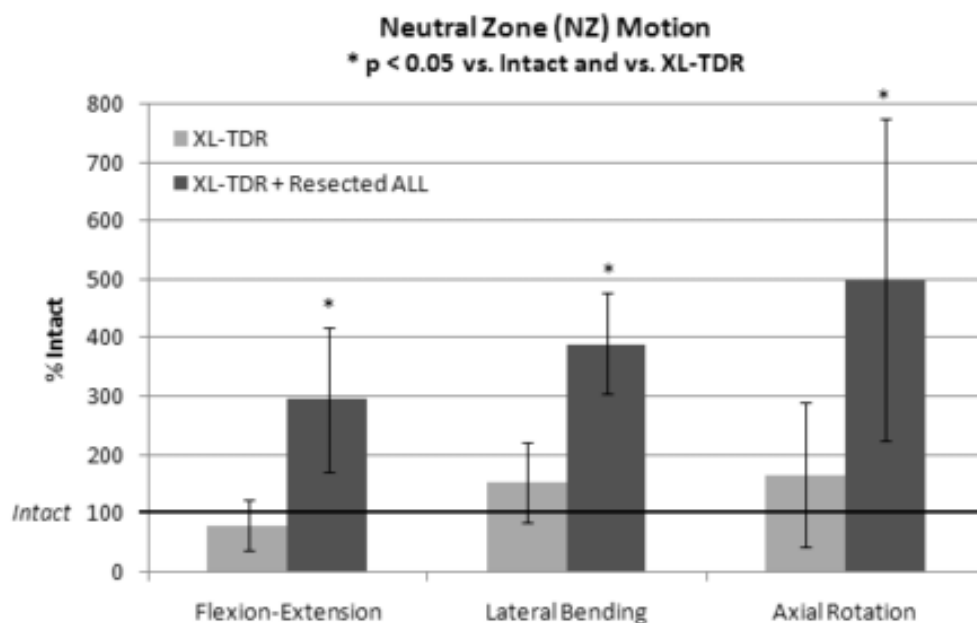


Figure 47: The XL TDR neutral zone motion in flexion/extension, lateral bending and axial rotation compared to the intact for both non and resected AF and ligaments conditions (Pimenta et al. 2015).

This study helped to support the rationale for the lateral implantation approach of the XL TDR.

5.3.3.3 Radiological Testing

X ray analysis at three years post XL TDR implantation found that initial average operated disc height increased from 7.2 mm preoperatively to 12.1 mm following implantation. The disc height then decreased to 10.7 mm three years postoperatively (Tohmeh & Smith 2015). Subsidence greater than 3 mm was found in one of the patients, who lost a reported 8 mm in disc height but was asymptomatic in terms of pain (Tohmeh & Smith 2015).

Flexion/extension RoM was preserved after the three years when compared to preoperative RoM ($p=0.471$).

5.3.3.4 Clinical Testing

A three-year clinical trial investigating the outcome of the XL TDR has been completed (Figure 65, Figure 66). The trial involved 64 patients with a mean age of 45.3 years. Average disc height increased following the procedure with an average increase of 10.7 mm postoperatively at 3 years (Tohmeh & Smith 2015). A clinically significant improvement was defined as a decrease of 15 points in ODI score and a 20 mm decrease in VAS score. At two years 78.3% and 88.3% of patients had a clinically significant improvement in VAS and ODI

pain scores respectively. This proportion of clinically significant improvement increased to 86.7% and 90.0% at three years postoperatively (Tohmeh & Smith 2015).

5.3.4 LP-ESP®

5.3.4.1 Design Features

The LP-ESP is a viscoelastic elastomer core TDR which allows 6 DOF and has shock absorbing properties (Lazennec et al. 2012). The design of the LP-ESP is based on a silent block brush. It comprises of silicone gel nucleus core; with micro voids filled with isobutane, surrounded by a polycarbonate urethane annulus. This disc like structure is then fixed between two titanium endplates (Lazennec et al. 2012). The titanium endplates are coated with a 60 µm T 40 titanium and hydroxyapatite coating and fitted with 5 pegs for initial stability.

Human implantation of the LP-ESP began in 2004, since then a further two generations of design have been developed. The last of which occurred in 2006 and is the current design available on the market (Lazennec et al. 2012). The LP-ESP went on to become the first elastomer core TDR to be validated and authorised for marketing in Europe once it acquired CE marking in 2005 (Lazennec et al. 2012).



Figure 48: CAD exploded view showing the LP-ESP inner silicone gel core and polycarbonate urethane ring (A-C). The actual LP-ESP TDR with titanium endplates and five spikes for fixation (D-G)(Lazennec et al. 2012).

5.3.4.1.1 Unique Design Features

The use of two different polymers in the core of the LP-ESP is unique. The use of female and male caps and inner pegs to stabilise the polycarbonate urethane annulus is also unique. The

components of the TDR are held together with an adhesive moulding technique in conjunction with peripheral grooving on the endplates. This component connection technique is also unique as other elastomer core TDR designs have relied on beads and adhesives alone to join the elastomer core to the endplates (Figure 49). The male and female caps also aid in the compressive properties of the TDR. They are utilised in conjunction with the compressive properties of the elastomer annulus. The contactless design of the two pegs allows compression of the inner core (Figure 49)(Lazennec et al. 2012). The pegs and caps also limit shearing of the core (Lazennec et al. 2012).

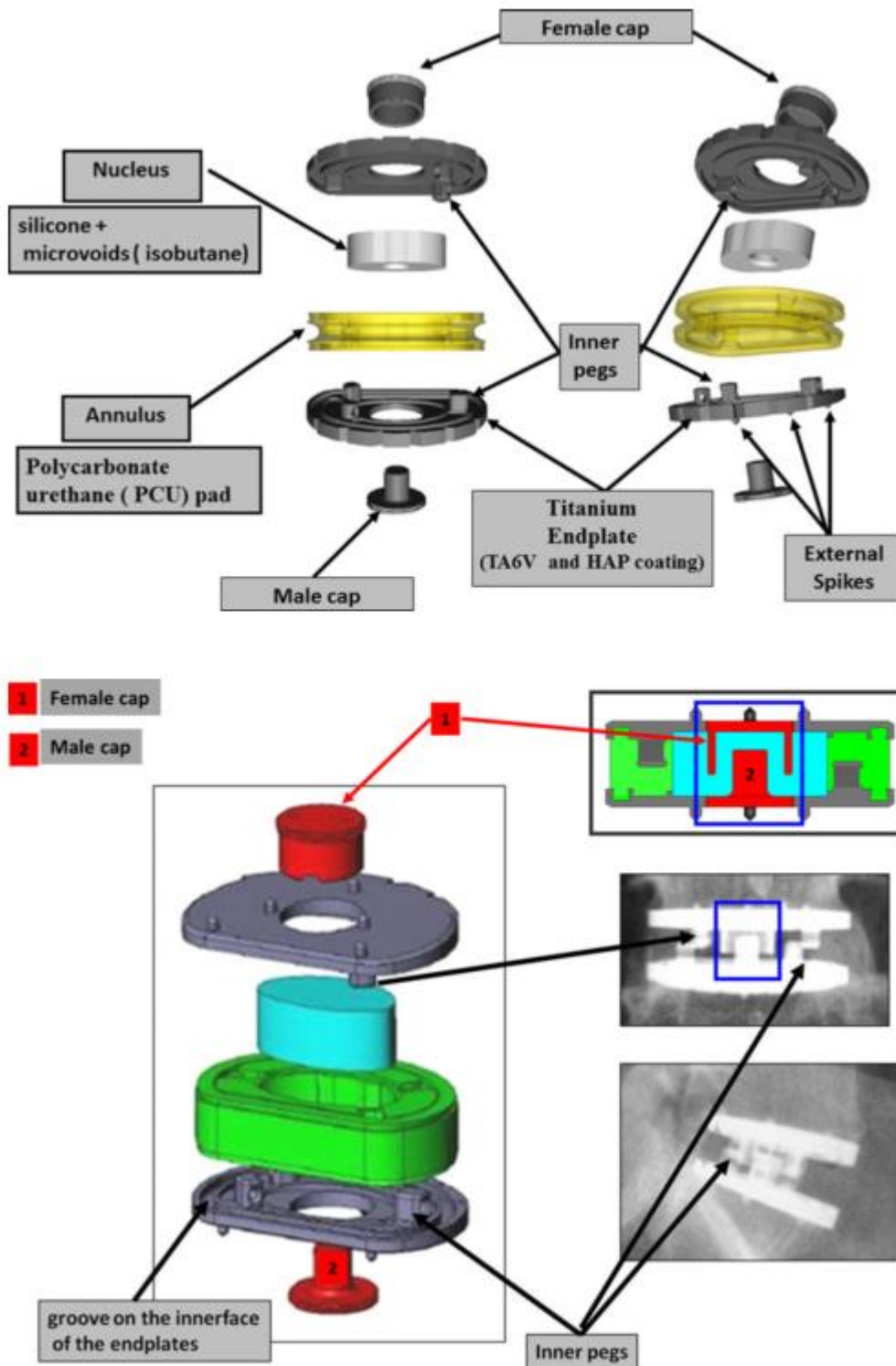


Figure 49: LP-ESP component schematic (Lazennec et al. 2012).

Compression of the annulus during translations occurs between the outer surface of the male peg and the inner surface of the female peg; between the pegs during rotation; and between the endplates during flexion (Lazennec et al. 2013). The endplate pegs and caps protrude into

the elastomer core to help resist loads in different directions; this is again unique to the LP-ESP design.

These design features can be modified in order to obtain an anisotropic loading response. Modifying the different peg and cap configurations by altering their geometric location and size, changes the return torque of the TDR (Lazennec et al. 2012). Altering the distance between the pegs will increase the stiffness of the TDR in rotation without modifying its translation or compressive properties. Decreasing the clearance between the female and male cap increases the stiffness in translation independently of the compressive or rotational properties of the TDR. Finally, changing the ratio of the outer upper and lower annulus diameters relative to the inner middle diameter, alters the return torque between flexion/extension, and lateral bending without altering the other mechanical properties (Lazennec et al. 2012).

5.3.4.2 Mechanical Testing

The LP-ESP has been tested in a range of different loading regimes and has demonstrated similar mechanical properties to the natural disc (Table 32).

Table 32: Comparison of the LP-ESP to the natural disc when loaded in flexion/extension, lateral flexion (also known as lateral bending), torsion, axial compression and elastic recovery (Lazennec et al. 2013; Lazennec et al. 2012).

Pure moments applied in increments up to a maximum value of 10 N/m	References	Level	Natural disk	LP-ESP 2 [®] prosthesis
Flexion–extension	Panjabi [22]	L4/L5	6°	6°
		L5/S1	4°	
	Campana [24]	L1/L2	4°	
		L4/L5	7°	
	Yamamoto [23]	L1/L2	5°	
		L4/L5	7.5°	
Lateral flexion	Panjabi [22]	L4/L5	4°	2.5°
		L5/S1	2°	
	Campana [24]	L1/L2	4.1°	
		L4/L5	6.1°	
	Yamamoto [23]	L1/L2	5°	
		L4/L5	5.7°	
Torsion	Panjabi [22]	L4/L5	2°	2°
		L5/S1	1°	
	Campana [24]	L1/L2	2.4°	
		L4/L5	3.4°	
	Yamamoto [23]	L1/L2	2.3°	
		L4/L5	2.2°	
Axial compression	Gardner-Morse [25]		2,420 N/mm	2,300 N/mm
Variable according to the loading speed, values retained for 0.1 m/s	Virgin [26]		3,000 N/mm	
	Kemper [27]		1,835 N/mm	
	Bouzakis [28]		1,700 N/mm	
Elastic recovery			Yes	Yes

These results support the claims of the LP-ESP that it mimics the natural disc's mechanical properties.

5.3.4.2.1 Creep

The LP-ESP was exposed to 1.25 kN of continuous compression for 122 days. The results showed minimal permanent height loss of 0.1 mm after an eight-hour recover period (Lazennec et al. 2012).

5.3.4.2.2 Combined compression and rotation

The pegs in the annulus were found to absorb approximate 50% of the torque when loaded in a combination of compression and rotation (Lazennec et al. 2012).

5.3.4.2.3 Adhesion of endplates to annuls

Both the 10 mm and 12 mm height LP-ESP TDRs were tested to identify the load needed to cause 1 mm of endplate displacement. The TDRs were tested in either the anteroposterior or mediolateral direction while the opposite endplate was fixed (Figure 50).

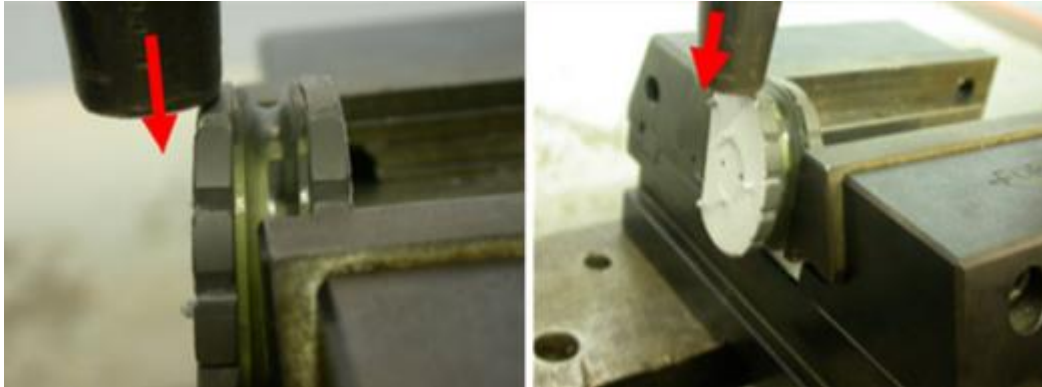


Figure 50: Test setup used to investigate the cohesion of the annulus to the endplates (Lazennec et al. 2012).

The 12 mm TDR needed 450 N to cause 1 mm of displacement in the anteroposterior direction as opposed to the 800 N needed for the 10 mm TDR. To displace the LP-ESP by 1 mm in the mediolateral direction 550 and 600 N respectively was needed for the 12 mm and 10 mm TDR variations (Lazennec et al. 2012).

5.3.4.2.4 Compression Tests

It has been suggested that the disc is permanently damaged after being loaded with 3 to 11 kN of force (Table 22)(Lazennec et al. 2012). The LP-ESP sustained 4.8 kN of load for 100 hours followed by a 9.2 kN load for 64 hours, with no irreversible damage to the TDRs was observed (Lazennec et al. 2012).

5.3.4.2.5 Endplate coating test

The endplates are plasma sprayed after the TDR is assembled. This spraying process is exothermic and compressed air is used to keep the temperature at 21°C during normal manufacturing operations. Two coats of the plasma spray were applied to the TDR without any cooling systems activated, to test that the polycarbonate urethane core does not reach temperature of 120°C where deterioration may occur. The temperatures did not reach a level that would pose a risk (maximum recorded temperature= 60.1°C) (Lazennec et al. 2012).

5.3.4.3 Clinical Trials

A two-year clinical trial where 120 patients were implanted the LP-ESP TDR has been completed (Figure 65, Figure 66). No device failures or major complications occurred during the clinical trials. ODI scores significantly decreased between the preoperative and 3 month scores and between the 3 and 6 month scores before stabilising (Lazennec et al. 2014). Flexion/extension ROM after two years was 5.4° on average with 76% of patients being deemed mobile (flexion/extension of at least 2°) at 24 months (Lazennec et al. 2014).

5.3.5 ActivL®

5.3.5.1 Design Features

The activL Lumbar disc replacement prosthesis was developed by Aesculap Implant Systems and is the most recent TDR to gain FDA approval (2015). It is recommended for use at a single lumbar index level at either the L4-L5 or L5-S1 level (FDA 2015b; Aesculap Implant Systems 2015). The ActivL utilises a mobile ball and socket design which is constrained to only allow translation in the sagittal plane to help reduce facet degeneration (B.Braun Australia 2015). The slightly convex endplates are made of cobalt chromium with a Plasmapore™ μ -CaP (titanium and microscopic calcium phosphate) coating which are joined by a polyethylene inlay (Figure 51)(Miller et al. 2016).



Figure 51: The ActivL different components. Inferior endplate (left), inlay (centre) and superior endplate (right) (Miller et al. 2016).

5.3.5.2 Unique Design Features

With an available constructed height of 8.5 mm the ActivL is the shortest TDR with FDA approval; only the Baguera-L has a smaller constructed height of 8.0 mm which is available outside of the US (Section 5.3.9)(Miller et al. 2016; FDA 2015b). The 8.5 mm total height variation was implanted in 87% of the patients enrolled in the ActivL IDE study (Aesculap Implant Systems 2015).

A unique characteristic of the ActivL is the shape of the S1 inferior endplate (Figure 52). The posterior edge is purposely rounded compared to the more square standard endplate to prevent the edges from protruding into the spinal canal (Miller et al. 2016).

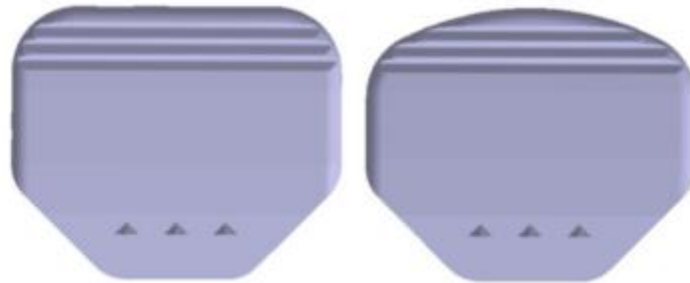


Figure 52: The standard shape of the ActivL TDR (left) and the specialised S1 endplate shape (right) (Miller et al. 2016).

Another unique characteristic is that the ActivL endplates are available in either keel or spike configuration to allow variability based on patient endplate shape and surgeon preference (B.Braun Australia 2015).



Figure 53: ActivL keel (left) and spike (right) endplate design(FDA 2015b).

5.3.5.3 Mechanical Testing

A series of mechanical tests were performed on the ActivL in order to gain FDA approval (Table 33)(FDA 2015b).

Table 33: Series of mechanical tests submitted as part of the ActivL FDA approval process (FDA 2015b).

Test Name	Purpose	Method	Acceptance Criteria	Results
Static Endplate Expulsion	To evaluate the loads required to expulse the activL® device.	Five (5) activL® spiked endplates and five (5) activL® keeled endplates were inserted onto custom grade 15 polycarbonate urethane foam blocks with a 1mm thickness of grade 80 foam on the surface to simulate the denser bone of the endplate. A 450 N axial load was applied. Shear load was applied to the endplate at 5 mm/min. The force necessary to dislodge the endplates was measured.	The shear load endured by the activL® endplates and simulated bone should exceed the maximum shear forces in the lumbar spine of 400 N.	The maximum shear force measured was 1258.82 ± 60.44 N in the activL® spiked endplates and 494.82 ± 13.88 N in the activL® keeled endplates.
Subsidence	To evaluate the activL® implant's resistance to subsidence into the vertebral endplate.	Five (5) activL® spiked endplates and five (5) activL® keeled endplates were compressed into custom grade 15 polycarbonate urethane foam blocks with a 1mm thickness of grade 80 foam on the surface to simulate the denser bone of the endplate ⁴ . Load was applied at 0.1mm/min. The maximum subsidence load was measured.	The fatigue loads endured by the activL® should exceed the maximum axial forces of 3400 N.	The maximum subsidence load was 5760.57 ± 391.47 N for the spiked endplates and 5567.74 ± 458.01 N for the keeled endplates.

Static Compression Shear	To evaluate the performance of the activL® under static compression-shear loading.	Five (5) activL® specimens with spiked endplates and five (5) activL® specimens with keeled endplates were tested under static compression-shear (10° angle) in saline at 37°C at a rate of 50N/sec until failure.	The loads endured by the activL® should exceed the fracture load of the L5 vertebral body (5500 N).	The mean yield load of the specimens was 6625.53 ± 272.49 N for the spiked specimens and 6911.44 ± 231.13 N for the keeled design.
Dynamic Compression Shear	To evaluate the performance of the activL® under dynamic compression-shear loading.	Seven (7) activL® specimens were tested under compression shear loads (10° angle) in saline at 37°C using a sinusoidal wave form with R = 10 at 5 Hz until 10 million cycles or failure.	The fatigue loads endured by the activL® should exceed the maximum in vivo axial forces (3400 N).	Four (4) activL® specimens ran out to 10 million cycles at 4000 N with no failure.
Creep Characterisation	To evaluate the creep characteristics of the activL® device.	Six (6) specimens of each the 14 mm (tallest) and 8.5 mm (shortest) activL® UHMWPE inlay was loaded in compression shear (10° angle) in saline at 37°C as follows: 1. Static: 300 N for 4 hours 2. Dynamic: 300 N to 1000 N (1 Hz) for 16 hours 3. Static: 300 N for 8 hours (relaxation phase) 4. Dynamic: 300 N to 2000 N (1 Hz) for 16 hours 5. Static: 300 N for 8 hours (relaxation phase)	The plastic deformations should be smaller than the diurnal changes of the intervertebral disc (1.5 mm).	The maximum displacements of approximately 0.5 mm observed were in the 14 mm inlay after the 3000 N cyclic loading. Maximum plastic deformations of approximately 0.16 mm were observed in the same 14 mm specimens.

		6. Dynamic: 300 N to 3000 N (1 Hz) for 16 hours 7. Static: 300 N for 8 hours (relaxation phase)		
Subluxation	To characterize the shear force necessary to cause subluxation of the superior endplate relative to the polyethylene core.	Twenty (20) activL® specimens were tested in the following configurations: five (5) in neutral position loaded posterior-to-anterior, five (5) in neutral position loaded medial-lateral, five (5) in maximum flexion loaded posterior-to-anterior, and five (5) in maximum lateral bending loaded medial-lateral. Specimens were loaded with a 500 N axial load. Testing was conducted in ambient air. The force necessary to sublux the superior endplate from the UHMWPE inlay was measured.	This test was performed for characterization only.	The mean subluxation force for the various scenarios described was as follows: 0° A-P: 351.82 ± 4.65 N 0° M-L: 324.14 ± 9.66 N 29° A-P: 272.15 ± 4.11 N
Wear/Durability	To determine the wear and durability characteristics of the activL® device under physiologic conditions.	Six (6) activL® specimens were tested per ISO 18192-1 (2004-04-30) to 10 million cycles. A complex loading profile combining flexion/extension, lateral bending, axial rotation, and axial load was applied at a frequency of 1Hz.	The amount of wear debris should be similar to that reported for other lumbar devices.	Average cumulative wear at 10 million cycles was 25.3mg and the mean wear rate was 2.7mg/million cycles. The test setup was unable to create any backside wear

		Specimens were tested in calf serum and deionized water solution with EDTA. Specimens were weighed prior to testing and at each 0.5 million cycle increment.		of the polyethylene inlay.
Impingement	To determine the wear and durability characteristics of the activL® under conditions simulating device impingement.	Six (6) activL® specimens with the largest endplates (XL) and smallest height (8.5 mm) were tested under impingement conditions to 1 million cycles along with two soak controls. Specimens were cycled in flexion-extension 2° past the device range of motion limits in both flexion and extension. A cyclic axial load was applied such that the flexion and extension moments were 8 Nm. Testing was conducted in calf serum in deionized water (20 g/L) at 37°C. Weight measurements and photo documentation was completed at 0, 0.125, 0.25, 0.5, and 1 million cycles. Particulate analysis was completed according to ASTM F1877.	This test was performed for characterization only.	Impingement behaviour of the activL® included contact between the cobalt chromium endplates. Based on gravimetric measurements, the mean total material loss from both endplates was 1.5 ± 0.4 mm ³ . The UHMWPE inlays gained mass during testing.

Wear Debris Particulate Animal Study	To characterize the local or systemic reactions potentially caused by UHMWPE wear debris implanted into the epidural space of New Zealand white rabbits.	Animals were injected with a control solution, low dose (10 million) particles, or high dose (25 million) particles. Animals were sacrificed at three (3) months and six (6) months. There were six (6) animals per group, for a total of 36 animals. Assessments included clinical and neurological observations, and hematological, histological, and gross pathologic methods.	There should be no evidence of neurotoxicity, systemic toxicity, or local effects associated with the UHMWPE particulate debris.	The study showed no evidence of neurotoxicity, systemic toxicity, or local effects associated with treatment with the test article wear debris.
--	--	---	--	---

The static endplate expulsion and dynamic compression test were also performed on a Prodisc-L control TDR. The Prodisc-L was able to only withstand 933 N and 400 N respectively in comparison to the ActivL (Miller et al. 2016).

5.3.5.4 Clinical Trials

A six-year clinical trial comparing the outcome of the ActivL and a Prodisc-L control group has been completed (Figure 65, Figure 66). Both ODI and VAS improvements from the preoperative baseline were superior in the ActivL group. VAS fell from an average of 87 to 9 for the ActivL group compared to 84 to 24 for the Prodisc-L control at 6 years postoperatively. ODI scores also fell from an average of 71 to 17 with the ActivL compared to 64 to 27 for the Prodisc-L (Miller et al. 2016).

5.3.6 Prodisc®-L

5.3.6.1 Design Features

The Prodisc-L was developed by Synthes Spine and was the second TDR device to gain FDA approval (2006). The Prodisc had been in use since the beginning of the 1990s outside of the US prior to FDA approval (Mayer & Siepe 2007; FDA 2006). The fixed ball and socket Prodisc-L endplates are made of ISO 583212 standard cobalt chromium alloy, that are plasma

sprayed with ISO/DIS 5832-2 compliant titanium (FDA 2006). The fixed core is made of UHMWPE and it indicated for single level use between the L3-S1 levels (FDA 2006). The superior and inferior endplates incorporate a keel and lateral spikes for initial stability (Figure 54).

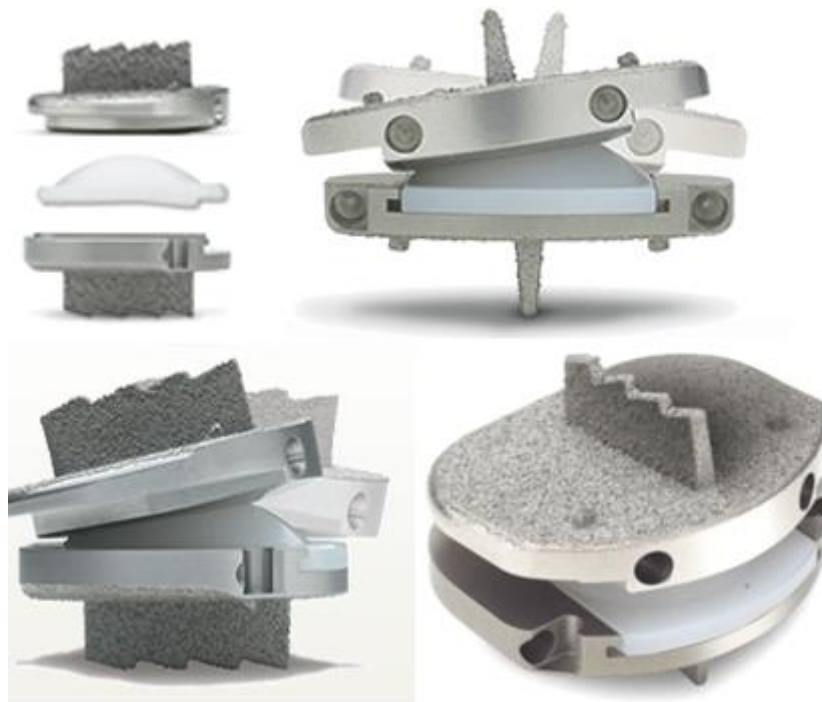


Figure 54: Prodisc-L exploded view showing the superior endplate, inlay core and inferior endplate (top left), the Prodisc-L in lateral bending (top right), the Prodisc-L in flexion and extension bottom left and an assembled Prodisc-L (bottom right) (Synthes Spine 2006).

The Prodisc-L comes in a number of configurations and is available in a number of different sizes (Table 40, Table 41, Table 42 and Table 43).

5.3.6.2 Mechanical Testing

Both the 10 mm and 14 mm height Prodisc-L TDRs were tested mechanically as part of the FDA approval process. The medium sized endplates with 6° of lordosis in the superior endplates were used for the tests (Table 40).

5.3.6.3 Static Compression Shear Test

The TDRs were tested at 10° and 5° of flexion or extension respectively at room temperature (20°C) after being kept in a 37°C water bath just prior to testing (FDA 2006). Axial load was applied at 1 mm/minute and stopped after 5 mm of displacement of the actuator or after 25 kN of force application (maximum possible by Zwick 1485 testing machine used in the experiment)(Table 34)(FDA 2006).

Table 34: Mean and standard deviation of the ultimate force and displacement at ultimate force from the Prodisc-L static compression shear test (FDA 2006).

Implant	Samples	Mean Ultimate Force (N)	Displacement at Ultimate Force (mm)
<u>10° Flexion</u>			
10mm	6	8625 ± 308	3.34 ± 0.38
14mm	6	7800 ± 191	2.80 ± 0.11
<u>5° Extension</u>			
10mm	6	18,883 ± 930	1.47 ± 0.07
14mm	6	19,617 ± 334	3.00 ± 0.05

The flexion group all failed due to shearing of the TDR off the inlay, whereas the extension group failed by shearing of the snap in feature used to lock the inlay into the inferior endplate (Figure 55). This resulted in anterior expulsion of the inlay (FDA 2006). These failure loads are much greater than expected in-vivo loads.

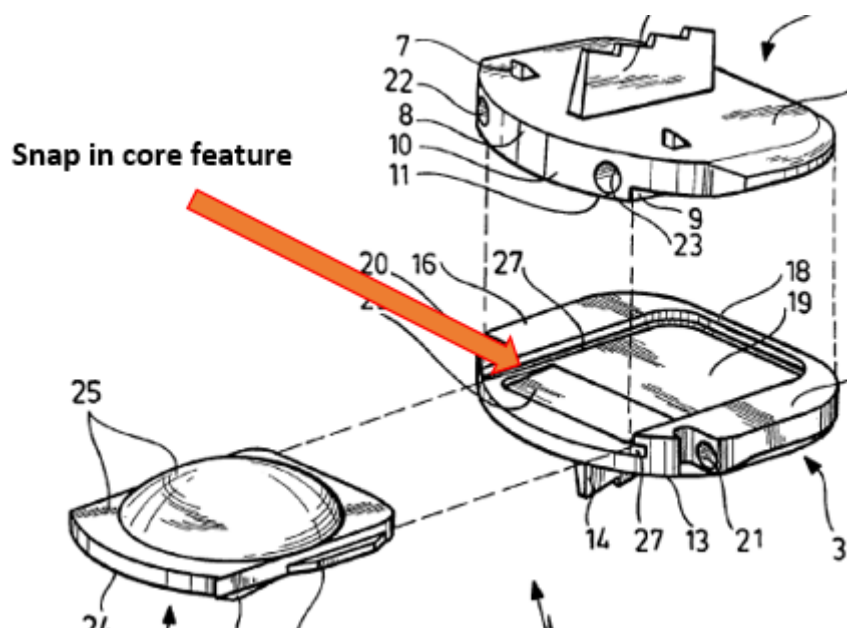


Figure 55: The Prodisc-L snap in core feature used to lock the inlay into place (Marnay & Beyersdorff 2005).

5.3.6.4 Dynamic Compression Shear Test

Fourteen TDRs were implanted into test blocks with fixation achieved using adhesive. They were then tested at a 10° to the horizontal shear angle, after being kept in a 0.9% saline solution in a 37°C water bath just prior to testing (FDA 2006). The axial load was applied at a load ratio of R=10 (load ratio = max load/min load) at 10Hz for 10 million cycles or to failure. Failure occurred after 2 mm of maximum displacement or metal to metal

impingement of the endplates (FDA 2006). The 10 mm and 14 mm TDRs both withstood the 2 million cycles at 3.114 kN and 2.669 kN respectively (within expected in vivo range) (FDA 2006).

5.3.6.5 Creep

Twelve TDRs; with adhesive bound endplates, were tested with a 38 hour 7 stage loading regime that incorporated both static and dynamic loading after being kept in a 0.9% saline solution at 37°C water bath just prior to testing. The inlay was positioned at a 10° angle to the horizontal and failure was defined to occur after 2 mm of displacement or failure of the implant (FDA 2006). The seven stages of testing were as followed:

1. A static 300N load applied for 3 hours.
2. A dynamic 300 to 1000 N load applied at 1 Hz for 3 hours.
3. A static 300 N load applied for 2 hours.
4. A dynamic 300 to 2000 N load applied at 1 Hz for 6 hours.
5. A static 300 N load applied for 4 hours.
6. A dynamic 300 to 3000 N load applied at 1 Hz for 12 hours.
7. A static 300 N load applied for 8 hours.

This loading regime was developed to represent the typical daily loads of the lumbar spine from activities such as walking, sitting and sleeping (FDA 2006). Displacement of the device was sampled after each of the seven stages of testing. Residual creep deformation was 0.345 mm and 0.349 mm for the 10 mm and 14 mm TDRs respectively.

5.3.6.6 Static Inlay Push Out Test

Six samples of every inlay size (anterior posterior width x lateral width (mm), 26 x 23 (M) and 29 x 25 (L)) (Table 42) for the 10 mm and 14 mm TDR heights were tested after being soaked in a 37°C water bath. The inlays were inserted into the appropriate endplate (Table 40) and an anterior shear load at 1mm/min was applied to the posterior face of the inlay until failure (Table 35)(FDA 2006).

Table 35: The mean and standard deviation ultimate force (N) and displacement (mm) at the ultimate force for the static inlay push out test (FDA 2006).

Implant Height	Implant Size	Ultimate Force	Displacement at Ultimate Force
10 mm	M	911 ± 15	2.43 ± 0.08
	L	875 ± 19	2.24 ± 0.07
14 mm	M	1105 ± 19	3.02 ± 0.04
	L	896 ± 45	2.09 ± 0.15

All failure occurred at the snap in feature of the inlay core at greater than expected in vivo shear loads (Figure 55).

5.3.6.7 Dynamic Inlay Push Out Test

A minimum of six samples of every inlay size (anterior posterior width x lateral width (mm), 26 x 23 (M) and 29 x 25 (L)) (Table 42) for the 10 mm and 14 mm TDR heights were tested while being soaked in a 37°C saline solution. A dynamic anterior directed pure shear force was applied to the posterior face of the inlay with a load ratio of R=10. Testing frequency varied between 1 and 10 Hz to a predefined run out load for 10 million cycles. Failure was defined as gross failure of the implant, when maximum machine load was reached, disengagement of the inlay, or the run out cycle limit was reached (Marnay & Beyersdorff 2005).

Table 36: Prodisc-L dynamic inlay push out test results.

Implant Height	Implant Size	Number of samples	Endurance Limit (N)
10 mm	M	7	500
	L	6	500
14 mm	M	6	500
	L	6	500

Similar to the static push out test (Section 5.3.6.6) all TDRs failed at the snap in core feature (Figure 55). These failure loads were less than those that occurred during the dynamic compression shear tests (Section 5.3.6.4). However, 500N of pure shear is not expect during normal in vivo activity (FDA 2006).

5.3.6.8 Wear Testing

Six 14 mm Prodisc-L TDR were tested at 10° to the horizontal in a 37°C bovine calve serum. They were tested at +6°/-3° flexion/extension at 1.1 Hz, lateral bending at ±2° at 1.05 Hz and axial rotation ±1.5° at 1.16 Hz. A sinusoidal 300 N valley and 1750 N peak load was applied at 1.57 Hz. Resulting in 14.28 million compressive cycles being applied for 10 million cycles of flexion/extension due to the different loading frequencies (FDA 2006). Specimens were weighed at various times to calculate wear rate. Wear debris was collected at 2, 5, 7, 8, 9 and 10 million cycles.

Mean wear rate from linear interpolation was found to be 5.73 mg/million cycles by averaging the amount of wear after 10 million cycles. Initial wear rate was greater during the first 2 million cycles. This reveals that wear will likely occur in vivo however it was found to be within biocompatible limits (FDA 2006).

5.3.6.9 Hysteresis Test

A total of 6 TDRs were tested in a 37°C water bath at 0.01 Hz for a 300 to 3600 N dynamic load range for 2000 cycles, to investigate the amount of permanent deformation. Stiffness and hysteresis of the inlay was measure every 100 cycles or until 2 mm of displacement. Four specimens made it to 200 cycles and two reached the 2 mm displacement failure criteria with none fracturing. Loads in this test are expect to be greater than those in vivo therefore hysteresis failure is unexpected (FDA 2006).

5.3.6.10 Expulsion Test

Six specimens were placed in polyurethane foam blocks and then loaded in anterior shear in ambient conditions until expulsion from the foam block occurred. This test was used to examine the load needed to cause the device to expel from the bone. The TDR was preloaded with 450 N of compression and had shear applied at 5 mm/min until they were expelled or had displaced 5 mm. Shear forces that are greater than 500 N are not expected in vivo and all of the tested TDRs withstood this (Table 37).

Table 37: Mean and standard deviation of the shear force needed to expel the Prodisc-L TDR from the polyurethane block and the corresponding displacement recorded (FDA 2006).

Implant Size	Number of Samples	Shear Force	Displacement
M	3	636 ± 82	1.17 ± 0.24
L	3	685 ± 93	1.40 ± 0.22

5.3.6.11 Clinical Trials

The Prodisc-L has demonstrated a positive clinical outcome over a ten year follow up study (Figure 65, Figure 66). The VAS scores decreased significantly after one and two years postoperatively ($p < 0.001$) (Park et al. 2016). VAS then slightly increased over the next eight years however they stayed significantly lower than the preoperative VAS scores. ODI scores also followed this trend, with a large decrease after two years. The scores then slightly increased over the remaining years. However, all ODI scores were significantly lower ($p < 0.001$) than preoperative scores (Park et al. 2016).

5.3.7 Maverick™

5.3.7.1 Design Features

The Maverick™ ball and socket TDR developed by Medtronic, comprises of a two ASTM standard Cobalt Chromium alloy metal on metal articulating endplates (Medtronic 2002; Marshall, Robert, Neta Raz, Brien & Burke 2014; Assaker et al. 2015). Both of the endplates are fitted keels and the whole endplate surface is plasma sprayed with hydroxyapatite (HA) to encourage bone ingrowth (Medtronic 2002). The ball and socket design constrains the CoR at a posterior position (Medtronic 2002). The Maverick is no longer marketed in the United States due to court ruling favouring the then owner; Synthes for patent infringement with respect to their Prodisc-L design (Premera Blue Cross 2016; Alison 2008).



Figure 56: The two different endplates of the Maverick TDR (left). Note the polished articulating core and an assembled Maverick TDR (right) (Serhan et al. 2011; Errico 2005).

5.3.7.2 Clinical Trials

A two-year clinical trial where 134 patients were implanted the Maverick TDR had been completed. Of the initial 134 patients 104 made it to the final follow up (Figure 65, Figure 66) (Assaker et al. 2015). ODI scores significantly decreased from the preoperative baseline (mean of 50.1) compared to the scores at 6, 12 and 24 months. 75.2% of patients met at 24 months met the FDA 15-point improvement in ODI criteria (Assaker et al. 2015). VAS score also decreased on average for a 10 mm scale from 7 preoperatively to 2.8 at 24 months (Assaker et al. 2015).

5.3.8 Freedom® Lumbar Disc

5.3.8.1 Design Features

The Freedom® Lumbar Disc is a one piece viscoelastic TDR that has been developed by Axiomed. It contains a CarboSil™ TSPU silicone polycarbonate urethane thermoplastic elastomer core, which is situated between two titanium endplates (Figure 57)(Axiomed 2008a).



Figure 57: The Freedom TDR from Axiomed (Axiomed 2008a).

5.3.8.2 Unique Design Features

The Freedom endplates utilises a vast number of teeth, in conjunction with a porous beaded coating, and a two part central keel on the top and bottom endcaps for initial stability into the vertebrae (Figure 58)(Axiomed 2008a).

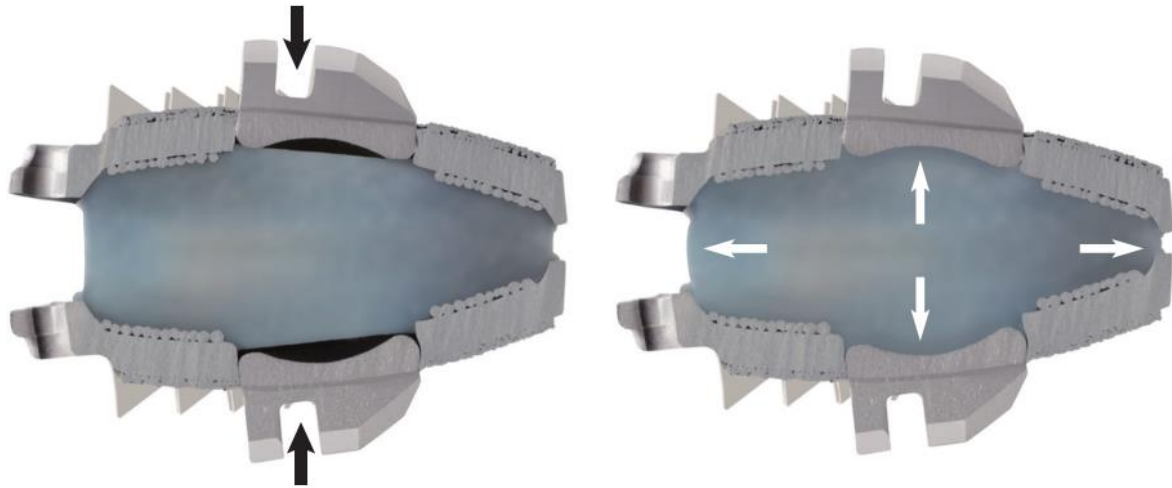


Figure 58: Cross section of the Freedom TDR. Illustrating the unique keels on the top and bottom top caps, void between the endplates, and the metal beads on both the outer endplate surface (for bone ingrowth) and inner endplate surface (for elastomer bond strength)(Axiomed 2008a).

The Freedom also utilised a void between the endplates and elastomer core, which allows the core to approximate the stiffness of the natural disc (Axiomed 2008a). The bonding of the endplates to the elastomer core was of great importance in the Freedom TDR design. A proprietary bonding technique which utilised both chemical and mechanical bonding techniques was used. This allows great bond strength while also having low retained stresses within the core itself (Axiomed 2008a).

5.3.8.3 Mechanical Testing

Majority of mechanical tests conducted on the Freedom were carried out on the worst case scenario size which has 26 x 36 mm endplates, an anterior height of 13 mm and lordotic angle of 12° (Axiomed 2008a). This sizing resulted in the smallest posterior height, core volume and endplate coverage area of the different available sizes of the Freedom. All test specimens were also pre sterilized and soaked in a 37°C saline bath for three days prior to testing to mimic in vivo conditions. Two different types of failure criteria were defined for the testing. Mechanical failure was defined as failure in respect to a defect in the material i.e. a crack in the material. Whereas, functional failure was defined by a permanent deformation or excessive wear which would render the TDR ineffective in vivo. It should be noted that mechanical behaviour can occur without functional failure.

5.3.8.4 Range of Motion

RoM analysis was performed using the 28 x 38 mm endplate variation of the Freedom. These variations had an anterior height of 16 mm and 12° of lordosis. The TDRs were tested under compression, rotation and flexion/extension.

5.3.8.4.1 Compression and Axial Rotation CoR

Axial compression and torsion RoM tests included quasi-static ramps and short term fatigue tests with loads ranging from 400 to 2000 N in compression and ± 6 Nm in torsion. A total of ten TDRs were tested. Displacement RoM data, static stiffness in the range of 400 – 600 N of axial compression or ± 4 Nm of torsion, the dynamic stiffness for one cycle and averaged over the last five cycles, and hysteresis (90th cycle compression, 190th for torsion) was calculated from the results (Table 38).

Table 38: Freedom RoM test results compared to human lumbar RoM (Benzel et al. 2011).

Parameter	VTDR results ^a	Properties of human lumbar disc
		ROM in compression
Stiffness	1.55–3.48 kN/mm	0.5–2.5 kN/mm [23–27]
ROM	0.7–1.3 mm under 2000 N load	0.8 mm under 330 N load [28]
		ROM in rotation
Stiffness	0.72–0.83 N m/deg ^b	2.0–9.6 N m/deg [25,26,29]
ROM	7.6–8.4 deg under 6 N m moment	0–2 deg in healthy volunteers [30]; 1–5.8 deg in cadavers [25,31,32]
		ROM in flexion/extension
Stiffness	Flexion: 1.4–2.12 N m/deg; extension: 1.4–2.14 N m/deg	Flexion: 0.8–2.5 N m/deg [26]; extension: 2.1 N m/deg [26]
ROM	Flexion: 3.0–5.3 deg at 8 N m moment; extension: 1.9–5.0 deg at 6 N m moment	Flexion: 5.5–13 deg [29,30,33]; extension: 1–5 deg [29,30,33]

^aFor worst case to large sized devices.

^bFor family of device sizes.

5.3.8.4.2 Flexion Extension RoM

Ten Freedom TDRs were tested for flexion/extension RoM. The testing regime included quasi-static ramps and short term fatigue tests ranging from 8 Nm in flexion to 6 Nm in extension. RoM and hysteresis at the 400th cycle was calculated from the tests. In addition, the static stiffness and dynamic stiffness at the 380th to the 420th cycles were calculated in the total loading range of 8 Nm to -6 Nm (Benzel et al. 2011)(Table 38).

5.3.8.5 Static Compression

Five Freedom TDRs were tested under displacement control and displaced at 0.2 mm/sec until the load cell maximum of 20,000 N was reached. The Freedom TDR has a nonlinear axial compression response (Figure 59) like the natural disc (Figure 19)(Benzel et al. 2011).

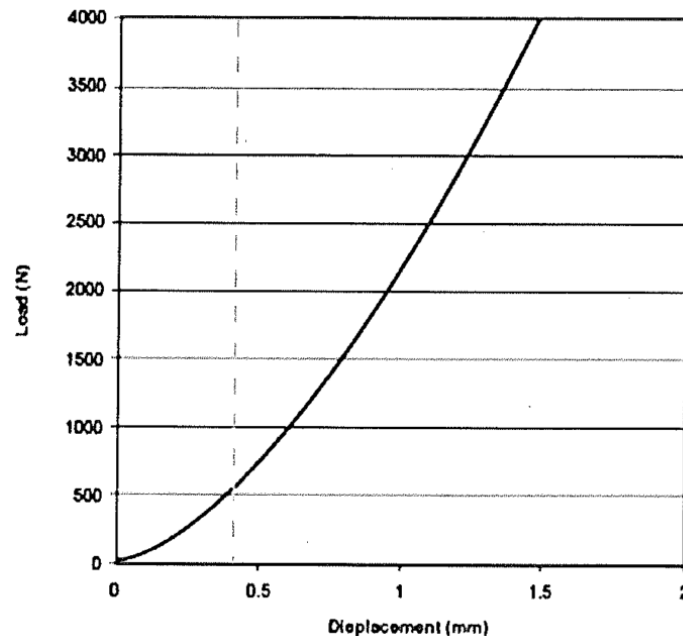


Figure 59: Freedom TDR compression stiffness test response. The dashed vertical line illustrates the boundary (displacement = 0.04 mm) between the neutral zone (left) and the elastic zone (right) (Benzel et al. 2011).

All of the TDRs tested reached the 20,000 N test machine limit with an average of 3.36 mm of displacement.

5.3.8.6 Fatigue

5.3.8.6.1 Compression

Eight TDRs were tested under the ASTM F2346 standard durability assessment method. The TDRs were tested at 3 Hz with varying levels of load to create a well-defined fatigue curve. Testing was performed until functional failure or after 10 million cycles (Benzel et al. 2011). Two devices were tested at compressive loads of 7000 and 6000 N for the 10 million cycles. An additional two TDRs were tested at a lower 2400 N for 50 million cycles. The worst case sized TDR survived for the whole 50 million cycles at 2400 N of compressive cyclic loading. These results favourably compared to average daily living loads, which have been reported to be 1200 N (Axiomed 2008a; Nachemson 1981). Both mechanical and functional failures

occurred for loads in the range of 6000 N to 17,500 N, however these loads are believed to be outside of the physiological range.

The generated fatigue curve shows no failure after 10 million cycles for loads less than 6000 N (Figure 60).

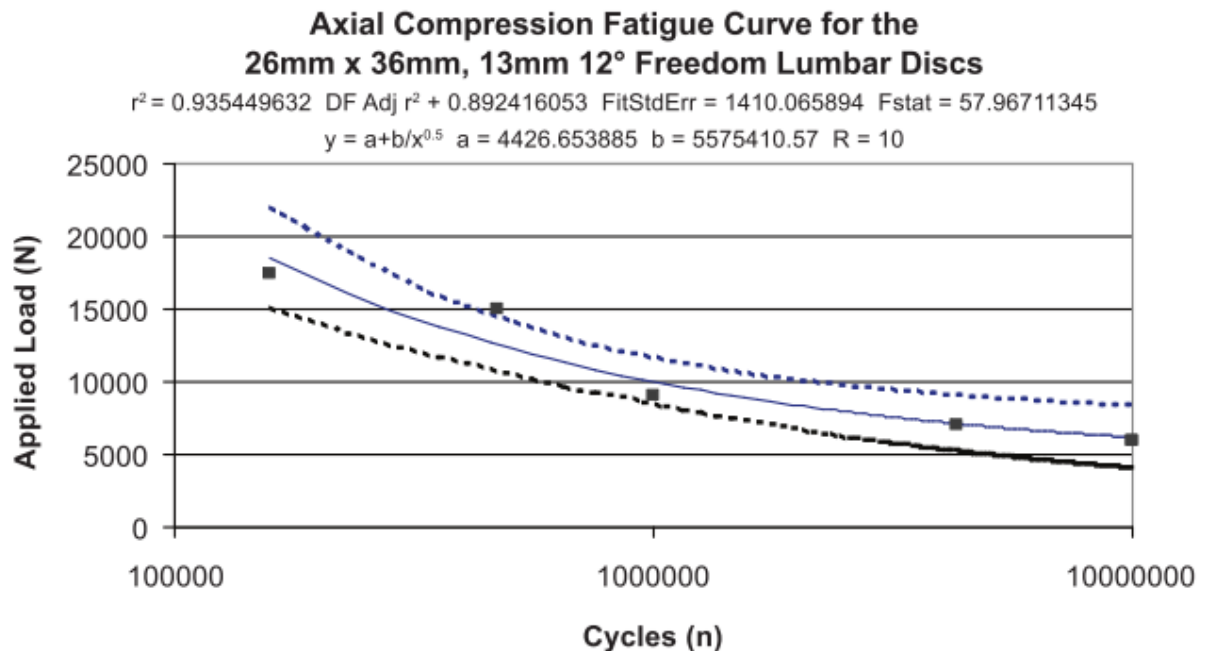


Figure 60: Axial compressive fatigue curve of the Freedom TDR (Benzel et al. 2011; Axiomed 2008a).

5.3.8.6.2 Compressive Shear

Ten Freedom TDRs were tested with a 45° compressive shear for ten million cycles. The devices were tested at 3 Hz and loads were set to range from 1200 to 2000 N. These loading values were derived from literature, which indicated that the fatigue strength of the human lumbar spine in anterior shear is 100 N. The maximum shear load on the human lumbar spine used to compare results was also derived from literature. This maximum shear load is approximately equal to 20 to 25% of the active daily compressive load (Axiomed 2008a). This 25% scaled load equates to approximately 300 N of shear. The converted shear component of load applied to the TDRs during the compressive shear tests was approximately 5 time larger than these maximum in vivo loads (300 N). Dynamic stiffness was calculated for the first 1000 cycles and the cycles to failure was also recorded. All of the TDR sizes including the worst case size survived an anterior shear load of 1697 N for 10 million cycles (Figure 61).

The bonding between the metal EPs and the elastomer core of the TDR has also been classified as a potential ‘weak point’ in the design of the one piece TDR (AxioMed 2008). By orientating the TDR at 45° during these cyclic tests it applies a more severe shear force than would be applied in vivo. The Freedom TDR experienced no endplate/core dislocation or tearing during these tests.

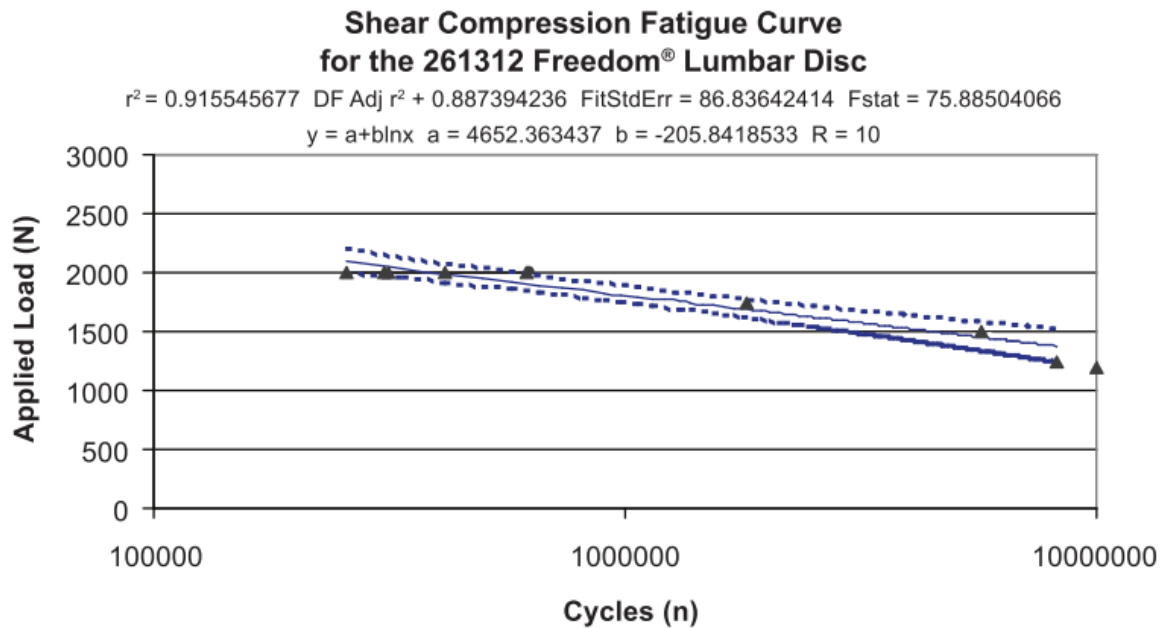


Figure 61: 45° compressive shear fatigue curve of the Freedom TDR. The applied compressive shear loads on 1200 to 2000 N correspond to 1697 to 2828 N of anterior shear load (Benzel et al. 2011; Axionmed 2008a).

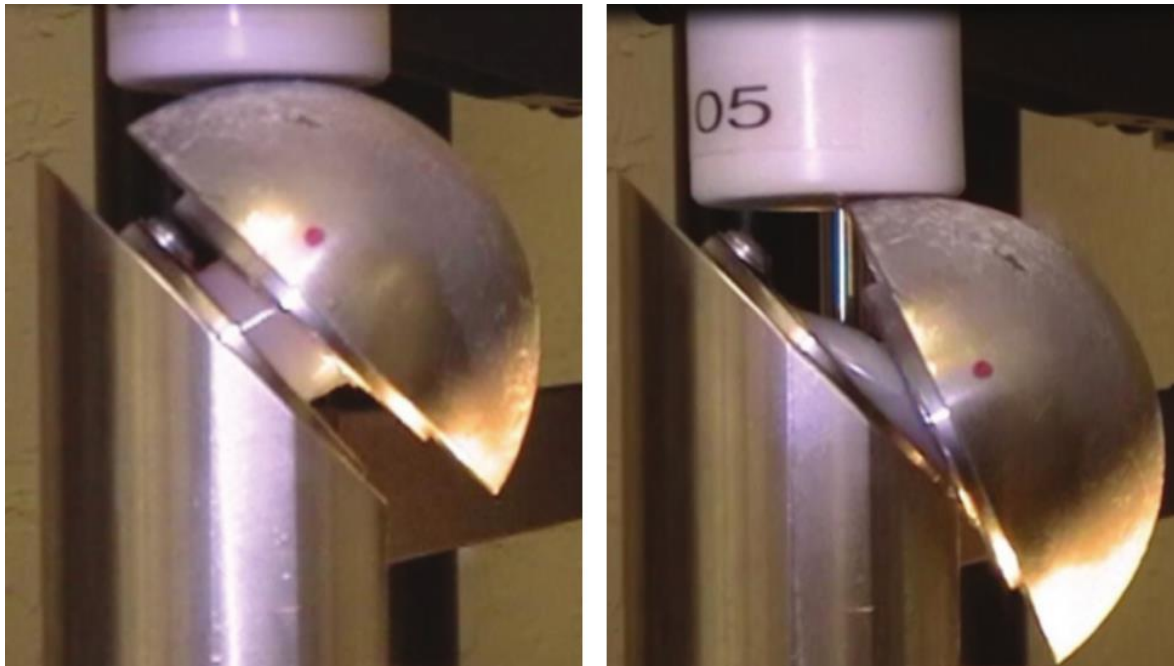


Figure 62: The Freedom TDR tested in a 45° compressive shear test. Note that the core and the endplates remain attached during testing (AxioMed 2008).

5.3.8.6.3 Wear Fatigue

Wear testing of the Freedom TDR comprised of two failure criteria. Firstly, to compare wear rates to the CHARITE and Prodisc-L TDR, and secondly, to assess the fatigue life of the worst case sized Freedom TDR. The Freedom was tested to investigate if it can last without functional or mechanical failure when subjected to ± 7 Nm of flexion/extension bending and ± 7.2 Nm of coupled lateral bending with axial rotation of $\pm 1.7^\circ$ for five million cycles with a 1200 N compressive preload.

Five TDRs were tested for 10 million cycles in each of flexion/extension, lateral bending and rotation, with no functional failures. It has been estimated that 125,000 significant bends occur per year (AxioMed 2008a). Using this estimate 30 million cycles equates to 240 years' worth of significant bends.

The wear rates of the Freedom from these fatigue tests were also compared to the CHARITE and Prodisc-L FDA Summaries of Safety and Effectiveness wear rates and wear particle size data (FDA 2004; FDA 2006)(Table 39).

Table 39: Comparison of the Freedom TDR (FLD) wear test data to the CHARITE and Prodisc-L data (Axiomed 2008a).

DEVICE	TEST DESCRIPTION	TOTAL NUMBER OF DEVICE CYCLES	WEAR RATE (MASS LOSS PER MILLION CYCLES)	AVERAGE PARTICLE DIAMETER
FLD	ASTM, 10M flex/ext + 10M lat bend + rotation	30 million	1.70 mg	1.90 μm
ProDisc-L	ISO, 10M flex/ext + lat bend + rotation	30 million	5.73 mg	0.44 μm
Charite	ASTM, 10M flex/ext + rotation, OR 10M lat bend + rotation	20 million	0.11 mg	0.2 μm

The Freedom wear rate was in between the values of the Prodisc-L and CHARITE given from the Summaries of safety and Effectiveness data. However, the average particle diameter was significantly larger than the other TDRs. This greater wear particle size has shown to be somewhat beneficial as they are less bioactive than smaller particles (Axiomed 2008b) It should be noted that the loading regimes differed for each TDR which may have influenced these differences in results.

5.3.8.7 Clinical Trials

The Freedom TDR has undergone a very successful clinical trial comparing the clinical outcome of Freedom TDRs to clinical data from the SWISSpine Registry (Figure 66). This was due to the Freedom TDR having statistically significant improvement in VAS compared to pooled data from a number of different TDRs on the SWISSpine Registry in a two year follow up study.

5.3.9 Baguera L

5.3.9.1 Design Features

The Baguera L is available as a fixed or mobile core TDR device (Spine Art 2010). It has titanium endplates; covered with a Diamolith® coating, that constrain a polymer core. Each of the endplates are fitted with five fins for initial stability (Figure 63).



Figure 63: Assembled Baguera L TDR (Spine Art n.d.).

5.3.9.2 Unique Design Features

The Baguera L TDR is MRI compatible due to its titanium endplates and Diamolith® coating. This unique Diamolith® coating also helps to reduce the risk of wear generation (Spine Art 2010; Spine Art n.d.; SSJ Health 2010). Another unique design feature of the Baguera L TDR is that it is available with a modular core allowing either a mobile or fixed core to be inserted before implantation depending on patient needs or surgeon preference (Spine Art 2010; Spine Art n.d.; SSJ Health 2010).

5.3.9.3 Clinical Trials

No clinical trials on the lumbar Baguera L TDR were found.

5.3.10 Physio-L

5.3.10.1 Design Features

The Physio-L; developed by Nexgen Spine, is a one piece polycarbonate polyurethane core TDR, intended for use in the L3-S1 lumbar spine (Pimenta et al. 2010; Med Gadget 2008). It has titanium endplates with a low profile keel and numerous titanium beads to allow bone in grow following implantation (Figure 64).



Figure 64: Physio-L TDR (Pimenta et al. 2010).

5.3.10.2 Radiographic RoM and Height Testing

The effect that the Physio-L TDR has on flexion/extension RoM at the operated and adjacent levels has been investigated. The total range of motion after one year increased slightly from $12.0^{\circ} \pm 6.2^{\circ}$ before surgery to $13.3^{\circ} \pm 5.5^{\circ}$. The adjacent level RoM also increased from $10.8^{\circ} \pm 5.5^{\circ}$ to $13.3^{\circ} \pm 5.0^{\circ}$, however RoM remained within normal ranges (Pimenta et al. 2010).

The disc height at the time of surgery, immediately after implantation and after a one-year follow-up was also measured. The mean and standard deviation pre-op disc height was 8.5 ± 2.7 mm and 8.7 ± 1.5 mm for the L4-L5 and L5-S1 levels respectively. Disc height then increased to 13.9 ± 1.6 mm and 15.7 ± 1.4 mm for the L4-L5 and L5-S1 levels immediately after implantation. Little changes in the disc height were measured after one year with the L4-L5 height increasing by 0.1 mm and the L5-S1 decreasing by 0.6 mm.

5.3.10.3 Clinical Trials

A one-year clinical trial where 12 patients were implanted with the Physio-L TDR has been completed (Figure 65, Figure 66). Throughout the clinical trial no signs of subsidence, migration or expulsion were evident (Pimenta et al. 2010). Mean ODI scores were 54.3 preoperatively and fell to 12.7 after one year. VAS scores also decreased from a mean value of 76 to 16.5 at the completion of the trial (Pimenta et al. 2010) . Full extension/flexion ROM was also restored to a mean value of 13.3° which was considered to be normal.

5.4 Summary of Clinical Trials

5.4.1 ODI

The FDA criteria for a TDR to gain approval requires a greater than or equal to 15 point improvement in ODI after 24 months (FDA 2004; Assaker et al. 2015; Miller et al. 2016). The ODI scores from a number of different clinical studies have been summarised (Figure 65). The Physio-L an elastomer core and ball and socket TDR has the best short term postoperative ODI score at 12 months compared to the other published clinical trials included in the analysis. However, in terms of long term clinical success the CHARITE has been found to have the most success in terms of ODI. However, of the TDRs currently on the market the Prodisc-L has the most long-term success in terms of ODI.

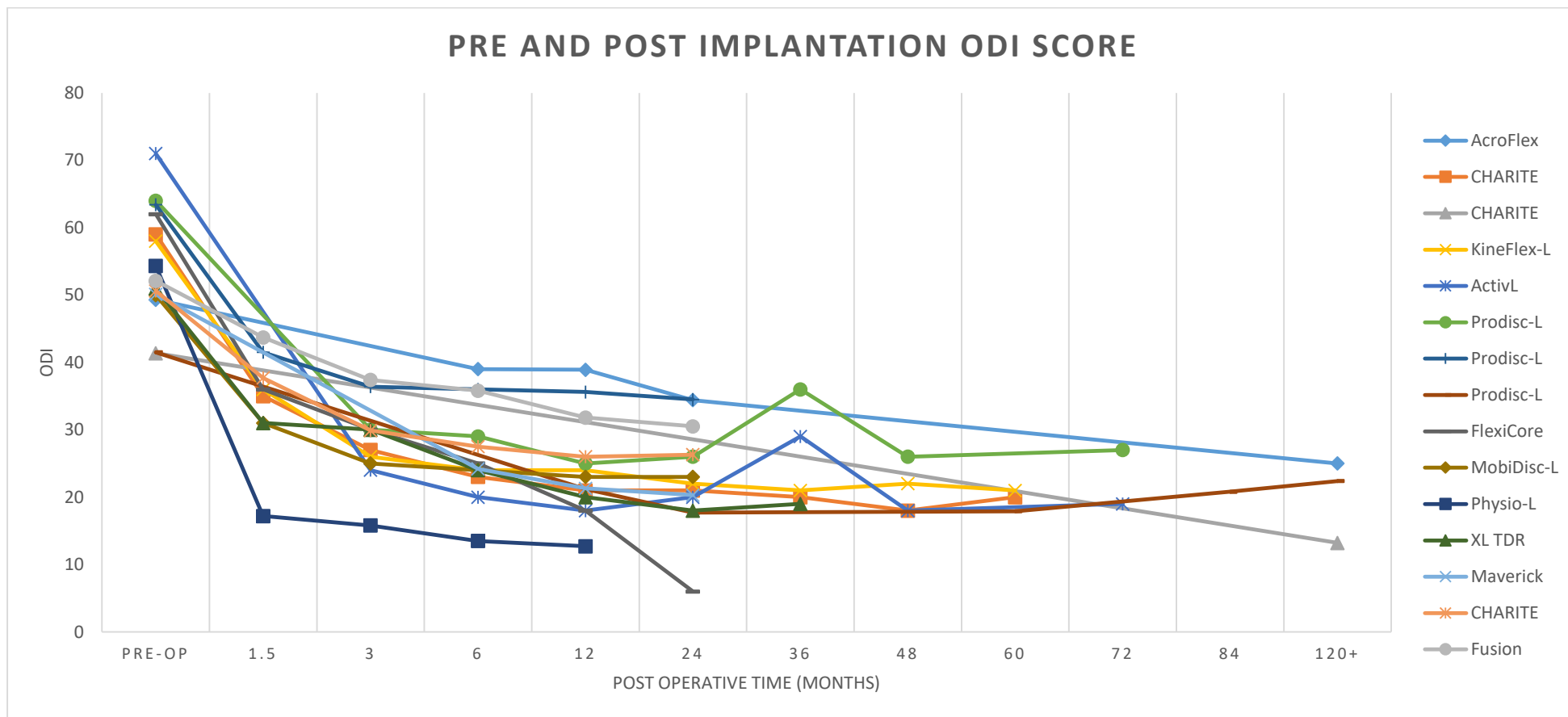


Figure 65: Comparison of mean ODI outcome of different TDR devices (For a tabulated comparison of the data and references to the clinical trials see Appendix C) (Pre-op=before operation).

5.4.2 VAS

In a similar fashion to the ODI scores an elastomer core (Freedom) TDR has had the superior clinical outcome in terms of VAS pain scores after 24 months' post implantation (Figure 66).

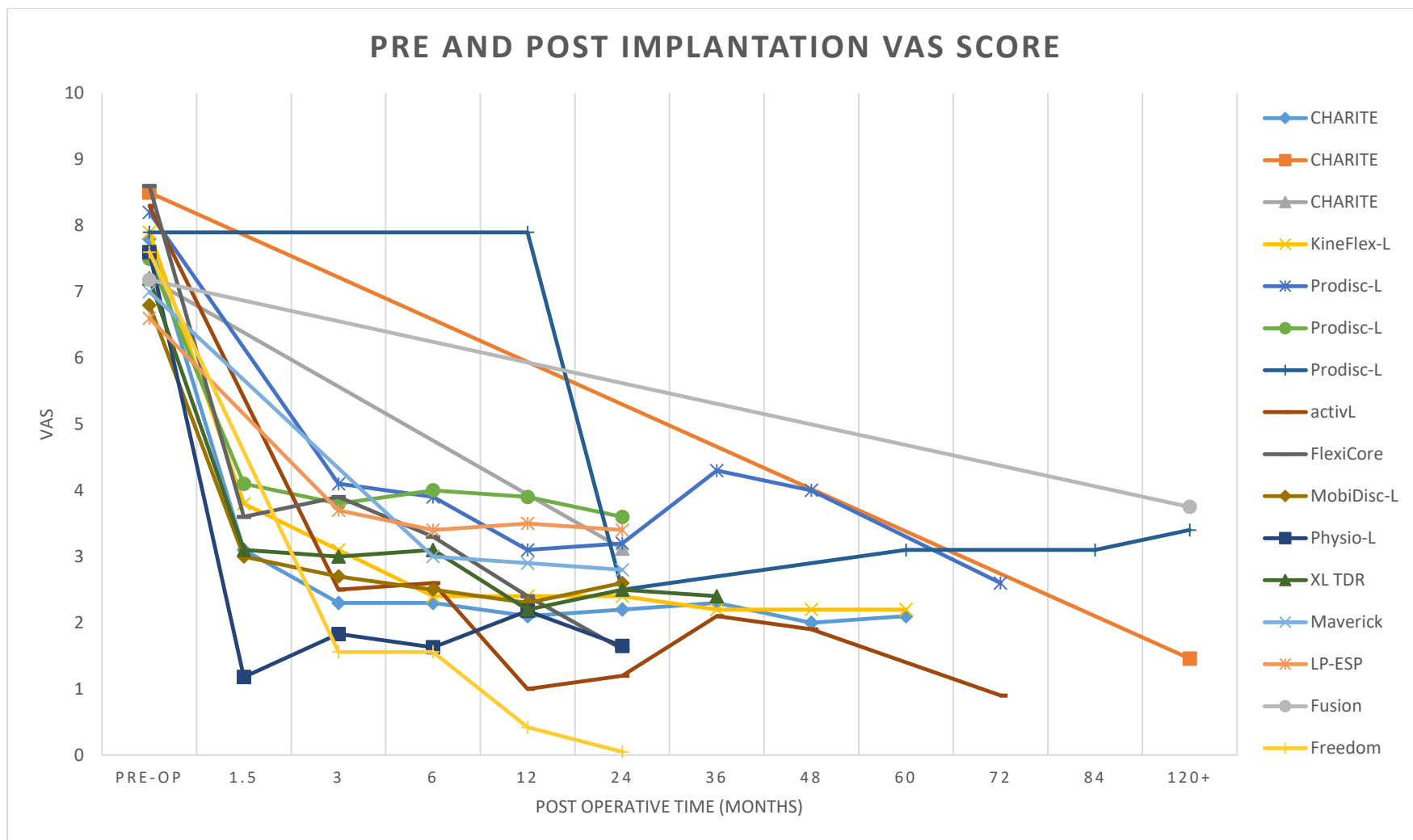


Figure 66: Comparison of VAS outcome of different TDR devices. (scores were scaled to 0-10 values) (For a tabulated comparison of the data and references to the clinical trials) (Pre-op=before operation) For a tabulated comparison of the data and references to the clinical trials see Appendix D) (Pre-op=before operation)..

5.5 Summary of Commercially Available TDR Parameters

A number of different design parameters from commercially available TDRs such as the total height, endplate anterior posterior width, lateral width, TDR height, lordosis angles and materials have been summarised (Tables 40 to 46). These parameters have been used in Chapter 6 to develop the final design specifications in conjunction with anatomical morphological studies (Section 4.2).

Table 40: A summary of the different anteriorposterior (top row) and lateral (bottom row) widths (mm) of a number of different total disc replacements endplates. Note the CHARITE sizes in the table correspond to the size 2,3,4 and 5 prosthesis and that the Mobidisc-L comes in two different lateral widths (34 and 39mm) for 3 different anteriorposterior widths.

Prosthesis	Small	Medium	Large	Extra Large	Reference
ActivL	26	28	30	33	(Michaela et al. 2008; FDA 2015b)
	31	34.5	39	40	
CHARITE	25	27	29	31	(Michaela et al. 2008; FDA 2004; Depuy Spine a Johnson & Johnson Company 2004)
	31.5	35.5	38.5	42	
M6-L		27	30		(Spinal Kinetics 2009)
		35	39		
Maverick	25	27	30		(Michaela et al. 2008; Medtronic 2002)
	32	35	39		
Mobidisc-L	27	30	33		(Michaela et al. 2008; LDR 2014)
	34				
	27	30	33		
	39				
Prodisc-L		27	30		(Michaela et al. 2008; Synthes Spine 2006; FDA 2006)
		34.5	39		
Kineflex	27	30	35		(Pettine & Hersh 2011)
	36.5	41	44		
FlexiCore	28	30			(Valdevit & Errico 2004)
	35	40			

Table 41: Summary of the different total heights of different TDRs (mm).

	Small	Medium	Large	Extra Large	References
ActivL	8.5	10	12	14	(FDA 2015b)
Baguera-L	8	10	12		(Spine Art 2010)
LP-ESP	10	12			(FH Orthopedics n.d.)
M6-L	10	12			(Spinal Kinetics 2009)
Maverick	10	12	14		(Medtronic 2002)
Mobidisc-L	10	11	12	13	(LDR 2014)
Prodisc-L	10	12	14		(FDA 2006)

Kineflex	11	12	12.75	13	13.75	
----------	----	----	-------	----	-------	--

Table 42: Summary of the different inlay sizes of different TDRs (mm).

	Prosthesis	Small	Medium	Large	Extra Large		References
<u>Inlay Height</u>	ActivL	5.3	6.8	8.8	10.8		
	CHARITE	7.5	8.5	9.5	10.5	11.5	(FDA 2004)
<u>Inlay Anterior Posterior Dimension</u>	ActivL	21	21	21	21		(FDA 2015b)
	Prodisc-L		26	29			(FDA 2006)
<u>Inlay Lateral Dimensions</u>	ActivL	21	21	21	21		(FDA 2015b)
	Prodisc-L		23	25			(FDA 2006)
<u>Inlay Diameter</u>	CHAIRTE	25	27	29	31		(FDA 2004)

Table 43: A summary of the different lordosis angles available from different TDR devices.

Prosthesis	Superior Endplate Angle			Inferior Endplate Angle		Total Lordosis Angles				References
ActivL	6	11		0	5	6	11	16		(FDA 2015b; Aesculap Implant Systems 2015)
Baguera-L						5	10			(Spine Art 2010)
CHARITE						0	5	7.5	10	(FDA 2004; Depuy Spine a Johnson & Johnson Company 2004)
LP-ESP						7	9	11		(FH Orthopedic s n.d.)
M6-L	3	6	10	0		3	6	10		(Spinal Kinetics 2009)
Maverick	3	6		3	6	6	9	12		(Medtronic 2002)
Mobidisc-L						5	10			(LDR 2014)

Prodisc-L (original design)	6	11		0	0	6	11			(Tsitsopoulos et al. 2012; Synthes Spine 2006)
Prodisc-L (improvised design)	3	3	3	8		6	11			
Kineflex						0	5	11		(Pettine & Hersh 2011)

Table 44: Summary of the RoM of different TDR devices. Merged flexion and extension data signifies the combined flexion/extension RoM.

Device	Flexion (°)	Extension (°)	Lateral Bending ±(°)	Axial Rotation (°)	References
Prodisc (manufactures quoted values)	13	7	10	3	(FDA 2006)
Charite (L3-L4 cadaver tests)	28		35	33	(Cunningham, Gordon, et al. 2003)
Charite (L4-L5 cadaver tests)	35		42	40	
Charite (L5-S1 cadaver tests)	37		23	27	
ActivL (L4-L5 cadaver tests)	9.0	3.2	9.0	5.4	(Ha et al. 2009)
ActivL (L5-S1 cadaver tests)	8.4	4.4	7.9	3.5	
MobiDisc-L (manufactures quoted values)	16.5		10	6	(LDR 2014)
MobiDisc-L (L4- L5 radiological clinical trial)	7.4				(Delécrin et al. 2007)
MobiDisc-L (L5- S1 radiological clinical trial)	6.5				
Physio-L (manufacture quoted values)	20		15		(Med Gadget 2008)
FlexiCore (manufactures quoted values)	15		15	5	(Errico 2005)

Table 45: The maximum ranges of motion of the ActivL TDR. *= The inlay translation is limited on endplate size which effect flexion RoM (FDA 2015b).

Device Size Combination (endplate size / inlay height)	Flexion Design Limit (inlay anterior) *	Flexion Design Limit (inlay posterior) *	Extension Design Limit	Lateral Bending Design Limit	Translational Design Limit (mm)
Small / 8.5mm	11.8°	11.5°	11.8°	±10.6°	1.5
Small / 10mm	19.5°	18.4°	18.7°	±15.6°	1.5
Small / 12mm	30.5°	26.6°	30.2°	±25.8°	1.5
Small / 14mm	43.5°	36.6°	43.5°	±34.1°	1.5
Medium / 8.5mm	11.7°	9.8°	11.7°	±9.2°	2
Medium / 10mm	17.5°	15.8°	17.5°	±14.3°	2
Medium / 12mm	27.3°	22°	27.3°	±25.8°	2
Medium / 14mm	37.8°	30.2°	37.8°	±32.9°	2
Large / 8.5mm	10.5°	9.5°	10.7°	±8.3°	2
Large / 10mm	17.5°	14.9°	17.8°	±12.9°	2
Large / 12mm	26.5°	22.9°	26.6°	±19.6°	2
Large / 14mm	34.5°	30.9°	34.5°	±26.1°	2
Xtra Large / 8.5mm	9°	8.2°	11°	±8°	2
Xtra Large / 10mm	14.2°	12.4°	17.6°	±12.6°	2
Xtra Large / 12mm	21.5°	19°	26.4°	±18.8°	2
Xtra Large / 14mm	28.8°	25.4°	35°	±25.4°	2

Biocompatibility is obviously a design requirement of all TDR devices. The metal EPs of the TDR prostheses form the interface between the prosthesis and the vertebral body. They are designed to allow initial fixation and stability and many designs also incorporate special coatings to allow osseointegration. A number of different biocompatible materials with varying material properties are often used in both TDR and orthopaedic devices (Table 46).

Table 46: Material properties of common orthopaedic biomaterials (Hallab et al. 2003).

Orthopaedic Biomaterial	ASTM Designation	Trade Name and Company (Examples)	Elastic Modulus (Young's Modulus) (GPa)	Yield Strength (Elastic Limit) (MPa)	Ultimate Strength (MPa)	Fatigue Strength (Endurance Limit) (MPa)	Hardness HVN	Elongation at Fracture (%)
Cortical bone*								
			15.2	114t	150c/90t	30–45	—	—
			40.8	—	400c–270t	—	—	—
Polymers								
			0.5–1.3	20–30	30–40t 30–40c	13–20	60–90 (Mpa)	130–500
			0.0018–0.009	28–40	28–40t 33–50c	21–30	50–120 (Mpa)	600–720
			1.8–3.3	35–70	38–80t	19–39	100–200 (Mpa)	2.5–6
Metals								
	ASTM F138	Protusul S30-Sulzer	190	792	930t	241–820	130–180	43–45
	ASTM F75	CoCrMo-Biomet Orthochrome-DePuy Protosul 2-Sulzer Vitallium C-Howmedica Zimaloy-Zimmer	210–253	448–841	655–1277t	207–950	300–400	4–14
	ASTM F90	Vitallium W-Howmedica	210	448–1606	1896t	586–1220	300–400	10–22
	ASTM F562	HS251-Haynes MP35N-Std Pressed Steel Corp.	200–230	300–2000	800–2068t	340–520	8–50 (RC)	10–40
	ASTM 1537	TJA 1537-Allevac Metasul - Sulzer	200–300	960	1,300t	200–300	41 (RC)	20
Ti alloys								
	ASTM F67	CSTi-Sulzer	110	485	760t	300	120–200	14–18
	ASTM 136	Isotan-Aesculap Werke Protosul 64WF-Sulzer Tilastan-Waldemar Link Tivaloy 12-Biomet Tivanium-Zimmer	116	897–1034	965–1103t	620–689	310	8

* Cortical bone is both anisotropic and viscoelastic thus mechanical properties listed are generalized
HVN = Vickers Hardness Number, kg/mm; C = Compression; t = tension; RC = Rockwell Hardness Scale.

The majority of TDR devices are made of titanium (Ti) or cobalt-chromium-molybdenum (Co-Cr-Mo) alloys (Taksali et al. 2004). Ti alloys offer the most superior corrosion resistance and has a Young's modulus more similar to that of natural bone when compared to other biocompatible alloys. Co-Cr-Mo alloys are less resistant to corrosion but offer superior wear resistance than Ti alloys (Hallab et al. 2003; Navarro et al. 2008).

5.6 Problems with TDR

5.6.1 Adjacent Disc Degeneration

The fate and degradation of adjacent level disc(s) following TDR is unfortunately a problem. Adjacent disc degeneration (ADD) has been linked to the RoM of adjacent segments (Huang et al. 2003). Radiographic asymptomatic ADD; which was evident by loss of adjacent disc height and anterior osteophyte formation, have been found in 24% of 42 participants in a first generation Prodisc follow up study. The link between the RoM at the TDR level and the presence of ADD at the superior level was significant, with a mean of 1.6° RoM for those with ADD and a mean of 4.7° for those without (Huang et al. 2003).

5.6.2 Facet Joint Degeneration

The motion preservation aspect of TDR design can be detrimental to the FJs if incorrect non physiological kinematics are introduced to the spinal segments. The associated changes in the biomechanical loading of the FJ are believed to lead to accelerated degeneration. This can in turn lead to disappointing pain relief even in successfully implanted devices (Shin et al. 2013).

There are a number of biomechanical studies that have investigated the affect TDR has on FJ loading. One study investigated a ball and socket style TDR with a verified finite element model. The model revealed that facet loads can be increased by as much as 250% due to malpositioning of the device in a more anterior placement (Dooris et al. 2001).

5.6.3 Subsidence

Subsidence of a TDR into the inferior vertebral EP has been identified as a relatively common complication. It has been identified to occur clinically in 52% of patients for a failed SB Charite III TDR group (Punt et al. 2013). Also mentioned in Section 4.2.2 the EP shape has been linked to subsidence and that the shape of a TDR should match as closely as possible to the size of the EP, in particular it should cover the cortical shell of the lumbar vertebrae which provides 45-75% of axial loading resistance (Michaela et al. 2008; Fraser et al. 2004). Mismatching in the sizing of CHARITE and Prodisc L in a total of 48 L4-L5 and L5-S1 EPs from 12 different patients has been investigated (Michaela et al. 2008). They took three measurements for each EP, the anterior posterior diameter and two different mediolateral easements taken at a third and two thirds of the anterior posterior diameter as seen in Figure 67.

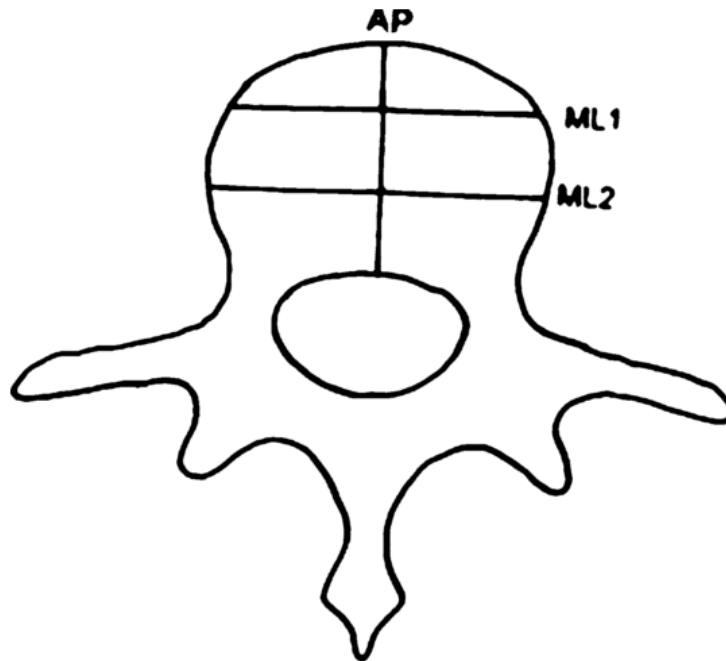


Figure 67: The sites at which the anterior posterior (AP) and two mediolateral (ML1 and ML2) measurement were taken to investigate endplate and total disc replacement endplate size mismatch (Michaela et al. 2008).

The failure criteria for the anterior posterior diameter was that the patient's EP diameter must match or be less than the TDR anterior posterior diameter. The mediolateral diameter failure criteria defined that the EP diameter must be within 10mm of the TDR; since the AF is preserved laterally. It was discovered that only 1.2% and 2.4% in the anterior posterior diameter, 20.7% and 48.8% in the mediolateral 1 (ML 1) diameter and 8.5% and 22.0% in the mediolateral 2 (ML 2) diameter were large enough for the Prodisc L and CHARITE TDRs respectively (Michaela et al. 2008).

Chapter 6. Specifications

The design specifications were sorted into three different sections. TDR type specification; which specifies if the desired design will be a ball and socket, mobile core or elastomer core TDR, material specifications; which identify the materials to be used in the design, mechanical specifications; which highlight the failure load criteria, and geometric specifications; that will constrain the dimensions of the design.

6.1 TDR Type

It was decided that the new design will be classed as an elastomer core TDR. This decision was made after the extensive literature review. Elastomer core TDRs do not constrain the CoR in a non-physiological manner, like ball and socket TDRs (Section 4.17.1). They also do not produce the metal on metal or metal on polymer wear particles that semi constrained mobile core TDRs emit (Section 4.17.2).

In addition, the clinical outcomes of elastomer TDRs have shown great promise in the available short term clinical studies (Section 5.4). Another major reason for deciding on developing an elastomer core TDR is that no elastomer core TDRs have gained FDA approval and hence represents a significant niche market that a potential design can target.

6.2 Material Specifications

As outlined in the design requirements the material selection of the design will be limited to already developed and biocompatible materials.

6.2.1 Elastomer Core

The elastomer core will be made from silicone polycarbonate urethane. This elastomer was chosen as it has been safely used in other elastomer core TDRs such as the LP-ESP (Section 5.3.4) and the Freedom TDR (Section 5.3.8). In addition, this type of elastomer has a proven track record of being biocompatible and has been used in a number of implantable medical products that require high levels of endurance (Mddiadmin 2000).

6.2.2 Metal Endplates

The endplates will be made of ASTM 1136 Ti-6Al-4V titanium alloy, which is the same alloy as the latest TDR to be granted FDA approval (ActivL).

6.3 Mechanical Specifications

The mechanical specifications of the design (Table 47) were derived from the failure loads reported in literature review (Section 4.9). A 1.5 safety factor has been incorporated into the mechanical failure specifications to insure that the device should be safe to implant. The specified failure loads were derived from the upper bounds of the failure loads of the FSU for the particular mode loading that were presented in literature (Table 22).

Table 47: Mechanical failure specifications.

Mechanical Failure Specifications	
Mode of loading	Failure Load
Compression	30 kN
Shear	3.2 kN
Torsion	132 Nm
Flexion	122.5 Nm
Extension	67.5 Nm
Lateral Bending	90 Nm

6.4 Geometric Specifications

6.4.1 Endplate Design Specifications

6.4.1.1 Lordosis of Endplates

The lordotic angle of a TDR is often caused by the inclination of either only the superior endplate or a combination of the superior and inferior endplates (Table 43). The initial Prodisc-L design had all of the lordotic inclination occurring at the superior endplate. This was then altered to have a distribution of inclination in the superior and inferior endplates (Tsitsopoulos et al. 2012).

The influence of the lordotic angle of the TDR coming purely superior endplate or a distributed lordotic angle in both endplates and its effect on the kinematics of the lumbar spine was investigated with the two different models of the Prodisc-L. The cadaveric study tested 12 human L1-S1 spines implanted at the L5-S1 level in flexion/extension (400 N follower load), lateral bending (0 N follower load) and axial rotation (0 N follower load) for

lordotic endplates with the following distributed or non-distributed superior/inferior lordotic angles ($6^{\circ}/0^{\circ}$, $3^{\circ}/3^{\circ}$, $11^{\circ}/0^{\circ}$ and $3^{\circ}/8^{\circ}$) (Table 48).

Table 48: The comparison of the range of motion of the lumbar spine in flexion/extension, lateral bending and axial rotation to the intact state for different TDR endplate lordosis angles (Tsitsopoulos et al. 2012).

	Intact	$6^{\circ}/0^{\circ}$	$3^{\circ}/3^{\circ}$	Intact	$11^{\circ}/0^{\circ}$	$3^{\circ}/8^{\circ}$
Flexion/Extension	$8.9 \pm 2.2^{\circ}$	$8.1 \pm 2.8^{\circ}$	$7.0 \pm 2.8^{\circ}$	$12.3 \pm 3.5^{\circ}$	$11.4 \pm 1.6^{\circ}$	$10.2 \pm 1.1^{\circ}$
Lateral Bending	$5.2 \pm 1.2^{\circ}$	$3.3 \pm 1.5^{\circ}$ *	$2.7 \pm 1.4^{\circ}$ *	$6.8 \pm 1.5^{\circ}$	$4.8 \pm 1.5^{\circ}$	$4.2 \pm 0.9^{\circ}$ *
Axial Rotation	$2.6 \pm 1.0^{\circ}$	$1.9 \pm 0.9^{\circ}$	$1.6 \pm 0.6^{\circ}$ *	$3.1 \pm 1.5^{\circ}$	$2.1 \pm 1.4^{\circ}$	$1.8 \pm 0.79^{\circ}$

*=statistically significant decrease from the intact state ($p < 0.05$)

Having the lordosis angle caused by the superior endplate or a combination of the superior and inferior endplate causes a decrease RoM, regardless of the loading type, compared to the intact state; although all of these reductions in RoM are not statistically significant (Table 48).

Although RoM decreases more for distributed lordosis angled endplates, compared to non-distributed lordosis endplates (Table 48). The CoR of the distributed endplates more closely resembled the intact state (Figure 68).

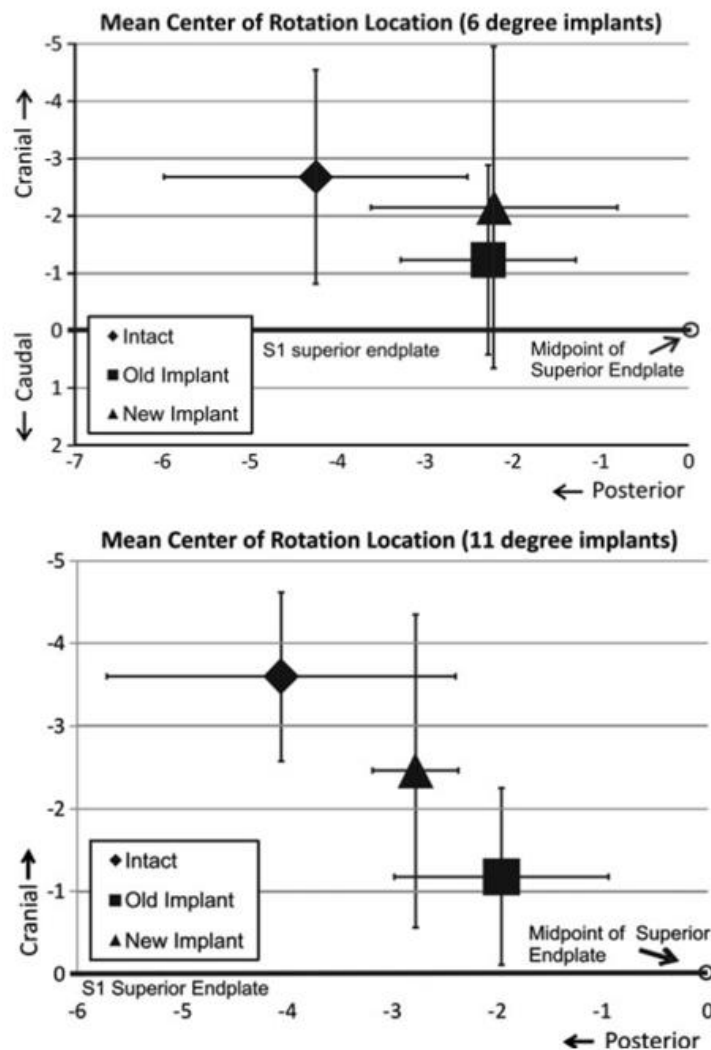


Figure 68: The location of the centre of rotation (CoR) for the 6° (top) and 11° (bottom) Prodisc-L prosthesis with non-distributed (old implant) and distributed (new implant) lordosis angle endplates compared to the intact CoR (Tsitsopoulos et al. 2012).

The CoR of the non-distributed lordotic endplates were more anterior and caudal when compared to the intact CoR location (Figure 68). Having the lordosis of the TDR contributed from both endplates more closely replicates to the natural disc geometrically compared to having it purely from the superior endplate (Tsitsopoulos et al. 2012). However, this study revealed that when using a fixed ball and socket TDR at the L5-S1 level it may be beneficial to have the lordosis only come from the superior endplate when the RoM is considered more important than the CoR.

The lordosis of the implant should be generated from the endplates, as opposed to the elastomer core. This decision was due to findings from a finite element analysis study that predicted better stress distribution between the rubber to endplate surface when this was the

case (Fraser et al. 2004). This is also consistent with all other TDRs that have been created that generate the inclination for lordosis at the endplates.

For simplicity in the early stages of design. No lordosis will be present in any of the prototype endplates. However, for future development the automated CAD design process does have lordosis capabilities already included.

Once implemented the lordosis angle that should be initially incorporated into the endplate design should come from both the endplates. This decision was made as the grand mean of lordotic angles of the relevant L4-L5 and L5-S1 were 15.2° and 27.53° respectively (Table 18). The largest commercially available total lordosis angle is from the recently FDA approved ActivL design (16°) (Table 43). The lordosis of the TDR design should approximate the natural lordotic angle as closely as possible and therefore a total lordosis angle of 15° should be first implemented into the design. It is impractical to have a single endplate produce all of this angle of inclination. This approach is also followed by commercially available TDRs which tend to produce majority of the lordotic angle from the superior endplate (largest angle = 11° for the ActivL). For a starting point in the design the superior endplate should produce 10° of lordosis and the remaining 5° should be produced from the inferior endplate. These values are also consistent with those used by commercial TDRs (Table 43).

6.4.1.2 Keel/spike Height

Based on the vertebral body measurements and the bone density findings the keels or spikes used for initial stability should rest in the superior or inferior third of the vertebral body (Section 4.2.1). A single keel has been integrated into the initial prototype design. A single keel was decided upon as it provides initial stability to axial rotation, increase surface area to allow osseointegration and can be used to help guide the TDR into position during implantation.

The keel height should be approximately one third of the maximum vertebral height dimension found in the literature review (30.8 mm (anterior L5 height)).

Keel height = 10 mm (approximately 1/3 of anterior L5 vertebral body height))

6.4.1.3 Endplate Shape

The general shape of the endplates of different commercial TDRs are quite similar (Figure 69).

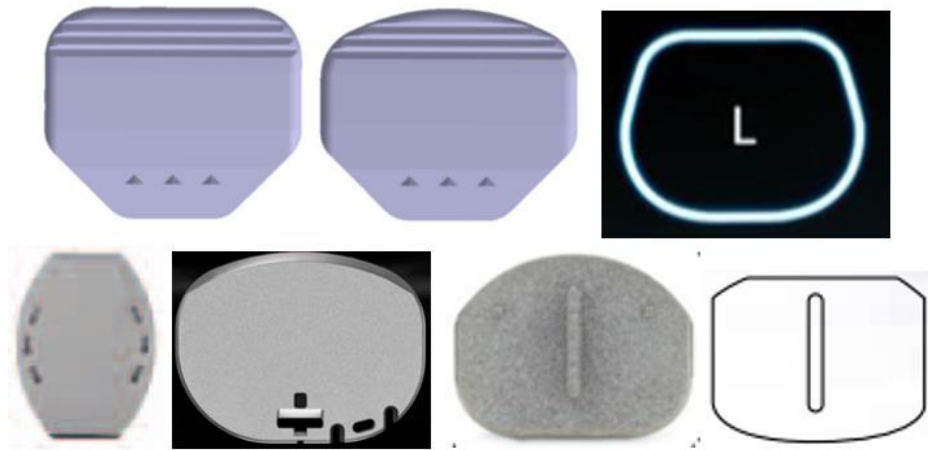


Figure 69: Different endplate shapes of various commercial TDRs. Activ-L standard endplate (top left), Activ-L S1 Endplate (top middle), Baguera-L (top right), CHARITE (bottom left), MobiDisc (bottom left-middle), Prodisc-L (bottom right-middle) and Maverick (bottom right).

For this early stage of design, a simple endplate shape resembling those found in pre-existing TDRs will be used. The variance of the published EP area is incorporated into the EP specifications.

6.4.1.4 Anterior Posterior Endplate Width

The anterior posterior width of the TDR endplate should lie on the cortical shell to prevent subsidence (Section 5.6.3). The mean endplate AP width was found to be approximately 35 mm (Section 4.2.2). However, the largest commercially available endplate AP width is 33 mm from the MobiDisc and ActivL TDRs. This under sizing is likely due to the size contains in the AP direction and that the endplates should not protrude posteriorly over the endplate into the spinal canal. Therefore, a AP width of 33 mm has been chosen for the prototype as it is constant with already developed TDRs and should still be able to lie on the anterior cortical bone when implanted.

6.4.1.5 Lateral Endplate Width

The lateral width of the vertebral EP is approximately 52 mm with approximately 19 mm of this covered by the lateral AF (Section 4.2.2 and 4.8). The widest commercially available endplate in the lateral direction was from the CHARITE, which measured 42 mm (Table 40). It is likely that during implantation surgery some of the lateral AF in particular in the transition zone between the AF and the NP is removed. Therefore, the width of the endplate should be greater than 33 mm (52-19 mm). The failure criteria of incorrectly sized TDR endplates in the lateral direction (Section 5.6.3) allowed for the TDR to be 10 mm shorter

than the lateral vertebral EP. A specification of having a 42 mm lateral width agrees with this criterion and also matches a size that has been made commercially available.

6.4.1.6 Endplate Area

The EP of the TDR design should cover at least 85% of the largest EP, plus two standard deviations to cover patient variability according to recommendations from the literature (Gornet et al. 2014). Using this criteria, the endplate area should be $\geq 1170 \text{ mm}^2$. This value was derived from using the Panjabi et al., area dimensions for the L4 lower endplate, as opposed to the Wang et al., area measurements (Table 7). The Panjabi measurements were derived by projecting the area onto a plane, Wang measured the actual surface area and took into consideration the concavity of the endplate. This explains why the Wang measurements are larger than those of Panjabi. The rationale for using the projected measurements is that the endplates are likely flattened during the implantation process and therefore this area more closely resembles the area that a TDR must sit on. The specification given represents 85% of the EP area equal to two standard deviations above the mean.

6.5 Range of Motion

RoM of the TDR should approximate the natural RoM of the lumbar spine (Section 4.12). The specifications for the RoM of the designed TDR (Table 49) were decided upon as they closely approximate the RoM of the specific L4-L5 and L5-S1 levels of interest. These specifications should also allow greater than 5° of flexion/extension RoM once implanted, which correlates with superior clinical outcomes (Huang et al. 2006). The specifications also took the mean values for the different lumbar spinal segments into consideration when deciding upon the values stated.

Table 49: The global mean RoM of the L4-L5 and L5-S1 spinal segments from literature and the final specified RoM.

Lumbar Level	Flexion ($^\circ$)	Extension ($^\circ$)	Lateral Bending ($^\circ$)	Axial Rotation ($^\circ$)
	Mean	Mean	Mean	Mean
L4-L5 Global Mean	13	3.83	6.63	3.23
L5-S1 Global Mean	9.5	5.93	4.35	1.75
Specification	10	4	5	2

6.6 Centre of Rotation

CoR is an important parameter in terms of quality of vertebral motion (Alain et al. 2016). The ICR of the lumbar spine migrates during different bending motions (Section 4.13). Due to the large patient variability in anatomical morphology, the specification of the CoR of the TDR design will be required to lie within 3 standard deviations of the mean extension to flexion ICR (Table 25). These values (Table 50) represent the proportion of the width (x) and height (y) of the inferior lumbar spinal segment of the particular lumbar level in the sagittal plane. Width is in the anterior posterior direction and height is in the inferior superior direction.

Table 50: Centre of rotation specifications. (values given as proportion of x=width and y=height of the inferior spinal segment).

Spine Level	3 standard deviations below mean		3 standard deviations above mean	
	x	y	x	y
L4-L5	0.15	-0.43	0.57	0.23
L5-S1	0.12	-0.39	0.54	0.63
Specification CoR must lie within	0.13	-0.40	0.55	0.43

6.7 Total Height

The mean height of the L4-L5 and L5-S1 lumbar discs; from different published sources, was found to be 10.47 mm (Table 19). The ActivL is available in an 8.5 mm constructed height which is the shortest of all FDA approved TDRs. This 8.5 mm height TDR was implanted in 87% of IDE patients (Section 5.3.5.2). However, a total height of 10 mm for the constructed TDR prototype was selected. This 10 mm height was chosen over a smaller size as this is closer to the mean physiological height and a vast majority commercial TDRs also have a 10 mm height variation of their design available (Table 41).

6.8 Summary of Key Design Specifications

Table 51: Summary of key design specifications.

Specification	Value
Total Constructed (Disc) Height	10 mm
Anterior-Posterior Width	33 mm
Lateral Width	42 mm
Lordosis	0° (accounted for in automated design for future work)
Keel Height	10 mm
Endplate Area	$\geq 1170 \text{ mm}^2$
Range of Motion	
Flexion	10°
Extension	4°
Lateral Bending	5°
Axial Rotation	2°
Centre of Rotation	
Relative to endplate width in the anterior-posterior direction of the sagittal plane	$13 < x < 55$ % of the endplate width relative the posterior superior corner of the relevant inferior vertebrae.
Relative to endplate height in the superior-inferior direction of the sagittal plane	$-40 < x < 43$ % of the endplate height relative the posterior superior corner of the relevant inferior vertebrae.

Chapter 7. Design Concepts

Four different design concepts of potential TDRs were generated and analysed in order to determine which design idea should be developed further.

7.1 Printed Magnetic Endplates

Polymagnet® Correlated Magnetics is a company based in the United States that has developed a novel technique that allows the printing of custom designed magnetic fields onto metal surfaces (Figure 70)(Polymagnet 2016).

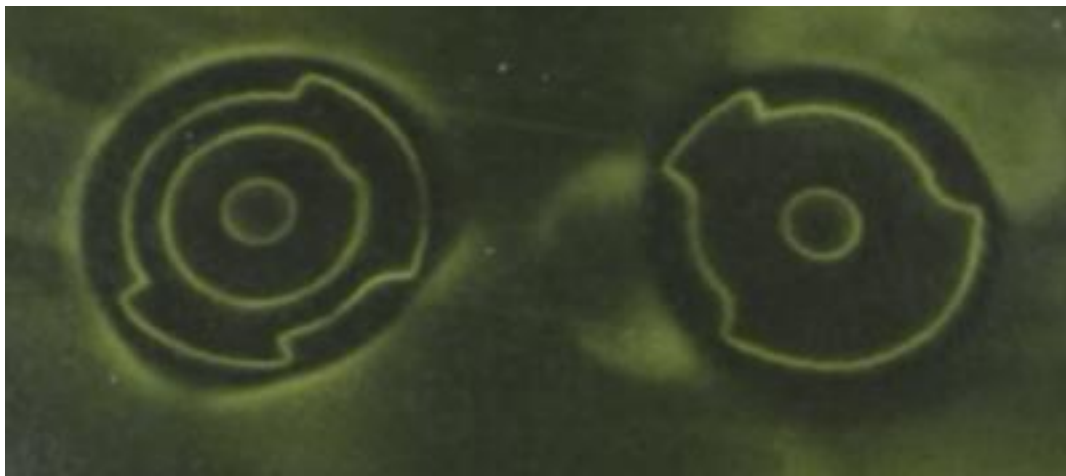


Figure 70: Example of two different 3D printed magnetic fields that are used to create a locking mechanism (Polymagnet 2016).

This inspired the idea of having a magnetic field that would be printed onto two separate biocompatible metal endplates. The magnetic fields would be developed in such a manner that they would oppose each other while also constrain the relative motion of the two endplates. The magnetic field would also allow for the mechanical behaviour of the TDR to be precisely tuned accordingly to mimic that of the natural disc.

7.1.1 Advantages

The major advantage of this design is that it would also provide frictionless, physiologically constrained motion of the endplates in all six degrees of freedom. The use of non-contacting endplates would also eliminate the risk of potential wear.

7.1.2 Disadvantages

The disadvantages of this design is that it is highly complex. There is limited expertise with this magnetic 3D printing technology, and it is unknown if this relatively new technology is even capable of producing such complex behaviour. Additional biocompatibility issues may

occur such as interference from external electronic devices. If the endplates were to become unconstrained it could result in catastrophic failure causing severe and potentially life threatening damage to the patient.

7.2 Internally Assembled Endplates

The implantation surgery of TDRs is highly invasive (Section 4.18). The idea of having internally assembled endplates was conceived in order to reduce the size of the TDR and in doing so reducing the size of the incision needed and overall invasiveness of the surgery. The endplates would join together once implanted.

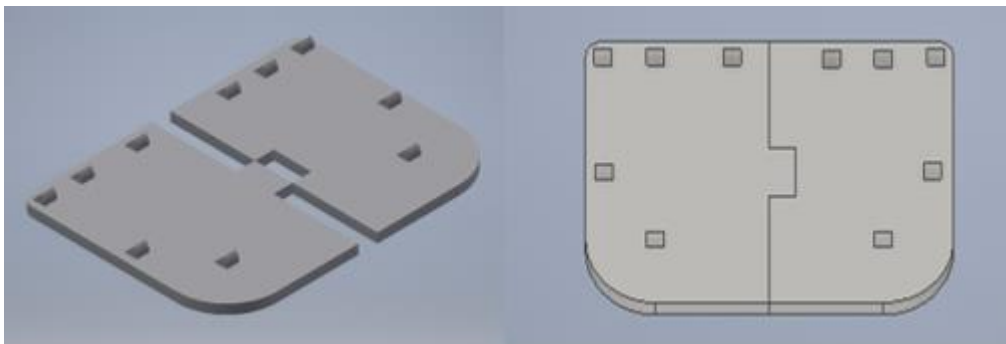


Figure 71: CAD drawing of the internally assembled endplate concept.

7.2.1 Advantages

The major advantage of this concept was that it reduces the invasiveness of the surgery.

7.2.2 Disadvantages

TDR surgery still requires the removal of the NP and some of the AF via discectomy. It may not be possible to minimise the invasiveness of the surgery, as these stages of the surgery would also still be needed before implantation. This would render the main advantage of this design useless. Additional problems that may occur include the development of stress concentrations along the joining edge between the different endplate components.

7.3 Modular Core

A modular core concept (Figure 72) was also proposed that consisted of an implantable inner elastomer core that locks into the endplate in a similar fashion to how the inlay of the Prodisc-L locks into its endplates (Figure 55).

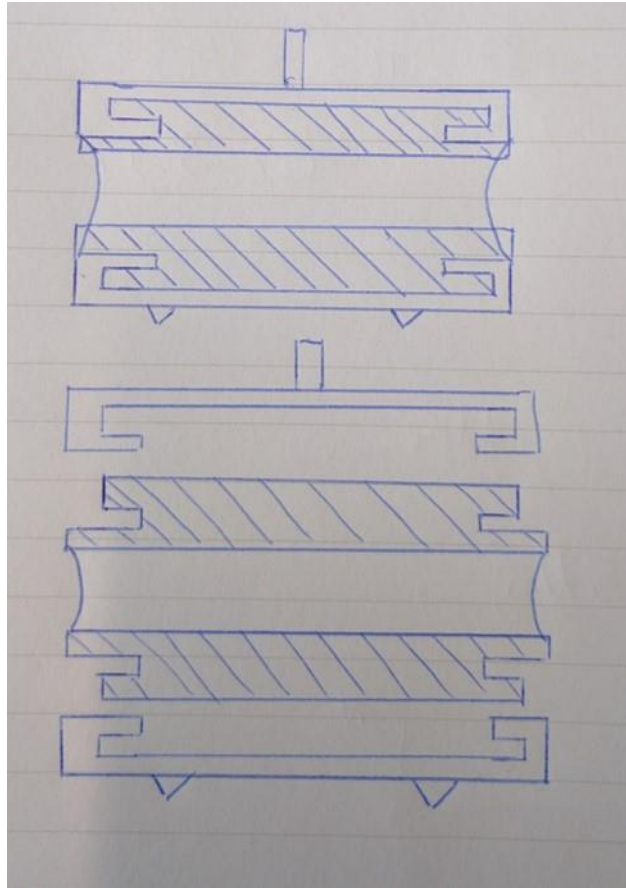


Figure 72: Drawing of the modular core concept assembled (top) and with the core unassembled (bottom).

7.3.1 Advantages

The advantages of having a modular core is that the height can be interchanged once the endplates have been fitted to ensure a correct fit. The modular core design also would have a contingency plan in case the elastomer core was to fail. The core could be replaced with another new core in the case of fatigue failure, or a stiffer more solid construct could be used to replace the core and essentially give the patient a revision spinal fusion.

7.3.2 Disadvantages

TDR replacement is highly invasive (Section 4.18) and having multiple revision surgeries is not advised. This means that the advantage of being able to replace the elastomer core in case of failure may not be a suitable option and the fusion construct should be used in case of revision. The snap in feature of the Prodisc-L was also shown to be a failure point in the static inlay push out testing. Although it did fail at loads at loads that exceeded those expected in vivo. A similar feature was going to be used in the modular core design which might be a potential weak point like the Prodisc-L.

7.4 Velodrome TDR

Upon investigation into a number of different TDRs that have been designed, it was noted that the ball and socket designs which have gained FDA approval clearly do not restore the natural biomechanics of the lumbar spine (Section 1.1). It is believed that elastomer core TDRs more closely mimics the disc's biomechanical behaviour, in particular by not constraining the discs CoR and by allowing a nonlinear mechanical response. This lead to the novel creation of a composite elastomer core concept that was proposed for the project. The design includes two main components; a bottom core and a top core. The bottom core resembles the shape of a velodrome (Figure 73) and the top core is moulded to the bottom core's shape creating the elliptic cylinder shape of the core.



Figure 73: A mini velodrome (Track Cycling News 2011)

7.4.1 Advantages

The velodrome shape of the bottom core allows the customisation of anterior, posterior and lateral sections. The geometry of these sides could then be designed in such a way that would allow for different mechanical response, CoR and RoM depending on direction of loading. For example, the posterior section of the velodrome shaped bottom core could be larger than the anterior section. This would increase the stiffness of the posterior section causing a reduction in extension RoM compared to flexion like the natural disc (Section 4.12). The bottom core would be made of a stiffer elastomer than the top core to accommodate this directional dependent behaviour.

The CoR would also not be completely constrained like the natural disc (Section 4.13) as the two elastomer cores would be able to deform in response to the natural movement of the lumbar spine.

7.4.2 Disadvantages

Having a multi part elastomer core may increase the risk of fatigue failure. In particular, the junction joining the bottom and top cores may be a potential weak spot and could cause separation when exposed to large forces.

Chapter 8. Ranking of Design Concepts

A decision matrix (Table 52) was developed to help justify the selection of which design concept to proceed with. The scoring system included factors such as surgical invasiveness, safety and biocompatibility, each of which was given a weighting out of 100% in terms of importance.

Table 52: Weighting matrix used to decide which design concept to pursue.

Criteria	Weighting (%)
Safety	20
Biocompatibility	20
Fatigue Life	15
Biomechanical Behaviour	12.5
Centre of Rotation	12.5
Reduced Surgical Invasiveness	5
Cost	2.5

8.1 Justification of Weighting

8.1.1 Safety

Safety is of the upmost importance when designing any medical device. The device should be safe to use once implanted and if failure was to occur it should fail in a contained manner and not cause significant damage to surrounding areas.

8.1.2 Biocompatibility

Like safety, biocompatibility is a must of any implanted medical device. Biocompatibility also considers potential wear particles that may be produced during loading of the TDR.

8.1.3 Range of Motion

Range of motion of a TDR has been correlated with clinical outcome (Section 4.12). Therefore, it is important that the TDR design meets the specified RoM.

8.1.4 Centre of Rotation

Centre of rotation correlates with sagittal imbalance, which if left uncorrected can cause poor clinical results (Section 4.13) (Pearcy & Bogduk 1988; Adams et al. 2013; Gornet et al. 2014; Tsitsopoulos et al. 2012; Le Huec et al. 2005). Therefore, it is important that the chosen design is able to meet specification.

8.1.5 Surgical Invasiveness

TDR implantation is a very invasive procedure partly due to the anatomical location of the lumbar discs, in particular the two most inferior segments (Section 4.18). The reduction in invasiveness is important, however due to the nature of the surgery this may be unnecessary to consider in the design of the TDR. As the implantation procedure still required the surgeon to gain access to the disc. Hence the low weight score given.

8.1.6 Cost

Cost is not of the utmost importance when it comes to such a life changing device. TDRs are also placed on the Australian prosthesis list so rebates are available if they must be implanted (Australian Government Department of Health 2016).

8.1.7 Fatigue Life

Fatigue life is very important when it comes to TDR design as they have been implanted in patients as young as 19 years (Delamarter et al. 2005)(Section 4.9.7). Therefore, it is important that the prosthesis can withstand the loading it is subjected to for 40-50 years or longer to prevent the need of potentially dangerous revision surgery.

8.1.8 Biomechanical Behaviour

The core justification for having a TDR is to alleviate LBP and restore motion. TDRs attempt to achieve this by restoring some or all of the natural biomechanics of the lumbar spine. Therefore, it ranked highly on the justification weighting.

8.2 Concept Scores

A score out of ten was then given to each of the design concepts for each of the different criteria, where 0 indicated that the design did not address the criteria at all, and 10 indicated that the design fully addressed the criteria.

8.2.1 Printed Magnetic Endplates

Table 53: Printed magnetic endplate decision matrix.

Criteria	Score	Weighting (%)	Score x Weighting
Safety	2	20	0.4
Biocompatibility	6	20	1.2
Range of Motion	7	12.5	0.875
Centre of Rotation	8	12.5	1
Surgical Invasiveness	8	5	0.4
Cost	2	2.5	0.05
Fatigue Life	9	15	1.35
Biomechanical Behaviour	6	12.5	0.875
		Total	6.15

The lack of information on the very new technology used to create the printed magnetic field design was a major factor for it ranking so low in some of the categories. Safety was a big issue as interference could potentially be a serious issue. Also if the magnets were to rapidly dis engage it could cause serious harm to the patient including possible death; hence the low safety score. This design would be no more invasive than current TDR and would potentially display exceptional fatigue lift due to the contact and frictionless bearing design. However, as previously stated, due to the early stage of this technology, the costs to manufacture this type of TDR would also be excessive compared to more conventional designs.

8.2.2 Internally Assembled Endplates

Table 54: Internally assembled endplate decision matrix.

Criteria	Score	Weighting (%)	Score x Weighting
Safety	8	20	1.6
Biocompatibility	8	20	1.6
Range of Motion	7	12.5	0.875
Centre of Rotation	8	12.5	1
Surgical Invasiveness	10	5	0.5
Cost	8	2.5	0.2
Fatigue Life	6	15	0.9
Biomechanical Behaviour	8	12.5	1
		Total	7.70

This concept was only for a component of a possible TDR design. It will be assumed that the endplates will be used in conjunction with an elastomer core for grading purposes. In terms of safety, biocompatibility, RoM, CoR, Cost and biomechanical behaviour this design should be

comparable to existing elastomer core TDRs. One of the main advantages of elastomer cores TDRs is that they allow moderate RoM and do not constrain the CoR (Section 4.17.3), thus they scored moderately high in these categories. If it is possible to reduce the surgical window to remove the disc prior to implantation, this design obviously would be superior in this category. Fatigue life may become an issue if stress concentrations form between the different endplate components.

8.2.3 Modular Core

Table 55: Modular core decision matrix.

Criteria	Score	Weighting (%)	Score x Weighting
Safety	8	20	1.6
Biocompatibility	8	20	1.6
Range of Motion	7	12.5	0.875
Centre of Rotation	8	12.5	1
Surgical Invasiveness	9	5	0.45
Cost	8	2.5	0.2
Fatigue Life	9	15	1.35
Biomechanical Behaviour	8	12.5	1
		Total	8.08

It is assumed that this design would have the same properties as an elastomer core TDR for safety, biocompatibility, RoM, CoR, surgical invasiveness, cost and biomechanical behaviour. This design ranks highly in fatigue life as the core could be replaced if needed as long as the endplates remain in suitable condition. This design also allows the option to use a fusion core if needed/desired during revision.

8.2.4 Velodrome TDR

Table 56: Velodrome TDR decision matrix.

Criteria	Score	Weighting (%)	Score x Weighting
Safety	8	20	1.6
Biocompatibility	8	20	1.6
Range of Motion	9	12.5	1.125
Centre of Rotation	7.5	12.5	0.9375
Surgical Invasiveness	8	5	0.4
Cost	8	2.5	0.2
Fatigue Life	7.5	15	1.125
Biomechanical Behaviour	9	12.5	1.125
		Total	8.11

The Velodrome design is assumed to be as safe, biocompatible and have similar costs to typical elastomer core TDRs. The main advantages of this design is that it can have tailored RoM depending on the bottom core configuration. This customisable bottom core could also be used to tune the mechanical repose in all 6 DOF. The CoR may be slightly constrained depending on the difference in stiffness of the upper and bottom core which may be undesirable. Fatigue life is a potential risk of this design due to the different core components and the challenge in adhering them together.

Chapter 9. Design Iterations of the Velodrome TDR

Based on the decision matrices (Chapter 8) the Velodrome TDR was revealed to be the superior design concept and therefore was developed further.

A number of different interactions of the chosen design concept were developed. The main factor that drove the changes to the design was the need to accommodate the automated CAD process that was implemented to maximise the designs unique bottom core shape. Initially the core was going to be comprised of two components a top core and a bottom core. The first design of the bottom core was very basic (Figure 74).

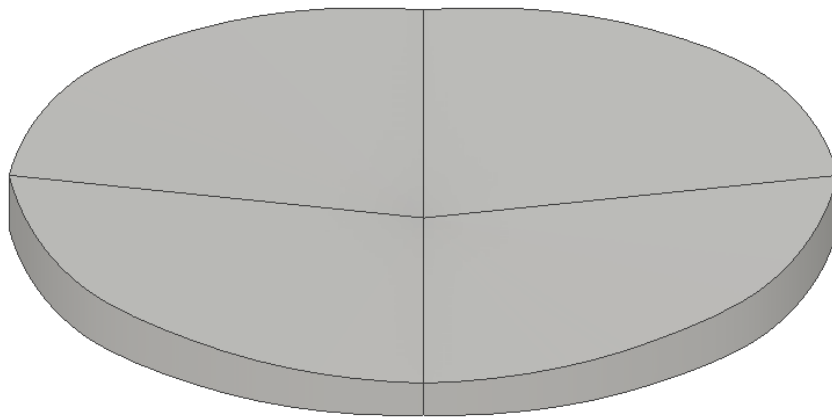


Figure 74: The first design of the bottom core.

It was developed by using the loft tool in inventor to join a series of trapezium shapes to create the different sized raised side edges (Figure 76).

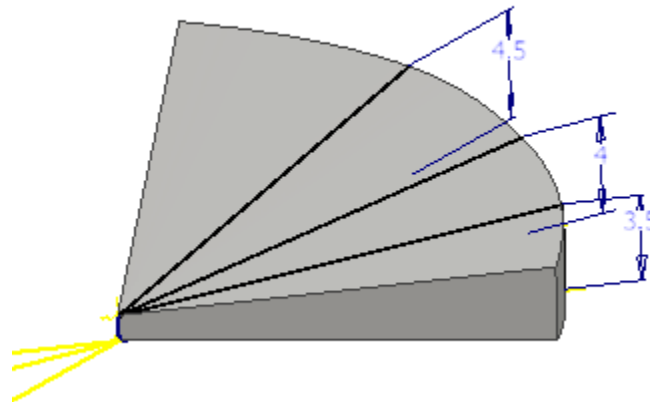


Figure 75: The sketches used by the loft tool to create the initial bottom core design.

This lofted geometry was then mirrored to create the complete core. Problems with this first design included that it was tedious to have to create all of the different trapezium shapes to achieve the desired raised edges of the design and that this design also meant that the lateral (right and left) edges and the anterior posterior (front and back) edges had to have the same dimensions. Having the same anterior, posterior and lateral edge heights was not according the original design concept plan.

The first major design iteration of the bottom core involved altering the shape so that it more closely resembled that of a velodrome. This involves not having the triangular like shaped edges revolve around the same axis but instead follow a pre created ellipse rail. This design also had a sharp edge along the top of the core (Figure 76).

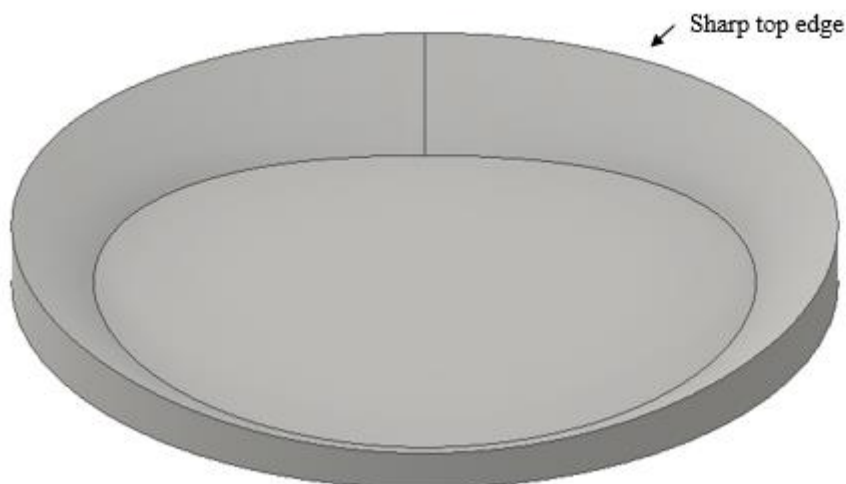


Figure 76: The initial bottom core design with a sharp top edge.

This top edge was then altered to be flat to create a larger surface area to a join the bottom core to the top core. The edge between the raised sides and the bottom of the core was also smoothed with a fillet (Figure 77).



Figure 77: First design iteration with flat top edge and fillet between raised edges and bottom of the bottom core.

9.1 The Final Design

The final bottom core design was altered into a ring shape due to limitations of the Autodesk Inventor software.

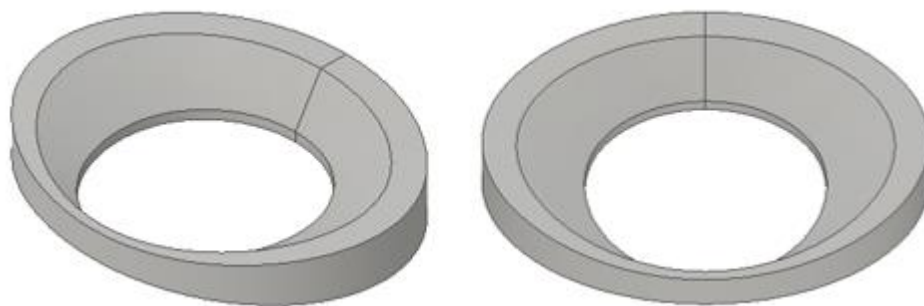


Figure 78: An iteration of the final bottom core design.

The main parameters that drive the bottom core geometry are the: top edge, outer height, base and inner height (Figure 79) of the trapezium internal geometry found at the anterior, posterior and lateral cross sections.

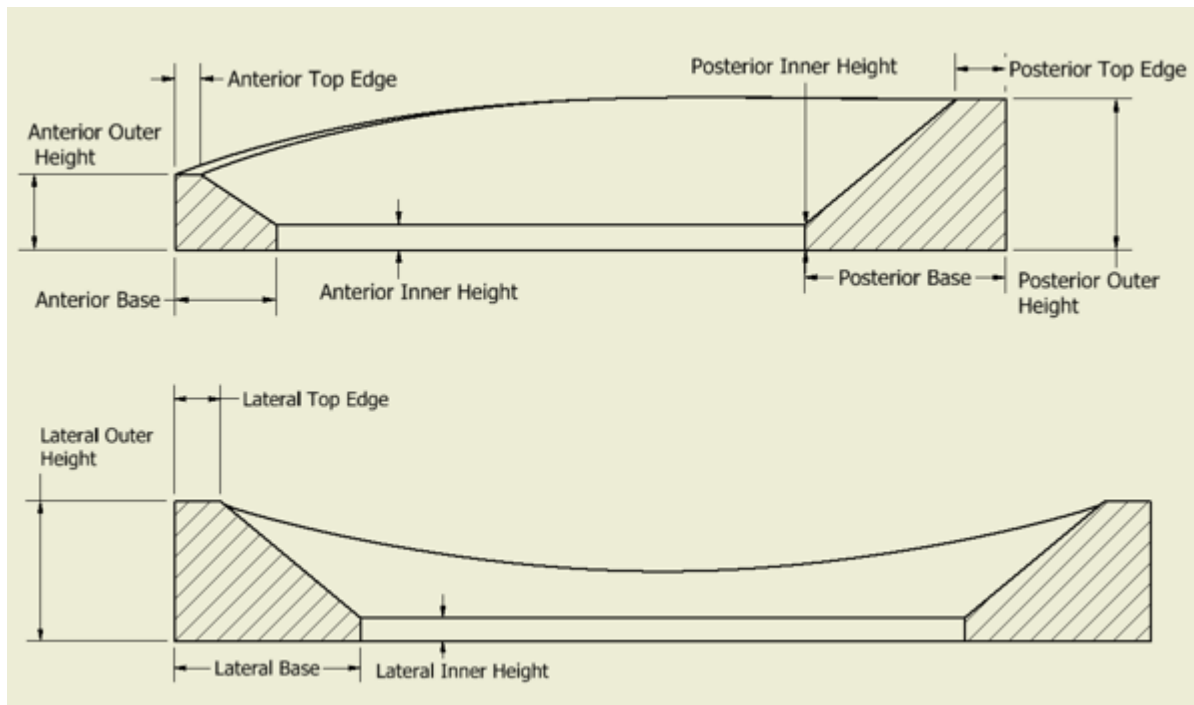


Figure 79: Cross section of the bottom core indicating the different geometric parameters that can be altered. A sagittal plane cross section (top) of the bottom core illustrating the anterior (left) and posterior (right) cross sections. A coronal plane cross section of the bottom core revealing the lateral cross sections (bottom).

The main limitation which drove the development of the ring shaped bottom core was the inability to incorporate the automation process to extrude the inner hole of the ring, without Inventor automatically generating an additional solid within the part. This was not desired as the bottom core was originally planned to consist of a single part. This issue also caused problems when attempting to open the exported CAD file into the Abaqus FEA software. This was a major limitation that had to be overcome as the bottom core is used to create a mould which is then used to derive the mating top core and therefore is critical to the design.

To overcome this problem an inner core (Figure 80) had to be developed that fits in the hole at the centre of the bottom core. In order to ensure a perfect fit between the inner core and the bottom core, the constraint of having the same inner height for the anterior, posterior and lateral sides of the bottom core had to be implemented into the design.

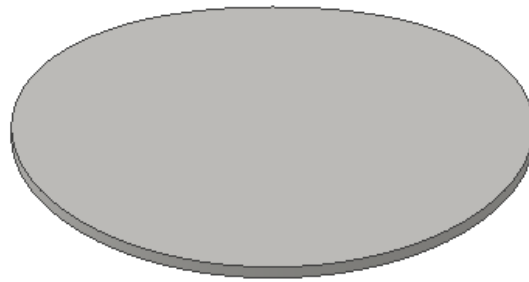


Figure 80: Inner core of the TDR design concept.

The inner core was developed in such a manner during the CAD automation process that it would always fit correctly in the hole of the bottom core ring. This method was also used to create a top core that mated correctly with the bottom core.

The inner core does not always have a perfect elliptical shape due to variability in the anterior, posterior and lateral base dimensions (Figure 80). The problem of not being able to simply create a matching ellipsoid cylinder to fit the bottom core inner hole, was overcome by creating a template inner core with dimensions that could be altered. This insured that it could be used as a mould to generate a perfect fit.

The template inner core has an elliptical shape which was updated in a manner so that it has the same height as the inner height of the bottom core. The inner core template is then updated again so that the anterior posterior diameter will lie in between the outer edge of the bottom core and the smaller dimension of the anterior or posterior base. This process is repeated for the lateral dimension so that the inner core template also lies between the outer edge of the bottom core and the lateral base dimensions (Figure 81).

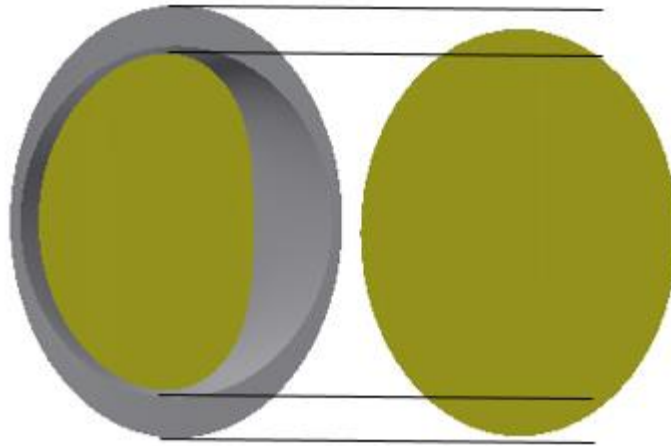


Figure 81: The assembled bottom core and inner core (left,) and the inner core (right) indicating the smaller size to the anterior posterior and lateral dimensions of the bottom core, but greater diameters than the base measurements.

The inner core is also developed so that it shares the same coordinate system as the bottom core. It is then placed in an assembly and constrained appropriately to the bottom core, to form an inner core mould. A new part is then derived from the assembled inner core mould that removes the bottom core geometry, leaving a perfectly matching inner core.

The need to create the inner core may have its advantages. The material properties of the inner core can be different from the other core components. This difference in material properties can be used to tune and improve the mechanical response of the TDR especially in compression.

The same method to create an assembly template of the upper core and then remove the bottom core was implemented for the top core. The top core template has an offset from the XZ axis which was updated according to the inner edge dimension. This was included so the inner core would still fit into the TDR core.

A problem unfortunately occurred during the removal of the bottom core to create the top core. If the top core template had the same lateral and anterior posterior dimensions as the bottom core, Inventor was unable to remove the bottom core geometry from the template. This error was caused by the overlapping edges. This meant that the top core design had to be altered so that it would be 0.07 mm smaller in both the anterior posterior and lateral dimensions compared to the bottom core. The value of 0.07 mm was chosen from a trial and error process.

The early endplate design was chosen (Figure 82) as it was basic, easy to create and resembled commercially available TDR endplates (Figure 69). Although it is undeveloped, the design was up to specification when combined with the specified anterior posterior and lateral widths dimensions as it provided an area of 1357 mm² (6.8).

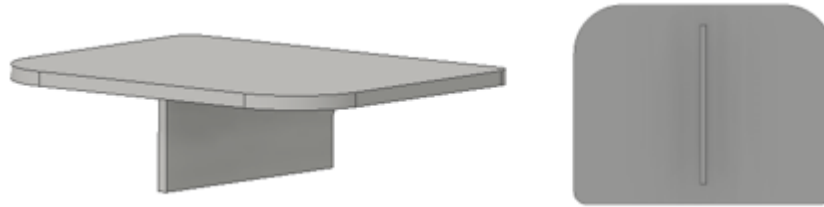


Figure 82: Early endplate design.

The same design was used for the inferior and superior endplates.

The final early stage design comprised of five parts; an inferior and superior endplate, and a bottom, inner and top core (Figure 83).

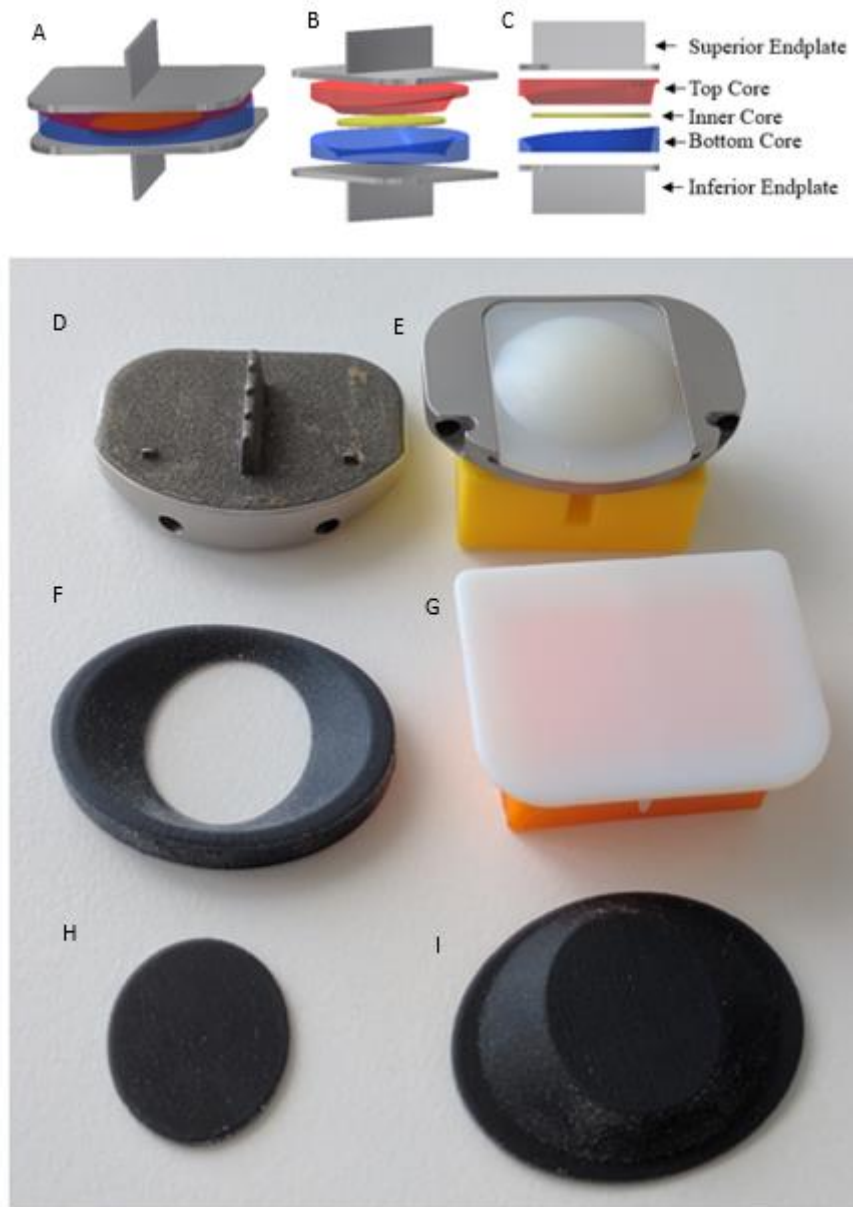


Figure 83: A CAD iteration of the final design chosen to proceed with the parametric analysis. (A) The assembled TDR and (B & C) exploded views illustrating the five different components of the design. (D-E) A picture of the Prodisc-L TDR components compared to (F-I) a 3D printed prototype of the Velodrome TDR concept components.

Chapter 10. CAD Automation

The major advantage of the final Velodrome design concept is that the three-part composite core allows for customisation and full utilisation of the planned CAD automation of the project.

With the introduction of the endplates there are a vast number of different parameters of the design which can be altered (Figure 84).

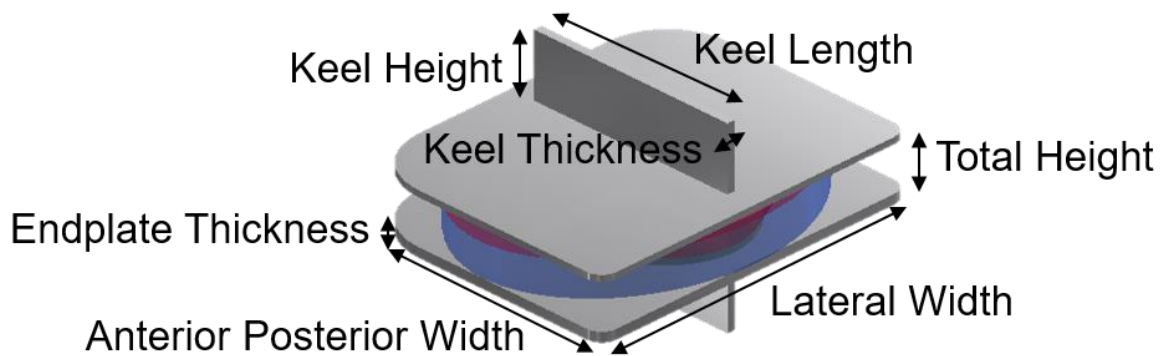


Figure 84: The different additional parameters of the endplates and total height of the TDR.

A summary of the different parameter of the Velodrome TDR design has been summarised in Table 57.

Table 57: Summary of different Velodrome TDR parameters.

Geometric Parameters
<u>Bottom Core</u>
Top Edge x 3
Outer Height x 3
Inner Height
Base x 3
Anterior Posterior Width
Lateral Width
<u>Endplate</u>
Anterior Posterior Width
Lateral Width
Thickness
Lordosis
<u>Keel</u>
Keel Length
Keel Height
Keel Thickness
<u>Total Height of TDR</u>

Material Parameters
Bottom Core Elastomer
Top Core Elastomer
Inner Core Elastomer
Endplate Material

10.1 Automation Justification

The main justification of automating the development of different parametric CAD models of the design was due to the large number of different parameters that could be altered (Table 57).

Replicating all the different dimensions of existing TDRs (Section 5.5) would result in 1000's of different possible combinations. Although this is not practical, having an automated system allowed for the easy integration of some of the commercial dimensions to be used in the design and then simulated.

Changing all of the parameters manually to create one completely new iteration of the design took eight and a half minutes. Whereas the automated system takes only 7 and a half minutes and is capable of making multiple iterations successively.

This project is also ongoing, since it is not practical to completely develop a TDR in a single year. Substantial time and effort was spent creating the CAD system as it will save significant time in the future as the design is further developed and refined.

10.1.1 CAD software

Autodesk Inventor 2016 was used to design the TDR. It was chosen for a number of reasons. The first reason was that the author had previous experience with using this software package and therefore time would not be spent becoming familiar with a different software package. The second reason to use Inventor was because a free student version is available as opposed to other CAD programs such as Solidworks (v2016 Dassault Systèmes, Providence, RI, USA).

The use of Autodesk inventor was not without its disadvantages. Although the software does have the ability to run macros it does not process the recording capabilities. This meant that a recorded macro template could not be altered to allow an automated parametric analysis of the multiple dimension combinations.

10.2 Initial CAD Automation System

Similar to the Velodrome TDR design the CAD automation system went through a number of design iteration stages.

Initially a third party freeware macro recorder (Perfect Automation Version 2.7.1 Gentee.Inc) was used to create a macro. The software recorded the user's mouse and keyboard operations to replicate the opening of the CAD part and updating the parameters by importing an appropriate XML file. Difficulty incorporating the parametric analysis component of the project was experienced with this method. This difficulty arose as the macro relied on the open window for opening parts in Inventor, being positioned in exactly the same location. It also required the location of the CAD part file and XML file used to update the part geometry being placed in the same location i.e. at the top of the file list before being opened. Early attempts to correct these issues involved the intelligent naming of the part and XML file names so they would be positioned at the top of the list and opened correctly. Another flaw with using this software was that it copied the exact location of the mouse while the recording occurred. This meant that any inefficiencies from the user in moving the mouse to click on icons was recorded and repeated in the macro.

10.3 Final CAD Part Automation System

The automation process was updated to remove the macro recorder software entirely. The new process used a mouse and keyboard commander from the import `java.awt.Robot` and import `java.awt.event.*` MATLAB library. The basic structure of the automation process for all of the CAD parts (including the template parts for creating moulds) followed the same process (Figure 85).

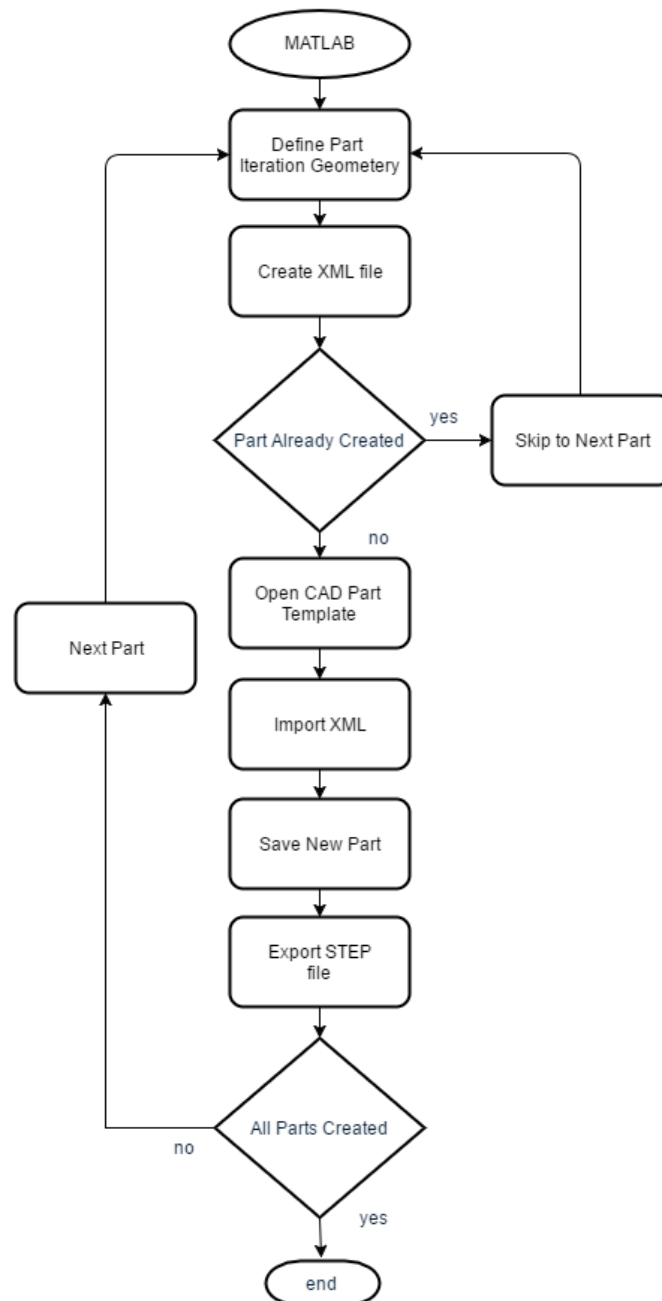


Figure 85: The automation process utilised to create different iterations of the CAD parts.

The automation process was generated in MATLAB. The system first generates all of the different part dimensions within a function. These dimensions are then passed to another

function where they are initially checked to make sure they abide by predefined limitations (Section 10.5).

The function then creates the XML files, and checks if the particular part had been already created. If it already exists, the program skips to the next component of the TDR. Otherwise the CAD part template file is opened, the XML file is imported and the dimensions are updated. The new updated part is then saved with the file name containing details on its dimensions, and then exported as a STEP file so it can be imported into the Abaqus FEA software. This process is repeated until all parts have been made.

10.3.1 Minor Functions

The main function for creating the CAD parts utilises a number of functions for repeated tasks throughout its execution (Table 58).

Table 58: Different subroutine functions that are used during the creation of the CAD parts.

Function	Summary
RemovePeriod	Removes ‘.’ from file names and replaces them with the valid ‘_’ character.
XML templates	Different XML templates unique to each part which is updated with the desired parameters and then saved and renamed accordingly.
ClickImportParamters	Clicks on the import parameters from XML button.
KeyType	Commands the keyboard to type the characters of a string that it is passed (used extensively for opening and saving files).
Convert2STEP	Clicks on the export CAD button and scrolls through with the keyboard to select the desired STEP format.
clickSave	Clicks save.

10.4 Assembly Creation

Additional steps were included in the code to generate the moulds needed to derive the inner and top core parts. These template parts would then be automatically placed in an assembly and constrained through the use of subroutine functions. This section of code was required to use the mouse controller and needed some innovation to ensure that it would work for every iteration (Figure 86). The function responsible for creating these assemblies performed the following tasks:

1. Click the place part icon.
2. Use the keyboard simulator to open the required part and press the enter key to import it.
3. Move the mouse onto the assembly window and place the part.
4. Collapse all of the folders in the model pane for consistency.
5. Expand the appropriate origin and part folders.
6. Use the keyboard to open the constrain option.
7. Constrain the first part to the centre point of the global coordinate system.
8. Constrain the second part to the centre point of the other part, to ensure correct orientation.
9. Save the mould assembly.

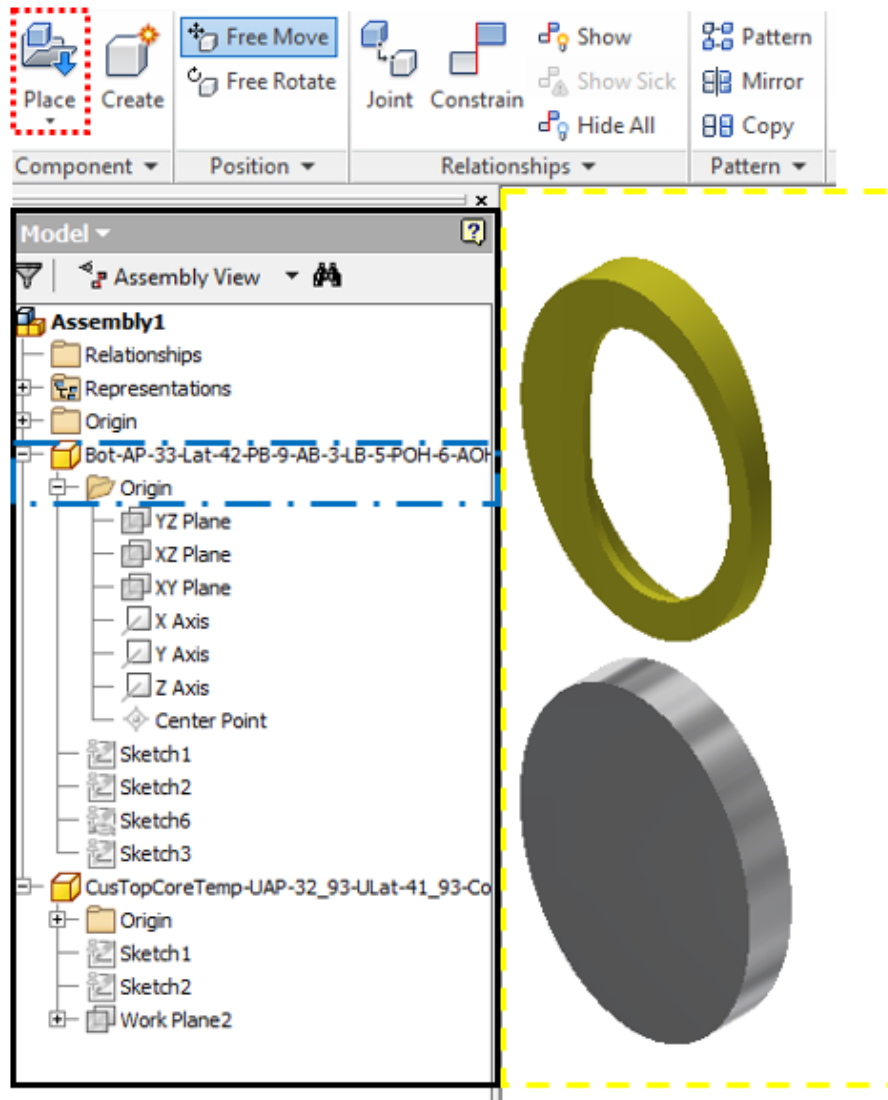


Figure 86: Section of the assembly creation window. The place button (red, dot dashed box), the model window (black, solid box), part and part origin box (blue, line dot line dashed box) and the assembly window (yellow, dashed line).

These mould were then used to derive a new part. The derive part window; needed to select which parts of the assembly to add or subtract to derive the new part, is not fixed in position; like the model window in the create assembly mode (Figure 86). The difficulty of the automating this process was further increased as the command to remove one part from the mould was not accessible through keyboard commands (TAB, down etc.). This issue was resolved by innovatively resizing the derive part window. The window was resized by accessing the resize window tab from the alt-space command. This was combined with the mouse controller to reshape the window to a consistent size and location. This allowed the mouse controller to be used to remove the unwanted part from the mould and create the desired mating part.

10.5 Dimension limitations

There are a number of limitations imposed on the dimensions of the bottom core to make sure the part is created correctly.

The manner in which the bottom core is made by lofting the different internal trapezium geometries around an ellipse rail (Figure 87) caused two main constraints on possible design iterations dimensions.

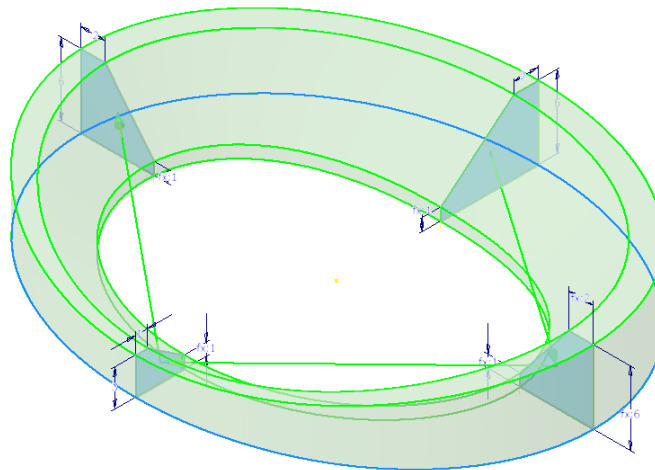


Figure 87: The internal trapezium geometries that are lofted around the outer ellipse rail.

These constraints were based on how the loft rotates about the centre of the ellipse. Therefore, in order to create the correct shape, the base dimensions and the top edge dimensions could not be greater than the respective radius of the ellipse. The top edge dimensions (Figure 79) were also compared to the base to make sure they were smaller so that the correct velodrome shape was generated.

Maximum bottom core outer height dimension constraints were also enforced. This limitation was due to imposing of a minimum outer height of 1 mm for the top core, preventing it from becoming too thin and becoming a weak point when joining the top core to the endplates. The maximum outer height dimension of the bottom core, was derived from the total TDR height parameter and was equal to the total TDR height minus the minimum top core outer height of 1 mm and the endplate thickness (Figure 88).



Figure 88: The maximum outer height of the bottom core = Total TDR height - 1 mm - Superior Endplate Thickness - Inferior Endplate Thickness.

If any dimensions did not meet the limitations the iteration was stopped before it proceeded to creating the CAD geometry and in doing so saved time and prevented errors.

10.6 Disadvantages of Automation System

The major disadvantage of the CAD automation process was the need to incorporate the mouse and keyboard controller. This unfortunately resulted in the computer being unable to be used while the automation system took control over the mouse and keyboard. In addition, pauses had to be incorporated into the software to account for loading time when waiting for operations such as opening template parts or saving the files. These pauses also had to take into consideration that subsequent parts would be made and that loading time may vary depending on processor speed.

The implementation of generating different iterations of the design was also not automated at this early stage of design. The different combinations were set manually before the CAD automation process would create the different iterations that have been specified. This reduced the time saving ability of the automation process.

A video of the CAD automation system in real time has been included on the accompanying disc provided.

Chapter 11. FEA Study

11.1 Aim of FEA

The aim of the FEA study was to investigate the different automatically generated design iterations to identify if the Velodrome design concept was feasible. The goals of the FEA was to simulate the designs in a simple loading scheme in order to:

1. Prove that the FEA component of the project could be automated.
2. Illustrate the customisable bottom core design concept.
3. Investigate if the CoR of the simulated TDR design was within physiological ranges.
4. Use the results to identify which dimensions could potentially be used to refine the TDR design.

11.2 Development of FEA model

The FEA model was developed in Abaqus/CAE. A structured approach was used to create the model, from the different part CAD geometries previously developed in an automated CAD system (Chapter 10). These CAD geometries were exported as STEP files so they could be imported to the Abaqus software.

The process of how the FEA models were developed involved a multistage process:

1. The STEP files of each part was imported into Abaqus.
2. The different surfaces of each part were defined.
3. Relevant parts were segmented.
4. New surfaces due to segmentation were defined if needed.
5. Sets were made containing the whole part geometries to allow material property assignment.
6. Material properties were defined.
7. The different parts were meshed.
8. Material properties were assigned to the different parts.
9. Node sets containing the tracking nodes were generated.
10. The parts were imported into the assembly.
11. Appropriate constraints were applied to the different parts.
12. Boundary conditions are applied to the model.
13. The Loading step is generated.
14. Output requests are created.

15. The FEA job is defined.

16. The input file is generated.

As slight variations of this process were to be repeated for the different design iterations, this procedure was also automated.

11.2.1 Additional Parts

Initially, only the parts generated from the CAD automation process (inferior endplate, bottom core, inner core, top core and superior endplate) were going to be used in the FEA. It was planned that a couple moment would be applied to the superior endplate by creating two oppositely directed vertical concentrated point loads at the front and back nodes in the centre of the top surface of the superior endplate. Unfortunately, this caused significant local deformation of the EP in close proximity to the load application (Figure 89). This significant deformation is generated due to the manner in which a point load is simulated, which essentially applies a stress over an infinitesimally small area.

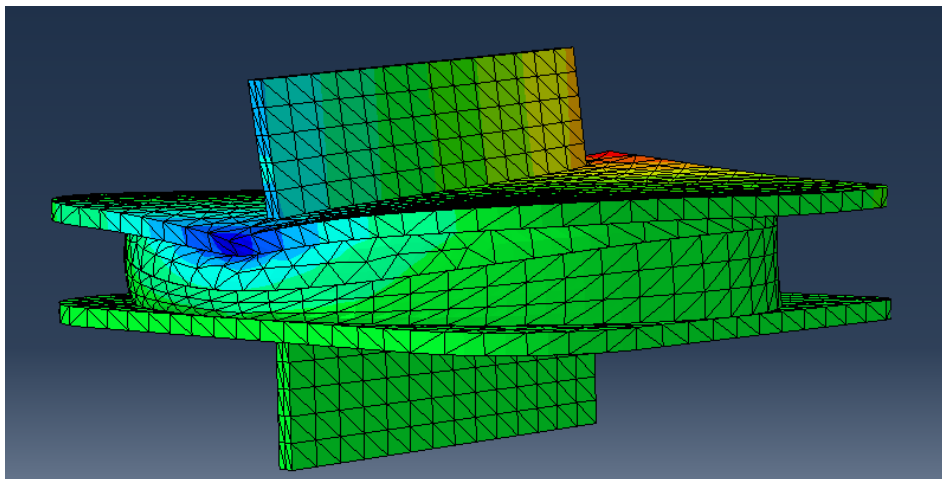


Figure 89: Initial point load simulation causing large local deformations.

Applying the concentrated forces at the top of the keels was also attempted in order to overcome this deformation problem however, this did not rectify the problem.

To overcome this issue, a box-like structure was generated which the superior endplate was then ‘implanted’ into (Figure 90). The application of applying the load to the model was also altered so that a pressure was applied to the front and back half of the top of the box instead of the endplate to prevent unrealistic deformation.

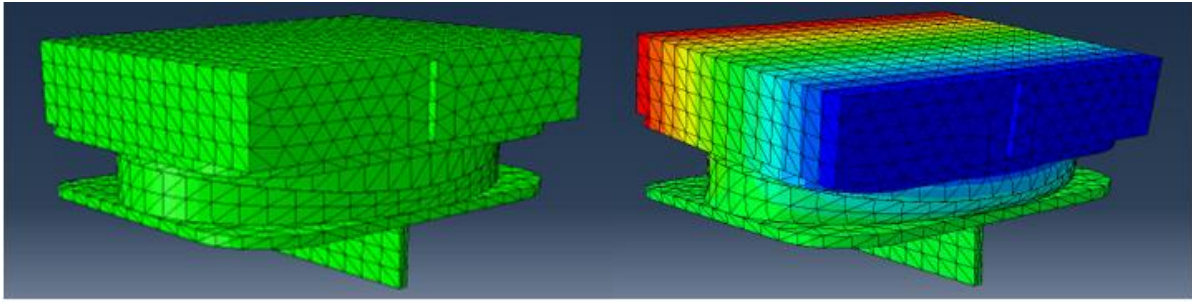


Figure 90: The developed model with the 'box like structure' used to apply the bending moment to the designed TDR. The model before deformation (left) and after (right).

11.3 Segmentation of Parts

When the parts are meshed the node coordinates are not generated in a consistent manner. These changes in node coordinates are known to occur due to alterations in part geometry and mesh density. This was an issue as the calculation of the CoR of the design required the consistent tracking of node coordinates. The location of these nodes relative to the geometry of the part, was required to be consistent to allow comparing of results between different design iterations.

Two nodes (anterior, posterior), on the bottom surface of the superior endplate in the mid sagittal plane were tracked to allow the CoR and RoM to be calculated. Segmenting the part prior to meshing causes the meshing algorithm of Abaqus to consistently generate a node at the desired locations. This allowed for the consistent tracking of the desired node's location throughout the loading cycle for ever design iteration (Figure 91).

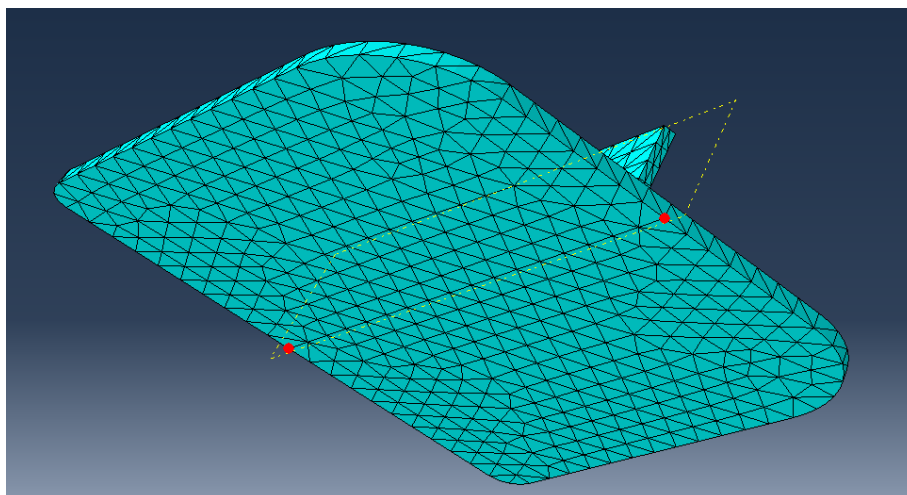


Figure 91: Superior endplate with the front and back tracking nodes selected in red. The box used to apply the couple bending moment to induce flexion to the designed TDR also had to be segmented to allow the definition of the front and back areas of the top

surface. These surfaces were then used to apply equal magnitude but opposite direction pressures to cause the bending (Figure 92).

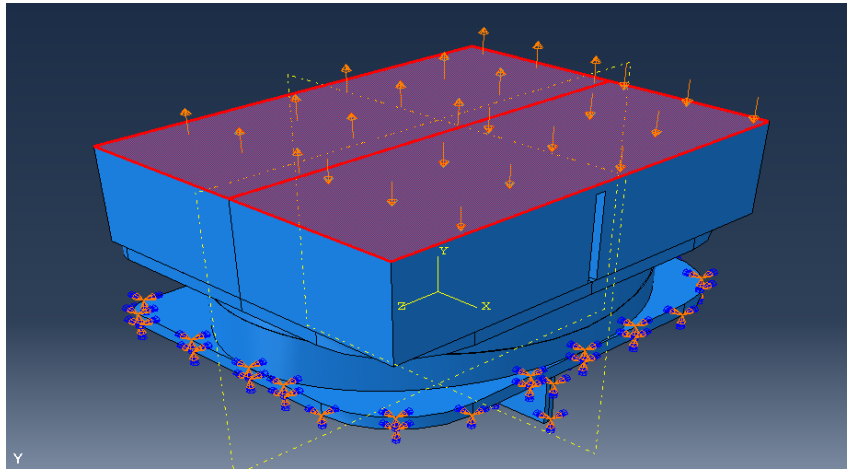


Figure 92: The pressure loads applied to the front and back halves of the 'box' part.

11.4 Material Properties

The Young's modulus and Poisson's ratio used for the titanium alloy in the FEA was 116 GPa and 0.342 respectively (Table 46)(ASM Aerospace Specification Metals Inc. n.d.; AZoM 2013). Vertebral cortical bone material properties were selected to be used for the box component of the FEA model. Bone materials were chosen to roughly approximate the conditions the TDR will be under in vivo, although the main purpose of the box was to apply the appropriate bending loads to the TDR. The material properties of the bone were derived from a previous FEA, well cited paper also simulating pure moments in the sagittal plane of the lumbar spine (Shirazi-Adl et al. 1986). The resulting Young's modulus and Poisson's ratio used in the developed model was 12000 MPa and 0.3 respectively.

The material properties of the composite core were much more difficult to derive. A major component of elastomer core TDRs is the material used for the elastomer core. Majority of these TDRs use silicone polycarbonate urethane. Silicone polycarbonate urethane is a copolymer and the material properties depend on the ratio of monomer units in the polymer. This has resulted in patents being filed for particular silicone polycarbonate urethane copolymers and the methods used to create them (Rega 2012).

The material properties of the silicone polycarbonate urethane used by commercial TDRs are often kept as trade secrets, as their development is a costly process. The Freedom TDR disclosed that the elastomer core is comprised of polymer developed by a third party called CarboSil™. Unfortunately, upon researching this polymer, the provided material summary

sheet from the manufacture's (DSM) website did not disclose the relevant Young's Modulus and Poisson's ratio needed to implement the material into Abaqus (DSM 2012).

In order to have a somewhat close representation of the potential rubbers that could be used to create the different core components. The rubber materials used in the model were derived from published online general material properties of silicone rubbers. The Young's Modulus and Poisson's ratio of the rubbers can vary between 0.001 and 0.05 MPa and 0.47 and 0.49 respectively (AZO Materials n.d.).

A major part of the proposed design is the three-part composite core which was designed to have each component made of different grade of rubber. For the purpose of this early stage of design the material properties were kept constant for all of the simulations. The bottom core was designed to be the stiffest of all the rubbers as it is used to somewhat constrain the RoM of the TDR. The rubbers were given the same Poisson's ratio of 0.45. This value was chosen; even though it lies just below the published values, as Abaqus has issues solving when the Poisson ratio is close to 0.5. The Young's Moduli of the rubbers were obtained through a trial and error process; within the given range, to ensure that an adequate amount of flexion occurred in the simulations (Table 59).

Table 59: Material properties of the elastomer core.

Component	Young's Modulus (MPa)	Poisson's Ratio
Bottom Core	10	0.45
Top Core	6	0.45
Inner Core	5	0.45

Isotropic linear elastic properties were applied to all parts of the model even though only the metal endplates are in fact comprised of an isotropic elastic material. This decision was made to shorten simulation time during this early proof of concept stage of the design, as the incorporation of hyper elastic material properties into the model would require further computational power.

11.5 Assembly

The parts were strategically made in Inventor so that they were already created in the pre-defined global coordinate system. Incorporating this feature removed the need of having to reposition the different parts of the design once they are imported. This made the automation system must easier to implement.

11.6 Constraints

All of the parts were constrained to the appropriate mating part/s with tie constraints. Tie constraints were implemented as it was assumed that all of the separate parts were perfectly bonded to one another. This also simplified the FEA by removing the need to incorporate contacts between parts which can potentially cause issues with the simulations. This however, is a limitation of the model used, but was considered acceptable during this early stage of design.

11.7 Boundary Conditions

The inferior endplate was constrained in all 6 DOF. This method is common in other FSU bending tests from literature (Michael Adams, Green, et al. 1994; Zhao et al. 2005).

11.8 Loading Regime

A simple 10 Nm couple moment, flexion test was simulated to investigate the CoR response of the Velodrome TDR. The implementation of applying 10 Nm of flexion was derived from testing performed on the LP-ESP (Lazennec et al. 2012). The required pressure need to create the 10 Nm couple moment was automatically scaled to the design iterations size to ensure a constant load was applied to all design iterations.

11.9 Parametric Study

One of the aims of the FEA is to use the results to investigate the Velodrome design concept. Due to the large number of different variations of the design possible and the development of the automated CAD and FEA systems, a parametric study was performed. The study investigated the influence of the bottom core parameters on the CoR and RoM of the designed TDR. The parametric study was designed to compare results to a control model which was derived by hypothesising the influences of the different parameters.

Multiple linear regression analysis was performed to investigate the influence of particular variables on the location of the CoR in order to reveal if a particular dimension can be used to alter the CoR into a more physiological location.

11.9.1 Control Parameters

Originally, two iterations of each of the nine different parameters tested and changed one at a time, while the remaining variables were kept to the control values.

The control design parameters were developed with inspiration from the range of motion section of the literature review (Section 4.12). It was discovered that the lumbar FSU has the

greatest range of motion in flexion, followed by lateral bending or extension; depending on lumbar index level. Therefore, the control values were selected to cause the internal trapeziums to be largest (stiffest) in the posterior region, moderate in the lateral regions and smallest in the anterior region, this would hopefully allow the composite core to have a RoM and CoR that is similar to the natural disc.

The logic behind having the posterior region of the bottom core larger than the anterior region was based on a simple spring analogy. Imagine two springs on the bottom of a beam at opposite ends. One spring is infinitely stiff the other is completely compliant. If a couple bending moment is applied to the top of the beam, the beam will rotate about the infinitely stiff spring. As the proportion of stiffness between the stiff spring and the compliant spring decreases the CoR will migrate towards the less stiff spring. This ideology is behind the velodrome shape of the design concept and will hopefully allow for the eventual tuning of the CoR so that it lies within two standard deviations of the physiological mean.

The early stage simulations kept the anterior posterior width, lateral width, keel height width and length, total core height, inner height, superior and inferior endplate thickness, and total core height constant for all simulations (Table 60). This was done to reduce the number of iterations needed to be simulated. These variables were also believed to have less of an impact in proving the main concept of the Velodrome TDR. The constant values were either derived from the specifications or estimated.

Table 60: Constant variables for FEA.

Anterior posterior width	Lateral width	Keel height	Keel thickness	Keel length
33 mm	42 mm	10 mm	1 mm	80 % of anterior posterior width (26.4 mm)
Total height	Inner height	Superior endplate thickness	Inferior endplate thickness	Total core height
10 mm	1 mm	1.5 mm	1.5 mm	Total height – superior and inferior endplate thickness (7 mm)

11.10 Investigated Design Iterations

The dimensions which were altered in the parametric study were the posterior, anterior and lateral base (PB, AB and LB), posterior, lateral and anterior outer heights (POH, LOH and

AOH) and posterior, anterior and lateral top edges (PTE, ATE and LTE). These parameters were chosen to be included in the early testing of the design as they are believed to have the most impact on the customisation of the mechanical response feature of the unique composite elastomer core (Table 61).

Table 61: The parameters used in the parametric analysis of the prototype design. (PB=Posterior base, AB= Anterior base, LB=Lateral base, POH=Posterior outer height, AOH=Anterior outer height, LOH=Lateral outer height, PTE=Posterior outer height, LTE=Lateral outer height).

Combination number	PB	AB	LB	POH	AOH	LOH	PTE	ATE	LTE
1	8	4	8	6	3	6	2	1	2
2	8	4	8	6	3	5	2	1	2
3	8	4	8	6	3	4	2	1	2
4	8	4	8	5	3	6	2	1	2
5	8	4	8	4	3	6	2	1	2
6	8	4	8	6	4	6	2	1	2
7	8	4	8	6	2	6	2	1	2
8	8	4	6	6	3	6	2	1	2
9	8	4	7	6	3	6	2	1	2
10	6	4	8	6	3	6	2	1	2
11	7	4	8	6	3	6	2	1	2
12	8	3	8	6	3	6	2	1	2
13	8	5	8	6	3	6	2	1	2
14	8	4	8	6	3	6	2	1	3
15	8	4	8	6	3	6	2	1	4
16	8	4	8	6	3	6	3	1	2
17	8	4	8	6	3	6	4	1	2
18	8	4	8	6	3	6	2	3	2
19	8	4	8	6	3	6	2	2	2

11.11 Measurement of CoR

The FEA was established in such a manner that the loading step of the simulation was separated into eight different equally spaced frames. This allowed the instantaneous CoR to be calculated for each of the frames of motion as the TDR underwent the flexion motion. This was a very important component of the analysis, as it revealed if the CoR is constrained or not.

The instantaneous centre of rotation was calculated as the intersection point between the perpendicular bisectors of the displacement vectors of the front and back tracking nodes for each of the frames of loading. This is the same method used in a number of publications

(Sears et al. 2006; Percy & Bogduk 1988). The paper used to compare the results to, in order to investigate if the CoR lies within two standard deviations of the mean also used this method (Percy & Bogduk 1988).

11.12 Measurement of RoM

The range of motion of the TDR when undergoing the simulated flexion bending was also calculated. It was calculated relative to the fixed inferior endplate by taking the tan of the slope of the line joining the two displaced tracking points. This assumed no deformation of the titanium endplates occurred during the simulated loading.

11.13 Convergence Study

A convergence study was performed on the generated FEA model to investigate what mesh size should be used during the simulations. A finer mesh gives more accurate results, which comes at the cost of requiring longer simulation times. A convergence study reveals that as the mesh density increases the outputs of the FEA study begin to converge. As the simulations converge the variance in results between different mesh sizes decreases. This is used to find an appropriate compromise between the result accuracy and time required to run the simulation.

11.13.1 Convergence Study Method

Five different mesh sizes were investigated in order to help determine which mesh size should be used for all of the simulations. A 1 % tolerance of percentage differences between meshes has been used to identify when the appropriate mesh has been applied.

Table 62: Convergence study results.

Mesh Size	RoM	Percent (%) difference to larger mesh size
2.5	6.6838	-
2.25	6.6388	-0.67
2	6.6439	+0.08
1.75	6.6037	-0.61
1.5	6.5855	-0.28
1.25	6.6166	+0.47

The results from the convergence study reveal the model converges immediately as there is always a percentage difference between results from different mesh sizes of less than 1 %. A mesh size of 2 was chosen. This mesh size was chosen even though it wasn't the coarsest mesh to converge to insure that it is appropriate to have other iterations of the design use the

same mesh size for consistency. In addition, the simulation time when using a mesh size = 2 was relatively short at approximately 20 minutes.

11.14 Mesh Size and Type

A tetrahedral mesh type was implemented due to the complex geometry of the design, and because a hexagonal mesh type would not allow for the automated FEA component of the project; as they have to be generated manually.

11.15 FEA Automation

Similar to the CAD section of the project it was decided that the FEA component of the project should also be automated. This was implemented to allow for the integration between the development of the CAD design iterations, and the following analysis.

Automating the FEA also made practical sense, as like the creation of a single CAD iteration of the design, creating a new FEA model for each of the different design iterations is a very timely process.

The FEA automation utilised the journal (.jnl) file that Abaqus CAE generates as the user creates their model. This journal file contains the python script which can be used to replicate the user's commands from the Abaqus command line.

One model was first generated manually and the accompanying generated jnl file was used as a template. This template was then recreated in MATLAB to generate the appropriate python script for each of the design iterations. The generation of the accompanying python script occurred concurrently with the CAD automation system. This allowed the relevant data from each design iteration to be easily integrated into the python script.

The odb files which contain the results following the simulations were then accessed through another automatically generated python script. This script allowed for the displacements and initial coordinates of the tracking nodes to be exported as a txt file for external post processing. The txt files were then automatically opened in MATLAB for the calculation of the CoR and RoM of all the different iterations. The results were first plotted in MATLAB to allow for the visualisation of the CoR. This allowed the CoR to be tracked as the different TDR iterations underwent flexion. This data was then used to investigate the proof of concept and to visually identify if the CoR lies within the desired physiological range. The results were then summarised in a table and exported to Excel (Microsoft Excel 2016) for multiple linear regression analysis.

11.16 Batch Analysis

One downside of the FEA component of the project was that the user did not have local access to an Abaqus license. Therefore, the automatically generated Abaqus python scripts and CAD STEP files had to be manually copied onto a remote server to perform the analysis.

The python script; once executed from the command line through MATLAB, generates an Abaqus input file. This input file is then run in a batch system; again via the Abaqus command line, from the same MATLAB script. The input file name is used to derive the name of the output txt files which contain the results after the FEA simulations have been run. It was initially planned that the input file names would contain information on all of the different parameters of the particular design iteration to make post processing easier.

Unfortunately, Abaqus enforces a 31-character limit on the input file name length. This limit was exceeded. This problem was resolved through the generation of a list that contains the parameter information of the different iterations that had been created. The input file names were then generated numerically in the order of where the particular iteration lay on the list. Once all of the simulations had been completed the resulting txt files; containing the displacements of the two tracking nodes as the TDR underwent flexion, were then copied back onto the user's computer for post processing.

11.17 Post Processing

The post processing component of the FEA section of the project was partially automated. The txt files containing the results were automatically imported into MATLAB and the parameters corresponding to the results are retrieved from the previously generated list.

The instantaneous CoR was then calculated for each of the frames of the simulation and stored appropriately. The final displaced tracking node coordinates are then plotted as the inferior corners of a box representing the superior vertebrae of a lumbar FSU. This box was sized to have an anterior posterior width equal to the anterior posterior width of the tested TDR design. The box was then given the same height as a typical lumbar vertebral body (30 mm) (Table 5). The same dimensions were given to the inferior fixed vertebrae to give a visual representation of the simulated FSU undergoing bending in the sagittal plane (Figure 93). The coordinates of the physiological CoR (derived from Table 25) was scaled (Table 63) to these box coordinates (Percy & Bogduk 1988).

Table 63: The model coordinates of the physiological CoR x and y coordinates and the two standard deviation ranges.

Lumbar segment	X model coordinate of mean CoR	Two standard deviations from the mean x CoR coordinate	Y model coordinate of mean CoR	Two standard deviations from the mean y CoR coordinate
L4-L5	-2.97	(-7.59, 1.65)	-1.2	(-9.6, 7.2)
L5-S1	-3.69	(-13.86, 5.94)	5.7	(-9.9, 21.3)

In order to investigate if the CoR lay within two standard deviations of the physiological CoR an ellipse was created which centred on the scaled physiological mean. The x and y radius of the ellipse was equal to the two standard deviations of the respective x and y physiological CoR locations.

The RoM was also calculated and the results from all the different iterations are summarised in a table which was then copied into Excel (v2016, Redmond, Washington, Microsoft) for statistical analysis.

11.18 Results

One of the main novel design features of the Velodrome TDR is the composite elastomer core. A main feature of this design is how it allows for customisation of the mechanical response depending on the bottom core dimensions. The FEA analysis illustrated that the mechanical response of the TDR; when subjected to 10 Nm of flexion, does alter for different iterations of the design (Figure 93).

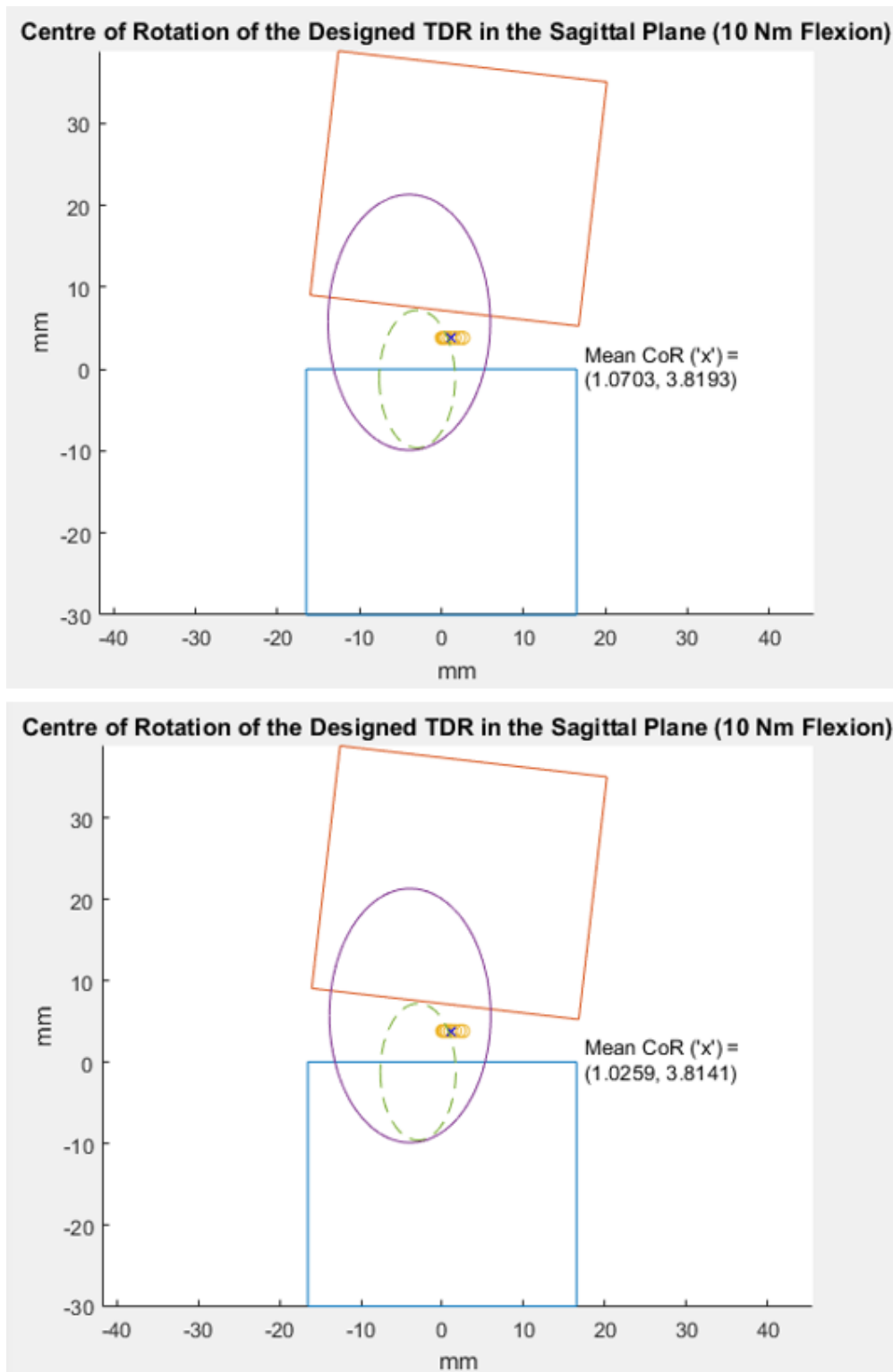


Figure 93: The results from two different iterations of the Velodrome TDR design. Dashed ellipse = two standard deviations from the L4-L5 CoR mean, solid ellipse = two standard deviations from the mean CoR for the L5-S1 index level, x = mean CoR of the TDR, o = the instantaneous change in position (posterior to anterior (left to right)) of the CoR as the TDR undergoes flexion.

The change in mechanical response was shown as the CoR of each of 19 interactions tested was different, although only slightly (Table 64).

Table 64: FEA simulation results for the 19 different design iterations. (Final instantaneous X CoR= The final frame CoR x coordinate, Final instantaneous Y CoR= The final frame CoR y coordinate, Mean CoR X = mean centre of rotation x coordinate, Mean CoR Y = mean centre of rotation y coordinate, RoM = range of motion).

Combination number	Final Instantaneous X CoR	Final Instantaneous Y CoR	Mean X CoR	Mean Y CoR	RoM (°)
1	2.580	3.791	1.047	3.805	6.604
2	2.583	3.822	1.044	3.812	6.599
3	2.604	3.796	1.055	3.795	6.587
4	2.544	3.926	1.03	3.845	6.618
5	2.545	3.957	1.037	3.864	6.612
6	2.599	3.858	1.055	3.839	6.595
7	2.540	3.886	1.035	3.831	6.633
8	2.613	3.879	1.057	3.857	6.605
9	2.599	3.860	1.053	3.841	6.602
10	2.612	3.873	1.068	3.847	6.615
11	2.597	3.888	1.055	3.854	6.606
12	2.544	3.800	1.026	3.814	6.634
13	2.624	3.818	1.07	3.819	6.575
14	2.589	3.861	1.048	3.833	6.599
15	2.610	3.836	1.062	3.818	6.591
16	2.572	3.792	1.047	3.808	6.614
17	2.570	3.835	1.044	3.82	6.616
18	2.602	3.794	1.06	3.802	6.598
19	2.602	3.884	1.059	3.843	6.6

The mean and standard deviation of the RoMs of the all the different TDR iterations was 6.605° and 0.0146° respectively. Another major design requirement was that the CoR should not be constrained like a ball and socket TDR (Section 4.17.1). This design feature of the Velodrome TDR design concept was also shown with the FEA analysis as the CoR is clearly not fixed, due to its changing position as it undergoes flexion (Figure 93).

11.18.1 Parametric Analysis

The mean CoR and the locations of the instantaneous CoRs as the TDR underwent flexion all lay within two standard deviations of the physiological mean for the L5-S1 lumbar segment level (solid ellipse (Figure 93)).

The location of the CoR of all of the TDR design iterations was shown to migrate anteriorly as it underwent flexion bending (Shown in the ResultsAnimation on the disc provided). This is not physiological and caused the CoR to drift outside of two standard deviations of the mean CoR location of the L4-L5 lumbar segment (Figure 93). The y coordinates of the CoRs however, were all within two standard deviation of the physiological mean for both the L4-L5 and L5-S1 values (Table 63).

The variable linear regression was performed; in Excel, on the different parameters to identify which of the nine dimensions altered most strongly correlates with the final instantaneous x coordinate of the CoR. This was performed to hopefully correct CoR location.

The resulting multiple variable regression equation was:

Equation 1: The resulting multiple variable linear equation to predict the x coordinate of the CoR.

$$\begin{aligned} \text{Final CoR } X_{\text{Coord}} &= -0.0108\text{PB} + 0.0222\text{AB} - 0.0058\text{LB} + 0.0067\text{POH} + 0.0101\text{AOH} \\ &\quad - 0.0034\text{LOH} - 0.0004\text{PTE} + 0.0085\text{ATE} + 0.0069\text{LTE} + 2.545 \end{aligned}$$

Following the multiple linear regression, the anterior base (AB) was shown to have the largest effect in moving the CoR in the x direction. The posterior base (PB) had the second largest negative correlation to the x coordinate of the CoR. This indicates that the PB dimension should be increased and the AB dimension should be decreased in order to hopefully tune the CoR to lie more posteriorly and within two standard deviations of the L4-L5 physiological mean. The fact that both the posterior and anterior dimensions of the bottom core influence the CoR location also make intuitive sense as these parameters influence the regions of the bottom core that undergo tension and compression respectively during flexion bending.

A major limitation of performing this analysis is that the different combinations of parameters were not generated randomly. Instead the parameters were estimated based on the geometric limitations outlined in the specifications (Section 6.4). This use of non-random iterations for the parametric study was implemented as the study was intended for investigative purposes; as opposed to the detailed analysis of the design. The small sample size imposed limitations to the regression analysis as it only incorporated three iterations of each of the nine dimension that were investigated. This essentially meant that three data

points were used for each of the linear regressions; resulting in a straight line with an extra point being used to derive the linear variable coefficients.

Luckily, due to the automation process that has been developed the number of iterations of each of the different dimensions was doubled which resulted in a total of 37 different iterations being tested (Table 65).

Table 65: Additional design iterations that were tested.

Combination number	PB	AB	LB	POH	AOH	LOH	PTE	ATE	LTE
20	8	4	8	6	3	3	2	1	2
21	8	4	8	6	3	2	2	1	2
22	8	4	8	3	3	6	2	1	2
23	8	4	8	2	3	6	2	1	2
24	8	4	8	6	5	6	2	1	2
25	8	4	8	6	6	6	2	1	2
26	8	4	5	6	3	6	2	1	2
27	8	4	4	6	3	6	2	1	2
28	5	4	8	6	3	6	2	1	2
29	4	4	8	6	3	6	2	1	2
30	8	6	8	6	3	6	2	1	2
31	8	2	8	6	3	6	2	1	2
32	8	4	8	6	3	6	2	1	5
33	8	4	8	6	3	6	2	1	1
34	8	4	8	6	3	6	5	1	2
35	8	4	8	6	3	6	6	1	2
36	8	4	8	6	3	6	2	4	2
37	8	4	8	6	3	6	2	5	2

The new additional iterations of the design that were tested (Table 65) should allow for a more substantial statistical analysis to be performed by increasing the sample size of each parameters; from three to five. The resulting CoR locations and RoMs were calculated for the new design iterations (Table 66).

Table 66: Additional iteration simulations results. (Final instantaneous X CoR= The final frame CoR x coordinate, Final instantaneous Y CoR= The final frame CoR y coordinate, Mean CoR X = mean centre of rotation x coordinate, Mean CoR Y = mean centre of rotation y coordinate, RoM = range of motion).

Combination number	Final Instantaneous X CoR	Final Instantaneous Y CoR	Mean X CoR	Mean Y CoR	RoM (°)
20	2.597	3.831	1.050	3.811	6.596
21	2.585	3.864	1.045	3.826	6.606
22	2.536	3.937	1.032	3.856	6.614
23	2.468	3.788	1.005	3.809	6.626
24	2.551	3.926	1.036	3.867	6.619
25	2.515	4.078	1.023	3.926	6.640
26	2.598	3.920	1.050	3.885	6.622
27	2.590	3.926	1.043	3.893	6.635
28	2.621	3.880	1.082	3.844	6.631
29	2.630	3.850	1.092	3.834	6.648
30	2.590	3.834	1.068	3.822	6.592
31	2.538	3.726	1.014	3.768	6.644
32	2.598	3.791	1.059	3.801	6.598
33	2.594	3.860	1.050	3.832	6.601
34	2.598	3.849	1.054	3.826	6.596
35	2.557	3.848	1.040	3.825	6.625
36	2.567	3.832	1.030	3.817	6.619
37	2.548	3.911	1.008	3.886	6.645

After expanding the parameter study the CoR was still found to migrate anteriorly outside two standard deviations of the L4-L5 physiological CoR. A new multiple linear regression was performed with the larger sample size.

Equation 2: The updated multi variable linear equation predicting the x coordinate of the CoR.

Final CoR X_{Coord}

$$= -0.013PB + 0.018AB - 0.005LB + 0.024POH - 0.013AOH - 0.003LOH \\ - 0.003PTE - 0.004ATE + 0.007LTE + 2.570$$

The new results indicated that increasing the posterior base (PB) and the anterior outer height (AOH) and decreasing the anterior base (AB) and posterior outer height (POH) should cause the CoR to shift closer to the L4-L5 anatomical mean. An additional iteration which applied these changes was also created and simulated (Table 67, Table 68).

Table 67: The refined iterations dimension parameters (PB=Posterior base, AB= Anterior base, LB=Lateral base, POH=Posterior outer height, AOH=Anterior outer height, LOH=Lateral outer height, PTE=Posterior outer height, LTE=Lateral outer height).

Combination number	PB	AB	LB	POH	AOH	LOH	PTE	ATE	LTE
38	10	2	8	3	6	6	2	1	2

Table 68: Refined iteration simulations results. (Final instantaneous X CoR= The final frame CoR x coordinate, Final instantaneous Y CoR= The final frame CoR y coordinate, Mean CoR X = mean centre of rotation x coordinate, Mean CoR Y = mean centre of rotation y coordinate, RoM = range of motion).

Combination number	Final Instantaneous X CoR	Final Instantaneous Y CoR	Mean X CoR	Mean Y CoR	RoM (°)
38	2.4377	3.8198	0.9722	3.8018	6.6803

The refined iteration did move the final instantaneous CoR x coordinate closer to the L4-L5 two standard deviation ellipse physiological range (-7.59, 1.65). However, the amount of movement was still very slight compared to the existing design iterations. This lack of substantial variation between the resulting CoR locations is likely due to variables that are kept constant throughout the different simulations. It is hypothesised that the material properties of the rubbers for the different core components are too similar (Table 59). This combined with the tie constraints joining the different core parts (Section 11.6) is believed to be causing the core to act as a single homogenous solid. The current ratio between the bottom core and top core elastic moduli is only 10:6. This may be limiting the influence that the bottom core has on manipulating the location of the CoR. This ratio was altered to 10:3 to investigate if this ratio between the stiffness of the bottom core components is the factor that is not allowing the changes in geometry to significantly influence the CoR.

The control and combination numbers 4 and 5 (Table 61) were restimulated with updated elastic modulus material properties.

Table 69: Updated material properties used to investigate the effect of the bottom core to top core elastic modulus ratio, on the variance between different design iterations.

	Bottom Core	Top Core	Inner Core	Bottom to Top Core Ratio
Original	10	6	3	10:6
Updated	10	3	1	10:3

The fourth and fifth design iterations were used in conjunction with the control parameters as they investigated the effect of the posterior outer height (POH) on the CoR location; which was the parameter shown to have the greatest influence on the CoR according to the multiple variable linear regression analysis (Equation 2).

Table 70: The original results (left column) compared to the updated results (right column).

Combination number	Final Instantaneous X CoR		Final Instantaneous Y CoR		Mean X CoR		Mean Y CoR	
1	2.580	2.537	3.791	4.430	1.047	0.994	3.805	4.343
4	2.544	2.625	3.926	4.499	1.03	1.020	3.845	4.350
5	2.545	2.625	3.957	4.533	1.037	1.027	3.864	4.370

11.19 Discussion

11.19.1 Automation Clarification

The first goal of the FEA component of the project was purely a proof of concept that the FEA could be successfully automated. This goal was somewhat achieved.

The developed system; once the correct files had been copied to the server for analysis; automatically simulated most of the models and the generated txt files containing the results of the working models for post processing.

The major issue which was encountered was due to use of the Abaqus CAE jnl file for automation of FEA analysis. The generated jnl file; which was used as a template to base the automation system on, uses the surface mask names in order to define the surfaces. These mask names are not accessible to the user and are not named in a logical manner. Therefore, the names of the specific surfaces that had to be defined could not be intuitively obtained and used in the automation process. This issue was overcome by utilising the Abaqus python scripting library. The Abaqus python library contains different functions that allow for surface selection. The two that were utilised by the automation process were the findAt() and the getByBoundingCylinder() commands. The findAt() command can receive two points which lie on the desired surface in order to define it. The getByBoundingCylinder() command requires two points which lie on a selecting cylinder's centre axis, and a value for the cylinder's radius. Any surface that lies within the cylinder will then be used in the surface definition.

Issues arose even when incorporating these commands. The `findAt()` function in particular had problems with selecting the desired surfaces, even when the points used to select the surface were found to lie on the surface (Figure 94).

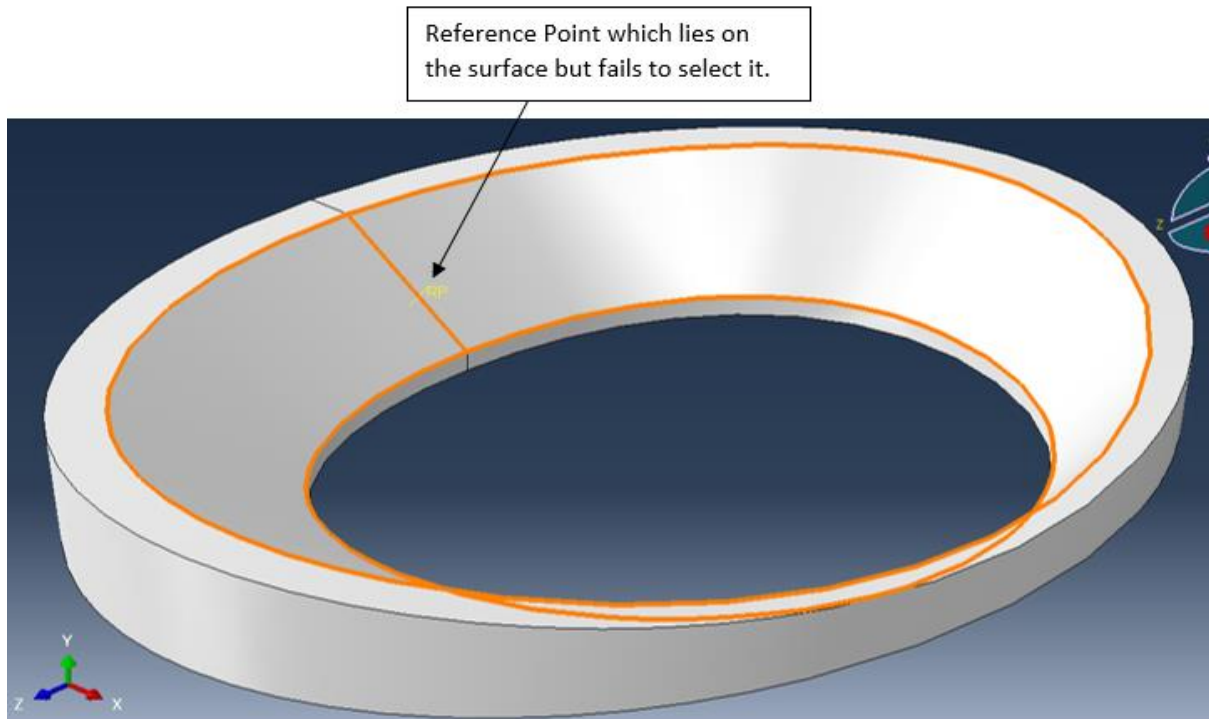


Figure 94: The bottom core sloped surface which would fail to be defined for particular design iterations. Note that the point used by the `findAt()` function does lie on surface as indicated by the reference point.

Luckily this problem was often overcome by using the `getByBoundingCylinder()` command instead of the `findAt()` command. The problem caused by the `findAt()` function is believed to be due to the imprecise geometry generated from using the loft tool to generate the bottom core (Section 10.5). The imprecise geometry was suspected as only geometries which were directly or indirectly (through using the bottom core as a template to derive parts i.e. the inner and top cores) influenced by this loft tool were affected by this issue.

The initial 19 design iterations of the design that were tested, were correctly and fully automatically generated and analysed in Abaqus. The developed python script and MATLAB automation system for running the simulations also worked.

However; when the sample size was doubled, five of the additional iterations developed for further analysis did not correctly define the surfaces of the different TDR parts. This was not a major issue as the batch system, takes advantage of the Abaqus input file submission examination. If the surface definitions are missing from the model, the affected design

iteration is not simulated and the process skips to the next design. The failed iterations are easy to locate as the odb file has a ‘_f’ suffix to indicate the failure. When the particular failed model is recreated manually using the python script a failure warning identifies the user which surfaces have to be manually defined. Once corrected all of the previously failed models were successfully simulated.

The automation system can still be branded as a success as it allows the efficient development of numerous CAD design iterations to be automatically developed. This alone saved and will continue to save significant time as the project progresses. The automated CAD system alone prevents human error when updating parts, has redundancy prevention when creating the different parts, and allows the user to work on other aspects of the project while the iterations are being developed.

11.19.2 Proof of Concept

Although the different iterations did exhibit different mechanical reposes in terms of CoR location, the standard deviations of the mean x and y coordinates of the CoR of the expanded 37 design iterations test was only 0.0186 and 0.0308 mm respectively. These low standard deviations indicate that the differences in the locations of the CoR of different iterations was slight. The cause of this lack of significant changes in the CoR could be contributed by a number of different factors.

The lack of analysis which investigates how combinations of parameters influence the CoR location could have contributed to the failure to identify the key parameter combinations needed to shift the CoR to the correct location. The low sample size may also have contributed. Expanding the parameter study further may highlight a significant factor that can cause greater variation between iterations and therefore sufficiently prove the customisation of the bottom core feature.

Although the ratio between the bottom core and the top core was increased the difference between the elastic moduli for the different components was only 7 MPa. This may not have been enough to prevent the two components from essentially acting as a single elastomer core.

The simple linear elastic material properties used for the core components may have caused the model to provide a non-realistic response as the TDR underwent flexion. This may have led to the lack of variability between the design iterations.

11.19.3 CoR location

The CoR of all of the different iterations of the design were found to lie within two standard deviations of the L5-S1 physiological mean. These results were promising nevertheless; this high level of success was likely contributed by the much larger standard deviation of the physiological mean for the L5-S1 level compared to the L4-L5 index level (Table 25). The anterior migration of the CoR out of the 2 standard deviation physiological range for the L4-L5 level (Figure 93) occurred for all iterations. Even when expanding the parametric study to increase sample size in the hopes of developing a superior multiple variable linear equation.

The resulting refined iteration failed to cause a significant shift in the CoR to have it lie within two standard deviations of the L4-L5 physiological range as it underwent 10 Nm of flexion. It should be noted however, that the refined iteration was the closest to the physiological range (Table 68) and the y position of the CoR remained within two standard deviation of the mean for all of the variations of the design tested.

11.19.4 Sample Size

The sample size of the number of iteration of each of the nine dimensions which were altered in the simulations is a major limitation of the analysis. Only three data points for each of the nine variable dimensions were initially included in the multiple variable linear regression analysis. Upon analysis of the results it was decided upon that the sample size should be doubled in the hopes to gain more reliable data. The expanded sample size although larger than the initial 19 different iterations is still relatively small. Increasing of the number of iterations for each of the dimensions tested and expanding the study to investigate additional parameters such as material properties of the different core components should allow for a more extensive analysis and may help to more clearly identify which parameters are the most important in terms of the CoR.

11.19.5 Additional Data

The FEA analysis involved only investigating the CoR in terms of three different parameters of the internal trapeziums of the Velodrome TDR design concept (base, outer height and top edge dimensions (Figure 79)). The analysis could utilise data that is already available from these parameters such as the slope generated by the parameters or the volume of the anterior posterior and lateral regions of the bottom core which may provide a greater understanding as to why no significant variation occurs between the designs.

11.19.6 Assumptions

A number of different assumptions and limitations were included into the FEA study. Majority of which were due to the early stage of design that the project was going aiming to complete and that it wasn't practical to develop a fully validated model and automate it in the given time frame. A number of limitations of the FEA model have been highlighted such as the use of linear material properties applied to the elastomer materials of the different core components.

The FEA also assumed that the bonding between the elastomer core components and the core to the endplates was ideal and that they were completely fused to one another. This is not the case in reality.

11.19.7 RoM

The mean RoM of the simulated TDRs was below the specification (6.605° instead of 10°). This was unfortunate however, the small differences in the overall RoM between the different design iterations (standard deviation = 0.0146) may indicate that the RoM strongly collates with one of the constant variables i.e. the material properties of the rubbers. Future expansion of the parametric analysis on the constant variables may reveal how to obtain a RoM that meets specification.

11.19.8 Specification and Design Requirement Priority

The FEA analysis only tested the different design iterations in 10 Nm of flexion and only investigated the RoM and CoR. This type of test was chosen for its simplicity and that it would allow a for a proof of the design concept. The tests were developed to show that different iterations of the Velodrome TDR have different mechanical responses and that the CoR is not constrained. Obviously other modes of loading such as compression, extension, axial rotation should also be investigated. A priority system should be developed in the future that specifies which characteristics of the design should be prioritised. This prioritisation will likely be needed as a particular combination may be optimal in flexion however be poor in compression. This trade off should not be considered lightly.

11.19.9 Further Analysis

Further analysis should be conducted in order to pinpoint how the design can be modified to have a more physiological CoR. It would be suitable to perform a stress analysis on the core as it underwent the flexion motion. This should reveal how the different components of the

core deformed under flexion bending and may reveal why there is so little variation between the different design iterations.

11.20 FEA Conclusion

The automation system which was developed to run the FEA simulations was for most part a great success. The majority of the FEA models were correctly generated through the use of the developed python script. Those that didn't, were easily identifiable and the problem was easily and efficiently rectified manually.

The results in terms of proof of concept; although disappointing, the FEA results can be used as an indicator that at least some; although small, variation in the CoR can be introduced through the alteration of the different bottom core component geometries. The refined iteration which was developed, did illustrate that the dimensions of the bottom core can be altered to cause a slight shift in the CoR to a more physiological location. However, further investigation is needed in order to validate that the use of a velodrome shaped bottom core to change the stiffness in specific regions of the core is a viable design concept.

The CoR of the simulated design iterations migrated anteriorly; as opposed to posteriorly, which is not physiological. However, this migration did illustrate that the design was at least physiological in terms of not constraining the CoR in a similar fashion to ball and socket TDRs. The different tested parameters were investigated with a multiple variable linear regression in the hopes of rectifying this problem. Although the CoR was not able to be shifted within two standard deviations of the L4-L5 physiological mean the final refined design iteration was the closest to achieving a CoR within the desired range. This may indicate that once more design iterations have been simulated and further analysis has been performed the significant variables in tuning the CoR may be identified. The analysis should also be expanded, as the FEA component of the project in its current status was developed more so as a proof of concept than an automated system.

Overall in terms of the aims of the FEA component of the project the FEA system was shown to be able to be automated, as majority of the design iterations were successfully simulated. The customisable bottom core concept of the Velodrome design was partially illustrated as different design iterations were shown to have slight differences in their mechanical response. The design concept had a non-constrained CoR which was a design requirement. The CoR of all the different design iterations lay within 2 standard deviations of the mean physiological L5-S1 CoR however, further development is needed to expand this success to other lumbar

index levels. Finally, the multiple variable linear regression analysis; although performed with a small non-random sample size, did highlight that the dimensions regarding the posterior and anterior regions of the bottom core have the greatest influence on the CoR. As the model is expanded and more design iterations are analysed; a more solid proof of concept of the Velodrome design could be developed.

11.21 CAD and FEA Automation System

One of the major deliverables of the project was the CAD and FEA automation system. The system successfully created all of the CAD part files for the Velodrome TDR design concept. The CAD files were exported in the appropriate file format to be automatically imported into the Abaqus FEA software via a generated Abaqus python script. This CAD and FEA integrated automation system has countless other applications. All design processes require the generation of numerous design iterations. The underlining automation system (Figure 95) can essentially be used for any design that requires different CAD iterations of the design and/or FEA analysis.

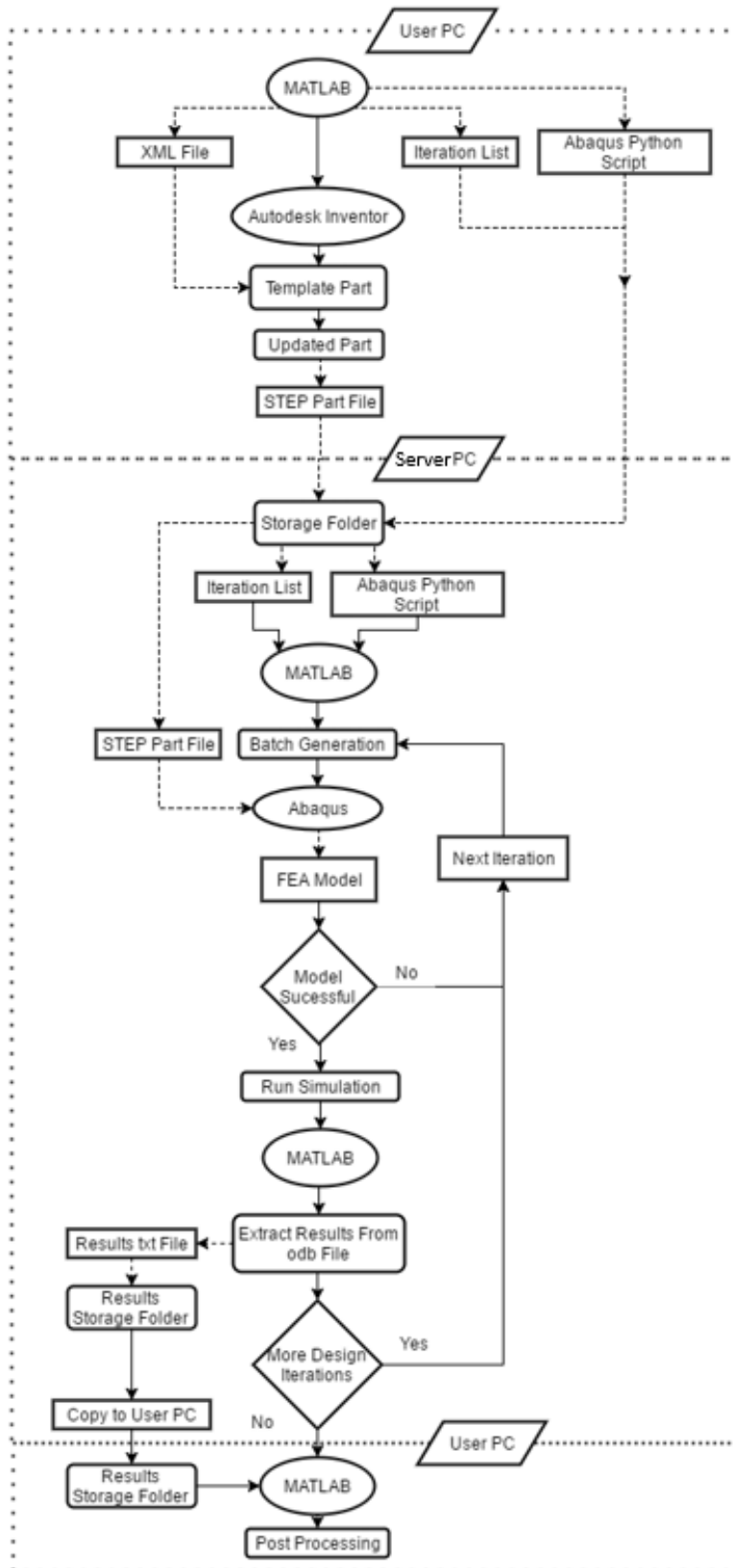


Figure 95: Summary of the CAD and FEA automation system.

The CAD automation system (Chapter 10) has been developed in a manner that allows for generation of different iterations of any CAD part file as long as the appropriate xml template file has been created. The automation system is controlled through MATLAB. The code first requires the desired parameters of the particular design iteration to be entered manually and assigned to variables in MATLAB. These parameters can be entered in a for loop so that a number of different iterations can be created in a queue. The code then uses the current parameters to update a template XML file which is to be uploaded into the Inventor CAD software. MATLAB then automatically opens Inventor by opening a template CAD file of the different components of the design. The part is then updated with the created XML file so that it has the required dimensions. The CAD file is then exported as a STEP file so that it can be used in the FEA software.

In the case where than one iteration is to be created, an iteration list is created so that the automated FEA software can also run the analysis in a batch. An Abaqus python script is also made for each of the different iterations. This script contains the information on the different files names of each of the CAD STEP files needed to be imported into Abaqus as well as the other parameters needed for the CAD model such as the materials properties and loading regime.

The CAD STEP files, the iteration list and the Abaqus python script are then copied to a server computer and stored in a designated folder. This storage folder is then accessed through a separate MATLAB script which uses the iteration list to generate a batch of the different analysis to be run. The python script then automatically imports the CAD STEP files into Abaqus and generates the FEA model. If the model generation fails, the system skips that iterations without running the FEA analysis and commences the next iteration. If the model is successfully constructed the simulation is run. The results from the FEA analysis are then again automatically extracted from the generated odb file and stored in a results folder.

This results fold contains the desired outputs from the model in the form of a number of txt files. These txt files each correspond to the desired output of the model for each of the frames of the FEA simulation. These file were then copied onto the user's computer for post processing or in the case of the project used to calculated the instantaneous centre of rotation.

The FEA results of the project were encouraging as the chosen design concept was shown to have the required properties of a non-constrained centre of rotation. The centre of rotation of

all the different design iterations was shown to lie within two standard deviations of the physiological mean of the L5-S1 lumbar spine segment. The FEA also helped to illustrate that the customisation concept of the Velodrome design, and how the different geometries of the bottom core can be altered to give a different mechanical response, was present. However, there is need for future investigation in order to validate that adequate variation between the design iterations can be achieved.

Without the development of this automation system the parametric analysis which was performed would not have been possible. The system in its current form allowed for the quick and simple creation, and simulation of 38 different design iterations. The following analysis revealed that the current design concept does require some modification however, without the automation system these findings may not have been possible.

With the increasing availability and performance of rapid prototyping patient specific implants are already being developed and it is estimated that they will become standard in the not so distant future (Synthes CMF 2005; Beer & Merwe 2013). Having this automation system already developed would allow for the simple integration of developing patient specific TDR design iterations in the future.

Chapter 12. Future Work

The aim of the project is to undergo the early design stages of a next generation total disc replacement. The complete research and development of such a device is very extensive and therefore there is still a substantial amount of work to complete before the design is market ready.

12.1 Expansion on levels of Intended Use

The existing design has been specified for use in only the L4 to S1 spine levels. Expanding the design to suit more levels of the spine (L3-L4 and L4-L5) would increase the applications of the design and increase potential market size.

12.2 Automatic Screen Scaling and Directory Creation

The current CAD automation system as mentioned in Chapter 10 utilises the mouse in order to click relevant buttons to allow for different iterations of the design to be created. There is one major downfall of having to incorporate this into the design. This disadvantage is caused by the differences in coordinates system of different computer screens depending on size and resolution. It is recommended that this problem is one of the first things corrected when continuing with the project. A possible solution to this would be to have a screen resolution check at the start of the automation MATLAB code. This would scale the coordinates correctly to ensure the correct buttons are pressed during the automation.

The MATLAB automation system also relies on consistent directory location in order to successfully call functions and access the CAD models and FEA result files. The software has been developed so that the directory definition occurs at the beginning of the code. This allows the user to assign where the files are to be kept before running the code. This system can and should be, further automated by having a script that the new user can highlight which drive the files should be stored on. The developed software then can create the appropriate directories and subdirectories needed. This would further the ease of use of the CAD and FEA automation system.

12.3 Automation of More Complex Post Processing

The post processing used to analyse the results was relatively simple. A more complex statistical method for investigating the influence of the different parameters on the mechanical response should be performed and automated.

In its current state the multiple linear regression only considers the effects of isolated parameters and how they influence the location of the TDR's CoR. The analysis should be expanded to investigate how combinations of the different parameters have on the overall performance of the particular iteration tested. This would provide a more detailed and in-depth analysis on how the different dimensions alter the CoR.

Although, the current system does automatically visualise the data of the different iterations and compile it in a single table to allow easy exportation of the result to Excel. This exportation can also be automated due to the existing integration between MATLAB and Excel which should be completed in the future.

12.4 Design of Experiment

Design of experiment is an important factor to consider especially when performing a parametric analysis. The project in its current stage did not undergo an extensive design of experiment as it was unnecessary for the main goals of the FEA during this early stage of design.

A full factorial design in the future would not be practical. The current system investigated nine different parameters with five different iterations of each. The full factorial design of experiment would result in 5^9 or over a million different combinations being tested. Running this many simulations even with the automation system would not be practical. The expansion of the project should also investigate the influence of the other parameters which were excluded from this early stage of design simulation (Table 57).

If all of the different parameters (28 in total when using a linear elastic material model) were to be tested at five different levels, 5^{28} simulations would be needed for the full analysis. This impractical number of simulations, also only takes into consideration one mode of loading at a single magnitude, further complicating the design of experiment.

Due to the larger number of different simulations that would be required to run all of the different design iteration combinations, a design of experiment optimisation process should be utilised. The appropriate design of experiment would decrease the number of simulations needed to be run, while still obtaining a suitable estimation of the different design parameters influence on the TDRs mechanical response. A fractional factorial design variation known as the Taguchi method has been recommended to be implemented as part of future work. The Taguchi method has been used in other orthopaedic FEA optimisation studies and would be a suitable starting point for future work (Lu et al. 2013).

Once implemented the design of experiment should allow a more detailed analysis on the different design iterations by taking into consideration the combination effects of different parameters.

12.5 Automation System Troubleshooting

The automation system which has been developed is not perfect. There were no issues with the automatic generation of the CAD parts, python script or batch simulation process. Issues arose when the models were automatically being created though the developed python script. The problems encountered related to the surface selection section of the python script; as all other components were successfully completed. The exact cause of the issue with surface selection is a mystery as the automated system worked for majority of the different iterations. The main surface that caused issues were the sloped sides of the bottom core and the mating top core. A potential fix would be to investigate the use of the `getByBoundingBox()` command which works in a similar manner to the `getByBoundingCylinder()` command; but requires the four coordinates of a box to select the required surfaces.

In addition, problems may arise when the number of iterations that are created is increased, due to changes in processor speed as the CAD models are generated. This may cause errors such as having the mouse click save before the current part has been updated.

The code in its current form skips the FEA analysis of the particular iteration if the input file used to run the analysis does not compile. This is an important aspect of the system as it means that the batch system does not stop, but will skip to the next simulation in the batch.

12.6 Automated Iteration Generation

The process of inputting different iterations of the design for the automation CAD system was currently done manually i.e. each iteration was changed one at a time by hand. A more automatic iteration generation method should be developed where the user can set bounds and increments so that the appropriate variable iteration combinations are created.

12.7 Validation of the FEA

Initial plans for the project were to use a CAD model donated from DePuy of the Prodisc-L TDR to help in validating the FEA component of the project. The donated model was to be simulated using the same methods from literature to help validate the FEA (Section 5.3.6.2). The choice to use the Prodisc-L was due to the University already having an existing agreement in aiding Depuy with research. The Prodisc-L was also chosen as it is also now the

longest serving TDR to have FDA approval that is still on the market; it has been used in the past as a control to get FDA approval (FDA 2015b); and it is one of the most commonly used TDRs on the market according to a number of resources including the 2010 Norwegian Hip Fracture Register (The Norwegian Hip Fracture Register 2010; Michaela et al. 2008).

Unfortunately, the existing agreement between Flinders and Depuy was not adequate for the project and a long legal process was needed to ensure confidentiality of the design. This meant that it was not feasible to obtain a CAD model in the given time frame of the project.

However, the project was fortunate enough to have a Prodisc-L donated from a collaborative surgeon. This Prodisc-L was then planned to be used to obtain a CAD model. Tragically, the 3D scanner of the University; which was to be used to accurately import the CAD geometry of the TDR, was broken once the Prodisc-L had arrived and therefore a CAD model is yet to be developed.

One of the first stages of future work will be the development of a scaled CAD model of the donated Prodisc-L so that it can be used as a reference in validating the FEA model. This Prodisc-L model can then be mechanically tested with the available facilities at Flinders University to obtain mechanical data which can be used to authenticate the FEA model.

12.8 Expand Parametric Analysis

At this early stage of design, only five iterations of each of the relevant bottom core parameters were investigated (Section 11.9.1). This parametric study should be expanded to include more iterations of the design and incorporate changes in the variables that were kept constant for this first stage of simulation.

12.9 Material properties

The material properties of the different rubbers were also kept constant for all of the simulations. A sweep of different material properties should also be performed to investigate how they influence the mechanical response of the proposed design.

12.10 Expansion of Mechanical Testing Simulation

The FEA simulation that was performed, was done purely as a proof of concept. The first expansion to the project in terms of mechanical loading should be to repeat the investigation of the TDR design iterations CoR, however also include extension and flexion and extension loading regimes. Luckily the paper used to help validate if the CoR lies within two standard deviations of the mean of the physiological also provides information on these modes of

bending (Pearcy & Bogduk 1988). This would allow for a more detailed analysis of the performance of the TDR design iterations.

As the project progresses further the design could be simulated in a wide range of different mechanical tests which other TDRs have been tested under. These tests have been highlighted in the literature review and will provide a good basis to build a case comparing the TDR to existing devices to aid in FDA approval.

As the FEA component of the project is already automated for the flexion loading regime, implementing other loading regimes should be relatively simple. Sections of the pre-existing automated FEA model which are already implemented; such as surface definition and setting up of constraints between the different parts, can be transferred to directly to the new loading regimes. The pre-existing python script will also provide a solid template to base the implantation of new loading regimes.

12.11 Mechanical Performance Prioritisation

The development of a TDR that provides optimal biomechanical properties in all 6DOF is not practical. Some modes of loading should gain priority over others when finalising which design iteration to use. It is recommending that compression and flexion initially gain precedence as these are the main modes of loading on the disc in vivo (Nevarro et al. 2008). The eDisc also took this approach of prioritising these modes of loading. Axial rotation should be of the least priority as the native FJs which are maintained after TDR implantation are responsible for restricting most of the axial rotation RoM (Section 4.10). This rational was used by the Prodisc-L which relies on the anatomy to constrain the TDR in axial rotation (Synthes Spine 2006).

12.12 In-vitro testing

As the design moves into the final stages and a substantial prototype has been completed, in vitro tests can be completed. The data from these tests can be used to further validate the FEA and provide additional data for analysis. These tests are also vital to gain FDA approval as evident by the extensive mechanical tests that approved devices have been subjected to (FDA 2015b; FDA 2004; FDA 2006).

12.13 Facet Joint Specifications

Facet joint degeneration (Section 2.3) is a source of LBP. Extreme FJ degeneration is a contraindication to the TDR procedure due to its influence to cause poor clinical outcomes

(Strube et al. 2013). Incorporating facet kinematics and boundary conditions into the FEA is a very complicated task. Therefore, since the aim of the project was to undergo the early stage of design they were not incorporated into the model. The literature review has covered the FJ dimensions to allow for this to be integrated in the future.

12.14 Endplate Optimisation

12.14.1 Endplate Lordosis

Lordosis was not introduced into the endplates used for FEA for this early stage of the project. Nevertheless, lordosis angle has been introduced into the inferior and superior endplates CAD geometries and is already integrated into the CAD automation system. The decision to not include lordosis into the FEA study was for simplification of the FEA at this early stage of design as it was not necessary for the proof of concept tests. The effects of lordosis on the mechanical response of the TDR should be investigated in the future.

12.14.2 Elastomer Core to Endplate Fixation

The early stage of the design assumed that the bonding between the endplates and the elastomer core of the device to be ideal. This was evident by the tie constraints used in the FEA analysis (Section 11.6). This interface between the endplates and the core is a potential weak point of elastomer core TDRs. As a result, this weak point has been accounted for in a number of different elastomer core designs in particular the Freedom TDR (Section 5.3.8.2).

How the endplates and elastomer core are going to be joined was briefly considered. The concept of potentially increasing the surface area on the mating surfaces of the endplates was derived. The idea involves ‘hollowing’ out this surface to form a pyramid-like shape which would increase the total surface area available to adhere the two surfaces together (Figure 96).

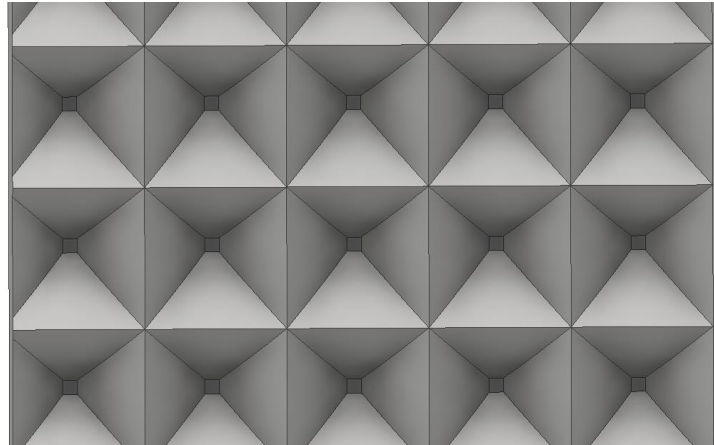


Figure 96: Hollow pyramid-like concept to increase surface area.

12.15 Hyper-elastic Mooney Rivlin Material Properties

As stated in Section 11.4 all materials were defined as linear elastic and isotropic. This was purposely done for simplicity of the early stage simulations. It is recommended that hyper elastic material properties are integrated into the next generation of the model. These type of material properties are already able to be integrated in Abaqus FEA software. Mooney Rivlin material properties were purposely chosen as they have been used to define elastomer material properties, and have also been applied to the disc in previous FEA studies (Feng & Hallquist 2012; Wagnac et al. 2011). Unfortunately, it may be difficult deriving the Mooney Rivlin materials of the different elastomers of the composite core as they are derived from experimental tests (Feng & Hallquist 2012). However, the coefficients or slight variations from disc models could be used as a starting point.

12.16 Design Optimisation

Once a fully automated system that develops different iterations of the design, simulates the iterations and then post processes the results has been developed. There is potential to include a multi objective optimisation system. The system could hypothetically ‘learn’ from previous iterations in order to intelligently develop new iterations of the design based on predefined success criteria. This system would allow for the reduction in the number of iterations needed to be run.

12.17 Patent Search and Application

Although not completely proven the Velodrome TDR design does have significant novel aspects behind its design. A patent search should be performed to confirm that the design is unique and then a decision to file a patent should be explored.

12.18 Single Core

One of the potential weaknesses of the Velodrome TDR design concept was that the fatigue life of the device may be inadequate due to the multi component core. Fears of failure occurring at the interfaces between the different components has raised this concern. A potential design change could possibly rectify this issue. If it is possible to manufacture, the three-part core could be integrated into a single component. Instead of having a mating surface between the different rubbers of varying stiffness's, the interface could incorporate a gradient change in the material properties while still hopefully maintaining the composite core's functions. This design iteration should be investigated in the future.

12.19 Additional Applications

The real underlying strength of the project is that the developed CAD and FEA integrated automation design system can be applied to any design. If the proposed Velodrome design is proven to be inappropriate after future analysis the developed system can still be applied to a new design concept.

Chapter 13. Conclusion

In this thesis a novel total disc replacement prosthesis design concept has been developed and presented. The project followed a structured design process to develop the proposed design.

The extensive literature review provided a solid foundation of which the design has been based upon. It contains in depth information on the lumbar anatomy and morphology which was used to derive design requirements and geometric specifications.

The biomechanics section of the literature review presents knowledge on the mechanical properties of the lumbar spine. This information was used to derive mechanical specifications of the design and as a reference to compare FEA results to make sure the investigated mechanical design requirements are met.

An extensive review of the different commercially available total disc replacements that have been released on to the market, provided information on how the different types of devices have performed in a clinical setting. Design features of the different devices have been described which were used as inspiration in the design process.

A number of different design concepts were developed before the Velodrome design was deemed superior following a ranking process. The proposed Velodrome design comprises of a unique composite three-part core. The bottom core which resembles the shape of a velodrome drives the design. It was developed in a manner which allows the customisation of the anterior, posterior and lateral regions, with the goal of producing unique biomechanical properties in all six degrees of freedom, like the natural disc.

A CAD model of the proposed Velodrome concept was created. Due to the novel customisable feature of the proposed design a CAD automation system was successfully developed which allows for the generation of different design iterations. These CAD geometries were then simulated using FEA to investigate the centre of rotation and range of motion of the different design iterations when the devices are subjected to flexion bending loading.

The FEA component of the project was also automated which allowed for the parametric analysis of the different dimensions of the bottom core to highlight the parameters that had the most influence on the iteration's centre of rotation.

The FEA results of the project were encouraging as the chosen design concept was shown to have desirable properties of a non-constrained centre of rotation. The centre of rotation of all the different design iterations was shown to lie within two standard deviations of the physiological mean of the L5-S1 lumbar spine segment. The FEA also helped to illustrate that the customisation concept of the Velodrome design and how the different geometries of the bottom core can be altered to give a different mechanical response was present. However, there is need for future investigation in order to validate that adequate variation between the design iterations can be achieved.

If the Velodrome design concept, once developed further is found to be ineffective, the underlying system which allows for both automation of CAD generation and FEA has a robust number of different applications. The design iteration phase is not unique to this project. Almost every design requires some refinement before the final design is finalised. The developed system can be applied to a vast number of different designs to allow for the relatively quick CAD development, FEA and parametric analysis of the applicable designs.

The automation system benefits are further amplified by the recent increase in 3D printing availability. The system will allow the different prototype iterations to be quickly developed to further aid in the design process and may potentially lead to the final design having patient specific features.

The goal of completing the early stage design of a novel total disc replacement has been accomplished. This thesis and the deliverables of the project have laid a strong foundation on which the project can progress.

If the Velodrome design is shown to be successful in achieving all of the design requirements once it has been fully developed, it will be a viable option in the surgical treatment of low back pain, which is a significant problem in today's society.

Chapter 14. Bibliography

- Adams, M. & Hutton, W.C., 1981. The relevance of torsion to the mechanical derangement of the lumbar spine. *Spine*, 6(3), pp.241–248.
- Adams, M.A. & Dolan, P., 1991. A technique for quantifying the bending moment acting on the lumbar spine in vivo. *Journal of Biomechanics*, 24(2), pp.117–126.
- Adams, M. a, Dolan, P. & Hutton, W.C., 1988. The lumbar spine in backward bending. *Spine*, 13(9), pp.1019–1026.
- Adams, M., Bogduk, N., Burton, K. & Dolan, P., 2013. *The Biomechanics of Back Pain* 3rd ed. A. Taylor & V. Watkins, eds., Elsevier.
- Adams, M., Green, T. & Dolan, P., 1994. The strength in anterior bending of lumbar intervertebral discs. *Spine*, 19(19), pp.2197–2203.
- Adams, M., McNally, D., Chinn, H. & Dolan, P., 1994. The clinical biomechanics award paper 1993 Posture and the compressive strength of the lumbar spine. *Clinical Biomechanics*, 9(1), pp.5–14.
- Aesculap Implant Systems, 2015. activL® Artificial Disc The First New Lumbar Total Disc Replacement.
- Aesculap Implant Sysytems, 2015. Lumbar Total Disc Replacement Intelligent Motion Technology. Available at: <https://www.aesculapimplantsystems.com/products/spine-solutions/lumbar-total-disc-replacement> [Accessed August 8, 2016].
- AIMIS Spine, 2014. Surgical Technologies Total Disc Replacement. Available at: <http://www.aimisspine.com/technology/total-disc-replacement> [Accessed August 9, 2016].
- Alain, J.L., Olivier, A., Jean, R. & Rakover, P., 2016. The innovative viscoelastic CP ESP cervical disk prosthesis with six degrees of freedom : biomechanical concepts , development program and preliminary clinical experience. *European Journal of Orthopaedic Surgery & Traumatology*, 26(1), pp.9–19.
- Alison, J., 2008. Medtronic Willfully Infringed Disc Patent: Jury - Law360. Law360. Available at: <http://www.law360.com/articles/79468/medtronic-willfully-infringed-disc-patent-jury> [Accessed August 9, 2016].
- Anekstein, Y., Floman, Y., Smorgick, Y., Rand, N., Millgram, M. & Mirovsky, Y., 2015. Seven years follow-up for total lumbar facet joint replacement (TOPS) in the management of lumbar spinal stenosis and degenerative spondylolisthesis. *European Spine Journal*, pp.2306–2314.
- Anon, 1983. The mechanical function of the lumbar apophyseal joints. *Spine*, 8(3), pp.327–330.
- Arun, R., Freeman, B.J.C., Scammell, B.E., McNally, D.S., Cox, E. & Gowland, P., 2009. 2009 ISSLS Prize Winner: What influence does sustained mechanical load have on diffusion in the human intervertebral disc?: an in vivo study using serial postcontrast magnetic resonance imaging. *Spine*, 34(21), pp.2324–2337.
- ASM Aerspace Specification Metals Inc., Titanium Ti-6Al-4V (Grade 5), Annealed - ASM

- Material Data Sheet. Available at:
<http://asm.matweb.com/search/SpecificMaterial.asp?bassnum=MTP641> [Accessed September 13, 2016].
- Assaker, R., Ritter-Lang, K., Vardon, D., Litrico, S., Fuentes, S., Putzier, M., Franke, J., Jarzem, P., Guigui, P., Nakach, G. & Le Huec, J.C., 2015. Maverick total disc replacement in a real-world patient population: a prospective, multicentre, observational study. *European Spine Journal*, 24(9), pp.2047–2055. Available at:
http://ovidsp.ovid.com/ovidweb.cgi?T=JS&CSC=Y&NEWS=N&PAGE=fulltext&D=emed13&AN=2015107372%5Cnhttp://sfx.ucl.ac.uk/sfx_local?sid=OVID:embase&id=pmid:&id=doi:10.1007/s00586-015-3918-x&issn=0940-6719&isbn=&volume=24&issue=9&spage=2047&pages=2047-2055&date=20.
- Australian Government Department of Health, 2016. The Prostheses List.
- Australian Institute of Health and Welfare, 2015. Musculoskeletal fact sheet Back problems Musculoskeletal fact sheet.
- Axiomed, 2008a. Fatigue Characterization of the Freedom® Lumbar Disc.
- Axiomed, 2012. Freedom® Lumbar Disc - Clinical Outcomes Benchmarked Against All TDRs in the SWISSpine Registry. Available at:
<http://www.axiomed.com/pdf/WPaperSWISSpineReg.pdf>.
- Axiomed, 2008b. Freedom® Lumbar Disc Wear Testing and Evaluation of Wear Debris in an Animal Model.
- Axiomed, 2008. Freedom Lumbar Disc.
- AZO Materials, Properties: Silicone Rubber. Available at:
<http://www.azom.com/properties.aspx?ArticleID=920> [Accessed October 13, 2016].
- AZoM, 2013. Grade 23 Ti 6Al 4V ELI Alloy (UNS R56401). Available at:
<http://www.azom.com/article.aspx?ArticleID=9365> [Accessed September 13, 2016].
- B.Braun Australia, 2015. actiL. Available at: <http://www.bbraun.com.au/cps/rde/xchg/cw-bbraun-en-au/hs.xsl/products.html?id=00020743280000000324&prid=PRID00004594>.
- Baliga, S., Treon, K. & Craig, N.J.A., 2015. Low back pain: Current surgical approaches. *Asian Spine Journal*, 9(4), pp.645–657.
- Battie, M.C., Lazary, A., Fairbank, J., Eisenstein, S., Heywood, C., Brayda-Bruno, M., Varga, P.P. & McCall, I., 2014. Disc degeneration-related clinical phenotypes. *European Spine Journal*, 23(SUPPL. 3).
- Battié, M.C., Videman, T., Levälähti, E., Gill, K. & Kaprio, J., 2008. Genetic and environmental effects on disc degeneration by phenotype and spinal level: a multivariate twin study. *Spine*, 33(25), pp.2801–2808.
- Been, E., Barash, A., Pessah, H. & Peleg, S., 2010. A new look at the geometry of the lumbar spine. *Spine*, 35(20), pp.E1014–E1017.
- Been, E. & Kalichman, L., 2014. Lumbar lordosis. *Spine Journal*, 14(1), pp.87–97. Available at: <http://dx.doi.org/10.1016/j.spinee.2013.07.464>.
- Beer, N. De & Merwe, A. Van Der, 2013. Patient-specific intervertebral disc implants using rapid manufacturing technology. *Rapid Prototyping Journal*, 19(May 2012), pp.126–

139. Available at: <http://www.emeraldinsight.com/10.1108/13552541311302987>.
- Benzel, E., Liebermsn, I., Ross, R., Linovitz, R., Kuras, J. & Zimmers, K., 2011. Mechanical Characterization of a Viscoelastic Disc for Lumbar Total Disc Replacement. *Journal of Medical Devices*, 5(March).
- Bogduk, N., 1997. *Clinical anatomy of the lumbar spine* 3rd ed., Churchill Livingstone.
- Bono, C.M. & Garfin, S.R., 2004. History and evolution of disc replacement. *The Spine Journal : official journal of the North American Spine Society*, 4(6 Suppl), p.145S–150S. Available at: <http://www.ncbi.nlm.nih.gov/pubmed/15541659>.
- Boonen, A., van den Heuvel, R., van Tubergen, A., Goossens, M., Severens, J.L., van der Heijde, D. & van der Linden, S., 2005. Large differences in cost of illness and wellbeing between patients with fibromyalgia, chronic low back pain, or ankylosing spondylitis. *Annals of the rheumatic diseases*, 64(3), pp.396–402. Available at: <http://www.pubmedcentral.nih.gov/articlerender.fcgi?artid=1755408&tool=pmcentrez&rendertype=abstract>.
- Boos, N., Weissbach, S., Rohrbach, H., Weiler, C., Spratt, K.F. & Nerlich, A.G., 2002. Classification of age-related changes in lumbar intervertebral discs: 2002 Volvo Award in basic science. *Spine*, 27(23), pp.2631–2644. Available at: <http://eutils.ncbi.nlm.nih.gov/entrez/eutils/elink.fcgi?dbfrom=pubmed&id=12461389&retmode=ref&cmd=prlinks%5Cnpapers3://publication/doi/10.1097/01.BRS.0000035304.27153.5B>.
- Bourne, A.M., Whittle, S.L., Richards, B.L., Maher, C.G. & Buchbinder, R., 2014. The scope, funding and publication of musculoskeletal clinical trials performed in Australia. *Medical Journal of Australia*, 200(2), pp.88–91.
- Briggs, A.M., Perilli, E., Parkinson, I.H., Kantor, S., Wrigley, T. V., Fazzalari, N.L. & Wark, J.D., 2012. Measurement of subregional vertebral bone mineral density in vitro using lateral projection dual-energy X-ray absorptiometry: Validation with peripheral quantitative computed tomography. *Journal of Bone and Mineral Metabolism*, 30(2), pp.222–231.
- Brinckmann, P., Biggemann, M. & Hilweg, D., 1988. Fatigue fracture of human lumbar vertebrae. *Clinical biomechanics (Bristol, Avon)*, 3 Suppl 1, p.i-S23. Available at: <http://www.sciencedirect.com/science/article/pii/S0268003388800019>.
- Brinckmann, P., Biggemann, M. & Hilweg, D., 1989. Prediction of the compressive strength of human lumbar vertebrae. *Clinical Biomechanics*, 4(SUPPL. 2).
- Brinckmann, P. & Grootenboer, H., 1991. Change of Disc Height, Radial Disc Bulge, and Intradiscal Pressue From Discectomy An in Vitro Investigation on Human Lumbar Discs. , 16(6), pp.641–646.
- van den Broek, P.R., Huyghe, J.M., Wilson, W. & Ito, K., 2012. Design of next generation total disk replacements. *Journal of Biomechanics*, 45(1), pp.134–140. Available at: <http://dx.doi.org/10.1016/j.jbiomech.2011.09.017>.
- Bron, J.L., Helder, M.N., Meisel, H.J., Van Royen, B.J. & Smit, T.H., 2009. Repair, regenerative and supportive therapies of the annulus fibrosus: Achievements and challenges. *European Spine Journal*, 18(3), pp.301–313.
- Cakir, B., Richter, M., Käfer, W., Puhl, W. & Schmidt, R., 2005. The impact of total lumbar

- disc replacement on segmental and total lumbar lordosis. *Clinical biomechanics* (Bristol, Avon), 20(4), pp.357–64. Available at: <http://www.ncbi.nlm.nih.gov/pubmed/15737442>.
- Cheung, K.M.C., Li, Y., Sham, P.C. & Chan, D., 2016. *Advanced Concepts in Lumbar Degenerative Disk Disease*, Available at: <http://link.springer.com/10.1007/978-3-662-47756-4>.
- Cortes, D. & Elliott, D., 2014. *The Intervertebral Disc: Molecular and Structural Studies of the Disc in Health and Disease*, Available at: <http://link.springer.com/10.1007/978-3-7091-1535-0>.
- Costi, J.J., Freeman, B.J.C. & Elliott, D.M., 2011. Intervertebral disc properties : challenges for biodevices. *Expert Reviews*, 8(3), pp.357–376.
- Cryon, B.M. & Hutton, W.C., 1978. the Fatigue Strength of the Lumbar Neural Arch in Spondylolysis. *The Journal of bone and joint surgery. UK volume*, 60–B(2), pp.234–238. Available at: <file:///C:/Users/rico/Documents/Lumbar Spine articles/THE FATIGUE STRENGTH OF THE LUMBAR NEURAL ARCH IN Spondylolysis Cryon 1978.pdf>.
- Cunningham, B.W., 2004. Basic scientific considerations in total disc arthroplasty. *Spine Journal*, 4(6 SUPPL.), pp.219–230.
- Cunningham, B.W., Dmitriev, A.E., Hu, N.B. & McAfee, P.C., 2003. General principles of total disc replacement arthroplasty - Seventeen cases in a nonhuman primate model. *Spine*, 28(20), pp.S118–S124.
- Cunningham, B.W., Gordon, J.D., Dmitriev, a E., Hu, N. & McAfee, P.C., 2003. Biomechanical evaluation of total disc replacement arthroplasty: an in vitro human cadaveric model. *Spine*, 28(20), pp.S110-7. Available at: http://www.ncbi.nlm.nih.gov/entrez/query.fcgi?cmd=Retrieve&db=PubMed&dopt=Citation&list_uids=14560182.
- Dagenais, S., Caro, J. & Haldeman, S., 2008. A systematic review of low back pain cost of illness studies in the United States and internationally. *Spine Journal*, 8(1), pp.8–20.
- Damasceno, L.H.F., Catarin, S.R.G., Campos, A.D. & Defino, H.L.A., 2006. Lumbar Lordosis : a Study of Angle Values and of Vertebral Bodies and Intervertebral Discs Role. *Acta Ortopedica Brasileria*, 14(4), pp.193–198.
- Davidson, M. & Keating, J.L., 2002. A Comparison of Five Low Back Disability Questionnaires: Reliability and Responsiveness. , 82, pp.8–24.
- Delamarter, R.B., Bae, H.W. & Pradhan, B.B., 2005. Clinical results of ProDisc-II lumbar total disc replacement: Report from the United States clinical trial. *Orthopedic Clinics of North America*, 36(3 SPEC. ISS.), pp.301–313.
- Delécrin, J., Allain, J., Steib, J., Beaurain, J., Dufour, T., Chataigner, H. & Aubourg, L., 2007. *Mobidisc Lumbar Arthroplasty : Multi-center Study with 2-Years Follow-Up.* , p.1.
- Depuy Spine a Johnson & Johnson Company, 2004. *Charite Artificial Disc Product Catalog*.
- Dooris, A.P., Goel, V.K., Grosland, N.M., Gilbertson, L.G. & Wilder, D.G., 2001. Load-sharing between anterior and posterior elements in a lumbar motion segment implanted with an artificial disc. *Spine (Philadelphia, Pa. 1976)*, 26(6), pp.122–129. Available at:

- http://www.ncbi.nlm.nih.gov/entrez/query.fcgi?cmd=Retrieve&db=PubMed&dopt=Citation&list_uids=11246394.
- Dreischarf, M., Albiol, L., Rohlmann, A., Pries, E., Bashkuev, M., Zander, T., Duda, G., Druschel, C., Strube, P., Putzier, M. & Schmidt, H., 2014. Age-related loss of lumbar spinal lordosis and mobility - A study of 323 asymptomatic volunteers. *PLoS ONE*, 9(12), pp.1–19.
- Dreischarf, M., Schmidt, H., Putzier, M. & Zander, T., 2015. Biomechanics of the L5-S1 motion segment after total disc replacement - Influence of iatrogenic distraction, implant positioning and preoperative disc height on the range of motion and loading of facet joints. *Journal of Biomechanics*, 48(12), pp.3283–3291.
- Drummond, M., 1992. Cost-of-illness studies: a major headache? *Pharmacoeconomics*, 2, pp.1–4.
- DSM, 2012. CarboSil Thermoplastic Silicone Polycarbonate Polyurethane (TSPCU). Available at: http://www.dsm.com/markets/medical/en_US/products-page/products-biostable-polyurethanes/product-pu-carbosil-tspcu.html.
- Dunlop, R.B., Hutton, W.C. & Adams, A., 1984. Space Facet Joints. *Surgery*, 66–B, pp.706–710.
- Duthey, B., 2013. Background Paper 6.24 Low back pain. *Priority Medicines for Europe and the World. Global Burden of Disease (2010)*, (March), pp.1–29.
- Ekman, M., Johnell, O. & Lidgren, L., 2016. The economic cost of low back pain in sweden in 2001 The economic cost of low back pain in Sweden in. , 3674(March).
- Enker, P., Steffee, A., McMillin, C., Keppler, L., Biscup, R. & Miller, S., 1993. Artificial disc replacement: preliminary report with a 3-year minimum follow-up. *Spine*, 18(8), pp.1061–1070. Available at: http://journals.lww.com/spinejournal/abstract/1993/06150/artificial_disc_replacement_preliminary_report.17.aspx.
- Errico, T.J., 2005. Lumbar disc arthroplasty. *Clin Orthop Relat Res*, (435), pp.106–117. Available at: http://www.ncbi.nlm.nih.gov/entrez/query.fcgi?cmd=Retrieve&db=PubMed&dopt=Citation&list_uids=15930927.
- Evcik, D. & Yücel, A., 2003. Lumbar lordosis in acute and chronic low back pain patients. *Rheumatology International*, 23(4), pp.163–165.
- Fairbank, J.C., Couper, J., Davies, J.B. & O'Brien, J.P., 1980. The Oswestry low back pain disability questionnaire. *Physiotherapy*, 66(8), pp.271–273.
- Fairbank, J.C. & Pynsent, P.B., 2000. The Oswestry Disability Index. *Spine*, 25(22), p.2940–52; discussion 2952. Available at: <http://www.ncbi.nlm.nih.gov/pubmed/11074683>.
- Farfan, H., 1973. *Mechanical Disorders of the Lower Back*. , pp.1–240.
- Fattor, J.A., Hollenbeck, J.F.M., Laz, P.J., Rullkoetter, P.J., Burger, E.L., Patel, V. V & Cain, C.M.J., 2016. Patient-Specific Templating of Lumbar Total Disk Replacement to Restore Normal Anatomy and Function. *Orthopedics*, 39(2), pp.97–102. Available at: <http://www.healio.com/orthopedics/journals/ortho/2016-3-39-2/%7B77ab237b-3957-4dc3-bf38-950d317168e3%7D/patient-specific-templating-of-lumbar-total-disk->

replacement-to-restore-normal-anatomy-and-function.

FDA, 2004. Charite Summary of Safety and Effectiveness-CHARITE. , pp.1–24.

FDA, 2015a. Device Advice: Investigational Device Exemption (IDE). Available at:
<http://www.fda.gov/MedicalDevices/DeviceRegulationandGuidance/HowtoMarketYourDevice/InvestigationalDeviceExemptionIDE/default.htm>.

FDA, 2006. SUMMARY OF SAFETY AND EFFECTIVENESS DATA - Prodisc-L. , pp.1–23.

FDA, 2015b. Summary of Safety and Effectiveness Data (SSED) activL. , pp.1–94.
Available at: http://www.accessdata.fda.gov/cdrh_docs/pdf10/P100034b.pdf.

Feng, W. & Hallquist, J., 2012. On Mooney-Rivlin Constants for Elastomers. 12th International LS-DYNA Users Conference, 1(1), pp.1–10. Available at:
<https://www.dynamore.de/de/download/papers/2012-internationale-ls-dyna-users-conference/documents/constitutivemodeling05-d.pdf>.

FH Orthopedics, ESP Elastic Spine Pad-Brochure.

Fibrosus, A., 2010. NIH Public Access. Journal of Biomechanics, 131(7), pp.1–10.

Fraser, R.D., Ross, E.R., Lowery, G.L., Freeman, B.J. & Dolan, M., 2004. AcroFlex design and results. Spine Journal, 4(6 SUPPL.).

Frelinghuysen, P., Huang, R.C., Girardi, F.P. & Cammisa, F.P., 2005. Lumbar total disc replacement part I: Rationale, biomechanics, and implant types. Orthopedic Clinics of North America, 36(3 SPEC. ISS.), pp.293–299.

Fritzell, P., Hagg, O., Wessberg, P. & Nordwall, A., 2001. 2001 Volvo Award Winner in Clinical Studies: Lumbar fusion versus nonsurgical treatment for chronic low back pain: a multicenter randomized controlled trial from the Swedish Lumbar Spine Study Group. Spine (Phila Pa 1976), 26(23), pp.2521–2524.

Frobin, W., Brinckmann, P., Kramer, M. & Hartwig, E., 2001. Height of lumbar discs measured from radiographs compared with degeneration and height classified from MR images. European Radiology, 11(2), pp.263–269.

Gaffey, J.L., Ghanayem, A.J., Voronov, M.L., Havey, R.M., Carandang, G., Abjornson, C. & Patwardhan, A.G., 2010. Effect of Increasing Implant Height on Lumbar Spine Kinematics and Foraminal Size Using the ProDisc-L Prosthesis. Spine, 35(19), pp.1777–1782. Available at:
<http://search.ebscohost.com/login.aspx?direct=true&db=c8h&AN=2010769284&site=ehost-live>.

Gallagher, S. & Marras, W.S., 2012. Tolerance of the lumbar spine to shear: A review and recommended exposure limits. Clinical Biomechanics, 27(10), pp.973–978. Available at: <http://dx.doi.org/10.1016/j.clinbiomech.2012.08.009>.

Garges, K.J., Nourbakhsh, A., Morris, R., Yang, J., Mody, M. & Patterson, R., 2008a. A Comparison of the Torsional Stiffness of the Lumbar Spine in Flexion and Extension. Journal of Manipulative and Physiological Therapeutics, 31(8), pp.563–569.

Garges, K.J., Nourbakhsh, A., Morris, R., Yang, J., Mody, M. & Patterson, R., 2008b. A Comparison of the Torsional Stiffness of the Lumbar Spine in Flexion and Extension.

- Journal of Manipulative and Physiological Therapeutics, 31(8), pp.563–569. Available at: <http://dx.doi.org/10.1016/j.jmpt.2008.09.002>.
- Geisler, F.H., 2006. The CHARITE Artificial Disc: design history, FDA IDE study results, and surgical technique. *Clinical neurosurgery*, 53, pp.223–228.
- Gellhorn, A.C., Katz, J.N. & Suri, P., 2013. Osteoarthritis of the spine: the facet joints. *Nature reviews. Rheumatology*, 9(4), pp.216–24. Available at: <http://www.pubmedcentral.nih.gov/articlerender.fcgi?artid=4012322&tool=pmcentrez&rendertype=abstract>.
- Goel, V.K., Mehta, A., Jangra, J., Faizan, A., Kiapour, A., Hoy, R.W. & Fauth, A.R., 2007. Anatomic Facet Replacement System (AFRS) Restoration of Lumbar Segment Mechanics to Intact: A Finite Element Study and In Vitro Cadaver Investigation. *SAS Journal*, 1(1), pp.46–54. Available at: [http://dx.doi.org/10.1016/S1935-9810\(07\)70046-4](http://dx.doi.org/10.1016/S1935-9810(07)70046-4).
- Gornet, M.F., Schranck, F., Wharton, N.D., Beall, D.P., Jones, E., Myers, M.E. & Hipp, J.A., 2014. Optimizing success with lumbar disc arthroplasty. *European Spine Journal*, 23(10), pp.2127–2135.
- Granhed, H., Jonson, R. & Hansson, T., 1987. The loads on the lumbar spine during extreme weight lifting. *Spine*, 12(2), pp.146–149.
- Green, T., Allvey, J. & Adams, M., 1994. Spondylolysis: Bending of the Inferior Articular Processes of Lumbar Vertebrae During Simulated Spinal Movements. *Spine*, 19(23), pp.2683–2691. Available at: <http://0-ovidsp.ovid.com.library.vu.edu.au/ovidweb.cgi?T=JS&PAGE=reference&D=ovftb&NEWS=N&AN=00007632-199412010-00016>.
- Grupp, T.M., Yue, J.J., Garcia, R., Kaddick, C., Fritz, B., Schilling, C., Schwiesau, J. & Blömer, W., 2014. Evaluation of impingement behaviour in lumbar spinal disc arthroplasty. *European Spine Journal*, 24(9), pp.2033–2046.
- Guyer, R.D., McAfee, P.C., Banco, R.J., Bitan, F.D., Cappuccino, A., Geisler, F.H., Hochschuler, S.H., Holt, R.T., Jenis, L.G., Majd, M.E., Regan, J.J., Tromanhauser, S.G., Wong, D.C. & Blumenthal, S.L., 2009. Prospective, randomized, multicenter Food and Drug Administration investigational device exemption study of lumbar total disc replacement with the CHARITÉ artificial disc versus lumbar fusion: Five-year follow-up. *Spine Journal*, 9(5), pp.374–386. Available at: <http://dx.doi.org/10.1016/j.spinee.2008.08.007>.
- Guyer, R.D., Pettine, K., Roh, J.S., Dimmig, T.A., Coric, D., McAfee, P.C. & Ohnmeiss, D.D., 2016. Five-Year Follow-Up of a Prospective, Randomized Trial Comparing Two Lumbar Total Disc Replacements. *Spine*, 41(1), pp.3–8. Available at: <http://content.wkhealth.com/linkback/openurl?sid=WKPTLP:landingpage&an=00007632-201601000-00002>.
- Ha, S.K., Kim, S.H., Kim, D.H., Park, J.Y., Lim, D.J. & Lee, S.K., 2009. Biomechanical study of lumbar spinal arthroplasty with a semi-constrained artificial disc (Activ L) in the human cadaveric spine. *Journal of Korean Neurosurgical Society*, 45(3), pp.169–175.
- Hahnle, U.R., Weinberg, I.R., Sliwa, K., Sweet, B.M. & de Villiers, M., 2007. Kineflex (Centurion) Lumbar Disc Prosthesis: Insertion Technique and 2-Year Clinical Results in

- 100 Patients. *SAS Journal*, 1(1), pp.28–35. Available at: [http://dx.doi.org/10.1016/S1935-9810\(07\)70044-0](http://dx.doi.org/10.1016/S1935-9810(07)70044-0).
- Haik, Y. & Shahin, T., 2011. *Engineering Design Process* second. R. Adams, T. Alterieri, & C. Valentine, eds., Global Engineering: Christopher Shortt.
- Hall, L.T., Esses, S.I., Noble, P.C. & Kamaric, E., 1997. Morphology of the lumbar vertebral endplates. *Spine*, 23(14), pp.1517-22–3. Available at: <http://www.ncbi.nlm.nih.gov/pubmed/9682307>.
- Hallab, N., Link, H.D. & McAfee, P.C., 2003. Biomaterial optimization in total disc arthroplasty. *Spine*, 28(20), pp.S139–S152.
- Hayes, M. a, Howard, T.C., Gruel, C.R. & Kopta, J. a, 1989. Roentgenographic evaluation of lumbar spine flexion-extension in asymptomatic individuals. *Spine*, 14(3), pp.327–331.
- Hedman, T., Kostuik, J., Fernie, G. & Hellier, W., 1990. Design of an Intervertebral Disc Prosthesis. *SPINE*, 16(6), pp.256–260.
- Hong, C.H., Park, J.S., Jung, K.J. & Kim, W.J., 2010. Measurement of the normal lumbar intervertebral disc space using magnetic resonance imaging. *Asian spine journal*, 4(1), pp.1–6. Available at: <http://www.pubmedcentral.nih.gov/articlerender.fcgi?artid=2900163&tool=pmcentrez&rendertype=abstract>.
- Hoy, D., March, L., Brooks, P., Blyth, F., Woolf, A., Bain, C., Williams, G., Smith, E., Vos, T., Barendregt, J., Murray, C., Burstein, R. & Buchbinder, R., 2014. The global burden of low back pain: estimates from the Global Burden of Disease 2010 study. *Annals of the Rheumatic Diseases*, 73(6), pp.968–974. Available at: http://gateway.ovid.com/ovidweb.cgi?T=JS&CSC=Y&NEWS=N&PAGE=fulltext&D=medl&AN=24665116%5Cnhttp://sfx.nottingham.ac.uk:80/sfx_local?genre=article&atitle=The+global+burden+of+low+back+pain%3A+estimates+from+the+Global+Burden+of+Disease+2010+study.&title=Annal.
- Huang, R.C., Girardi, F.P., Cammisa, F.P., Lim, M.R., Tropiano, P. & Marnay, T., 2005. Correlation between range of motion and outcome after lumbar total disc replacement: 8.6-year follow-up. *Spine*, 30(12), pp.1407–1411.
- Huang, R.C., Girardi, F.P., Cammisa Jr, F.P., Tropiano, P. & Marnay, T., 2003. Long-term flexion-extension range of motion of the prodisc Total Disc Replacement. *J Spinal Disord Tech*, 16(5), pp.435–440.
- Huang, R.C., Tropiano, P., Marnay, T., Girardi, F.P., Lim, M.R. & Cammisa, F.P., 2006. Range of motion and adjacent level degeneration after lumbar total disc replacement. *Spine Journal*, 6(3), pp.242–247.
- Huber, G., Nagel, K., Skrzypiec, D.M., Klein, A., Püschel, K. & Morlock, M.M., 2016. A description of Spinal Fatigue Strength. *Journal of Biomechanics*, 49(6), pp.875–880. Available at: <http://linkinghub.elsevier.com/retrieve/pii/S0021929016301221>.
- Le Huec, J.C., Basso, Y., Mathews, H., Mehbod, A., Aunoble, S., Friesem, T. & Zdeblick, T., 2005. The effect of single-level, total disc arthroplasty on sagittal balance parameters: A prospective study. *European Spine Journal*, 14(5), pp.480–486.
- Hunt, M.W., Baxter, D., Mckay, T., Brody, B.L., Miller, J., LeGendre, V. & Ward, W.G., 2007. *Materials and Processes for Medical Devices*. Advanced Materials & Processes,

(January).

- Hyde, P.J., Tipper, J., Fisher, J. & Hall, R.M., 2015. Wear and biological effects of a semi-constrained total disc replacement subject to modified ISO standard test conditions. *Journal of the Mechanical Behavior of Biomedical Materials*, 44, pp.43–52. Available at: <http://dx.doi.org/10.1016/j.jmbbm.2014.12.001>.
- Jackson, R. & McManus, A., 1994. Radiographic Analysis of Sagittal Plane Alignment and Balance in Standing Volunteers and Patients with Low Back Pain Matched for Age, Sex, and Size. *Spine*, 19(14), pp.1611–1618.
- Jaumard, N. V & Welch, William C, Winkelstein, B.A., 2011. Spinal Facet Joint Biomechanics and Mechanotransduction in Normal , Injury and Degenerative Conditions. *Journal of biomechanical engineering*, 133(August 2011).
- Jaumard, N. V, Welch, W.C. & Winkelstein, B.A., 2011. Spinal facet joint biomechanics and mechanotransduction in normal, injury and degenerative conditions. *Journal of biomechanical engineering*, 133(7), p.71010. Available at: <http://www.pubmedcentral.nih.gov/articlerender.fcgi?artid=3705911&tool=pmcentrez&rendertype=abstract>.
- St. John, K.R., 2014. The use of polyurethane materials in the surgery of the spine: A review. *Spine Journal*, 14(12), pp.3038–3047. Available at: <http://dx.doi.org/10.1016/j.spinee.2014.08.012>.
- Jongeneelen, C.J.M., 2006. Biomechanics in the intervertebral disc, a literature review. , (March), pp.1–21.
- Katz, J.N., 2006. Lumbar disc disorders and low-back pain: socioeconomic factors and consequences. *The Journal of bone and joint surgery. American volume*, 88 Suppl 2, pp.21–24.
- Krijnen, W.P., Sullivan, K., Mahalik, J., Eagly, A., Johannesen-Schmidt, M., Ragins, B.R., Cotton, J.L., Narcotta, E.M., Petersen, J.C., Johnson, S.R., Young, D., Chandler, C., Benishek, L.A., Bieschke, K.J., Park, J., Slattery, S.M., Shary, T., Dixon, M.A. et al., 2004. Report Information from ProQuest. *European Physical Education Review*, 8(3), pp.191–204. Available at: <http://www.ncbi.nlm.nih.gov/pubmed/9635332%5Cnhttp://epe.sagepub.com/cgi/doi/10.1177/1356336X020083004%5Cnhttp://www.scopus.com/inward/record.url?eid=2-s2.0-0002905043&partnerID=40&md5=64180cf1ce1f95c31597a9225a964218%5Cnhttp://prooxy.govst.edu:2048/login?url=ht>.
- Kurtz, S.M., Villarraga, M.L. & Ianuzzi, A., 2009. *The Clinical Performance of UHMWPE in the Spine Third Edit.*, Elsevier Inc. Available at: <http://dx.doi.org/10.1016/B978-0-323-35401-1/00014-4>.
- Lazennec, J., Brusson, A. & Aaron, A., 2013. The LP-ESP Lumbar Disc Prosthesis: Concept, Development and Clinical Experience. *Arthroplasty - Update*, pp.217–219. Available at: <http://cdn.intechopen.com/pdfs-wm/42824.pdf>.
- Lazennec, J.Y., Aaron, A., Brusson, A., Rakover, J.P. & Rousseau, M.A., 2012. The LP-ESP lumbar disc prosthesis with 6 degrees of freedom: Development and 7 years of clinical experience. *European Journal of Orthopaedic Surgery and Traumatology*, 23(2), pp.131–143.

- Lazennec, J.Y., Even, J., Skalli, W., Rakover, J.P., Brusson, A. & Rousseau, M.A., 2014. Clinical outcomes, radiologic kinematics, and effects on sagittal balance of the 6 df LP-ESP lumbar disc prosthesis. *Spine Journal*, 14(9), pp.1914–1920. Available at: <http://dx.doi.org/10.1016/j.spinee.2013.11.016>.
- Lazennec, J.Y., Ramaré, S., Arafati, N., Laudet, C.G., Gorin, M., Roger, B., Hansen, S., Saillant, G., Maurs, L. & Trabelsi, R., 2000. Sagittal alignment in lumbosacral fusion: relations between radiological parameters and pain. *European spine journal : official publication of the European Spine Society, the European Spinal Deformity Society, and the European Section of the Cervical Spine Research Society*, 9(1), pp.47–55. Available at: <http://www.pubmedcentral.nih.gov/articlerender.fcgi?artid=3611353&tool=pmcentrez&rendertype=abstract>.
- LDR, 2014. Mobidisc L Brochure.
- Lindergren, B., 1981. Costs of illness in Sweden, 1964-1975, University of Michigan.
- Liu, J., Ebraheim, N. a, Haman, S.P., Shafiq, Q., Karkare, N., Biyani, A., Goel, V.K. & Woldenberg, L., 2006. Effect of the increase in the height of lumbar disc space on facet joint articulation area in sagittal plane. *Spine*, 31(7), pp.E198--E202.
- Longo, U.G., Loppini, M., Denaro, L., Maffulli, N. & Denaro, V., 2010. Rating scales for low back pain. *British Medical Bulletin*, 94(1), pp.81–144.
- Lu, L.-M., Chao, C.-K., Hsu, C.-C., Hsu, W.-H. & Lin, J., 2013. Applications of Finite Element Analyses-Based Taguchi Methods for Subsidence Problem of Vertebral Body Cages Used in Cervical Spine. *Biomedical Engineering: Applications, Basis and Communications*, 25(4), p.1350040. Available at: <http://www.worldscientific.com/doi/abs/10.4015/S1016237213500403>.
- Lu, S.-B., Hai, Y., Kong, C., Wang, Q.-Y., Su, Q., Zang, L., Kang, N., Meng, X.-L. & Wang, Y., 2015. An 11-year minimum follow-up of the Charite III lumbar disc replacement for the treatment of symptomatic degenerative disc disease. *European spine journal : official publication of the European Spine Society, the European Spinal Deformity Society, and the European Section of the Cervical Spine Research Society*, pp.2056–2064. Available at: <http://www.ncbi.nlm.nih.gov/pubmed/25895882>.
- Lu, W.W., Luk, K.D.K., Holmes, A.D., Cheung, K.M.C. & Leong, J.C.Y., 2005. Pure shear properties of lumbar spinal joints and the effect of tissue sectioning on load sharing. *Spine*, 30(8), pp.E204--E209.
- Luk, K.D.K. & Ruan, D.K., 2008. Intervertebral disc transplantation: A biological approach to motion preservation. *European Spine Journal*, 17(SUPPL. 4), pp.504–510.
- Maniadakis, N. & Gray, A., 2000. The economic burden of back pain in the UK. *Pain*, 84(1), pp.95–103.
- Mannion, A.F., Balagué, F., Pellisé, F. & Cedraschi, C., 2007. Pain measurement in patients with low back pain. *Nature clinical practice. Rheumatology*, 3(11), pp.610–618.
- Manuscript, A. & Proximity, I., 2011. NIH Public Access. , 4(164), pp.744–753.
- Marchand, F. & Ahmed, a M., 1990. Investigation of the laminate structure of lumbar disc annulus fibrosus. *Spine*, 15(5), pp.402–410.

- Marnay, T. & Beyersdorff, B., 2005. Intervertebral implant. , 2(12). Available at: <https://www.google.com/patents/US6936071>.
- Marshall, Robert, Neta Raz, Brien, M.O. & Burke, F., 2014. Applications of Lumbar Spinal Fusion and Disc Replacement. , pp.2717–2727. Available at: <http://link.springer.com/10.1007/978-3-642-34746-7>.
- Mayer, H.M. & Siepe, C., 2007. (iii) Total lumbar disc arthroplasty. *Current Orthopaedics*, 21(1), pp.17–24.
- McAfee, P.C., Geisler, F.H., Saiedy, S.S., Moore, S. V, Regan, J.J., Guyer, R.D., Blumenthal, S.L., Fedder, I.L., Tortolani, P.J. & Cunningham, B., 2006. Revisability of the CHARITE artificial disc replacement: analysis of 688 patients enrolled in the U.S. IDE study of the CHARITE Artificial Disc. *Spine*, 31(11), pp.1217–1226.
- McMillin, C.R., 2006. Biomedical Applications of Rubbers and Elastomers. *Rubber Chemistry and Technology*, 79(3), pp.500–519. Available at: <http://www.rubberchemtechnol.org/doi/abs/10.5254/1.3547948>.
- Mddiadmin, 2000. Thermoplastic Silicone-Urethane Copolymers: A New Class of Biomedical Elastomers | MDDI Medical Device and Diagnostic Industry News Products and Suppliers. *Medical Device and Diagnostic Industry*. Available at: <http://www.mddionline.com/article/thermoplastic-silicone-urethane-copolymers-new-class-biomedical-elastomers> [Accessed October 4, 2016].
- Med Gadget, 2008. Physio-L Lumbar Artificial Elastomeric Disc Gets EU OK | Medgadget. *Med Gadget*. Available at: http://www.medgadget.com/2008/08/physiolr_artificial_disc_gets_eu_ok.html [Accessed August 8, 2016].
- Medtronic, 2002. Maverick Total Disc Replacement Brochure. , p.6.
- Meir, A.R., Freeman, B.J.C., Fraser, R.D. & Fowler, S.M., 2013. Ten-year survival and clinical outcome of the AcroFlex lumbar disc replacement for the treatment of symptomatic disc degeneration. *The Spine Journal*, 13(1), pp.13–21. Available at: <http://www.sciencedirect.com/science/article/pii/S1529943013000247>.
- Michaela, G., Denise, H., Liebensteiner, M. & Michael, B.C., 2008. Footprint mismatch in lumbar total disc arthroplasty. *European Spine Journal*, 17(11), pp.1470–1475.
- Miller, J.A.A., Schultz, A.B., Warwick, D.N. & Spencer, D.L., 1986. Mechanical properties of lumbar spine motion segments under large loads. *Journal of Biomechanics*, 19(1), pp.79–84.
- Miller, L.E., Yue, J. & Garcia, R., 2016. The activL® Artificial Disc: a next-generation motion-preserving implant for chronic lumbar discogenic pain. *Medical Devices: Evidence and Research*, p.75. Available at: <https://www.dovepress.com/the-activlreg-artificial-disc-a-next-generation-motion-preserving-impl-peer-reviewed-article-MDER>.
- Murray, C.J.L., Vos, T., Lozano, R., Naghavi, M., Flaxman, A.D., Michaud, C., Ezzati, M., Shibuya, K., Salomon, J.A., Abdalla, S., Aboyans, V., Abraham, J., Ackerman, I., Aggarwal, R., Ahn, S.Y., Ali, M.K., Alvarado, M., Anderson, H.R. et al., 2012. Disability-adjusted life years (DALYs) for 291 diseases and injuries in 21 regions, 1990–2010: A systematic analysis for the Global Burden of Disease Study 2010. *The Lancet*,

- 380(9859), pp.2197–2223.
- Nachemson, A., 1981. Disc Pressure Measurements. *Spine*, 6(1).
- Navarro, M., Michiardi, a, Castaño, O. & Planell, J. a, 2008. Biomaterials in orthopaedics. *Journal of the Royal Society, Interface / the Royal Society*, 5(October), pp.1137–1158.
- Nerurkar, N.L., Elliott, D.M. & Mauck, R.L., 2010. Mechanical design criteria for intervertebral disc tissue engineering. *Journal of Biomechanics*, 43(6), pp.1017–1030. Available at: <http://dx.doi.org/10.1016/j.jbiomech.2009.12.001>.
- Neubert, A., Fripp, J., Engstrom, C., Gal, Y., Crozier, S. & Kingsley, M.I.C., 2014. Validity and reliability of computerized measurement of lumbar intervertebral disc height and volume from magnetic resonance images. *Spine Journal*, 14(11), pp.2773–2781. Available at: <http://dx.doi.org/10.1016/j.spinee.2014.05.023>.
- Nevarro, R., Theken, R., Anathan, R., Cole, C., Price, J., Park, C., Geol, V., Miller, S. & Yuan, H., 2008. Theken eDisc: A second-Generation Lumbar Artificial Disc, Saunders/Elsevier. Available at: [https://books.google.com.au/books?id=NsIz03qSgy8C&pg=PA367&lpg=PA367&dq=eDisc+mechanical&source=bl&ots=YAATFti0eM&sig=1wEA_g87hX6tu8ogiywU5E30ndg&hl=en&sa=X&ved=0ahUKEwj5oNqo9ZTOAhXKkpQKHQl5AJkQ6AEIJjAB#v=onepage&q=eDisc mechanical&f=false](https://books.google.com.au/books?id=NsIz03qSgy8C&pg=PA367&lpg=PA367&dq=eDisc+mechanical&source=bl&ots=YAATFti0eM&sig=1wEA_g87hX6tu8ogiywU5E30ndg&hl=en&sa=X&ved=0ahUKEwj5oNqo9ZTOAhXKkpQKHQl5AJkQ6AEIJjAB#v=onepage&q=eDisc%20mechanical&f=false).
- Noren, R., Trafimow, J., Andersson, G.B. & Huckman, M.S., 1991. The role of facet joint tropism and facet angle in disc degeneration. *Spine*, 16(5), pp.530–532.
- OpenStax College, 2013. *OpenStax College Anatomy & Physiology*. , pp.493–532.
- Ostelo, R.W.J.G. & de Vet, H.C.W., 2005. Clinically important outcomes in low back pain. *Best Practice and Research: Clinical Rheumatology*, 19(4), pp.593–607.
- Panjabi, M., Goel, V., Oxland, T., Takata, K., Duranceau, J., Martin, K. & Price, M., 1992. Human Lumbar Vertebrae Quantitative Three-Dimensional Anatomy. *Spine*, 17(3), pp.299–206.
- Panjabi, M.M., Oxland, T., Takata, K., Goel, V., Duranceau, J. & Krag, M., 1993. Articular facets of the human spine. Quantitative three-dimensional anatomy. *Spine*, 18(10), pp.1298–1310. Available at: <http://www.ncbi.nlm.nih.gov/pubmed/8211362>.
- Park, C.K., 2015. Total Disc Replacement in Lumbar Degerative Disc Diseases. *The Korean Neurosurgical Society*, 58(5), pp.401–411.
- Park, S.-J., Lee, C.-S., Chung, S.-S., Lee, K.-H., Kim, W.-S. & Lee, J.-Y., 2016. Long-term Outcomes Following Lumbar Total Disc Replacement Using ProDisc-II Average 10-year follow-up at a single institute. *Spine*, 41(11), pp.971–977. Available at: <http://www.ncbi.nlm.nih.gov/pubmed/26909840>.
- Pearcy, M., Portek, I. & Shepherd, J., 1984. Three-dimensional x-ray analysis of normal movement in the lumbar spine. *Spine (Phila Pa 1976)*, 9(3), pp.294–297. Available at: <http://www.ncbi.nlm.nih.gov/pubmed/6374922>.
- Pearcy, M.J. & Bogduk, N., 1988. Instantaneous axes of rotation of the lumbar intervertebral joints. *Spine*, 13(9), pp.1033–41. Available at: <http://ukpmc.ac.uk/abstract/MED/3206297%5Cnhttp://www.ncbi.nlm.nih.gov/pubmed/3206297>.

- Pearcy, M.J. & Tibrewal, S.B., 1984. Axial rotation and lateral bending in the normal lumbar spine measured by three-dimensional radiography. *Spine*, 9(6), pp.582–587.
- Pettine, K. & Hersh, A., 2011. Kineflex lumbar artificial disc versus Charit?? lumbar total disc replacement for the treatment of degenerative disc disease: A randomized non-inferiority trial with minimum of 2 years' follow-up. *SAS Journal*, 5(4), pp.108–113. Available at: <http://dx.doi.org/10.1016/j.esas.2011.07.003>.
- Pilitsis, J.G., Gleiss, A., Rengachary, S.S., Iddrissu, M.I., Awe, O.O., Gonzalez, L.F., Hasan, D., Maltenfort, M. & Rossenwasser, R., 2007. Biomechanics of the Posterior Lumbar Articulating Elements. *Neurosurg Focus*, 22(1), pp.1–11. Available at: <papers3://publication/uuid/CB3BFBA8-02C7-477C-94FA-5FEDB509FD60>.
- Pimenta, L., Turner, A., Cornwall, G., Eisermann, L. & Cappuccino, A., 2015. Controlled Motion with the XL-TDR Lateral-approach Lumbar Total Disc Replacement: In vitro Kinematic Investigation. *J Neurol Surg A Cent Eur Neurosurg.*, pp.1–2. Available at: <http://www.ncbi.nlm.nih.gov/pubmed/25545808>.
- Pimenta, L., Springmuller, R., Lee, C.K., Oliveira, L., Roth, S.E. & Ogilvie, W.F., 2010. Clinical performance of an elastomeric lumbar disc replacement: Minimum 12 months follow-up. *SAS Journal*, 4(1), pp.16–25. Available at: <http://dx.doi.org/10.1016/j.esas.2009.12.002>.
- Polymagnet, 2016. Home - Correlated Magnetics. Available at: <http://www.polymagnet.com/> [Accessed September 29, 2016].
- Premera Blue Cross, 2016. Artificial Intervertebral Disc: Lumbar Spine. Medical Policy Number 7.01.87, (70187), pp.3–5.
- Productivity Commission, 2013. An Ageing Australia: Preparing for the Future, Melbourne: Media and Publications Productivity Commission. Available at: <http://www.pc.gov.au/research/completed/ageing-australia>.
- Punt, I., Van Rijsbergen, M., Van Rietbergen, B., Ito, K., Van Rhijn, L., Van Ooij, A. & Willems, P., 2013. Subsidence of SB Charité total disc replacement and the role of undersizing. *European Spine Journal*, 22(10), pp.2264–2270.
- Rajaei, S.S., Bae, H.W., Kanim, L.E. & Delamarter, R.B., 2012. Spinal fusion in the United States: analysis of trends from 1998 to 2008. *Spine*, 37(1), pp.67–76. Available at: <http://www.ncbi.nlm.nih.gov/pubmed/21311399>.
- Reeks, J. & Liang, H., 2015. Materials and Their Failure Mechanisms in Total Disc Replacement. , (Cdc), pp.346–364.
- Rega, J., 2012. SILICONE-URETHANE COPOLYMERS. , 2(12).
- Rothwell, A., Larmer, P., Hobbs, T. & Rothwell, A., 2014. THE NEW ZEALAND JOINT REGISTRY Annual Report Editorial Committee. Nzjr, (January 1999).
- Ruiz, F.K., Bohl, D.D., Webb, M.L., Russo, G.S. & Grauer, J.N., 2014. Oswestry Disability Index is a better indicator of lumbar motion than the Visual Analogue Scale. *Spine Journal*, 14(9), pp.1860–1865. Available at: <http://dx.doi.org/10.1016/j.spinee.2013.10.027>.
- Safe Work Australia, 2013. Australian Workers ' Compensation Statistics , 2012 - 13, Available at:

- <http://www.safeworkaustralia.gov.au/sites/SWA/about/Publications/Documents/897/australian-workers-compensation-statistics-2012-13.pdf>.
- Safe Work Australia, 2015. Key Work Health and Safety.
- Salomon, J.A., Vos, T., Hogan, D.R., Gagnon, M., Naghavi, M., Mokdad, A., Begum, N., Shah, R., Karyana, M., Kosen, S., Farje, M.R., Moncada, G., Dutta, A., Sazawal, S., Dyer, A., Seiler, J., Aboyans, V., Baker, L. et al., 2012. Common values in assessing health outcomes from disease and injury: Disability weights measurement study for the Global Burden of Disease Study 2010. *The Lancet*, 380(9859), pp.2129–2143.
- Sasso, R.C., Foulk, D.M. & Hahn, M., 2008. Prospective, randomized trial of metal-on-metal artificial lumbar disc replacement: initial results for treatment of discogenic pain. *Spine*, 33(2), pp.123–131.
- Van Schaik, Jan, Verbiest, Henk, Van Schaik, F., 1984. The Orientation of the Laminae and Facet Joints in the Lower Lumbar Spine. , p.10:59-63.
- Schätz, C., Ritter-Lang, K., Gössel, L. & Others, 2015. Comparison of Single-Level and Multiple-Level Outcomes of Total Disc Arthroplasty: 24-Month Results. *International journal of spine surgery*, 9, p.14. Available at: <http://www.pubmedcentral.nih.gov/articlerender.fcgi?artid=4442630&tool=pmcentrez&rendertype=abstract>.
- Schroeder, Y., Wilson, W., Huyghe, J.M. & Baaijens, F.P.T., 2006. Osmoviscoelastic finite element model of the intervertebral disc. *European Spine Journal*, 15(SUPPL. 3), pp.361–371.
- Sears, W.R., McCombe, P.F. & Sasso, R.C., 2006. Kinematics of Cervical and Lumbar Total Disc Replacement. *Seminars in Spine Surgery*, 18(2), pp.117–129.
- Serhan, H. a, Varnavas, G., Dooris, A.P., Patwadhan, A. & Tzermiadianos, M., 2007. Biomechanics of the posterior lumbar articulating elements. *Neurosurgical focus*, 22(1), p.E1.
- Serhan, H., Mhatre, D., Defosse, H. & Bono, C.M., 2011. Motion-preserving technologies for degenerative lumbar spine: The past, present, and future horizons. *SAS Journal*, 5(3), pp.75–89. Available at: <http://dx.doi.org/10.1016/j.esas.2011.05.001>.
- Shin, M.H., Ryu, K.S., Hur, J.W., Kim, J.S. & Park, C.K., 2013. Association of facet tropism and progressive facet arthrosis after lumbar total disc replacement using ProDisc-L?? *European Spine Journal*, 22(8), pp.1717–1722.
- Shinohara, S., Okada, M., Keira, T., Ohwada, M., Niitsuya, M. & Aizawa, Y., 1998. Prognosis of accidental low back pain at work. *The Tohoku journal of experimental medicine*, 186(4), pp.291–302.
- Shirazi-Adl, A., Ahmed, A.M. & Shrivastava, S.C., 1986. A finite element study of a lumbar motion segment subjected to pure sagittal plane moments. *Journal of Biomechanics*, 19(4), pp.331–350.
- Showalter, B.L., Beckstein, J.C., Martin, J.T., Elizabeth, E., Orías, A.A.E., Schaer, T.P., Edward, J. & Elliott, D.M., 2012. Comparison of Animal Discs Used in Disc Research to Human Lumbar Disc: Torsion Mechanics and Collagen Content. *Spine*, 37(15), pp.1–17.

- Siepe, C.J., Mayer, H.M., Heinz-Leisenheimer, M. & Korge, A., 2007. Total lumbar disc replacement: Different results for different levels. *Spine*, 32(7), pp.782–790. Available at: <http://www.scopus.com/inward/record.url?eid=2-s2.0-34147154146&partnerID=40&md5=c1ec5462eb301109f30faa30b89466ad>.
- Da Silva Baptista, J., De Vasconcellos Fontes, R.B. & Liberti, E.A., 2015. Aging and degeneration of the intervertebral disc: Review of basic science. *Coluna/ Columna*, 14(2), pp.144–148.
- Skrzypiec, D.M., Klein, A., Bishop, N.E., Stahmer, F., Püschel, K., Seidel, H., Morlock, M.M. & Huber, G., 2012. Shear strength of the human lumbar spine. *Clinical Biomechanics*, 27(7), pp.646–651. Available at: <http://dx.doi.org/10.1016/j.clinbiomech.2012.04.003>.
- Spinal Kinetics, 2009. M6-L Artificial Lumbar Disc Brochure. , p.6. Available at: <http://ovidsp.ovid.com/ovidweb.cgi?T=JS&PAGE=reference&D=ovftf&NEWS=N&AN=00002352-200303000-00029>.
- Spine Art, 2010. Baguera-L - Features. , p.2.
- Spine Art, Baguera®L Lumbar Disc Prothesis. Available at: <http://www.spineart.com/product-platforms/motion/9/product/baguera%25C2%25AEI/128> [Accessed August 8, 2016].
- SSJ Health, 2010. Baguera L - Lumbar Disc Prothesis. Available at: http://www.signaturespine.com.au/product.php?prod=baguera_l_-_lumbar_disc_prothesis [Accessed August 8, 2016].
- Sterling, P. & Sterling, P., 2014. Financial year average exchange rates Australian dollar 2011 / 12 – 2014 / 15 Financial year average exchange rates. , pp.1–7.
- Strube, P., Hoff, E.K., Schmidt, H., Dreischarf, M., Rohlmann, A. & Putzier, M., 2013. Parameters influencing the outcome after total disc replacement at the lumbosacral junction. Part 2: Distraction and posterior translation lead to clinical failure after a mean follow-up of 5 years. *European Spine Journal*, 22(10), pp.2279–2287.
- Synthes CMF, 2005. PSI - Patient Specific Implants. Derived from CT data for excellent reconstructive results.
- Synthes Spine, 2006. ProDisc-L Total Disc Replacement - Product information. , p.9.
- Taksali, S., Grauer, J.N. & Vaccaro, A.R., 2004. Material considerations for intervertebral disc replacement implants. , 4, pp.231–238.
- Tang, R., Gungor, C., Sesek, R.F., Foreman, K.B., Gallagher, S. & Davis, G.A., 2016. Morphometry of the lower lumbar intervertebral discs and endplates: comparative analyses of new MRI data with previous findings. *European Spine Journal*. Available at: <http://link.springer.com/10.1007/s00586-016-4405-8>.
- Thavaneswaran, P. & Vandeppeer, M., 2014. Lumbar artificial intervertebral disc replacement : a systematic review. , 84, pp.121–127.
- The Norwegian Hip Fracture Register, 2010. Annual Report 2010, <http://nrlweb.ihelse.net/eng/>,
- Tohmeh, A.G. & Smith, W.D., 2015. Lumbar total disc replacement by less invasive lateral

- approach: a report of results from two centers in the US IDE clinical trial of the XL TDR[®] device. *European Spine Journal*, 24, pp.331–338.
- Tournier, C., Aunoble, S., Le Huec, J.C., Lemaire, J.P., Tropiano, P., Lafage, V. & Skalli, W., 2007. Total disc arthroplasty: Consequences for sagittal balance and lumbar spine movement. *European Spine Journal*, 16(3), pp.411–421.
- Track Cycling News, 2011. Red Bull Mini-Drome for Glasgow. Available at: <http://www.trackcyclingnews.com/minidrome glasgow.html> [Accessed October 3, 2016].
- Tsitsopoulos, P.P., Wojewnik, B., Voronov, L.I., Havey, R.M., Renner, S.M., Zelenakova, J., McIntosh, B., Carandang, G., Abjornson, C. & Patwardhan, A.G., 2012. Effect of prosthesis endplate lordosis angles on L5-S1 kinematics after disc arthroplasty. *European Spine Journal*, 21(SUPPL. 5), pp.585–591.
- Valdevit, A. & Errico, T.J., 2004. Design and evaluation of the FlexiCore metal-on-metal intervertebral disc prosthesis. *Spine Journal*, 4(6 SUPPL.), pp.276–288.
- Van, ZJ, Van, K., 2005. Low back pain: from algorithm to cost-effective- ness? *Pain Pract*, pp.179–189.
- Veruva, S.Y., Steinbeck, M.J., Toth, J., Alexander, D.D. & Kurtz, S.M., 2014. Which design and biomaterial factors affect clinical wear performance of total disc replacements? A systematic review. *Clinical orthopaedics and related research*, 472(12), pp.3759–3769.
- Vialle, R., Levassor, N., Rillardon, L., Templier, A., Skalli, W. & Guigui, P., 2005. Radiographic analysis of the sagittal alignment and balance of the spine in asymptomatic subjects. *The Journal of bone and joint surgery. American volume*, 87(2), pp.260–267.
- Vital, J.-M. & Boissière, L., 2014. Total disc replacement. *Orthopaedics & traumatology, surgery & research : OTSR*, 100(1 Suppl), pp.S1-14. Available at: <http://www.sciencedirect.com/science/article/pii/S1877056813002806>.
- Vrtovec, T., Pernuš, F. & Likar, B., 2009. A review of methods for quantitative evaluation of spinal curvature. *European Spine Journal*, 18(5), pp.593–607.
- Wagnac, E., Arnoux, P.-J., Garo, A., El-Rich, M. & Aubin, C.-E., 2011. Calibration of hyperelastic material properties of the human lumbar intervertebral disc under fast dynamic compressive loads. *Journal of Biomechanical Engineering*, 133(10), p.101007. Available at: <http://www.ncbi.nlm.nih.gov/pubmed/22070332>.
- Walker, B.F, Muller, R., Grant, W.D.D., 2003. Low Back Pain in Australian Adults: The Economic Burden. *Asia-Pacific Journal of Public Health*, 15(2), pp.79–87. Available at: <http://www.ncbi.nlm.nih.gov/pubmed/15038680>.
- Wang, J.C., Arnold, P.M., Hermsmeyer, J.T. & Norvell, D.C., 2012. Do Lumbar Motion Preserving Devices Reduce the Risk of Adjacent Segment Pathology. , 37(22), pp.133–143.
- Wang, Y., Battie, M.C. & Videman, T., 2012. A morphological study of lumbar vertebral endplates: Radiographic, visual and digital measurements. *European Spine Journal*, 21(11), pp.2316–2323.
- Wang, Y.X.J. & Griffith, J.F., 2011. Menopause causes vertebral endplate degeneration and decrease in nutrient diffusion to the intervertebral discs. *Medical Hypotheses*, 77(1), pp.18–20. Available at: <http://dx.doi.org/10.1016/j.mehy.2011.03.014>.

- Whatley, B.R. & Wen, X., 2012. Intervertebral disc (IVD): Structure, degeneration, repair and regeneration. *Materials Science and Engineering C*, 32(2), pp.61–77. Available at: <http://dx.doi.org/10.1016/j.msec.2011.10.011>.
- Wieser, S., Horisberger, B., Schmidhauser, S. & Eisenring, C., 2011. Cost of low back pain in Switzerland in 2005. , pp.455–467.
- Wieser, S., Horisberger, B., Schmidhauser, S., Eisenring, C., Br??gger, U., Ruckstuhl, A., Dietrich, J., Mannion, A.F., Elfering, A., Tamcan, ??zg??r & M??ller, U., 2011. Cost of low back pain in Switzerland in 2005. *European Journal of Health Economics*, 12(5), pp.455–467.
- Yamamoto, I., Panjabi, M.M., Crisco, T. & Oxland, T., 1989. Three-dimensional movements of the whole lumbar spine and lumbosacral joint. *Spine*, 14(11), pp.1256–60. Available at: <http://www.ncbi.nlm.nih.gov/pubmed/2603060>.
- Young, D.S., Sachais, B.S. & Jefferies, L.C., 2000. The costs of disease. *Clinical Chemistry*, 46(7), pp.955–966.
- Yue, J.J. & Mo, F.F., 2010. Clinical study to evaluate the safety and effectiveness of the Aesculap Activ-L artificial disc in the treatment of degenerative disc disease. *BMC surgery*, 10, p.14.
- Zhao, F., Pollintine, P., Hole, B.D., Dolan, P. & Adams, M. a, 2005. Discogenic origins of spinal instability. *Spine*, 30(23), pp.2621–2630.
- Zhou, S.H., McCarthy, I.D., McGregor, A.H., Coombs, R.R. & Hughes, S.P., 2000. Geometrical dimensions of the lower lumbar vertebrae--analysis of data from digitised CT images. *European spine journal : official publication of the European Spine Society, the European Spinal Deformity Society, and the European Section of the Cervical Spine Research Society*, 9(3), pp.242–8. Available at: <http://www.pubmedcentral.nih.gov/articlerender.fcgi?artid=3611390&tool=pmcentrez&rendertype=abstract>.
- Zimmer Biomet, 2016. Mobidisc® L Lumbar Disc Prosthesis. Available at: <https://fr.ldr.com/english/Products/Thoracolumbar/Mobidisc%25C2%25AELLumbarDiscProsthesis> [Accessed August 8, 2016].

Chapter 15. Appendix

Appendix A: Modified Stauffer-Coventry scoring system (Huang et al. 2005)

Parameter	Grade					Total
	0	1	2	3	4	
Low back pain	Permanent	Frequent	Moderate	None		3
Radicular pain	Permanent	Frequent	Effort	None		3
Neurologic deficit	Major		Moderate		None	4
Medication	Major	Moderate	None			2
Day living activities	Impossible		Normal			2
Work status postoperatively	No work	Frequently stopped	Change	Same work >6 mos. Change <3 mos	Normal	4
Psychiatric status	Preoperative	Secondary to pathology	None			2
Total		20				

Appendix B: ODI version 1.0 (left) and ODI version 2.0 (right) questionnaires (Fairbank & Pynsent 2000; Fairbank et al. 1980; Longo et al. 2010)

ODI Version 1.0

This questionnaire has been designed to give the doctor information as to how your back pain has affected your ability to manage in every day life. Please answer every section, and mark in each section only the *one* box which applies to you. We realize you may consider that two of the statements in any one section relate to you, but please just *mark the box which most closely describes your problem.*

Section 1—Pain intensity

I can tolerate the pain I have without having to use painkillers.
 The pain is bad but I manage without taking painkillers.
 Painkillers give complete relief from pain.
 Painkillers give moderate relief from pain.
 Painkillers give very little relief from pain.
 Painkillers have no effect on the pain and I do not use them.

Section 2—Personal care (washing, dressing, etc.)

I can look after myself normally without causing extra pain.
 I can look after myself normally but it causes extra pain.
 It is painful to look after myself and I am slow and careful.
 I need some help but manage most of my personal care.
 I need help every day in most aspects of self-care.
 I do not get dressed, wash with difficulty and stay in bed.

Section 3—Lifting

I can lift heavy weights without extra pain.
 I can lift heavy weights but it gives extra pain.
 Pain prevents me from lifting heavy weights off the floor, but I can manage if they are conveniently positioned, e.g. on a table.
 Pain prevents me from lifting heavy weights but I can manage light to medium weights if they are conveniently positioned.
 I can lift only very light weights.
 I cannot lift or carry anything at all.

ODI Version 2.0

Could you please complete this questionnaire It is designed to give us information as to how your back (or leg) trouble has affected your ability to manage in everyday life. Please answer **every section**. Mark **one box only** in each section that most closely describes you **today**.

Section 1—Pain intensity

I have no pain at the moment.
 The pain is very mild at the moment.
 The pain is moderate at the moment.
 The pain is fairly severe at the moment.
 The pain is very severe at the moment.
 The pain is the worst imaginable at the moment.

Section 2—Personal care (washing, dressing, etc.)

I can look after myself normally without causing extra pain.
 I can look after myself normally but it is very painful.
 It is painful to look after myself and I am slow and careful.
 I need some help but manage most of my personal care.
 I need help every day in most aspects of self care.
 I do not get dressed, wash with difficulty and stay in bed.

Section 3—Lifting

I can lift heavy weights without extra pain.
 I can lift heavy weights but it gives extra pain.
 Pain prevents me from lifting heavy weights off the floor but I can manage if they are conveniently positioned, e.g. on a table.
 Pain prevents me from lifting heavy weights but I can manage light to medium weights if they are conveniently positioned.
 I can lift only very light weights.
 I cannot lift or carry anything at all.

Section 4—Walking

Pain does not prevent my walking any distance.
Pain prevents me walking more than 1 mile.
Pain prevents me walking more than 1/2 mile.
Pain prevents me walking more than 1/4 mile.
I can only walk using a stick or crutches.
I am in bed most of the time and have to crawl to the toilet.

Section 5—Sitting

I can sit in any chair as long as I like.
I can sit in my favourite chair as long as I like.
Pain prevents me sitting more than 1 hour.
Pain prevents me from sitting more than 1/2 an hour.
Pain prevents me from sitting more than 10 minutes.
Pain prevents me from sitting at all.

Section 6—Standing

I can stand as long as I want without extra pain.
I can stand as long as I want but it gives me extra pain.
Pain prevents me from standing for more than 1 hour.
Pain prevents me from standing for more than 30 minutes.
Pain prevents me from standing for more than 10 minutes.
Pain prevents me from standing at all.

Section 7—Sleeping

Pain does not prevent me from sleeping well.
I can sleep well only by using tablets.
Even when I take tablets I have less than 6 hours sleep.
Even when I take tablets I have less than 4 hours sleep.
Even when I take tablets I have less than 2 hours sleep.
Pain prevents me from sleeping at all.

Section 4—Walking

Pain does not prevent me walking any distance.
Pain prevents me walking more than 1 mile.
Pain prevents me walking more than than 1/2 of a mile.
Pain prevents me walking more than 100 yards.
I can only walk using a stick or crutches.
I am in bed most of the time and have to crawl to the toilet.

Section 5—Sitting

I can sit in any chair as long as I like.
I can sit in my favourite chair as long as I like.
Pain prevents me from sitting for more than 1 hour.
Pain prevents me from sitting for more than 1/2 an hour.
Pain prevents me from sitting for more than 10 minutes.
Pain prevents me from sitting at all.

Section 6—Standing

I can stand as long as I want without extra pain.
I can stand as long as I want but it gives me extra pain.
Pain prevents me from standing for more than 1 hour.
Pain prevents me from standing for more than 1/2 an hour.
Pain prevents me from standing for more than 10 minutes.
Pain prevents me from standing at all.

Section 7—Sleeping

My sleep is never disturbed by pain.
My sleep is occasionally disturbed by pain.
Because of pain I have less than 6 hours sleep.
Because of pain I have less than 4 hours sleep.
Because of pain I have less than 2 hours sleep.
Pain prevents me from sleeping at all.

Section 8—Sex life

My sex life is normal and causes no extra pain.
My sex life is normal but causes some extra pain.
My sex life is nearly normal but is very painful.
My sex life is severely restricted by pain.
My sex life is nearly absent because of pain.
Pain prevents any sex life at all.

Section 9—Social life

My social life is normal and gives me no extra pain.
My social life is normal but increases the degree of pain.
Pain has no significant effect on my social life apart from limiting my more energetic interests, e.g. dancing, etc.
Pain has restricted my social life and I do not go out as often.
Pain has restricted social life to my home.
I have no social life because of pain.

Section 10—Travelling

I can travel anywhere without extra pain.
I can travel anywhere but it gives me extra pain.
Pain is bad but I manage journeys over two hours.
Pain restricts me to journeys of less than one hour.
Pain restricts me to short necessary journeys under 30 minutes.
Pain prevents travel except to the doctor or hospital.

Section 8—Sex life (if applicable)

My sex life is normal and causes no extra pain.
My sex life is normal but causes some extra pain.
My sex life is nearly normal but is very painful.
My sex life is severely restricted by pain.
My sex life is nearly absent because of pain.
Pain prevents any sex life at all.

Section 9—Social life

My social life is normal and causes me no extra pain.
My social life is normal but increases the degree of pain.
Pain has no significant effect on my social life apart from limiting my more energetic interests, e.g. sport, etc.
Pain has restricted my social life and I do not go out as often.
Pain has restricted social life to my home.
I have no social life because of pain.

Section 10—Travelling

I can travel anywhere without pain.
I can travel anywhere but it gives extra pain.
Pain is bad but I manage journeys over two hours.
Pain restricts me to journeys of less than one hour.
Pain restricts me to short necessary journeys under 30 minutes.
Pain prevents me from travelling except to receive treatment.

Appendix C: Comparison of mean ODI outcome of different TDR devices (*=values estimated from graphs found in appendices) (Pre-op=before operation).

Prosthes is	Pre-op	Post-operative (Months)											Referenc es	
		1.5	3	6	12	24	36	48	60	72	84	120 +		
AcroFlex (average of pilot 1 and pilot 2 device)	49.3			39	38.9	34.4							25	(Fraser et al. 2004; Meir et al. 2013)
CHARI TE	59*	35*	27*	23*	21*	21*	20*	18*	20*					(Guyer et al. 2016)
	41.36												13.21	(Lu et al. 2015)
	50.6	37.7	29.9	27.5	26	26.3								(FDA 2004)
KineFlex-L	58*	36*	26*	24*	24*	22*	21*	22*	21*					(Guyer et al. 2016)
ActivL	71*		24*	20*	18*	20*	29*	18*		19*				(Miller et al. 2016)
Prodisc-L	64*		30*	29*	25*	26*	36*	26*		27*				(Miller et al. 2016)
	63.4	41.5	36.4	36	35.6	34.5								(FDA 2006)
	41.5				21.2	17.7			17.9		20.8	22.4		(Park et al. 2016)
FlexiCore	62	36	30	25	18	6								(Sasso et al. 2008)
MobiDisc-L	50	31	25	24	23	23								(Delécrin et al. 2007)
Physio-L	54.3	17.2	15.8	13.5	12.7									(Pimenta et al. 2010)
XL TDR	51*	31*	30*	24*	20*	18*	19*							(Tohmeh & Smith 2015)
Maverick	50.1			24.2	21.3	20.3								(Assaker et al. 2015)
LP-ESP	47.6		30.3	24.5	21.8	20.6								(Lazenne c et al. 2012)
Fusion	52.1	43.7	37.4	35.8	31.8	30.5								(FDA 2004)

Appendix D: Comparison of VAS outcome of different TDR devices. (scores were scaled to 0-10 values) (*=values estimated form bar graphs found in appendices) (Pre-op=before operation).

Prosthesi s	Pre -op	Post-operative (Months)											Referenc es
		1.5	3	6	12	24	36	48	60	72	84	120 +	
CHARI TE	7.8	3.1	2.3	2.3	2.1	2.2	2.3	2	2. 1				(Guyer et al. 2016)
	8.5											1.46	(Lu et al. 2015)
	7.2					3.1 2							(FDA 2004)
KineFle x-L	7.9	3.8	3.1	2.4	2.4	2.4	2.2	2.2	2. 2				(Guyer et al. 2016)
Prodisc- L	8.2 *		4.1 *	3.9 *	3.1 *	3.2 *	4.3 *	4*		2.6 *			(Miller et al. 2016)
	7.5 *	4.1	3.8	4.0	3.9	3.6							(Synthes Spine 2006)
	7.9				7.9	2.5			3. 1		3. 1	3.4	(Park et al. 2016)
activL	8.3 *		2.5 *	2.6 *	1*	1.2 *	2.1 *	1.9 *		0.9 *			(Miller et al. 2016)
FlexiCor e	8.6	3.6	3.9	3.3	2.4	1.6							(Sasso et al. 2008)
MobiDis c-L	6.8	3.0	2.7	2.5	2.3	2.6							(Delécrin et al. 2007)
Physio-L	7.6	1.1 8	1.8 3	1.6 3	2.1 8	1.6 5							(Pimenta et al. 2010)
XL TDR	7.2 *	3.1 *	3*	3.1 *	2.2 *	2.5 *	2.4 *						(Tohmeh & Smith 2015)
Maveric k	7			3	2.9	2.8							(Assaker et al. 2015)
LP-ESP	6.6		3.7	3.4	3.5	3.4							(Lazenne c et al. 2012)
Freedom	7.6		1.5 6	1.5 6	0.4 2	0.0 5							(Axiome d 2012)
Fusion	7.1 8											3.75	(FDA 2004)

Appendix E: CHARITE (Control) and KineFlex-L (Investigational) bar graphs used to estimate mean ODI (Guyer et al. 2016).

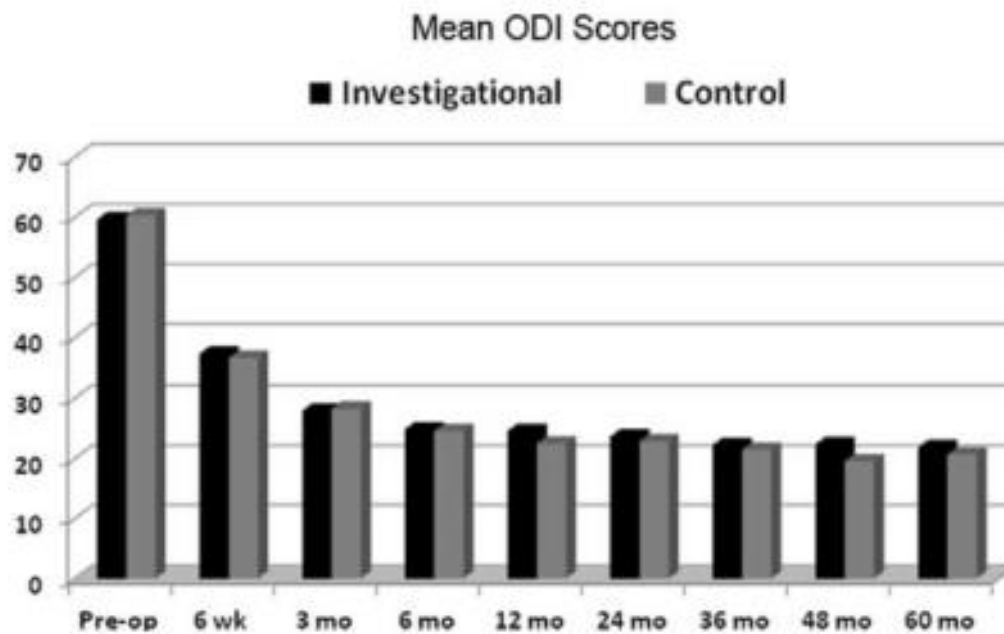


Figure 1. The mean Oswestry Disability Index scores in both treatment groups improved significantly by 6-week follow-up and remained stable and improved ($P < 0.01$) throughout 5-year follow-up.

Appendix F: ActivL and ProDisc-L graph used to estimate ODI (Miller et al. 2016).

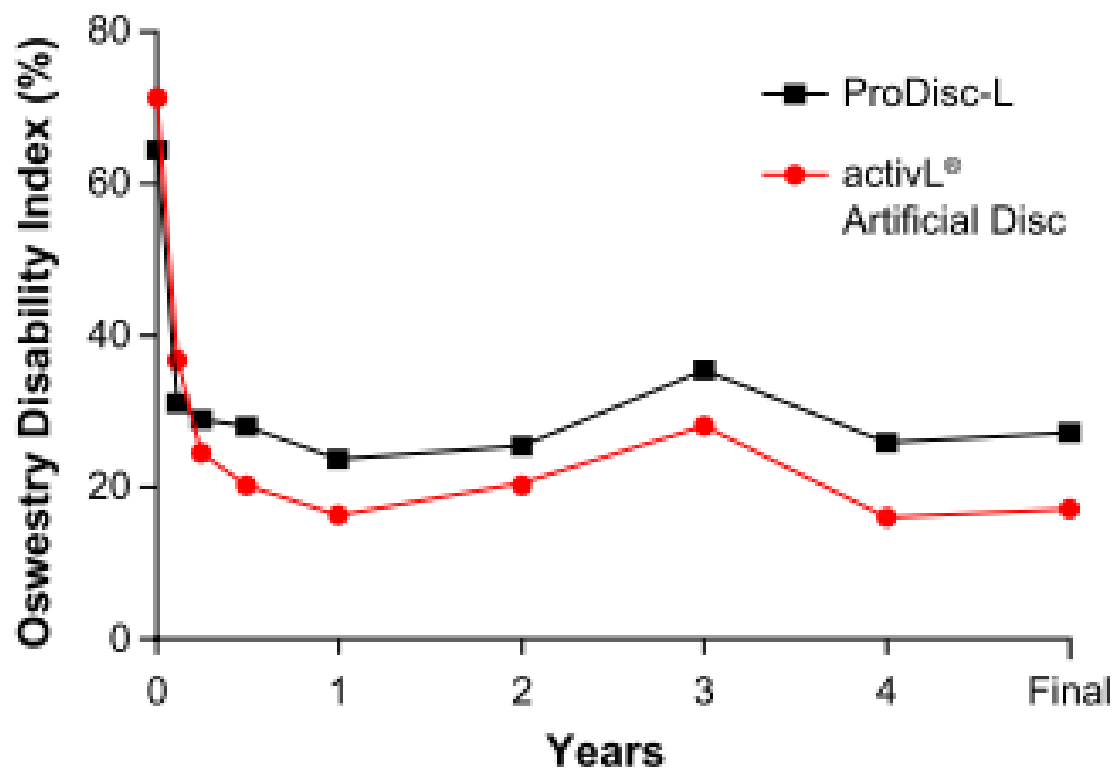


Figure 7 Changes in Oswestry Disability Index over 6-year mean follow-up with activL Artificial Disc versus ProDisc-L.

Appendix G: ActivL and ProDisc-L graph used to estimate VAS (Miller et al. 2016).

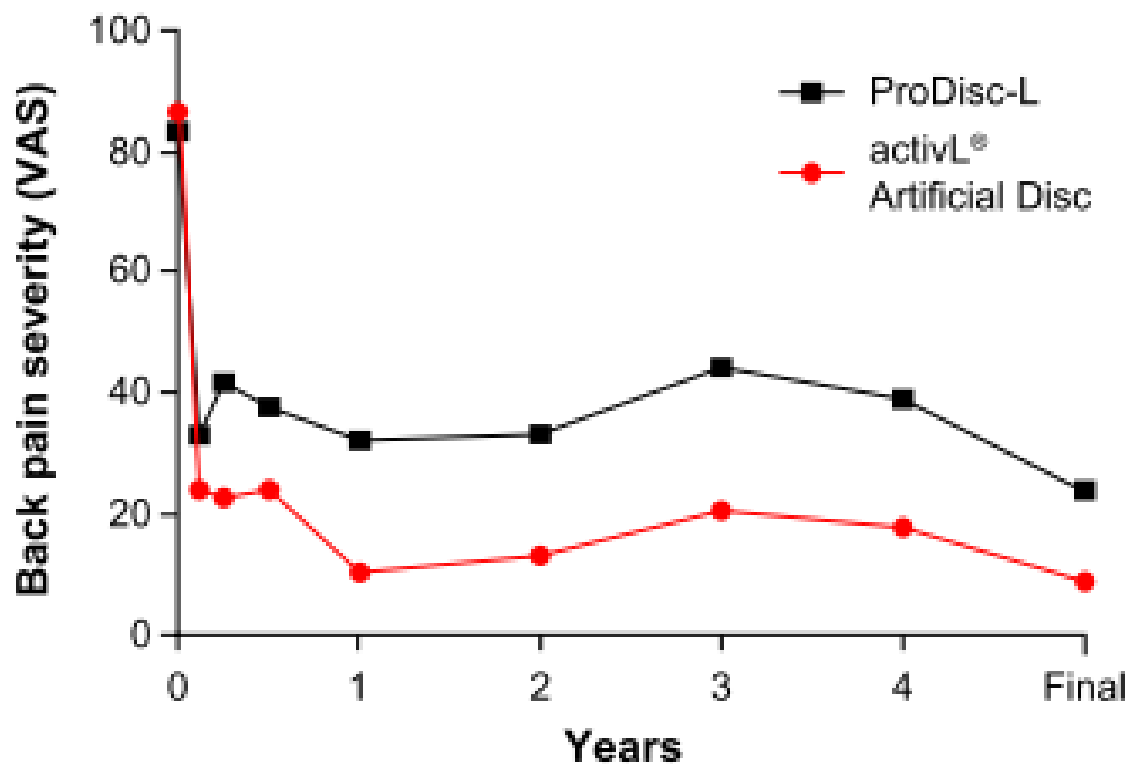
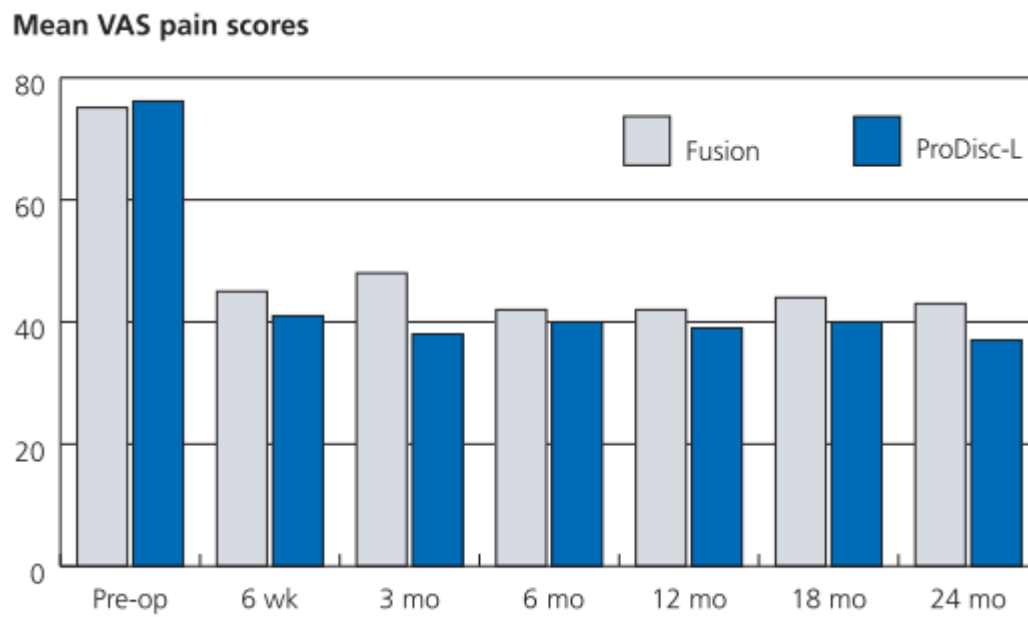


Figure 6 Changes in back pain severity over 6-year mean follow-up with activL[®] Artificial Disc versus ProDisc-L.

Abbreviation: VAS, visual analog scale.

Appendix H: ProDisc-L 24 month VAS bar graph (Synthes Spine 2006).



Appendix I: Graph used to estimate both the ODI and VAS scores of a three year clinical trial of the XL TDR (Tohmeh & Smith 2015).

